TAL TECH

DOCTORAL THESIS

A Multi-Method Approach to Solid Insulation Aging Based on Partial Discharge Measurement

Maninder Choudhary

TALLINNA TEHNIKAÜLIKOOL
TALLINN UNIVERSITY OF TECHNOLOGY
TALLINN 2025

TALLINN UNIVERSITY OF TECHNOLOGY
DOCTORAL THESIS
86/2025

A Multi-Method Approach to Solid Insulation Aging Based on Partial Discharge Measurement

MANINDER CHOUDHARY

TAL TECH PRESS

TALLINN UNIVERSITY OF TECHNOLOGY
School of Engineering
Department of Electrical Power Engineering and Mechatronics
This dissertation was accepted for the defines of the degree 28/10/2025

Supervisor: Prof. Ivo Palu
Department of Electrical Power Engineering and Mechatronics,
Tallinn University of Technology,
Tallinn, Estonia

Co-supervisor: Dr. Ivar Kiitam
Department of Electrical Power Engineering and Mechatronics,
Tallinn University of Technology,
Tallinn, Estonia

Opponents: Prof. Saulius Gudzius
Department of Electrical and Power Systems,
Kaunas University of Technology (KTU),
Kaunas, Lithuania

Prof. Muzamir Bin Isa
School of Electrical System Engineering,
University Malaysia Perlis (UniMAP),
Perlis, Malaysia

Defense of the thesis: 28/11/2025, Tallinn

Declaration:
Hereby I declare that this doctoral thesis, my original investigation, and achievement, submitted for the doctoral degree at Tallinn University of Technology has not been submitted for doctoral or equivalent academic degree.

Maninder Choudhary

---
signature

European Union
European Regional
Development Fund

Investing
in your future

Copyright: Maninder Choudhary, 2025
ISSN 2585-6898 (publication)
ISBN 978-9916-80-409-4 (publication)
ISSN 2585-6901 (PDF)
ISBN 978-9916-80-410-0 (PDF)
DOI https://doi.org/10.23658/taltech.86/2025
Printed by Koopia Niini & Rauam

Choudhary, M. (2025). *A Multi-Method Approach to Solid Insulation Aging Based on Partial Discharge Measurement* [TalTech Press]. https://doi.org/10.23658/taltech.86/2025

TALLINNA TEHNIKAÜLIKOOL
DOKTORITÖÖ
86/2025

Osalahenduste mõõtmisel põhinev mitmemeetodiline lähenemine tahke isolatsiooni vananemisele

MANINDER CHOUDHARY

TAL TECH
KIRJASTUS

Contents

List of Publications

The list of author's publications, on which the thesis is based:

I **M. Choudhary**, M. Shafiq. I. Kiitam, A. Hussain, I. Palu and P. Taklaja, "A Review of Aging Models for Electrical Insulation in Power Cables," Energies, vol. 15, issue 9. 2022. doi: https://doi.org/10.3390/en15093408.

II **M. Choudhary**, M. Shafiq, I. Kiitam, I. Palu, and P. Taklaja, "Study on the Progression of Surface Partial Discharge in Power Cables", IEEE 63rd Annual International Scientific Conference on Power and Electrical Engineering of Riga Technical University (RTUCON), 2022, doi: https://10.1109/RTUCON56726.2022.9978804.

III **M. Choudhary**, I. Palu, I. Kiitam, M. Shafiq, P. Taklaja and A. Bhattarai, "Denoising and Extraction of Partial Discharge Pulse Characteristics Using Wavelet Denoising and Local Maxima Method," 2024 IEEE International Conference on Power and Energy (PECon), Kuala Lumpur, Malaysia, 2024, pp. 221–225, doi: https://doi.org/10.1109/PECon62060.2024.10827085.

IV **M. Choudhary**, I. Palu, I. Kiitam, M. Shafiq and P. Taklaja, "Study of Partial Discharge Characteristics in Medium Voltage Cable Insulation with Internal Defect," 2024 IEEE International Conference on High Voltage Engineering and Applications (ICHVE), Berlin, Germany, 2024, pp. 1–4, doi: https://doi.org/10.1109/ICHVE61955.2024.10676188.

V **M. Choudhary**, M. Shafiq. I. Kiitam, I. Palu, W. Hassan, P. Singh, "Investigation of Partial Discharge Characteristics in XLPE Cable Insulation Under Increasing Electrical Stress," Engineering Failure Analysis, Elsevier, 2024. doi: https://doi.org/10.1016/j.engfailanal.2024.108006

VI **M. Choudhary**, M. Shafiq, I. Kiitam, I. Palu and W. Hassan, "Partial Discharge Pulse Shape Analysis for Progression of Insulation Degradation in Medium Voltage Cable," 2023 International Electrical Engineering Congress (iEECON), Krabi, Thailand, 2023, pp. 332–336, doi: https://doi.org/10.1109/iEECON56657.2023.10126589.

VII **M. Choudhary**, M. Shafiq, A. Bhattarai, I. Kiitam, I. Palu, P. Taklaja, "A Comprehensive Study of Partial Discharge based Extrinsic Aging in Nomex Insulation Films: Modeling, Simulation and Measurement", Electric Power Systems Research, Elsevier, 2025, doi: https://doi.org/10.1016/j.epsr.2025.111663.

VIII **M. Choudhary**, I. Kiitam, I. Palu, "Electrical Aging and Lifetime Study of Nomex Insulation Influenced by Partial Discharges", Electric Power Systems Research, Volume 249, 2025, doi: https://doi.org/10.1016/j.epsr.2025.112000.

IX **M. Choudhary,** I. Kiitam, I. Palu, "An Integrated Approach for Pulse Detection and Classification of Partial Discharge Signals", IEEE 66th International Scientific Conference on Power and Electrical Engineering of Riga Technical University (RTUCON), 2025. (Accepted for publication).

Author's Contribution to the Publications

The author's contributions to the papers in this thesis are:

I Maninder Choudhary is the main author of this article. He conducted a literature review of various aging models, factors that accelerate aging, and the role of partial discharge measurement in aging studies. He reviewed various research articles, structured the contents, and drafted the article.

II Maninder Choudhary is the main author of this article. He analyzed the progression of partial discharge in a surface discharge defect created in MV cable. He analyzed data and structured the paper draft.

III Maninder Choudhary is the main author of this article. He developed an efficient tool that denoises PD data and extracts major PD characteristics from PD pulses. He structured the ideas and prepared the full paper draft.

IV Maninder Choudhary is the first author of this article. He analyzed the behavior of internal discharges in XLPE cable insulation under increasing voltage. He analyzed the data and prepared the draft of the article.

V Maninder Choudhary is the primary author of this article. He analyzed the behavior of surface discharges in XLPE cable insulation under increasing voltage. He analyzed the data and structured the paper draft.

VI Maninder Choudhary is the primary author of this article. He analyzed the behavior of pulse shape characteristics in XLPE cable with a surface discharge defect. He analyzed the data, extracted shape features, and drafted the article.

VII Maninder Choudhary is the first author of this article. He implemented a three-leg approach to estimate the partial discharge inception voltage (PDIV) of Nomex films. He authored a full article draft.

VIII Maninder Choudhary is the first author of this article. He investigated the behavior of Nomex films under the influence of partial discharges. He designed the experiment setup, collected and analyzed data. He also prepared the full draft of the article.

IX Maninder Choudhary is the first author of this article. He developed an integrated approach for classification of PD signal. He also prepared the full draft of the article.

1 Introduction

The resiliency and reliability of the power system assets heavily rely on the condition and durability of assets, particularly their insulation system. Insulation is a primary protection as it isolates conductive parts of equipment, thereby preventing unintended outages. Deterioration of the insulation system may cause a discontinuity of supply. As power system networks evolve, driven by increased loads, the integration of distributed energy generation, renewable energy sources, and dynamic operating conditions, the deterioration of insulation has become a major concern for insulation system designers, asset managers, and power system planners. The Insulation system of power system assets must be able to cope with modern operating conditions.

Insulation deterioration or aging is a complex phenomenon caused by various stresses, thermal, electrical, ambient, and mechanical (TEAM) stresses, and defects that occur during manufacturing and installation. These stresses and defects accelerate the aging rate and cause premature failure of assets. Partial discharge (PD) is one of the prominent factors that contribute to insulation deterioration. PD is a localized breakdown that occurs at the weak points in the insulation system; its long-term progression contributes to insulation aging and breakdown. Consequently, understanding and observing PD behavior is crucial for the efficient design of the insulation system, early detection of faults, and forecasting the useful life of the insulation.

Historically, the aging of insulation has been examined by phenomenological, physical, and thermodynamic models, encompassing thermal, electrical, and thermodynamic aging laws using statistical life models, like the inverse power law and Arrhenius equation. Several combined thermal and electrical models are also available in the literature. Although these models offer significant insight, the applicability of these models is tested on certain materials; also, these models do not incorporate the parameters or quantities that describe the effect of PD on insulation, which is a critical deteriorating phenomenon, and the fact that these models do not account for modern grid-operating conditions.

PD measurement is an important topic that has significantly advanced in recent years. Despite considerable progress in quantifying PD apparent charge (Q_a), the conventional methods are inapplicable to online measurements and for detailed investigations. On the other hand, the interest in non-conventional technologies for detecting and quantifying PD, such as the use of high-frequency current transformers (HFCT), ultrasonic sensors, and ultra-high frequency (UHF) antennas, has grown as PD pulses and corresponding features describe the physics behind the PD activity.

PD measurement relies on efficient sensor technologies and efficient data analytics tools. Numerous sensor technologies are empirically evaluated for their implication, accuracy, and performance. This brings us to the subsequent phase in the development of novel tools. In recent years, hybrid techniques have emerged as potential solutions. These techniques integrate data-driven tools and physics-based concepts behind PD mechanisms to analyze PD data and PD behavior in various insulating materials. These techniques offer high-resolution analysis of PD data using signal processing and machine learning (ML) tools backed by the physics of the PD phenomenon, providing a more precise and detailed understanding of insulation aging behavior. The prominent indicators or quantities with aging models enable the tracking of aging mechanisms and the lifetime prediction of insulation.

Differentiating between different types of PD is a complex challenge. Internal discharge refers to the most common type of discharge that occurs in gaseous spaces, cavities, and cracks in solid insulation. It develops carbonized channels within the insulation. These channels grow with time and intensity of the electric field and spread over the insulation's thickness, leading to a fault or breakdown. Since cross-linked polyethylene (XLPE) has poor resistance to PD, it is preferable to detect these defects at earlier stages before failure. PD can also develop at the points where solid insulation meets air, such as cable terminations. However, it causes surface contamination and is typically not as severely harmful as internal. However, depending on their location and type of equipment, surface discharge can also cause a fault. Therefore, the correct identification of PD source enables utility and asset managers to implement targeted preventive measures, thereby increasing the reliability and life of power system assets.

PD measurement is not as simple as PD data may contain noise and different types of PD sources simultaneously, which may affect insulation differently. This makes result interpretation difficult; in most cases, expert opinion is needed to find potential causes or sources of PD within measured PD data. There is a potential need for tools that reliably interpret the results with reduced or minimal supervision.

The PD phenomenon is highly dependent on the electrical field distribution within the insulation system. Electric field profiles play a crucial role in the prediction of PD behavior, as these profiles show the regions where PD activity is likely to initiate. COMSOL, with its finite element method (FEM) capabilities, allows the design of physical electrode configuration and insulation system, enabling computation of electrical field profiles at insulation surfaces. These profiles are useful for estimating the partial discharge inception voltage (PDIV), a key parameter in insulation design.

The lifetime study of solid insulation is a critical aspect that ensures the lifetime reliability and performance of electrical assets. For this, surface erosion-based accelerated aging methods are useful as a shorter time is needed to conduct tests from PD inception until breakdown. These tests are useful for those assets where surface discharges are a major risk for their insulation system. A well-defined framework includes partial discharge testing, identifying stages of degradation, and the behavior of PD characteristics at each stage. Microscopic investigation gives an edge to this investigation as it validates stages of degradation, thereby highlighting the internal changes in insulation structure at distinct stages of aging.

To address the above aspects, this thesis provides a multi-method approach designed for aging and degradation studies based on PD measurement. It includes state-of-the-art approaches for analyzing PD data that include denoising, pulse detection, feature extraction, optimum feature selection, classification and clustering, and identification of the type of PD source (in case different types of PD sources are present in acquired PD data) using unsupervised methods that require reduced or minimal human intervention. Further, it delves into the behavior of different types of defects within medium voltage XLPE cables and validation of the aging stages of Nomex insulation. The framework also incorporates a COMSOL-based simulation model, which is utilized for the determination of PDIV of Nomex insulation film, facilitating the calculation of electrical field profiles that are used for PDIV estimation. Additionally, this framework provides the methodology for the aging and lifetime study of solid insulation under the influence of surface discharges. This methodology contributes to the design of predictive maintenance strategies and long-term reliability analysis of solid insulation. Collectively, this thesis offers a holistic

methodology for the aging and degradation study of solid insulation used in medium and high voltage equipment.

The aim is to establish a thorough framework for evaluating insulation integrity using PD features, guided by physical principles and data-driven insights, to improve asset durability under modern operating conditions.

1.1 Hypothesis

This thesis hypothesizes that data-driven and FEM modeling approaches can make a significant contribution to the investigation of aging and degradation behavior of solid insulation based on partial discharge measurement. This thesis aims to integrate these approaches with ML tools, and the physical concept of the PD phenomenon can enhance the investigation of PD in electrical assets and play a crucial role in the aging and degradation study of solid insulation. This leads to improved diagnostics and predictive capabilities. The thesis encompasses the following key hypotheses:

- An integrated approach consisting of signal processing, principal component analysis (PCA), hierarchical clustering, and fuzzy logic-based techniques is useful for efficient PD pulse detection, investigating the PD behavior in power cables, and determining the aging or degradation trends in solid insulation.
- The FEM model, combined with the surface discharge model, is useful for the determination of electric field profiles and estimation of partial discharge inception voltage of solid insulation.
- Surface erosion-based accelerated aging tests are effective in evaluating the lifetime performance of solid insulation over a short duration under the influence of surface discharges.

1.2 Contribution and Dissemination

During the doctoral study period, the author contributed 11 publications as a main and co-author. The research findings and results have been disseminated through participation in international conferences, doctoral schools, and peer-reviewed journals. This thesis is based on 8 research articles, including 4 journal articles and 4 conference articles.

1.2.1 Scientific Novelties

- Development of an integrated approach for denoising partial discharge pulse detection, feature extraction, optimum feature selection, classification, and identification of PD data.
- Development of a systematic measurement methodology for investigating partial discharge behavior in solid insulation.
- Implementation of the three-leg approach for estimation of PDIV in Nomex film.
- Determination of the four-stage aging behavior in Nomex film using surface erosion-based accelerated aging test.

1.2.2 Practical Novelties

- Implementation of an integrated tool for comprehensive analysis of partial discharge behavior in medium voltage XLPE cable samples with typical defects and for validation of different aging stages of Nomex film.

- Development of an FEM model for the implementation of the three-leg approach.
- Comparison of various electrode geometries to optimize surface erosion-based accelerated aging test.
- Mapping of aging stages of Nomex film with PRPD patterns, PD characteristics, and microscopic assessment.

1.3 Thesis Outline

The thesis comprises five chapters, each focusing on essential elements of PD-based investigation of solid insulation.

Chapter 2 describes the factors that contribute to aging and degradation of solid insulation and a holistic comparison of aging models developed in the past few decades. This chapter also discusses major aspects of the partial discharge phenomenon, measurement procedure, and its importance.

Chapter 3 focuses on the design of an efficient approach for PD data analysis, from PD data collection to source identification, which includes wavelet denoising and the local maxima method for denoising, detection, and extraction of PD pulse and features from PD data. Additionally, it describes the application of principal component analysis (PCA) for optimum feature selection and ML tools such as hierarchical clustering for clustering and classification of PD data. Finally, the fuzzy logic algorithm has been implemented for the identification of type PD source. The designed approach has been implemented on various data sets obtained during PD measurement on various insulation defects in MV XLPE cable insulation and the lifetime data of Nomex insulation.

Chapter 4 emphasizes the implementation of a three-leg approach used for PDIV estimation of Nomex insulation film. It explains how the COMSOL-based FEM model and surface discharge model are used to determine the PDIV of Nomex film. This chapter also discusses the behavior of electric field profiles at different configurations of electrodes and voltages. It also describes the experimental methodology adopted for validation of the three-leg approach since theoretical PDIV is validated with measured PDIV obtained through PD experiments on Nomex insulation.

Chapter 5 focuses on surface erosion-based accelerated aging of Nomex insulation. It describes the methodology for the PD-based lifetime study of solid insulation. It implements the concept of four-stage degradation, which describes how insulation undergoes various stages of aging or degradation from PD inception until breakdown. This four-stage degradation is observed through PRPD (phase-resolved partial discharge) patterns, PD characteristics, and microscopic investigations.

Lastly, Chapter 6 presents a summary of research findings and implications of research and outlines potential future research directions.

Abbreviations

AC	Alternating current
DSO	Digital storage oscilloscope
DWT	Discrete wavelet transform
FEM	Finite element modeling
FIS	Fuzzy inference system
FFT	Fast Fourier transform
GIS	Gas-insulated switchgear
HFCT	High-frequency current transformer
HV	High voltage
HVDC	High-voltage direct current
IPL	Inverse power law
MI	Measuring instrument
ML	Machine learning
MV	Medium voltage
PCs	Principal components
PCA	Principal component analysis
PD	Partial discharge
PDIV	Partial discharge inception voltage
PEC	Power electronic converters
PRPD	Phase-resolved partial discharge
SISO	Single input and single output
TEAM	Thermal, electrical, ambient, and mechanical
UHF	Ultra-high frequency
XLPE	Cross-linked polyethylene

List of Symbols

a	Pre-exponential constant (scaling factor)
A^*	Critical fraction of converted moieties (damage threshold)
$A_{eq,\,AC}(E)$	Space charge model parameter or equilibrium conversion function
b	Accelerated aging factor
B	Arrhenius model parameter (ratio of activation energy and Boltzmann constant
b	Model scaling factor
b_1, b_2, b_3, b_4	Model constants depend on temperature, frequency, and electrical stress
C	Correlation factor
C'	Material-specific constant
C_a	Capacitance of the void or cavity (pC)
C_b	Capacitance of insulation in series with the void (pC)
C_c	Capacitance of the PD-free bulk of insulation (pC)
d	Exponent in probability model
D_5	Thermodynamic parameter combining entropy and enthalpy effects
E	Electric field strength or applied electrical stress (kV/mm)
E'	E-E_O (kV)/mm)
E'_{to}	Threshold electrical stress corresponding to θ_a (kV/mm)
E_1	Electric field in solid insulation (kV/mm)
E_2	Electric field in a gaseous medium (kV/mm)
E_a	Activation energy (J/mol)
E_b	Breakdown field constant (kV/mm)
E_n	Pulse energy (V^2)
E_o	The gradient below which electrical aging is neglected (kV/mm)
E_s	Surface discharge inception field (kV)/mm)
E_t	Threshold electrical stress (kV)/mm)
E_{tAC}	Activation threshold field constant (kV)/mm)
E_{thAC}	Threshold AC electrical stress (kV)/mm)
f	Frequency (Hz)
$f(s)$	Stress-dependent function (electrical or mechanical)
$F(t, Qi,E)$	Failure probability function
$F(T_f)$	Failure probability at specified stress or time
f_1	Frequency level 1 (Hz)
f_2	Frequency level 2 (Hz)
f_d	Dominant frequency (Hz)
F^{PCs}	Feature matrix transformed after PCA
F^{PCs}_i	Feature score vector for the i^{th} observation after PCA transformation
$F^{PCs}_{i,\,J}$	Feature score of the i^{th} observation on the j^{th} principal component

h	Height of cavity or vertical distance from triple point (mm)
h	Planck's constant (6.62×10^{-34} J)
h_c	Vertical distance between two electrodes (mm)
h_e	Exponential model parameter (reciprocal of electrical life slope)
i_i	Index or position of the detected odd peak
j	Imaginary unit
k_5	Rate constant in the failure model
K_B	Boltzmann constant (1.38×10^{-23} J/K)
k_e	Model constant
k_t	Reaction rate constant
k_t, k_s, k_z	Model scaling factors
l	Creepage distance or horizontal distance from the triple point (mm)
L_0	Life under normal conditions or reference life
l_1 and l_2	points where $E_{max} = E_{ps}$ (mm)
$L_1, L_2, \ldots L_n$	Life under individual stresses $S_1, S_2, \ldots S_n$
L_{AC}	Lifetime under AC voltage
L_E	Life under electrical stress
L_{f1}, U_1	Lifetime at frequency of_1 and voltage U_1
L_{f2}, $U2$	Lifetime at frequency of_2 and voltage U_2
L_m	Life under multistress conditions
L_o	Life at room temperature without electrical stress for no threshold materials
L_{PD}	Length of the PD data
L_T	Insulation life under thermal stress
n	Field or stress exponent
N	Number of samples
n_{ap}	Number of detected odd peaks
N_b	Number of breakable bonds
N_d	Number of discrete Fourier transform points
n_e	Voltage endurance exponent
N_f	Total number of features
P	Pressure (101.325 kPa)
$p(f)$	Energy spectral density
P_d	Pulse width (number of samples)
P_e	End position of a pulse
P_{loc}	Sample location of pulse
$P_{loc}(i)$	Location (index or time position) of the i^{th} detected peak
P_{odd}	Magnitude of detected PD peaks
P_s	Start position of a pulse
Q_i	Initial charge or energy input (pC)

R	Rate of reaction
r	Universal gas constant (8.314 J/mol K)
S_k	Skewness
T	Absolute temperature or thermal stress (K)
T	Temperature (K)
t	Time or aging time
t_0	Insulation life or reference lifetime when $E = E_t$
t_{AC}	Time of one AC cycle (ms)
T_B	Characteristic breakdown temperature (K)
t_f	Fall time (ns)
t_f	Time to failure
t_{int}	Interval between two samples
t_{loc}	Time of occurrence of PD pulse (s)
t_o	Reference time (s)
t_r	Rise time (ns)
T_{to}	The highest threshold temperature corresponds to E_o (s)
t_{wo}	Pulse width (ns)
$U_b(E)$	Energy for breaking bonds (J/mol)
U^i_m	Measured PDIV (kV)
U^i_{th}	Theoretical PDIV (kV)
$U_r(E)$	Energy for forming bonds (J/mol)
V_m	Peak pulse amplitude (mV)
V_s	Applied voltage (kV)
$X(k)$	Discrete FFT at index k
x_i	Feature vector for the i^{th} observation
x_j	Feature vector for J^{th} observation
α	Weibull scale parameter
β	Weibull shape parameter
γ	Temperature exponent
$\Delta G_{K,\,AC}$	Gibbs free energy change under AC condition (J/mol)
ΔH	Activation enthalpy (J/mol)
ΔS	Entropy of reaction(J/mol/K)
η	Number of broken bonds
η_c	Critical number of broken bonds remaining
μ	Mean
σ^2	Variance
ε_{r2}	Relative permittivity of XLPE (F/m)

2 Insulation Aging Mechanism, Review of Aging Models, and Various Aspects of Partial Discharge Phenomenon

This chapter discusses insulation aging mechanisms, a brief review of different aging models proposed in the past few decades and highlights the role of PD measurement in insulation aging and lifetime studies.

2.1 Insulation Aging Mechanism

The operational lifespan of power system assets is contingent on the reliability of their insulation system. Insulation aging or deterioration is a prominent cause of failure, particularly in medium and high-voltage assets. According to general failure statistics of power system assets, 40–60% of the faults in the power system assets are caused by insulation failure. Figure 1 shows the failure statistics of different power system assets and the contribution of insulation-related faults in the failure of power system assets [1–4]. These unforeseen failures result in considerable economic and operational risks on both the utility and customer side. Therefore, a greater insight into the insulation aging mechanism and its progression can enable the prediction of faults in critical network assets, thereby reducing the disruption in industrial, economic, and commercial processes.

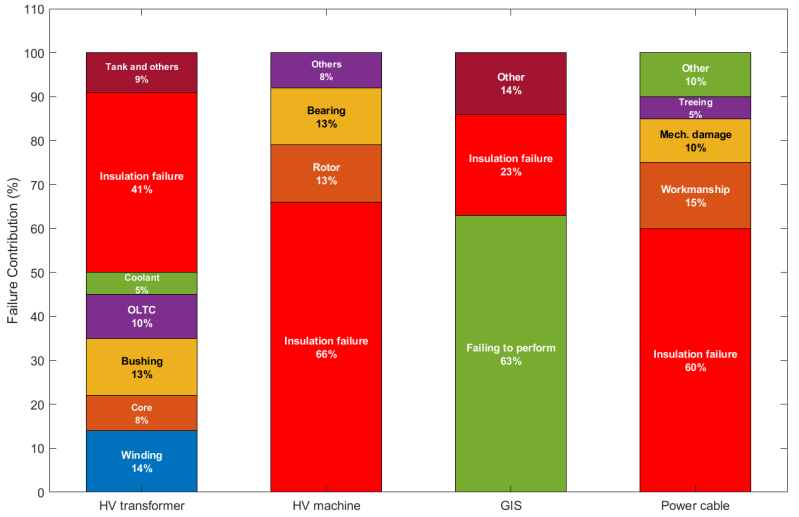

Figure 1. General statistics of insulation-related failure in power system assets and causes.

The aging mechanism in insulation is categorized into distinct processes, i.e., intrinsic and extrinsic. Intrinsic aging is a natural process that causes irreversible changes in the dielectric properties of insulation. It is an intuitive process that results in physiochemical changes in insulation, impacting a significant portion of the insulation. The chemical kinetic process causes the breaking of chemical bonds. These bonds are continually disrupted and reorganized by the electric field that generates moieties. These moieties accumulate over time and change the microscopic and eventually macroscopic properties of insulation, resulting in the fast deterioration of insulation. Intrinsic aging causes gradual deterioration over a long time. Extrinsic aging occurs due to cavities, protrusions, defects, and voids arising from inadequate production, transportation, installation, and

operation [5–7]. Under field operating conditions, electrical stress is not only the primary factor that causes degradation. Instead, it is influenced by the combination of stresses. These stresses are the result of increasing temperature, tensile compression or bending, moisture, or voids present in the insulation. The intensity of these stresses triggers irreversible phenomena, including oxidation, space charge, partial discharges, and electrical treeing. Consequently, these aging mechanisms lead to a deterioration of material characteristics, resulting in a localized reduction of dielectric strength that progressively extends throughout the insulation between conductive components. This results in an electrical breakdown of the insulation, leading to component failure [8–10]. Figure 2 illustrates the progression of insulation degradation from aging causes to consequences.

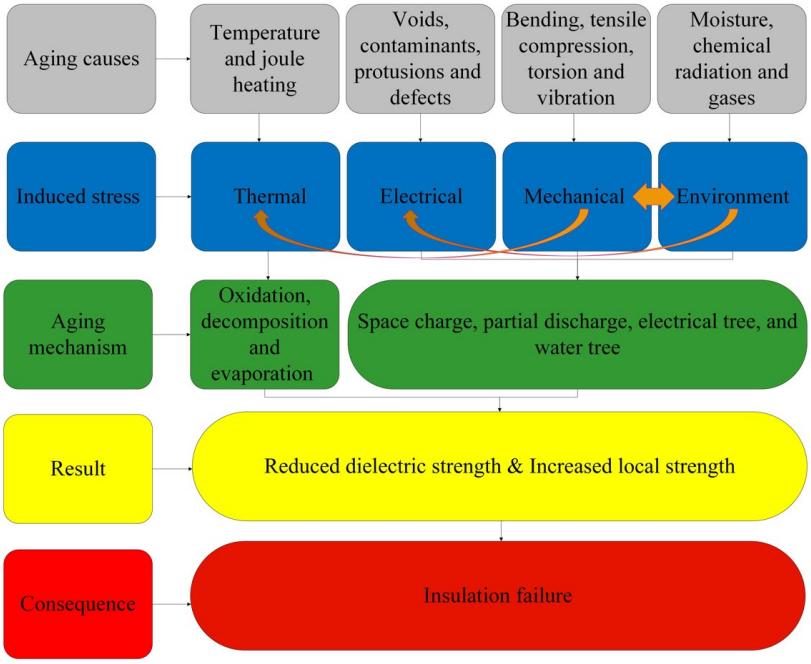

Figure 2. Insulation degradation and aging from causes to consequences [Paper I].

Underground cables are an essential part of the power system, and solid insulation is a major part of their design. Figure 3 illustrates common defects found in the cables. Mostly, the defects are in the primary insulation layer, which separates the conductor from the shielding or surrounding environment or shielding layer. These defects reduce the dielectric strength of insulation, causing PD or failure eventually. Water treeing is also a major risk in power cables, especially in moist environments, where the water infiltration creates favorable conditions for the initiation and growth of water trees. These trees are microstructures within cross-linked polyethylene (XLPE) insulation, which reduces dielectric strength and may consequently accelerate aging. Water trees can evolve into electrical trees under prolonged electrical stress, particularly in the presence of cavities and voids in the insulation. These trees develop due to continuous PD activity, leading to the progressive local degradation of insulation. Both water trees and electrical trees typically propagate in the direction of the local electric field, as electric field strength influences the growth and path of these microstructures [11–13].

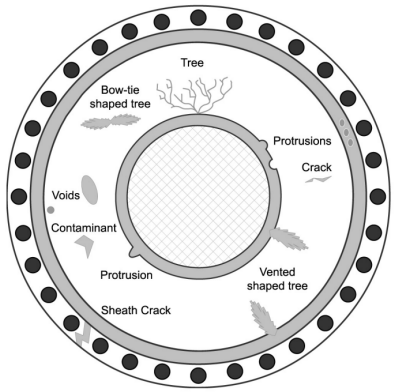

Figure 3. Typical defects found in power cables [13].

2.2 Aging Models

Over the years, aging models have made significant progress from the Montsinger thermal aging model, the Dakin physical model [6], to the Simoni multistress life models [14–16] and Dissado space charge model [17]. These models are utilized for the lifetime prediction of insulation under single and multistress conditions. Usually, multiple stresses are not cumulative; they are coactive and may exert direct, indirect, or sequential impact on insulation [18]. While accelerated aging tests effectively assess insulation state, life prediction at a specific service point necessitates statistical methods and life models. The subsequent part examines aging models based on thermal and electrical stresses. Considering the impact of different stresses on insulation, both single-stress and multistress models are examined [19]. Multistress models are further categorized as phenomenological, physical, and thermodynamic models, as shown in Figure 4.

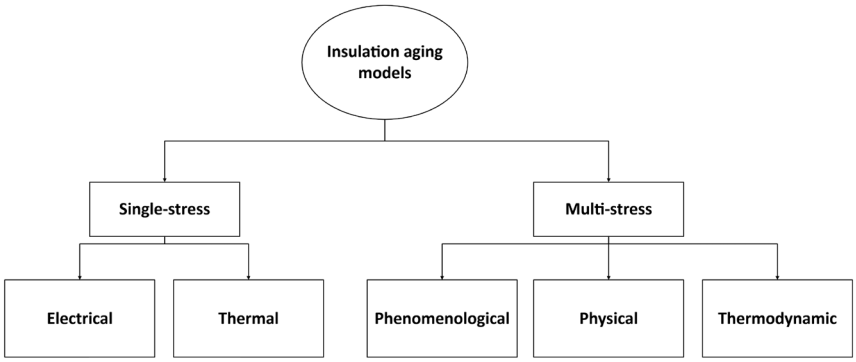

Figure 4. Classification of insulation aging models [Paper I]

2.2.1 Single Stress Models

Aging models in which a single stress, i.e., thermal or electrical stress, is considered as a major factor that contributes to aging. These models describe the lifetime of insulation or the time of failure under a single stress.

2.2.1.1 Electrical Aging Models

Electrical aging occurs due to the presence of free electrons and other charge carriers. At low concentrations, free electrons regularly collide with the lattice of dielectric materials, ionizing molecules of insulating substances by energy transfer. At increasing electrical stress, this collision releases additional free electrons, which collectively generate an avalanche effect that causes current flow within the insulation [20]. The additional current produces heating in the insulating materials, hence accelerating aging. The inverse power law (IPL) defines the relationship between electrical stress and the lifetime of insulation using (1)

$$t_f = aE^{-b} \ (a > 0) \tag{1}$$

Where: t_f – lifetime of insulation or time to failure.
E – applied electrical stress;
a – pre-exponential constant (scaling factor);
b – voltage endurance coefficient.

The parameter b is defined as the slope of the life graph correlating applied electrical stress with lifespan. Life prediction by IPL is based on the experimental results of accelerated aging tests, as it correlates electrical stress with time to failure [21]. It is described that insulation lifetime data can be accurately characterized by a two-parameter Weibull distribution [22]. The cumulative distribution function for the Weibull distribution is (2),

$$F(t_f) = 1 - e^{-\left(\frac{t_f}{\alpha}\right)^{-\beta}} \tag{2}$$

Where: $F(t_f)$ – failure probability at specified stress or time;
α – scale parameter ($\alpha > 0$);
β – shape parameter ($\beta > 0$).

Parameter α denotes the voltage or time at which $F(t_f)$ reaches 63.2%, whereas β represents the dispersion of data, such as variance in a normal distribution. Experimental observations showed that at lower levels of electrical stress, the insulation life graph approaches the electrical threshold E_t. The exponential model accurately characterizes this behavior (3)

$$t_f = t_0 \, e^{-b(E-E_t)} \tag{3}$$

Where: t_0 – insulation life or reference lifetime when $E = E_t$;
E_t – electrical threshold stress.

The model determines the voltage endurance of the insulation using a threshold value [23]. It is found that the lifetime curve tends to be flat below a certain threshold value called the threshold effect. Based on this observation, the inverse power model can be modified as (4). Model (5) incorporates both IPL and exponential models with threshold [14], [24].

$$t_f = t_0 \left(\frac{E}{E_t}\right)^{-b} \tag{4}$$

$$t_f = t_0 \left(\frac{k_e}{E - E_t}\right) e^{b(E-E_t)} \tag{5}$$

Where: k_e – scaling constant.

2.2.1.2 Thermal Aging Models

Thermal stress is one of the major causes that contribute to the aging of insulation. It induces irreversible reactions that result in increased dissipation factor or conductance. Dakin et al. [6] identified three phenomena that contribute to the thermal aging of insulation:

- Change in the dissipation factor and conductance as a result of oxidation.
- Brittleness of insulation due to the reduction in plasticizer effect.
- Depolarization of insulation at high temperatures.

Montsinger described that aging is directly proportional to temperature and lifetime. According to Montsinger, a temperature increase of 8…10 °C reduces the asset life by half. Arrhenius described the relationship between temperature and chemical reactions that occur due to thermal stress. It is defined as the rate of a chemical reaction that is directly proportional to temperature (6) [25–26].

$$R = k_t \, e^{-\frac{E_a}{rT}} \tag{6}$$

Where: R – rate of reaction;
k_t – reaction rate constant;
T – absolute temperature;
E_a – activation energy;
r – Universal gas constant (8.314 J/mol K).

The E_a can be found from the slope of the line representing the relationship between the rate of reaction and the inverse of temperature. A revised form of (6) is proposed as (7) since (6) describes kinematics (reaction rates) exclusively in gaseous states. However, (7) can describe heterogeneous reactions, i.e., two more states of matter (liquids, gases, and solids) contribute as reactants, described as,

$$R = \frac{K_B T}{h} \, e^{\left(\frac{\Delta S}{r} - \frac{\Delta H}{rT}\right)} \tag{7}$$

Where: K_B – Boltzmann constant (1.38×10^{-23} J/k);
h – Planck's constant (6.62×10^{-34} Js);
ΔH – activation enthalpy;
ΔS – entropy of reaction.

Insulation life under thermal stress can be defined as (8)

$$L_T = k_t e^{-\frac{E_a}{rT}} \tag{8}$$

The linearity of the thermal life graph relies on the consistency of the reaction rate across all temperature ranges and on the condition that the material experiences only thermal stress. Various lifetime tests conducted under combined electrical and thermal stress show that the thermal life graph lines exhibited curved patterns under high electrical stress [27–28]. This curved behavior describes the concept of thermal threshold. Eyring modified the thermal life model by adding the concept of threshold using an exponential function (9)

$$L_T = K_1 T^{\gamma} e^{\left(K_2 + \frac{K_3}{T f(s)} - \frac{T_B}{T}\right)} \tag{9}$$

Where: $f(s)$ – stress-dependent function (electrical or mechanical);
K_1, K_2, K_3 – empirical constants related to activation processes;
γ – temperature exponent;
T_B – characteristic breakdown temperature;
k_t – scaling factor.

2.2.2 Multistress Models

During operation, electrical assets undergo multiple stresses simultaneously. Understanding aging behavior under the impact of multiple stresses gives a comprehensive understanding of the aging behavior of insulation. For example, if thermal stress is a primary cause of aging, its interaction with electrical stress results in a temperature rise and may cause a tracking phenomenon. On the other hand, if electrical stress is the primary cause, then thermal stress may change the inception voltage or intensity of partial discharges. Therefore, multistress models are highly effective as they consider the synergetic effect of stresses in the lifetime study of insulation [24], [27]. The generalized multistress model can be represented using (10)

$$\frac{L_M}{L_0} = \frac{L_1}{L_0}\frac{L_2}{L_0} \dots \frac{L_n}{L_0}\, C(S_1 S_2, \dots S_N) \tag{10}$$

Where: L_m – life under multistress conditions;
L_0 – life under normal conditions or reference life;
$L_1, L_2, \dots L_n$ – Life under individual stresses $S_1, S_2, \dots S_n$;
C – Correlation factor.

2.2.2.1 Phenomenological Models

Phenomenological models are based on the aging phenomenon. These are empirical models based on parameters without necessarily modeling the physical details of the material. However, their parameters rely on theories or principles of the aging phenomenon. These models are designed using lifetime data obtained by accelerated aging tests on insulating materials. The following are the major characteristics of phenomenological models [29].

- Illustrate the relationship between applied stresses and insulation life based on the experimental investigation.
- Insulating materials can be characterized based on experimental evidence rather than physical properties.
- Using extrapolation or regression methods, the life of insulation can be predicted at any stage.

2.2.2.2 Physical Models

Physical models are based on parameters described by physical and chemical mechanisms that cause deterioration of insulation over time. Unlike phenomenological models, which rely on empirical data for lifetime prediction, the parameters in physical models have physical meaning, representing material properties and aging mechanisms [29]. Major advantages of these models include:

- These models help to understand the dominant aging mechanism, e.g., oxidation, PD erosion, or electrochemical breakdown.
- They are useful considering the design and selection of insulation based on physical parameters (since parameters are linked to material properties).
- These models can be generalized based on physical mechanisms (e.g., voltage levels, materials, or temperatures).

2.2.2.3 Thermodynamic Models

These models describe aging as a result of thermodynamic reactions, i.e., energy transformations, chemical and physical changes. These changes occur due to heat, temperature, pressure, and electric field. High activation energy causes bond breaking,

polymer chain scission, and other chemical processes that deteriorate insulation [30]. Major advantages of these models include:

- These models are useful in understanding insulation aging behavior at the molecular level.
- Also, these models play a vital role in insulation system design, as model parameters relate to the physical and chemical properties of insulating material.

A detailed review of aging models is performed in [10]. Table I gives a brief overview of various multistress models proposed over the years. The following are some observations that limit the general viability of the proposed models.

- Most models are material-oriented, as their validity is assessed based on specific materials. Table I indicates that most of the models are evaluated on XLPE and ethylene-propylene rubber (EPR) cables. However, insulation properties and aging behavior vary with material type and operating conditions. For example, the lifespan of cables with identical insulation varies across different networks. Insulation aging behavior depends upon the environment and operational conditions. As operational conditions change, the degradation rate is altered, thereby affecting the time to failure. This limits the general viability of models.
- Experimental studies [16] demonstrate significant variability in the life graphs of different insulating materials subjected to single or combined stresses. The uncertainty in the results does not show a visible trend that insulation follows during aging. Also, it is difficult to accurately integrate data into a single model.
- Insulation life model equations incorporate multiple parameters, as shown in Table I. Their parameters are determined using several statistical techniques, including maximum likelihood and linear regression methods. Parameters in the models are like variables in an equation. Therefore, managing the number of variables in the experimental investigation of combined thermal and electrical stress is a complex task.
- Considering modern grid operating conditions, such as power electronics converters (PEC), being integrated into the modern grid, reveals that existing models do not account for their impact. A model proposed in [31] examines the influence of PEC and articulates the overall aging or degradation rate as the summation of electrical stress (peak-to-peak voltage values) at a nominal frequency (50 Hz) and the impulse frequency. However, there is no constructive relation between stresses, specifically voltage and impulse frequency. Also, the model does not account for the impact of thermal stress since the model parameters only incorporate the influences of electrical stress and frequency.
- Considering PD as a deteriorating phenomenon, a model was proposed in [32] that predicts insulation life based on electrical tree length. Since the initiation of an electrical tree represents severe deterioration, it is essential to assess the lifetime of insulation before the occurrence of trees.

Table I. Summary of major multistress (thermal and electrical) stress aging models [Paper I].

Model Equation	Type	Parameters	Ref.
$L_m = L_0 \frac{e^{(-h_e E' - BT + bE'T)}}{\left(\frac{E'}{E'_{to}} + \frac{T}{T_{to}} - \frac{(bTt_o E'T)}{(h_e E'_{to} T_{to})} - 1\right)^{\beta}}$	Phenomenological	6 (t_s, E_s, E_T, μ, β, B, h_e)	[16]
$L_{f_2,U_2} = L_{f_1,U_1}\left(\frac{U_1}{U_2}\right)^{n_e}\left(\frac{f_1}{f_2}\right)$	Phenomenological	1 (n_e)	[31]
$L_{AC} = \frac{h}{2K_B T}\frac{e^{D_5}\ln\left(\frac{A_{eq,AC(E)}}{A_{eq,AC(E)-A^*}}\right)}{\cosh\left(\frac{\Delta_{GK,AC-C'E^{4b}}}{2T}\right)}$	Thermodynamic	6 (D_5 , C', b, A^*, $\Delta_{GK,ac}$, $A_{eq,ac}$	[32]
$t = \int_{N_b}^{\eta_c}\left[\frac{K_B T}{h}\left\{e^{\left(\frac{-U_r(E)}{k_B T}\right).(N_b-\eta)} - e^{\left(\frac{-U_b(E)}{K_B T}\right).(\eta)}\right\}\right]^{-1} d\eta$	Thermodynamic	5 (t, η_c , N_b, Ur(E), $U_b(E)$)	[33]
$t_b = \frac{1}{f b_1[e^{b_2(E-E_{thAC})} - 1]\, e^{b_3(E_b)} + b_4}$	Physical	4 (b_1, b_2, b_3, b_4)	[34]
$F(t, Q_i, E) = 1 - e^{\left[-\left(\frac{tk_5(E-E_T)^n}{ln[(\frac{Q_i}{k_2})+1]^d}\right)\right]^{\beta}}$	Physical	6(k_5, E_t, n, k_2, d, β)	[35]

2.3 Role of Partial Discharge Measurement

Partial discharge measurement is widely used for fault detection, determination of insulation integrity, and diagnostics of medium and high-voltage assets. According to IEC 60270, it is a localized breakdown that partially bridges the insulation between conductors [36]. PD can occur near the sharp edges, called corona discharge, or at the insulation surface, called surface discharge, or within cavities embedded in the insulation, called internal PD. It occurs in regions of high electrical stress and reduced dielectric strength, such as voids or cavities, contaminations on insulation surfaces, or insulation defects [37].

The electric field distribution within insulation that contains embedded cavities can be used to describe the PD phenomenon. Consider a cavity within a solid insulation as shown in Figure 5, where ε_{r1} represents the relative dielectric permittivity of the material and ε_{r2} represents dielectric permittivity of the cavity. The permittivity of both media affects the electric field along the polar axis of the cavity. It is assumed that ε_{r1} = 2.3 for solid insulation (XLPE), while $\varepsilon_{r2} \approx 1$ for gaseous void, because of the cavity being filled with gas. In this scenario, the electric field strength ratio within the insulation E_1 and the cavity E_2 is determined using (11)

$$\frac{E_1}{E_2} = \frac{\varepsilon_{r2}}{\varepsilon_{r1}} \tag{11}$$

The value of E_2 in the cavity will be (12)

$$E_2 = E_1 \frac{\varepsilon_{r1}}{\varepsilon_{r2}} \tag{12}$$

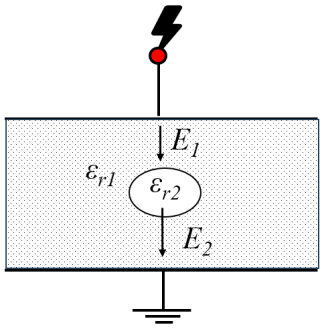

Figure 5. Behavior of the electric field in a gas-filled cavity and the bulk of insulation [38].

This shows that the enhancement of E_2 within the cavity is due to characteristics of the adjacent insulation. If E_2 is sufficiently high, a discharge will occur within the cavity. The magnitude of E_2 that causes discharges is affected by the geometry, size, and location of the cavity. Initiation of PD needs a high electric field and the presence of a free electron to initiate the electron avalanche. This avalanche results in the breakdown of the gas within the cavity. Initially, this electron is unavailable; however, when the electric field increases above the PD inception field, it creates favorable conditions for ionization of gas molecules within the cavity. However, the ionization may not occur instantaneously [37].

The primary concern about PD activity is the deleterious impact that PDs may have on insulation over an extended period. PD causes degradation of insulation, as persistent PD activity often generates conditions that are conducive to the occurrence of additional PD events. Solid and liquid insulation systems may undergo deterioration because of continuous PD activity. Polymers commonly used in power cables are more susceptible to PD. However, materials such as mica used in rotating machine insulation can withstand mild to moderate PD without experiencing permanent damage. The impact of free electron bombardment on the insulation surface exposed to the discharges is associated with the degradation mechanism of insulation affected by PD. The material can be degraded because of chemical and physical changes and breaking of C-C and C-H covalent bonds by high-energy electrons [39–40].

2.4 Types of Partial Discharge

There are three major types of PD found in the electrical assets, namely corona, surface, and internal discharge, as shown in Figure 6 (a, b, c). Electrical treeing behavior is also considered a separate class of discharge. These trees are the result of long-term internal PD activity. There are various subclasses of discharge depending on the equipment, location, and nature of the defect [37].

2.4.1 Corona Discharges

These discharges occur at the interfaces of a conductor and surrounding gaseous insulation. Corona is observed at places where a non-uniform electric field is present, such as pointed edges and cable terminations. Typically, the corona has a minimal impact on insulation since the material is not directly exposed to energized particles associated with discharges. It might indirectly affect insulation through the corrosive influence of

emitted gases (e.g., O_3 and NO_x) and ultraviolet light; however, in practical terms, the significance of these impacts is minimal, except in certain specific situations. PD in the gaseous medium can demonstrate different behavior depending on the gas type, pressure, electrical polarity, and electric field characteristics, among other factors [39–40]. Considering the PRPD pattern, corona discharge pulses are likely to appear in the negative half cycle of the applied voltage, as shown in Figure 7 (b). However, at high voltage levels, these pulses can appear in the positive half cycle of the applied voltage.

2.4.2 Surface Discharge

Surface discharge takes place at the boundary between a solid or liquid insulation and air or insulating gas or along the insulation surfaces. Surface discharge is particularly prevalent in components that exhibit abrupt changes in insulation system geometry, such as cable terminations and transformer bushings. A sufficiently strong tangential component of an electric field across the insulation's surface induces surface discharge. This may happen when conductive materials or particles are present on the insulating surface, or when the component has incurred damage in regions subjected to elevated electric field stress. The interaction of impurities and moisture on the insulating surface can potentially initiate discharges. Surface discharges become problematic over an extended duration of continuous operation due to the degradation of the insulating material's surface. Few materials have greater susceptibility to tracking, specifically the development of conductive pathways on the dielectric surface. Tracking leads to the continuous deterioration of the insulation [41–42]. Considering the PRPD pattern, surface discharge activity is asymmetrical between positive and negative half cycles of the applied voltage, as shown in Figure 7 (c).

2.4.3 Internal Discharges

These discharges take place in cavities or voids. Their behavior is influenced by the external electric field and the space charges that have accumulated on the void boundaries due to previous PD activity. Continuous PD activity increases the conductivity of the walls of the PD-inducing defect, which changes the chemical and physical properties of the insulation. [42]. In comparison to the minimum voltage required to initiate a discharge, the extent of overvoltage across the cavity influences the shape of the PD pulse. A Townsend-like discharge is induced by a small overvoltage, which is characterized by low amplitude and a wide pulse. Conversely, a streamer-like discharge is produced by a high overvoltage, which is characterized by a high amplitude and a narrow pulse. The discharge activity is influenced by crystals of hydrated oxalic acid ($[COOH]_2 \cdot 2H_2O$) at higher stages of PD-related deterioration. These crystals form within the cavity, alongside other organic molecules that contain carboxyl groups. Because PD accumulates at the tips of these crystals, the pulse form is characterized by low amplitude and intermediate width [42–43]. Considering the PRPD pattern, internal discharge activity is symmetrical between the positive and negative half cycles of the applied voltage, as shown in Figure 7(d).

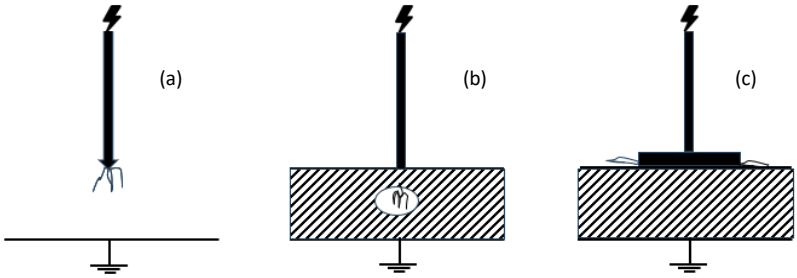

Figure 6. Three major PD types found in electrical assets are a) Corona, b) Internal, and c) Surface.

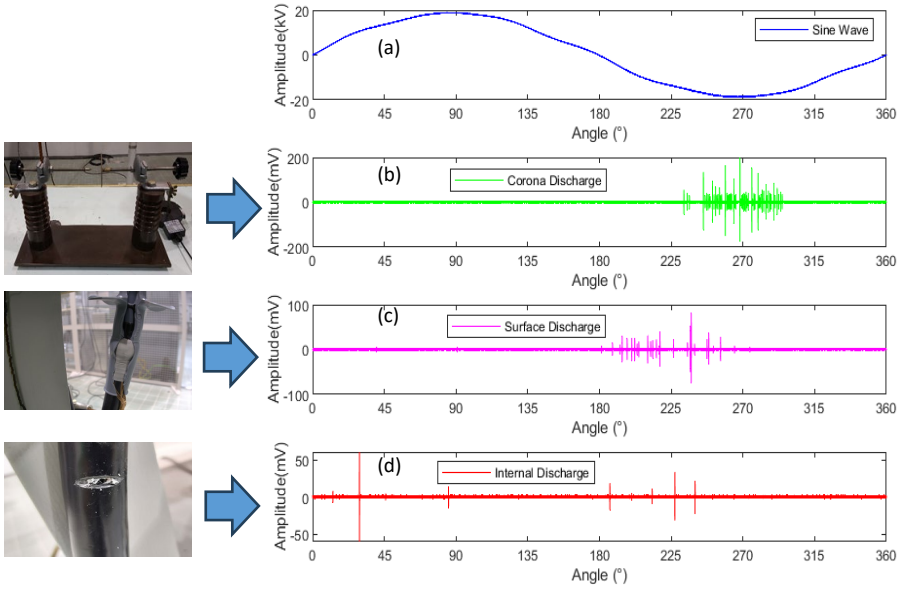

Figure 7. PRPD patterns of major types of PD sources found in power cables: a) Sine wave, b) Corona, c) Surface, d) Internal PD [Paper III].

2.5 Measurement of Partial Discharges

The PD phenomenon can be modelled using two models, i.e., the capacitive model (abc model) or the dipole model. The simple approach to describe the PD phenomenon is abc model, introduced by Whitehead and Kruger in 1950. Figure 8 shows the schematic of the abc model. It is extensively used to link the measured external charge from the measurement system, also called the apparent charge, and the charge available at the cavity site. The capacitance C_a represents the capacitance of the void or cavity, C_b represents the capacitance of insulation in series with the void, and C_c represents the capacitance of the PD-free bulk of insulation. When the voltage across *a* and *b* is raised, it is divided into two paths: a series path. $C_{ab} = C_a C_b / C_a + C_b$ and parallel path C_c. As the voltage reaches the critical value, $V_{c,}$ the voltage may exceed the breakdown voltage of the gas within the void; at that time, a discharge may occur within the cavity or void through the capacitor $C_{a,}$ generating a sharp current or voltage pulse. As it does not cause a full breakdown, it is called partial discharge.

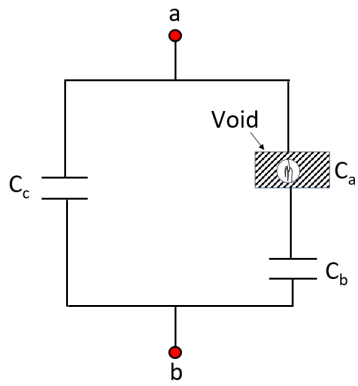

Figure 8. abc model for PD phenomenon.

The PD measurement can be conducted using a variety of methodologies and instruments. The detection and quantification of discharge current and voltage pulses is an essential component of the PD measurement. PD pulse amplitude is measured in millivolt or milliampere, while the apparent charge is measured in picocoulomb (pC) or nanocoulomb (nC) range. IEC 60270 defines the standard procedure for PD measurement [36]. However, this procedure has a few limitations, as it is suitable for offline PD measurements. It requires proper calibration and galvanic connection of the measuring circuit and HV terminals of the test specimen, the need for calibration of the circuit by injecting a charge of known magnitude using a PD calibrator, and the fact that IEC 60270-compliant instruments are expensive.

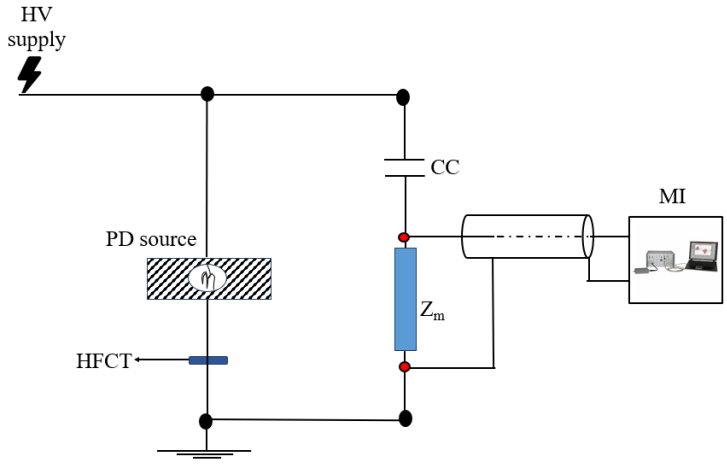

Figure 9. Primary circuit configuration for PD measurement, IEC 60270-based setup with an additional HFCT sensor connected to the ground of the test specimen. HFCT-High frequency current transformer, CC – Coupling capacitor, Z_m – Measuring impedance, MI – Measuring instrument.

PD signals can be measured by connecting capacitive or inductive sensors, or both can be used simultaneously to capture discharges [44–45]. Some detectors can be integrated during the installation of cable accessories such as joints [46–48]. Figure 9 depicts the PD measurement setup, using CC and the HFCT sensors. In addition to the above sensors, the optical and acoustic sensors can also be used for the PD detection [49].

One key distinction between the IEC 60270 measurement technique and non-conventional methods is the quantification of PD. Accurate apparent charge magnitude is a core objective of measurement systems based on IEC 60270. Considering HFCT as one of the non-conventional methods, it is well-suited for several reasons.

- It enables the processing of data using various digital signal processing techniques. PD data collected through HFCT sensors can be analyzed using both frequency and time domains.
- PD signals are more distinguishable from low-frequency noise and interference as HFCT operates in a high-frequency range (typically > 100 kHz).
- It requires no calibration, as conventional PD measurement systems do.
- It enables online PD measurement without shutting down the system.
- It is cost-effective and scalable, i.e., various HFCT sensors can be implemented at separate locations to measure and locate PD.

However, the charge associated with the discharge procedure is complex to measure. The PD pulse shape can be accurately reproduced by sensors with a wide bandwidth. This pulse can be numerically integrated to determine the apparent charge (Q_a) proportional to the transferred charge. However, a proportionality coefficient is required that accurately converts the sensor response into Q_a, as measured in pC [50].

3 An Integrated Approach for PD Data Analysis, Denoising, Pulse Detection, Multiple Feature Extraction, Classification, Clustering, and Identification of the Type of PD

Phase-resolved partial discharge (PRPD) patterns and IEC 60270 features have been used to describe the unique behavior of PD activity under alternating current supply over the past two decades [51–55]. Energy shift, characterized by the proliferation of renewable energy sources, electrified transportation, and high voltage direct current (HVDC) systems, has altered the methodologies for PD monitoring and analysis [52–56]. This transition led to the adoption of high-frequency sensors, including HFCT for cables and gas-insulated substations (GIS), UHF sensors for transformers and GIS, and acoustic and optical sensors for PD measurement [49]. Among these sensors, HFCT is widely used for the detection of high-frequency pulses generated during PD activity in cables, terminations, and converter stations. PD pulse contains useful information that can describe the physics of PD activity in the insulation [57]. Extraction and analysis of PD pulse features can enable engineers to identify and locate insulation-related faults in power system assets at an early stage. From a research and design perspective, these pulse features are important for analyzing the behavior of various defects and lifetime assessment [58–61].

PD measurement through the HFCT sensor is usually accompanied by external noise and a large volume of data, and it may account for different types of PD (internal, surface, corona) within one PD data set [62, 63]. To address the noise issue and transform acquired data into useful information, there is an efficient need for sophisticated tools that can denoise PD data, detect actual PD pulses, extract and optimize major PD features, classify, and identify if multiple sources are present in the data set. Literature shows that the data-driven tools for analyzing PD data are scarce, primarily due to challenges in achieving universal applicability across various power system assets. These tools consider pulse height and phase distribution features to be key criteria for separation of types of PD sources [64–65]. Moreover, the existing methods are designed for specific assets, e.g., rotating machines. In contrast, the proposed method provides an integrated approach that denoises data, detects the first occurring PD pulse while removing oscillation introduced by the measuring circuit. In the subsequent stage, it extracts multi-dimensional features from each pulse to increase the likelihood of accurately distinguishing between types of PD sources existing in the acquired PD data.

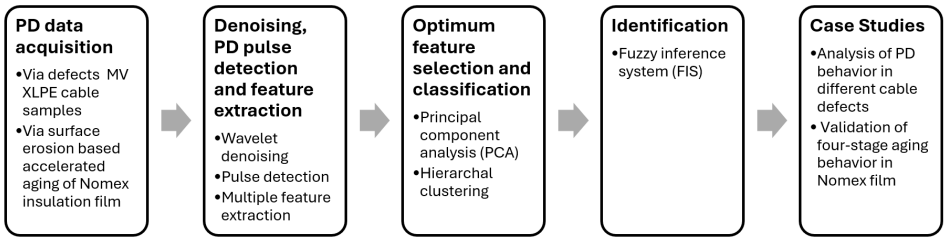

Figure 10. Data-driven approach for denoising, pulse detection, multiple feature extraction, classification, clustering, and identification of PD data.

In the next stage, the developed approach utilizes PCA and Hierarchical clustering for the selection of optimum features and clusters from the acquired PD data. In the final stage, it utilizes a fuzzy logic approach for the identification of clusters based on the Weibull shape parameter (β) criteria. The developed tool is implemented on various data sets obtained from artificially created defects in two MV XLPE cable samples and by performing surface-erosion-based accelerated aging of Nomex film. Figure 10 depicts a step-by-step process adopted for the implementation of this approach.

3.1 PD Data Acquisition

Data-driven tools operate on data collected through detailed experiments. In this thesis, the data is collected through two methods.

- By modeling two physical defects (internal and surface) in MV XLPE cable samples.
- By performing a surface erosion-based lifetime accelerated aging test on Nomex insulation film.

Figure 11 shows the schematic of the PD experiment setup for both methods. Usually, the PD experiment setup includes a high voltage source, a CC or HFCT sensor, measuring impedance (Z_m), a test object, a commercial PD measurement instrument for measurement through a CC, and a digital storage oscilloscope (DSO) for measuring PD pulses from HFCT. The details of the laboratory-based experiment setup and modeled defects will be described in the case study section.

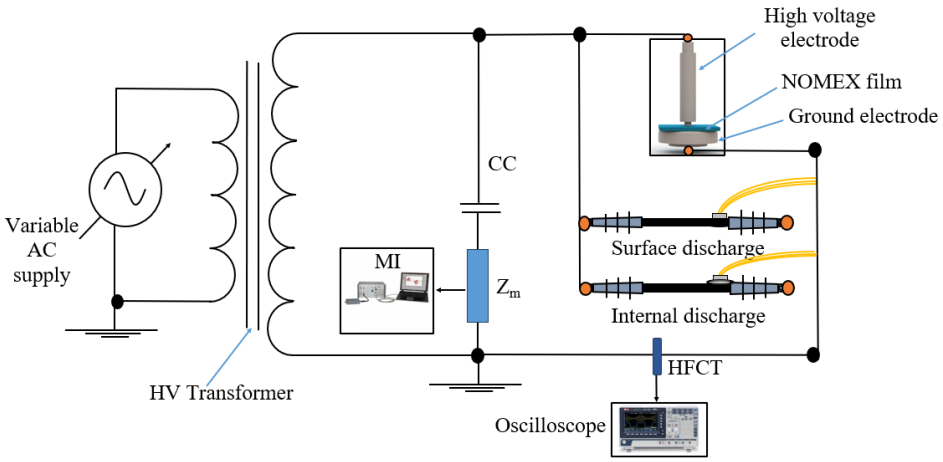

Figure 11. Schematic of the experiment setup designed in the laboratory for PD measurement.

3.2 Denoising, Pulse Detection, and Feature Extraction

This section discusses the operation of an algorithm designed for noise removal, PD pulse detection, and feature extraction.

3.2.1 Denoising and Pulse Detection

Partial discharge signals are accompanied by several types of noise, including electromagnetic interference from communication equipment and noise from the environment. Elimination of noise is crucial for effective PD data analysis and feature extraction. Literature indicates that wavelet denoising is an effective technique for

denoising PD data, as wavelets provide multiresolution analysis in both frequency and temporal domains, unlike the standard Fourier transform, which allows analysis of signals only in the frequency domain [62]. To address the noise, a discrete wavelet transform (DWT) combined with an adaptive thresholding technique is implemented. The overall methodology of wavelet denoising, peak detection, and feature extraction is described in [66]. Figure 12 shows the flow chart of wavelet denoising and the local maxima algorithm.

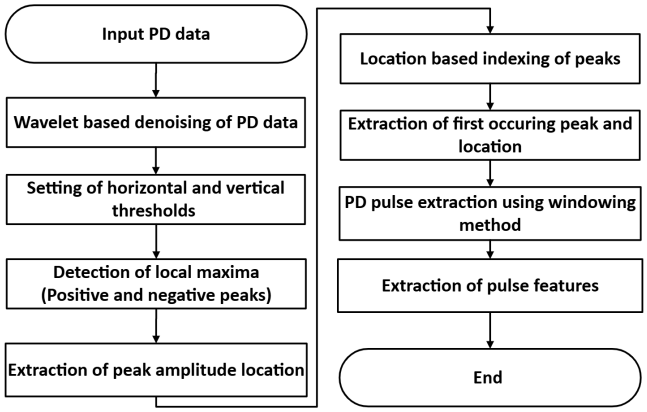

Figure 12. Flow chart of wavelet denoising and local maxima algorithm [Paper III].

The DWT-based denoising procedure consists of three steps:

- **Selection of the mother wavelet:** Selection of the mother wavelet depends on the input signal's shape characteristics. PD pulse resembles Daubechies db2 and db8 wavelets [67]. Therefore, these two mother wavelets are compared.
- **Number of decomposition levels:** This parameter depends on the signal length and sampling frequency. For this, the cross-correlation coefficient (C_c) and SNR indices are calculated. Figure 13 shows that db8 with decomposition level 9 has the optimum value of C_c and SNR value [66].

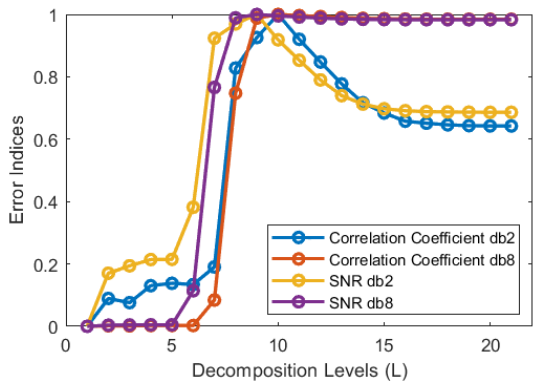

Figure 13. Indices for selection of optimal decomposition level [Paper III].

- **Thresholding:** For this, Stein's unbiased risk estimate (SURE) method is used since it automatically calculates the threshold value without prior knowledge of the noise level.

Based on the above input, the DWT reconstructs the PD data. Figure 14 shows the noisy and the denoised signal.

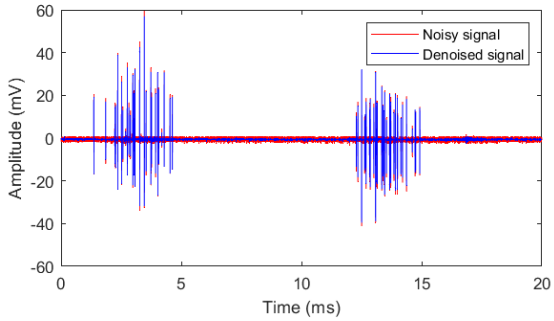

*Figure 14. Denoising of PD data using DWT-*based *denoising method [Paper III].*

In the next stage, a local maxima or peak detection method is implemented to detect peaks [64]. It works based on the vertical (V_{th}) and horizontal (H_{th}) thresholds. The former is set to identify peaks above a specified threshold, while the latter is set to compensate for the dead time of pulses, as shown in Figure 16. It decides after how many samples the algorithm detects the next peak. The optimal selection of threshold values is essential for the effective detection of PD peaks. The peak identification is executed utilizing MATLAB's peak function, which detects local maxima in the PD dataset based on vertical and horizontal thresholds. Initially, it identifies the positive and negative peaks of an individual pulse collected during 20 ms or under one AC cycle. Upon identification of positive and negative peaks, it performs indexing of peaks consecutively as P_1, P_2, P_3, ..., P_n. Let us consider that the P_n represents the total count of peaks. After identification of the first peak, P_1, each odd-indexed peak is considered a peak of the PD pulse.

Figure 15 illustrates the time-resolved partial discharge pattern, associated positive and negative peaks, and the first occurring peak of pulses. The indices of these peaks can be mathematically stated as (13). The term $i|i$ mod 2 = 1 ensures only odd indices are selected and restricts indices to within the range of detected pulses; n_{pk} is the number of peaks.

$$i_i = \{i \mid i \ mod\ 2 = 1 \ and \ i \leq n_{pk}\} \tag{13}$$

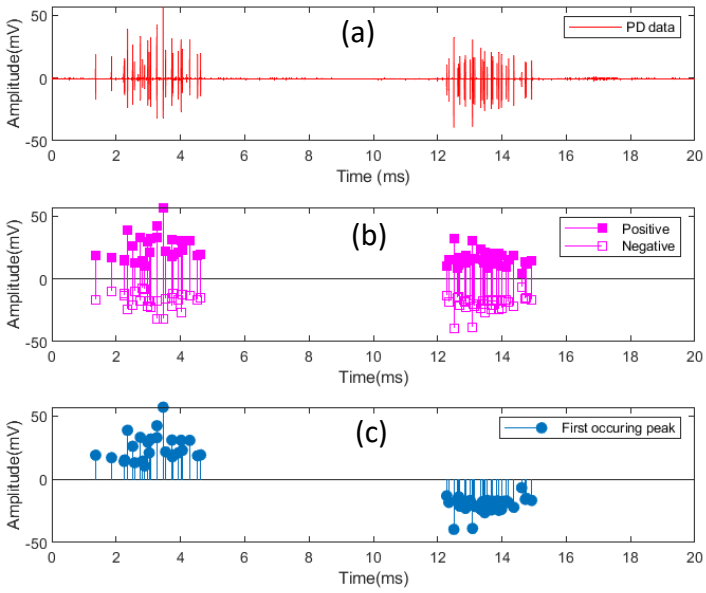

Figure 15. PD pulse detection using peak detection algorithm: a) Time resolved PD pattern, b) Positive and negative peaks, c) First occurring peak of individual PD pulse [Paper III].

Corresponding peak amplitudes are extracted using (14). Subsequently, the time and phase location of the individual peak is calculated using (15) and (16)

$$P_{odd} = \{P(i) \mid i \in i_i\} \tag{14}$$

$$t_{loc} = t_{int} * P_{loc} \tag{15}$$

$$\varphi_{loc} = \frac{t_{loc} * 360}{t_{AC}} \tag{16}$$

Where: t_{loc} – time of occurrence of PD pulse;
t_{int} – interval between two samples;
P_{loc} – sample location of pulse;
t_{AC} – time of one AC cycle.

After the detection of the peak, the next stage is to extract the pulse using the peak location. For this stage, the windowing method is used to extract the pulse using the peak value and location. Equations (17), (18), and (19) describe the extraction of the PD pulse. Here, P_d represents the width of the pulse.

$$P_s = \max\left(1, \quad P_{loc}(i) - \frac{P_d}{2}\right) \tag{17}$$

$$P_e = \min\left(l_{PD}, \quad P_{loc}(i) + \frac{P_d}{2}\right) \tag{18}$$

$$Pulse = P_s : P_e \tag{19}$$

Where: $P_{loc}(i)$ – location of i^{th} detected peak;
P_s – start of pulse;
L_{PD} – length of PD data;
P_d – pulse width (number of samples);
P_e – end of pulse.

The optimum value of pulse duration (window) is set considering the duration of the lowest pulse and the highest pulse appearing in the time-resolved PD pattern. It is observed that a window of 250 samples efficiently extracts the PD pulse. Figure 16 shows the PD pulse extracted using the windowing method. PD pulse is well structured, where the noise has random behavior. This randomness can be measured using linear prediction. The residuals related to PD pulse bear high skewness (3.0), and those related to noise have a low skewness (0.9). The PD pulse follows an asymmetric distribution, whereas noise has a symmetrical distribution, like the Gaussian distribution. Therefore, the skewness parameter can be used to differentiate the actual PD signal and noise.

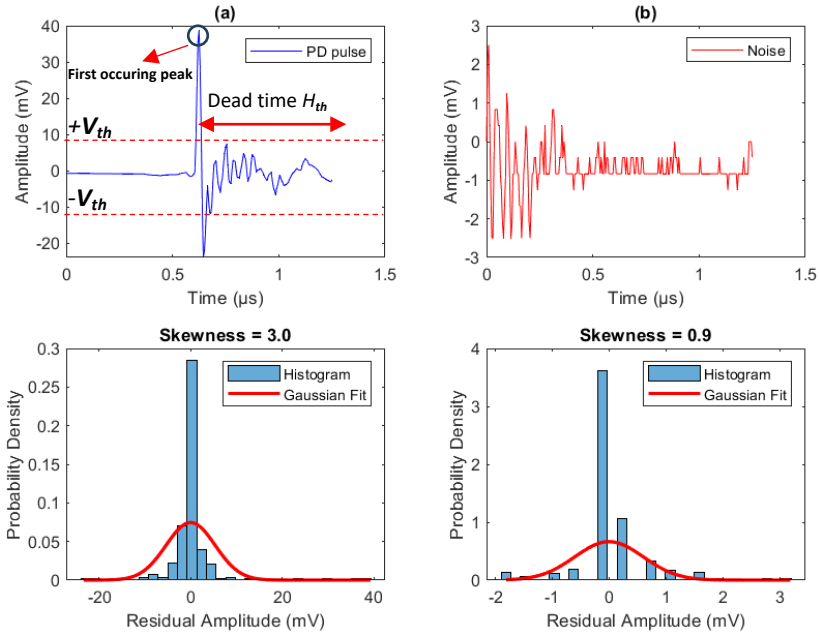

Figure 16. Typical PD and noise pulse obtained from Nomex film: a) PD pulse and distribution of residual of linear prediction, b) Noise pulse with residual of linear prediction [Paper IX].

3.2.2 Multiple Feature Extraction

PD pulse features can differentiate between pulses from various discharge sources (e.g., surface, internal, or noise). Research indicates that statistical features, time, and frequency domain attributes can efficiently distinguish different types of PD sources [64], [68]. The developed tool extracts multiple features, including time and frequency domain features, pulse shape, and statistical features. In total, 11 features have been extracted. An iterative approach is utilized that extracts these features from individual pulses and

stores them in tabular form. Table II shows PD features extracted using the developed tool. The rationale for considering the number of features is to enhance the probability of identifying a two-dimensional PCA map where clusters from distinct sources can be separated efficiently.

3.2.2.1 Peak Pulse Amplitude (V_m)

It is characterized as the peak value reached by a PD pulse. The peak amplitude of PD pulses can be described by an extreme value distribution or a two-parameter Weibull distribution [64]. Consequently, the pulses that follow the Weibull curve are classified as PD pulses, whereas others are considered noise. The cumulative distribution function of the Weibull criterion is elucidated using (20)

$$f(V_m) = 1 - e^{\left(\frac{V_m}{\alpha}\right)^{-\beta}} \quad \alpha, \beta > 0 \tag{20}$$

3.2.2.2 Pulse Energy (E_n)

It is the measure of the strength of a signal over a specified duration. It is mathematically defined as (21). Where *x[n]* represents the number of samples per pulse.

$$E_n = \sum |x[n]|^2 \tag{21}$$

3.2.2.3 Dominant frequency (f_d)

The highest frequency amplitude occurs in the frequency spectrum of the pulse. It is found using three stages. The Fast Fourier transform (FFT) of the pulse is initially computed using equation (22).

$$X(k) = \sum_{n=0}^{N-1} x[n] e^{-j\left(\frac{2\pi kn}{N}\right)} \quad , k = 0,1,2 \dots N-1 \tag{22}$$

Where: $X(k)$ – discrete FFT at index k;
j – imaginary unit;
N –number of samples;

In the second stage, the magnitude spectrum of the FFT is computed using the power spectral density value (23). The dominant frequency is subsequently determined using equation (24).

$$p(f) = |X(k)|^2 \tag{23}$$

$$f_d = \frac{\text{argmax}_k |X(k)|}{N_d} . f_s \tag{24}$$

Where: $p(f)$ – energy spectral density;
f_s – sampling frequency;
f_d – dominant frequency component;
N_d – number of discrete Fourier transform points;
argmax_k – function that gives the index or location of the maximum amplitude in the single-sided spectrum.

3.2.2.4 Pulse Shape features

Partial discharge pulse shape features describe the mechanisms and physics of discharges [41]. Figure 17 illustrates three major pulse shape features. These features are defined as follows:

Rise time (t_r): Time taken by PD pulse to rise from 10% to 90% of Vm.

Fall time (t_f): Time taken by PD pulse to fall from 90% to 10% of V_m.

Pulse width (t_w): The time interval recorded between two points when the pulse amplitude reaches 50% of V_m.

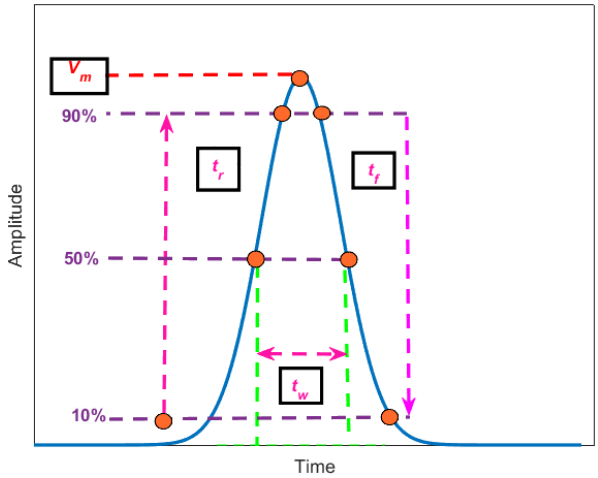

Figure 17. Typical PD pulse and shape features [Paper VI].

3.2.2.5 Statistical features

Statistical attributes like mean(μ), variance(σ^2), and skewness (S_k) are significant indicators for distinguishing various sources. They are mathematically defined as (25), (26), (27). respectively. Here σ is the standard deviation.

$$\mu = \frac{\sum_{i=1}^{N} x_i}{N} \tag{25}$$

$$\sigma^2 = \frac{1}{N}\sum_{i=1}^{N}(x_i - \mu)^2 \tag{26}$$

$$S_k = \frac{N}{(N-1)(N-2)}\sum_{i=1}^{N}\left(\frac{x_i - \mu}{\sigma}\right)^3 \tag{27}$$

Table II. Multiple PD features obtained from ten pulses from surface erosion-based accelerated aging of Nomex film after 330 minutes of aging.

No.	V_p (mV)	E_n (V^2)	t_{loc} (ms)	φ_{loc} (º)	f_d (MHz)	μ (mV)	σ^2 $(mV)^2$	S_k	t_r (ns)	t_f (ns)	t_w (ns)
1	38.7	7233	2.4	42.4	23.9	0.6	28.6	3.0	12.1	9.9	18.8
2	33.1	4976	2.8	49.6	3.98	0.5	19.7	3.9	9.6	10.9	18.8
3	29.4	4393	3	53.7	23.9	0.6	17.2	2.2	12.8	9.1	17.7
4	31.8	4146	3.1	55.3	23.9	0.4	16.4	2.6	13.0	8.3	15.1
5	42.3	9225	3.3	58.8	23.9	0.4	36.7	1.9	13.3	7.6	17.0
6	57	17276	3.5	62.3	3.98	0.4	68.9	2.9	13.1	11.1	20.9
7	30.8	4235	4.3	77.2	3.98	0.5	16.8	3.6	12.6	15.4	19.8
8	39.6	7902	12.5	225.0	23.9	0.7	31.1	1.2	12.4	7.6	16.9
9	38.9	6910	13.1	235.5	23.9	0.7	27.2	1.6	12.3	8.0	15.3
10	26.5	2968	13.5	242.3	23.9	0.6	11.5	1.2	12.8	7.4	13.6

3.3 Optimum Feature Selection and Hierarchical Clustering

This section presents PCA and hierarchical clustering methods used for optimum feature selection and clustering of PD data.

3.3.1 Optimum Feature Selection Using PCA

Principal component analysis (PCA) is an effective tool used for dimensionality reduction and optimal feature selection. It converts the original dataset or features into a new set of elements referred to as principal components (PCs). It performs optimal feature selection by using the first *N* principal components. Let us consider that the feature matrix of 11 features is processed under PCA, the feature matrix $Fe^{M\times N}$ to $Fe^{M\times R,}$ as expressed by (28). Figure 18 shows the flow chart describing PCA operation.

$$\boldsymbol{F^{PCs}} = \begin{bmatrix} \boldsymbol{F_1^{PC_s}} \\ . \\ . \\ \boldsymbol{F_i^{PC_s}} \\ . \\ . \\ \boldsymbol{F_{N_f}^{PC_s}} \end{bmatrix} = \begin{bmatrix} \boldsymbol{F_{1,1}^{PC_s}} & .. & \boldsymbol{F_{1,j}^{PC_s}} & .. & \boldsymbol{F_{1,k}^{PC_s}} \\ . & & . & & . \\ . & & . & & . \\ \boldsymbol{F_{i,1}^{PC_s}} & .. & \boldsymbol{F_{i,j}^{PC_s}} & & \boldsymbol{F_{i,k}^{PC_s}} \\ . & & . & & . \\ . & & . & & . \\ \boldsymbol{F_{N_f,1}^{PC_s}} & .. & \boldsymbol{F_{N_f,j}^{PC_s}} & & \boldsymbol{F_{N_f,k}^{PC_s}} \end{bmatrix} \tag{28}$$

Where: F^{PCs} – feature matrix transformed after PCA;
N_f – total number of features;
k – number of selected PCs after dimensionality reduction;
$F^{PCs}{}_i$ – feature score vector for the i^{th} observation after PCA transformation;
$F^{PCs}{}_{i,j}$ – feature score of i^{th} observation on j^{th} principal component.

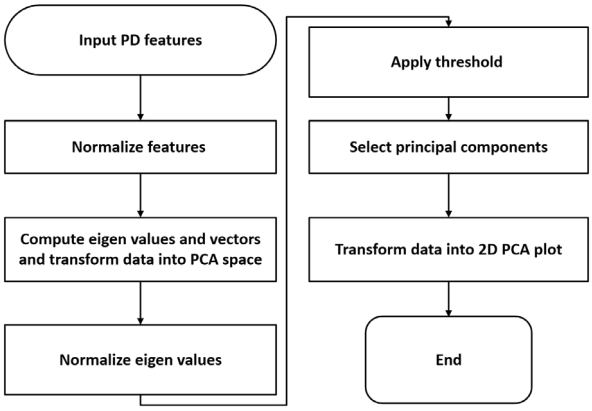

Figure 18. Flow chart of PCA-based selection of PD features.

The selection of the number of PCA components is determined by the variance plot. Figure 19 illustrates the variance plot derived from PCA. The first seven principal components exhibit a variance of 95%. Thus, these seven features are chosen for clustering and classification of PD data.

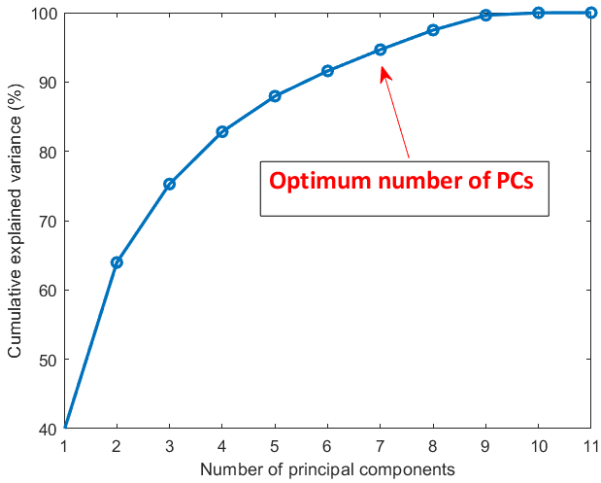

Figure 19. PCA-based optimum selection of PD features [Paper IX].

3.3.2 Hierarchical Clustering

PCA analysis identifies optimal features suitable for data clustering. The next step after optimum feature selection is classification and clustering. For this, a hierarchical clustering method is used. One of the major advantages is that it does not require prior information about the number of clusters. In addition to this, Ward's method is used, which reduces variance within clusters at each step of the hierarchical clustering and merging process. Similarity among data points is calculated using the Euclidean distance method. For each pair of data points, x_i and x_j, the Euclidean distance $d(x_i, x_j)$ is calculated using (29)

$$d(x_i,\ x_j) = \sum_{m=1}^{k} (x_{i,m} - x_{j,m})^2 \qquad (29)$$

Where: m – feature index;
x_i – $[x_{i,1}, x_{i,2}, x_{i,3} \ldots, x_{i,k}]$ feature vector for the i^{th} observation;
x_j – $[x_{j,1}, x_{j,2}, x_{j,3} \ldots, x_{j,k}]$ feature vector for J^{th} observation.

The optimum number of clusters is determined by utilizing the knee heuristic (second derivative) method. Overclassification is one of the key issues that occur during clustering of PD data, i.e., two clusters may overlap. A cross-correlation approach is employed to merge clusters when similarities are identified between them. A threshold of 0.8 is set for merging similar clusters [65]. Figure 20 (a, b, c) illustrates the PRPD pattern, PCA map, and PRPD pattern after clustering of PD data.

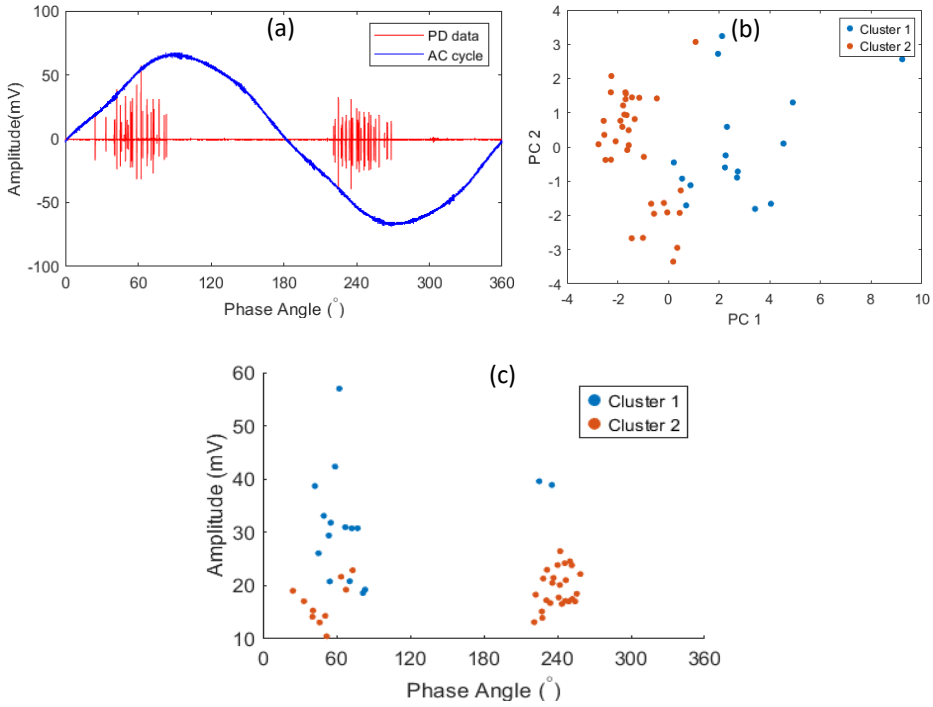

Figure 20. Hierarchical clustering of PD data: a) PRPD pattern, b) PCA map, c) Clusters of different types of PD sources [Paper IX].

3.4 Identification of Type of PD

The subsequent stage following the clustering of PD data is the identification of PD types that correspond to specific clusters. Numerous features documented in the literature can be employed for the classification and labelling of clusters. Nevertheless, the shape parameter (β) of the Weibull distribution is identified as an effective parameter for the identification of partial discharge sources, including surface, internal, and corona discharges. The scale parameter (α) is directly associated with the mean of the distribution. In PD analysis, it is influenced by the mean integrated pulse height and mathematically

linked through the gamma function, while β denotes the dispersion of pulse height, elucidating the physics underlying the PD phenomena. Experimental investigations indicate that low β signifies surface discharges, medium β denotes internal discharges, and high β corresponds to corona discharges. For example, in [63] it is illustrated that β between 1…2 represents surface PD, 3…10 represents internal PD, and $\beta > 10$ represents corona discharge. Considering phase angle or phase distribution, a low phase inception (Φ_i) shows internal PD, a medium Φ_i shows surface PD, and a high Φ_i shows corona discharges. Considering the phase span, it is observed that Φ_i, an overlap of phase inception may occur, particularly between internal and surface or internal and corona [63–65]. Therefore, the β is the only criterion set for the identification of PD type. In this work β is set as 1…3.5 for surface PD, 3.5…10 for internal PD, and $\beta > 10$ for corona discharge. These values are found from PD data sets acquired from surface erosion of Nomex films at different stages of aging.

Fuzzy logic is an effective tool that resembles human decision-making, particularly in scenarios where there is uncertainty or limited information. Fuzzy inference systems (FIS) are based on rules. These rules are linguistic variables established by experts based on the behavior of partial discharges in various defects [69]. Here, β is considered for the identification of different clusters found in the PD data or PRPD pattern. At the initial level, a single-input and single-output (SISO) FIS is designed since β is the only parameter used for the identification of sources.

Typically, the input attributes are represented using binary values of 0 or 1 called crisp inputs. These inputs range from 0 to 1. Depending on the severity or percentage of the type of source present in a PRPD pattern, these crisp inputs can be set. The second advantage is that it is a simple method of designing an unsupervised and automated system for identifying clusters that represent a particular PD source. Figure 21 illustrates the block diagram of the FIS developed. Fuzzy inputs and outputs are represented by trapezoidal and triangular membership functions (MF), respectively. Trapezoidal MFs are flexible and effective, particularly during a gradual transition between categories [69]. In contrast, the Triangular MFs are simpler and ensure that the resulting crisp output aligns precisely with the center of the intended class, which simplifies centroid calculation.

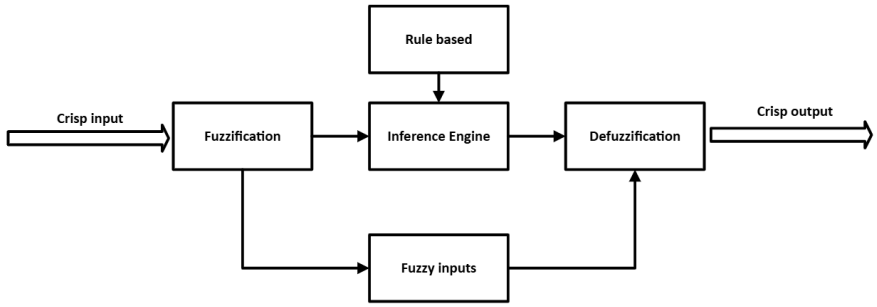

Figure 21. Block diagram of fuzzy inference system (FIS) for identification of PD type [Paper IX].

Examples of if-then fuzzy rules are illustrated below. These rules are set in keeping with the literature and based on the physics of the PD phenomena [64–65]. Initially, three rules were designed.

If β is **low**, THEN the cluster represents Surface discharge
If β is **medium**, THEN the cluster represents Internal PD
If β is **high**, THEN the cluster represents Corona PD

Additional rules can be designed based on experimental investigation and expert advice. The FIS offers flexibility to incorporate different rules based on the severity and physics of PD activity.

3.5 Case Studies

This integrated tool has been implemented in two cases. In the first case, two artificial defects are created in MV XLPE cable samples. In the second case, lifetime PD measurements were performed on Nomex film using a surface erosion-based accelerated aging method. The details of each case study are given as follows:

3.5.1 Behavior of Internal and Surface PD in MV XLPE Cable

Figure 22 (a) shows a laboratory-based experiment setup and defects created in the MV XLPE cable. The surface discharge defect is created by damaging the cable termination, and the internal defect is made by introducing a tiny incision in the external sheath of an MV cable sample approximately three meters long, which extends into the main insulation as shown in Figure 22 (b, c). PDIV for the former was found to be 5.4 kV, and for the latter, it was found to be 5.9 kV.

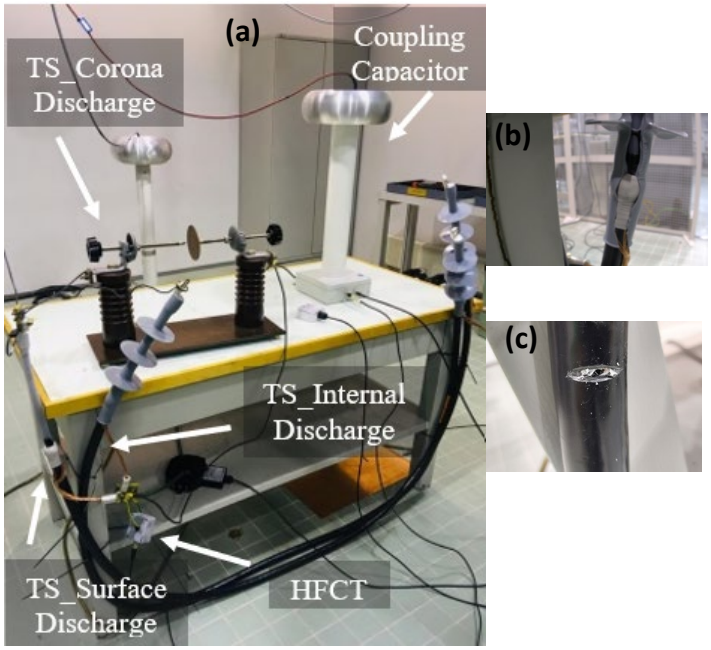

Figure 22. a) Laboratory-based experiment setup for PD measurement in b) Surface defect c) Internal defect [Paper III].

PD data were recorded at increasing electrical stress. The setup utilizes a high-voltage AC source, CC, HFCT, and oscilloscope with a bandwidth of 80 MHz. PD data is measured at different voltage levels at a sampling rate of 250 MS/s. PD behavior in modeled defects is analyzed under increasing electrical stress. Initially, the applied voltage is increased with a step size of 0.1 kV until the PDIV is found. After finding PDIV, the voltage is increased at various levels.

3.5.1.1 Internal Defect

Figure 23 (a, b, c, d) shows PPRD patterns obtained during PD measurement at different voltage levels. Three voltage levels are considered after PDIV, i.e., 6.4, 9.4, and 12.4 kV. Considering the PRPD patterns, internal PDs are symmetrical in both the positive and negative half-cycles of the applied voltage. Considering phase distribution, PD pulses usually occur near the zero crossing, i.e., between 0…90° in the positive half cycle and 180°…270° in the negative half cycle of the applied voltage.

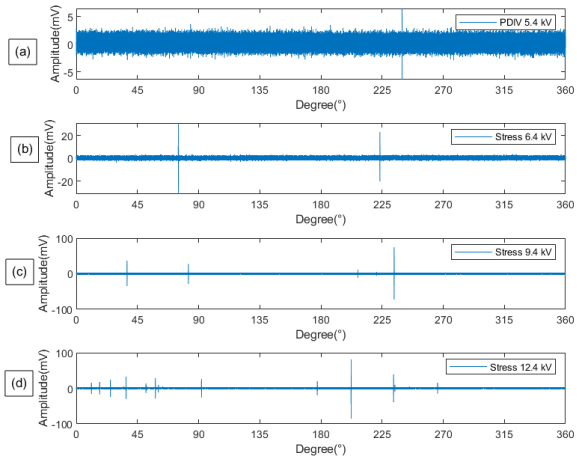

Figure 23. PRPD patterns obtained through modelled internal defect in XLPE cable insulation under different voltage levels: a) PDIV, b) 6.4 kV, c) 9.4 kV, d) 12.4 kV [Paper IV].

Table III. PD features extracted from the modeled internal defect [Paper IV].

No.	***V_m*** **(mV)**	***V_{mabs}*** **(mV)**	***V_{app}*** **(kV)**	***t_{loc}*** **(ms)**	***Φ_{loc}*** **(°)**	***t_r*** **(ns)**	***t_f*** **(ns)**	***t_w*** **(ns)**	***Φ_{span}*** **(°)**
1	30.7	30.7	3.9	1	17.3	69.8	30.3	64.5	
2	17.7	17.7	8.4	1.6	29	43.8	32.4	71.8	
3	35.9	35.9	11.8	2.6	47.5	48	37.2	73.5	77.1
4	23.5	23.5	14.1	3.7	65.8	49.1	32.5	72.2	
5	13.6	13.6	16.5	5.2	94.4	61.6	28.9	74	
6	-32.3	32.3	-0.7	10.1	182.1	46.6	31.6	61.8	
7	-11.1	11.1	-7.9	11.5	206.2	63.8	34.3	73.9	
8	-56.2	56.2	-14.3	12.2	219.6	52.5	32.8	70	69.2
9	-32.9	32.9	-15.7	13.6	244.4	13.1	15.1	28.8	
10	-21.7	21.7	-18.1	14	251.3	45.9	37.2	71.7	

After measuring PD data through an oscilloscope, the data is processed using the integrated tool, and major PD features are extracted. Table III shows major features. These features include basic pulse features like peak pulse amplitude (V_m), absolute value of peak pulse amplitude (V_{mabs}), applied instantaneous voltage (V_{app}), pulse location features ($V_{loc,}$ $t_{loc,}$ and Φ_{loc}), pulse shape features (t_r, $t_{f,}$ and t_w) [70]. Three major features,

including peak pulse amplitude (V_m), phase distribution or phase span (Φ_{span}), and number of pulses (n_p), are considered to analyze the behavior of internal PD defect under the influence of PD. Figure 24 illustrates the major features.

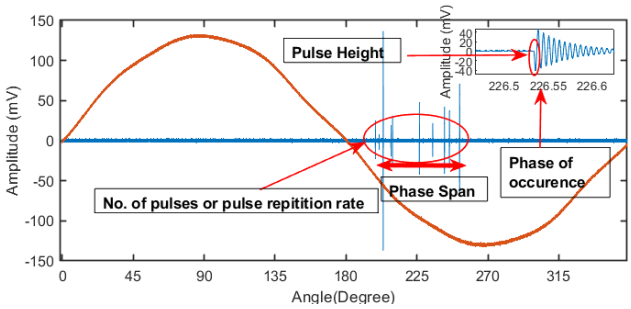

Figure 24. PD features considered for analysis of surface and internal defects [Paper V].

Figure 25 shows polar plots and PRPD patterns illustrating the behavior of peak pulse height (V_M)and Φ_{loc} of individual PD pulses observed during an acquisition time of 200 ms. The results indicate obvious variation in PD features at different voltage levels. The key findings of this investigation are:

- With increasing voltage, there is an increase in V_M. At 6.4 kV, V_M ranges between 5…30 mV, and at 9.4 kV, it ranges between 10…60 mV. However, at 12.4 kV, there is a slight increase in V_M as only a few peaks of amplitude more than 60 mV are observed. It is interesting to note that, at higher voltage levels, there is no significant increase in the V_M, but the occurrence of pulses increases near the zero crossing of the applied voltage.
- It is observed that with increasing voltage, the n_p increases. The increase is observed in both positive and negative pulses, as shown in Figure 26.
- An increased phase span is observed at increasing voltage, at 6.4 kV PD activity span was found between 210°…250° in the negative half cycle of the applied voltage and only single peak found in positive half cycle of the applied voltage, at 9.4 kV phase span increased ranges between 20° …60° in the positive half cycle of the applied voltage and 180°…270° in negative half cycle of the applied voltage and at 12.4 kV it is further increased ranges between 0°…90° in positive half cycle of the applied voltage and 180°…270° in negative half cycle of the applied voltage.
- It is also observed that with increasing voltage, PD activity becomes denser near the zero crossing of the applied voltage.

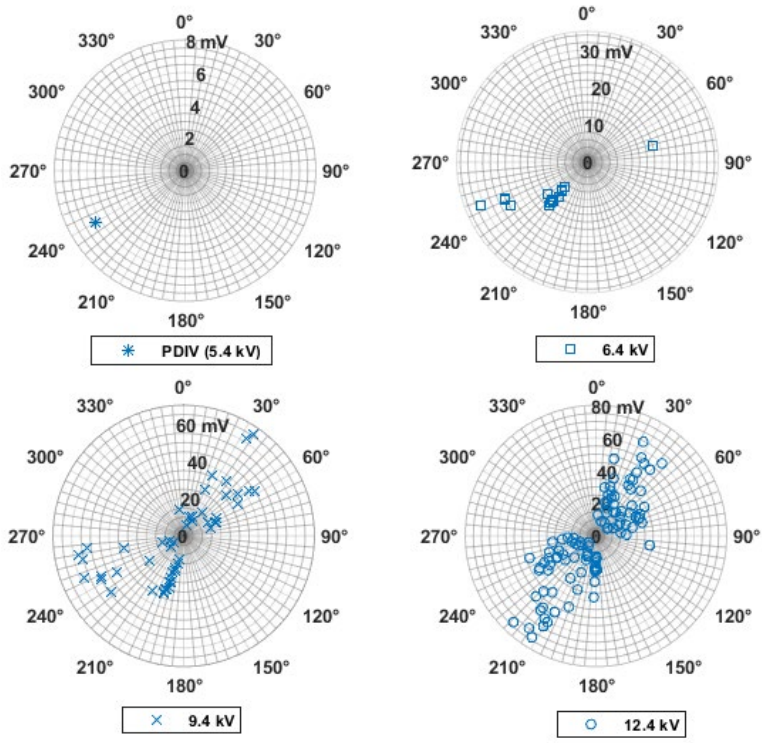

Figure 25. Polar plot showing peak pulse amplitude (V_m) and phase location (Φ_{loc}) of an individual pulse of internal discharge defect [Paper IV].

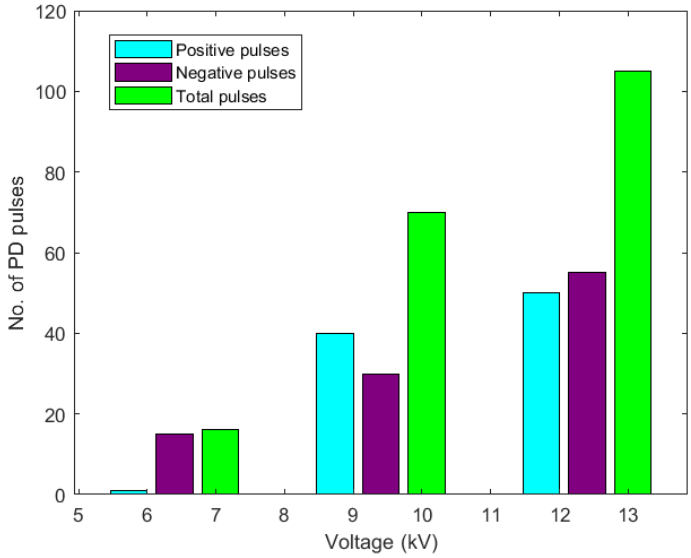

Figure 26. Behavior of the number of pulses (positive and negative) for internal defect [Paper IV].

3.5.1.2 Surface Discharge Defect

Figure 27 shows PPRD patterns obtained during PD measurement at different voltage levels. Eight voltage levels are considered after PDIV, ranging between 5.9…13.3 kV. Considering the PRPD patterns, surface PDs are asymmetrical in both the positive and negative half-cycles of the applied voltage. Considering phase distribution, PD pulses are mostly observed during the negative half cycle of the applied voltage between 180°… 290°.

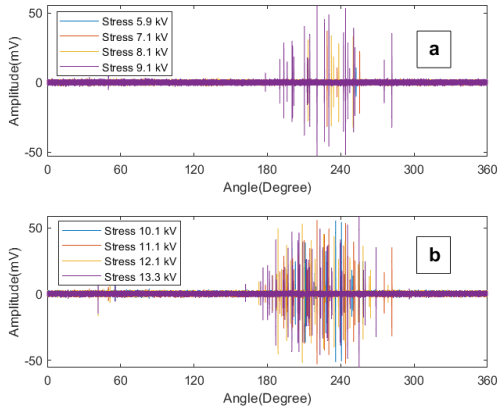

Figure 27. PRPD pattern obtained from the surface discharge defect at different voltages

Figure 28 shows polar plots illustrating the behavior of V_M and Φ_{loc} of individual PD pulses acquired from the surface discharge defect. Polar plots contain pulses found during an acquisition time of 200 ms. The key findings of this investigation are as follows:

- PD activity in surface discharge defects is observed in two stages. At the initial stage, between 5.9…9.1 kV, V_M increases proportionally with applied voltage, ranging between 10…100 mV. However, at a later stage between 10.1…13.3 kV, the V_M consistently ranges between 20…60 mV. It is noticed that at the second stage, the occurrence of pulses increases near zero crossing, as a cloud of peaks appears near zero crossing, as shown in the polar plots in Figure 28. Considering the n_p, there is an obvious increase in the n_p. At the initial stage, there is a slight increase in pulses. However, at higher voltage levels, the n_p increases drastically.
- Considering the phase span of PD activity, the activity span increases with applied stress. At the initial level, the activity span ranges between 210°…270°. This phase span increased after 10.1 kV, ranging between 180°…270° in the negative half cycle of the applied voltage.
- In addition to the above features, pulse shape features including rise time (t_r), fall time (t_f), and pulse width (t_w) are investigated for surface discharge defect. These features are extracted using the developed tool. MATLAB functions are used to extract these values, as shown in Figure 29. The results show that pulse features show an increasing trend with applied voltage. However, there is a high dispersion in the pulse shape feature values at higher voltage levels.

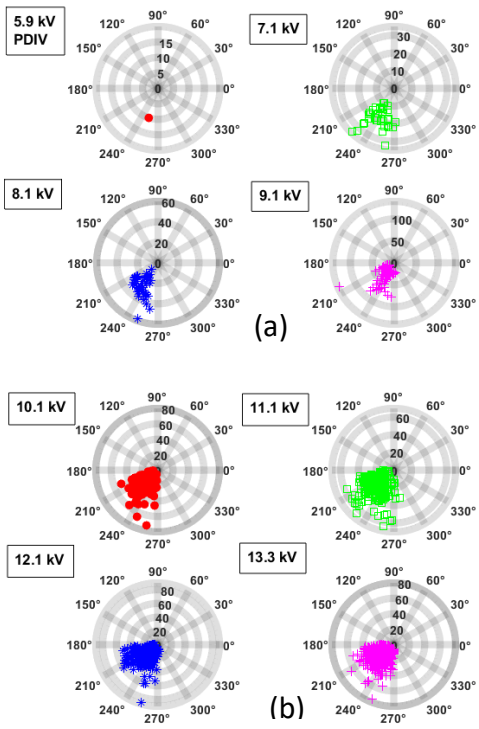

Figure 28. Polar plot showing peak pulse amplitude (V_m) and phase location (Φ_{loc}) of individual peaks of surface discharge defect [Paper V].

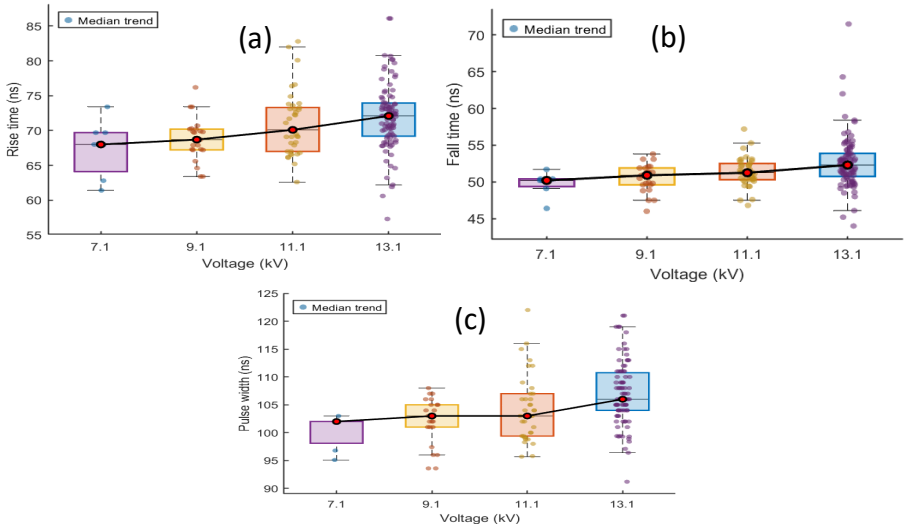

Figure 29. Behavior of pulse shape features at different voltage levels with surface discharge defect: a) rise time, b) fall time, c) pulse width [Paper VI].

3.5.2 Classification and Identification of Four Stages of Aging in Nomex Films Under Surface Erosion-Based Accelerated Aging

Figure 30 (a, b) shows a laboratory-based experiment setup and a two-electrode configuration utilized. Major components are outlined as follows:

- A 150 kV-rated test transformer is coupled with a voltage regulator.
- A two-electrode arrangement featuring an HV electrode and a ground electrode. The upper electrode, functioning as the HV electrode, features a flat surface with a diameter of 6 mm and a contoured radius of curvature of 0.25 mm at the corners. The ground electrode has a smooth surface with a diameter of 51.5 mm, as shown in Figure 30 (b).
- Charge calibrator for the calibration of conventional PD measurement systems.
- A capacitor with a capacitance of 1 nF and a voltage rating of 36 kV is connected in series with a partial discharge sensor for measuring discharges and in parallel with a two-electrode arrangement and an HV AC supply, as illustrated in Figure 30 (a).
- Conventional PD measurement device with a quadrupole for capturing PRPD patterns and PD characteristics, as illustrated in Figure 30 (a).

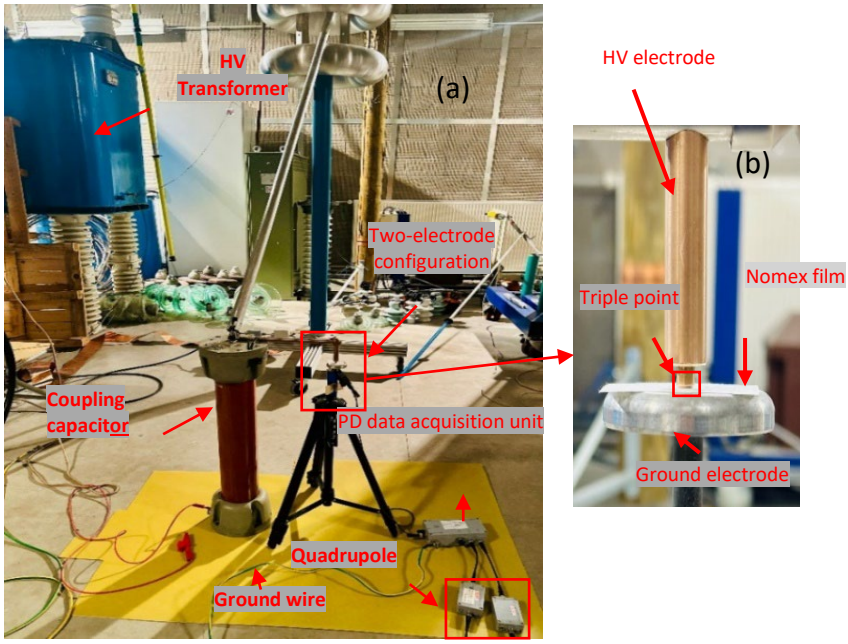

Figure 30. Laboratory-based experiment setup designed for lifetime study of Nomex film: a) experimental setup, b) electrode configuration [Paper VII].

The electrodes are specially designed for the surface erosion-based accelerated aging. The high voltage electrode has a flat surface with a contour at the edges that controls the electric field, and a ground electrode with a flat surface. The specification of the experimental setup and two-electrode configuration is mentioned in [71]. The square shape of Nomex film is sandwiched between two electrodes, creating a triple point. Lifetime PD data is measured at 2×PDIV with a sampling rate of 200 MS/s.

Surface erosion-based accelerated aging test was performed on Nomex film to observe PD behavior throughout its lifetime. The analysis of PRPD patterns revealed that aging on Nomex film follows four distinct stages from inception until breakdown. These major variations are observed in the PRPD patterns and microscopic analysis [61].

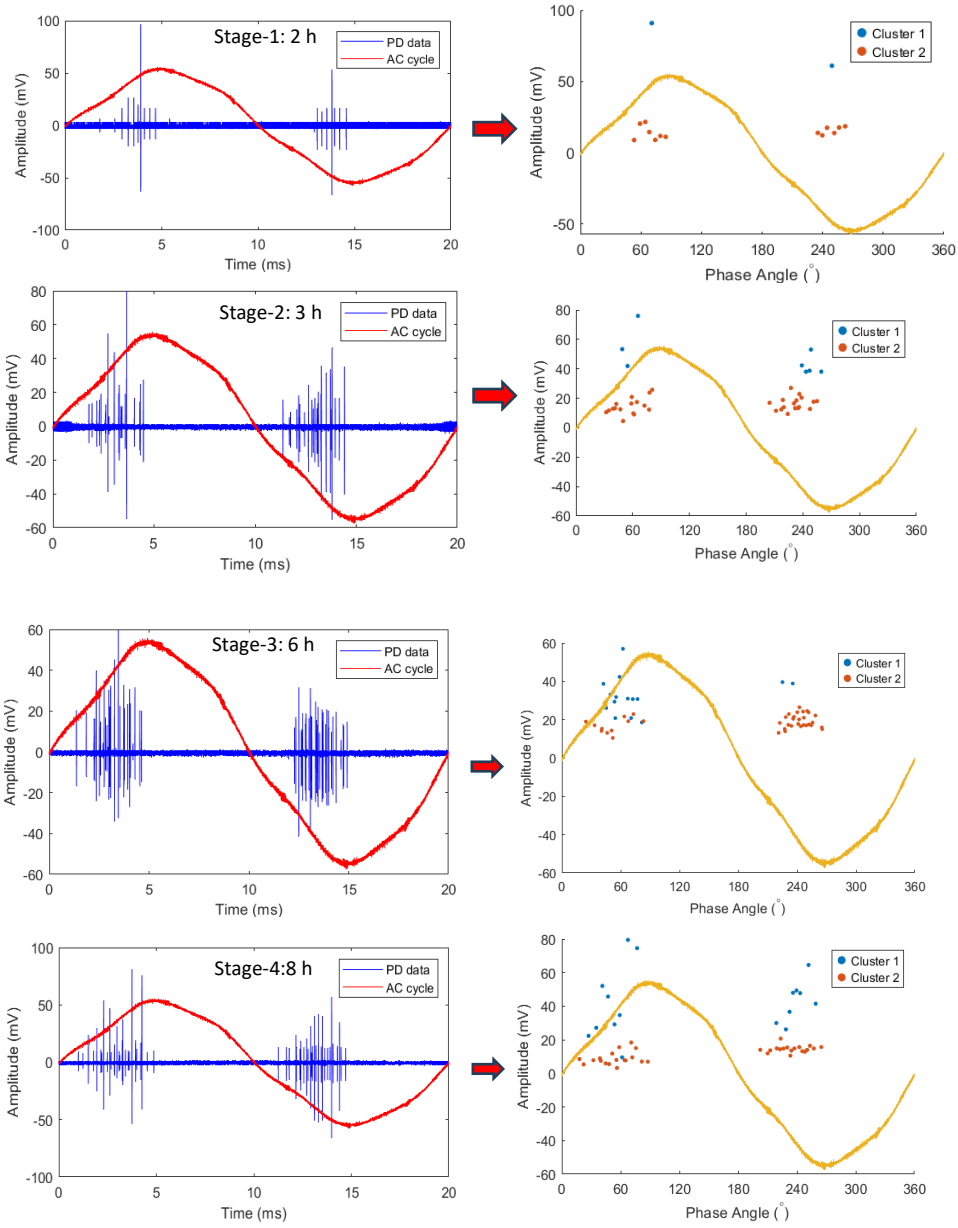

Figure 31. PRPD patterns at different stages of aging of Nomex film, corresponding PCA maps, and PRPD patterns after classification of PD data [Paper IX].

These variations are mapped with the concept of four-stage aging, i.e., surface discharge inception, surface erosion, surface tracking, treeing, and finally pitting and breakdown [70]. It is assumed that initially surface discharges occur at the insulation surface; thus, the PRPD pattern contains discharges that represent only surface discharges. However, continued PD activity may track within the bulk of the insulation. It is observed that at the third stage, PD activity tends towards zero crossing of the applied voltage, which can be an indication of the inception of internal discharges or tracking. The details about the lifetime study of Nomex film and four-stage aging are described in Chapter 5 of this thesis. To validate this four-stage aging phenomenon, oscilloscope-based PD measurements are collected. Subsequently, the data is analyzed through a developed approach.

Figure 31 (a, b, c, d) illustrates the time-resolved PD patterns corresponding to PCA maps and PRPD patterns showing different clusters. Initially, PD pulses and pulse features are extracted using the local maxima algorithm. In the next stage, PCA-based optimum features are selected, and based on the features, clustering is performed. The next stage after clustering is the identification of defects. For this, β is calculated for each cluster at four stages as shown in Table IV.

Table IV. Weibull shape parameter (β) for different clusters at four stages of aging of Nomex insulation.

Stage	Aging time (Hours)	Cluster	Weibull shape parameter (β)
1	2	1	6.0
		2	3.5
2	3	1	4.4
		2	3.3
3	6	1	3.5
		2	5.5
4	8	1	2.5
		2	4

At stages 1 and 2, the surface discharge activity is predominant as cluster-2 has a higher number of discharges and low β compared to cluster-1. This shows that PD activity is mostly on the surface of insulation, causing surface discharges. However, there are a few traces of internal activity at stage 2 shown by cluster 1. At stages 3 and 4, the internal discharge activity is dominant as cluster-2 has a higher number of discharges and a higher β compared to cluster-1. This shows that PD activity entered within the bulk of insulation due to tracking that causes internal discharges to increase compared to surface discharge. It can be noticed that PD activity tends towards zero crossing of the applied voltage, particularly at stage 4, which is an attribute exhibited by the PRPD pattern of internal PD [66]. The observed transition in PD activity from surface to internal discharges indicates the four-stage aging of Nomex film. The four-stage aging process is further described in Chapter 5.

4 PDIV Estimation Using A COMSOL-Based Simulation Model with Two Electrode Configurations: FEM Simulation, Modelling, And Experimental Validation

Surface discharges are one of the major causes of failure in various electrical assets and aerospace devices. Due to their high voltage rating and compact size, these discharges pose a severe risk to insulation systems, particularly in low-pressure and HV environments. Nomex is widely used in aerospace devices and has vast applications in various power system assets. PDIV is a critical parameter used to assess the condition of insulation. It also plays a key role in the insulation system design. As insulation deteriorates, PDIV starts decreasing, which can be an indication of cracks, damage, voids, or tracking of discharges within the insulation. In this chapter, a three-leg approach has been implemented to calculate the PDIV of Nomex film. An electrode configuration is used, and a thin Nomex film is placed between the electrodes, thereby creating a triple point. Figure 33 shows the two-electrode configuration and triple point. The following steps are taken for the implementation of the three-leg approach:

- Design of FEM-based simulation model in the COMSOL environment and calculation of tangential and normal field profiles for electrodes with different contours or radii of curvature.
- Use of tangential field profiles and surface discharge model for estimation of PDIV.
- Design of physical experiment setup for validation of theoretical PDIV ($U_i^{th)}$ estimated using the first two legs with measured PDIV ($U_i^{m)}$ found in the third leg.

4.1 FEM-based Simulation Model

A two-dimensional axisymmetric simulation model is designed to illustrate the spatial configuration of electric field profiles on solid insulation. These field profiles were calculated utilizing the electrostatics module in the AC/DC division. Figure 32 illustrates the methodology adopted to determine electric field profiles.

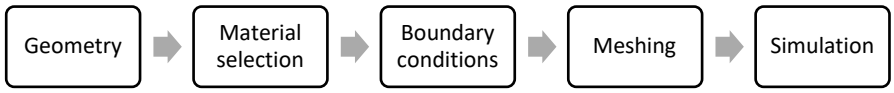

Figure 32. Methodology for FEM-based modeling [Paper VII].

4.1.1 Geometry

The geometrical model of the electrode configuration consists of a cylindrical high-voltage electrode and a circular/disk-shaped ground electrode, as shown in Figure 33. The high-voltage electrode has a diameter of 6 mm and a corner contour of 0.25 mm, whereas the ground electrode has a diameter of 51.5 mm. A square Nomex specimen of 5 x 5 cm with a thickness of 0.13 mm is sandwiched between two electrodes with no air gap. A 2D axisymmetric model provides a method to simplify a 3D model into a 2D geometric representation. This approach offers three primary advantages:

- Improved computing efficiency relative to 3D models.
- Enables the evaluation of the field distribution along the contour.

- Simplify the implementation of boundary conditions and speed up the meshing process.

Based on the modelled electrode configuration, two types of discharges can be initiated. Surface discharge on the insulation surface along direction *l* and internal discharge *h.* However, the electrode design is made in such a way that the surface discharge inception voltage will be lower than the internal discharge inception voltage [71–73]. Therefore, only surface discharge occurs, which causes erosion on the material surface. This electrode configuration is particularly designed to investigate the behavior of surface discharge on insulation using the erosion method.

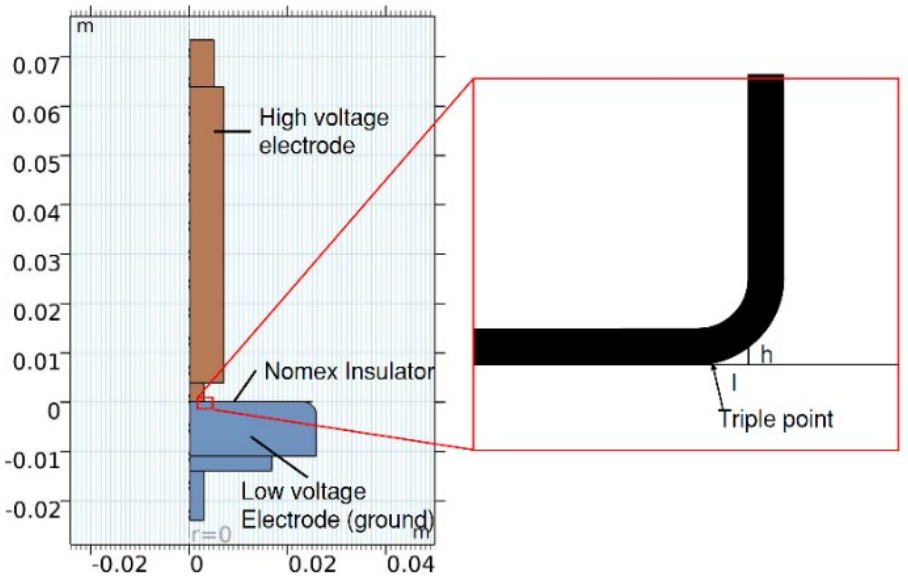

Figure 33. Geometry of two-electrode configuration and Nomex film in COMSOL environment [Paper VII].

4.1.2 Material Selection

Nomex is extensively used in electrical equipment due to its excellent dielectric strength, mechanical durability, and thermal stability. The modelled system utilizes Nomex 410 film with a thickness of 0.13 mm, which possesses an AC dielectric strength of 28 kV/mm and a full-wave impulse strength of 55 kV/mm. Additional details regarding Nomex film are given in [74].

4.1.3 Boundary Conditions and Meshing

Boundary conditions are established to determine the behavior of the electric field at specified places and scenarios. For this, Dirichlet boundary conditions are set as shown in Figure 34. They have extensive applicability in mechanics, heat transfer, fluid dynamics, and electrostatics. They offer two principal benefits:

- Input parameters or boundary conditions remain unchanged during the solution. For instance, the voltage of both electrodes remains constant throughout the solution.

- It facilitates correlation of experimental investigations to FEM solutions, as these conditions can be controlled at the initial stages. Consequently, solutions can be derived under different conditions. For instance, the behavior of tangential and normal fields is determined at various voltage levels ranging from PDIV to breakdown.

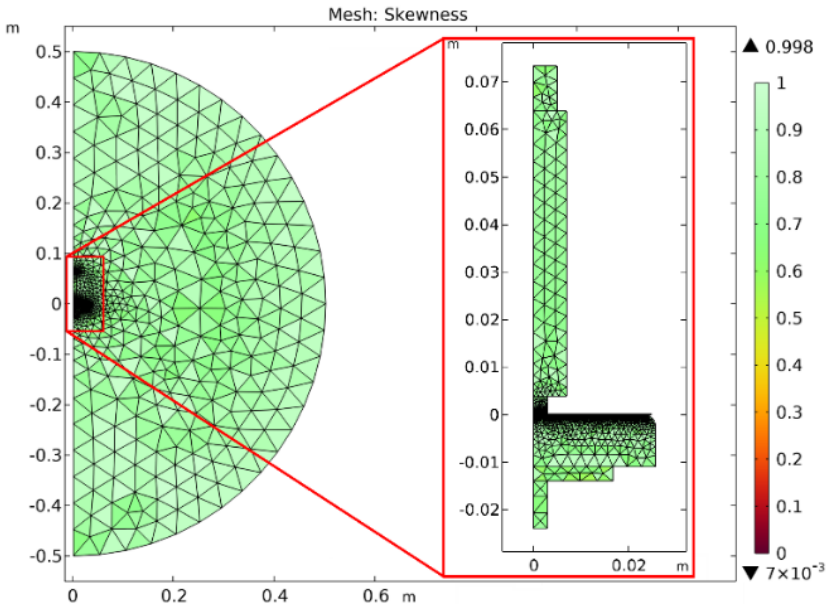

Figure 34. Boundary condition and meshing for determination of normal and tangential field profiles at triple point [Paper VII].

The mesh size and quality are two critical parameters. Triangular meshing is used as it provides effective surface approximation and accurately represents complex shapes. The electrodes and the surrounding air are integrated using a predetermined, coarser mesh to reduce processing time.

4.1.4 Simulation

Simulation involves the solution of partial differential equations to determine the behavior of electric fields (normal and tangential) under set boundary conditions. For this, electrical field profiles are determined at different radii of curvature and at various AC voltage levels ranging from 1 to 3 kV. The radius of curvature for field profiles at different voltage levels is set at 0.25 mm. Figure 35 depicts a FEM-based two-dimensional simulation model of the electrodes, including the electrical field distribution at the insulation surface and near the contour of the HV electrode.

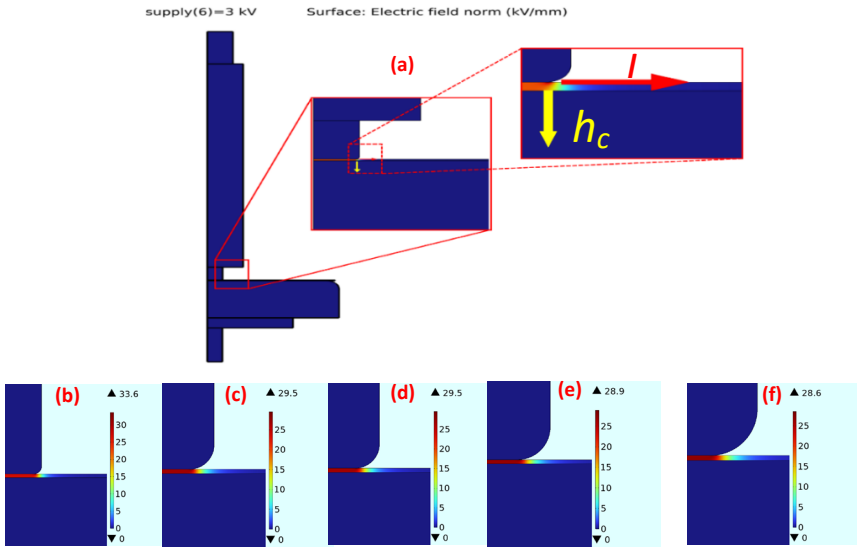

Figure 35. FEM based simulation model a) Direction of tangential distance along l and normal distance along h and behavior of tangential (orange) and normal (aqua blue) at different radii of curvature of HV electrode b) 0.25 mm c) 0.5 mm d) 0.75 mm e) 1 mm f) 1.25 mm [Paper VII].

Two types of electric field profiles were identified based on the simulated electrode configuration [75], the tangential electric field along the horizontal direction *l*, illustrated by the red arrow. Secondly, a normal electric field along the vertical direction *h,* illustrated by the yellow arrow. Corresponding field distributions at different electrode contour radii are shown in orange and aqua blue colour in Figure 35 (b…f). The gap between the electrode contour/radius of curvature at the corner and the insulation surface forms an air cavity. It is classified as a gas or an internal cavity. Figure 35 (b... f) shows the magnitude of the tangential and normal field at the triple point at different radii of curvature (contours). With increasing contour size from 0.25 to 1.25 mm, the tangential field decreased from 33.6 kV to 28.6 kV. Figure 36 (a…d) illustrates the tangential and normal field profiles at different radii of curvature of high voltage electrodes and under different voltages along *l* and *h*, respectively. Three major points were observed by these profiles:

- The tangential field increases from zero to its maximum near the triple point, while the normal is maximum at the triple point and then decreases exponentially, as shown in Figure 36 (a…d). A continuous decline in both fields is noted as the distance from the triple point increases along *l* and h_c, e.g., a consistent decline is noted after 0.2 mm as shown in Figure 36 (a, c).
- With increasing radius of curvature at the corner of the HV electrode, both normal and tangential fields are decreased as shown in Figure 36(a, c).
- Although the amplitude of the normal field is much higher than that of the tangential field, the erosion on the material surface will occur only due to the tangential field, as it has a direct impact on the material surface; also, the surface PDIV is lower than the internal PDIV.
- With increasing voltage, both tangential and normal field increases proportionally as shown in Fig. 36 (b, d).

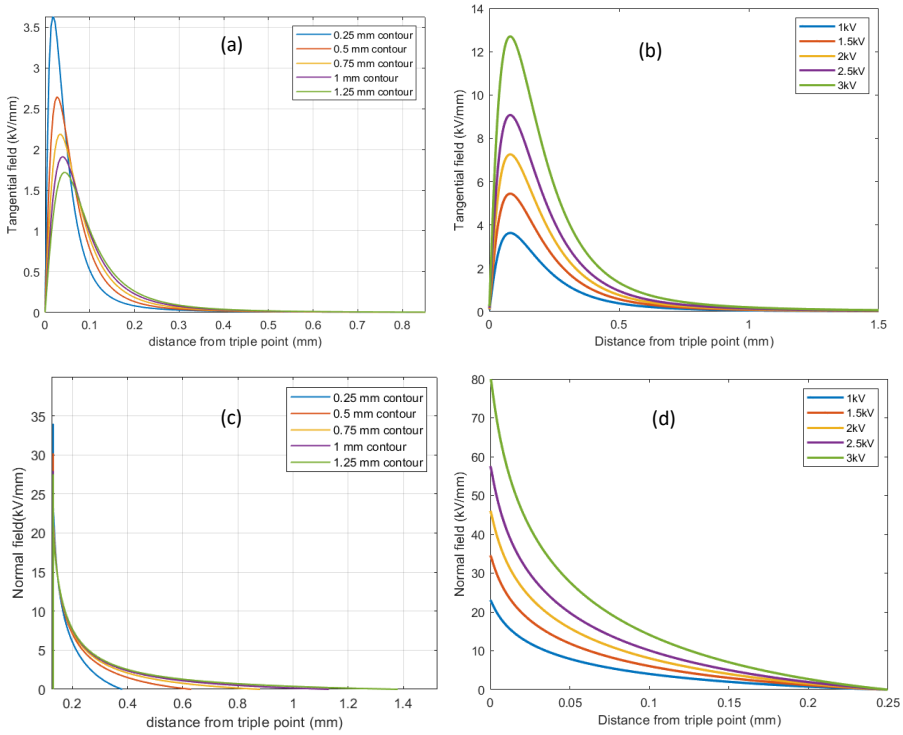

Figure 36. Behavior of tangential and normal field profiles a and c) Under different radius of curvature of high voltage electrode b and d) At different voltage levels with radius of curvature 0.25 mm [Paper VII].

4.2 Estimation of PDIV Using the Tangential Field Profile and Surface Discharge Model

The partial discharge inception voltage is a crucial parameter in insulation design, lifetime, and aging studies of insulation. As per IEC 60270, PDIV is the minimum voltage at which recurrent partial discharges are initially identified. PDIV is induced by the inception electric field (E_s). In [76], E_s is found using (30), referred to as the surface discharge model. This is a modified version of the Niemeyer model for internal discharges, which describes the inception field in internal or gas discharge (32). E_g refers to gas or internal discharges within an air-filled cavity. The quantity U_i^{th} is determined using (33).

$$E_s = 8p\left(1 + \frac{4.3}{\sqrt{pk_s l}}\right) \tag{30}$$

$$k_s \sim \left(\frac{l_2(0.95E_{max})^+ - l_1(0.95E_{max})^-}{l}\right) \tag{31}$$

$$E_g = 25.2p\left(1 + \frac{8.6}{\sqrt{ph_c}}\right) \tag{32}$$

$$\frac{V_S}{E_{PS}} = \frac{U_i^{th}}{E_s} \tag{33}$$

Where: P – pressure (101.325 kPa);
h_c – vertical distance or characteristic distance between two electrodes;
l– horizontal distance from triple point or creepage distance;
V_s – applied voltage;
U_i^{th} – theoretical PDIV;
E_s – surface discharge inception field;
l_1 and l_2 – points where $E_{max} = E_{ps}$;
k_s – scaling factor.

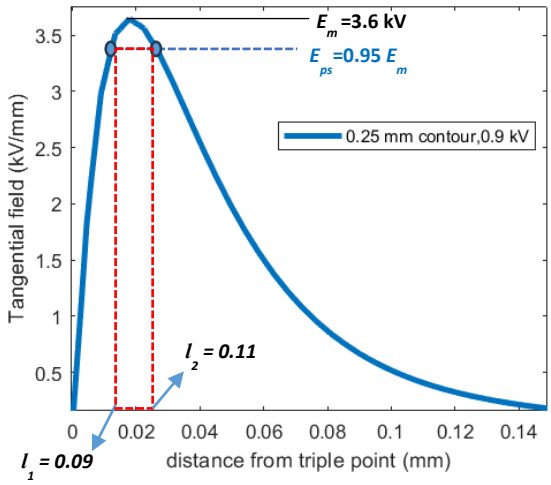

Figure 37. Tangential field profile at 0.9 kV, with circular points illustrating $E_{ps} = 0.95E_m$ and the corresponding distances l_1 and l_2 [Paper VII].

The justification for this assumption ($E_{ps} = 0.95E_m$) is that the occurrence of a PD event is more probable in the vicinity of the maximum field. A rectangle is constructed at $0.95E_m$ on the tangential field profile. The points l_1 and l_2 correspond to where the tangential field reaches $E_{ps} = 0.95E_m$, as illustrated in Figure 37. Intersecting points are utilized for the computation of the k_s [22]. The normal field is not further addressed here, as the tangential field is responsible for the surface discharge; E_s is computed using (30).

Table V presents the values of the parameters. By correlating the simulated tangential electric field profile with the surface partial discharge inception field derived from the partial discharge inception model (31), the electric field strength E_s and $PDIV_{th}$ are determined.

Table V. PDIV estimation under different radii of curvature of high voltage electrode.

R (mm)	E_m (kV/mm)	l_1 (mm)	l_2 (mm)	k_s	E_s (kV/mm)	U_i^{th} (kV)
0.25	3.65	0.09	0.11	0.0004	3.26	0.9
0.5	2.65	0.02	0.03	0.0002	4.27	1.7
0.75	2.19	0.023	0.048	0.0005	3.00	1.4
1	1.91	0.031	0.052	0.0004	3.20	1.8
1.25	1.72	0.03	0.06	0.0006	2.81	1.7

4.3 Experimental Validation

To validate the U_i^{th} with U_i^m, the PD experiment setup was established in the laboratory as shown in Figure 30.

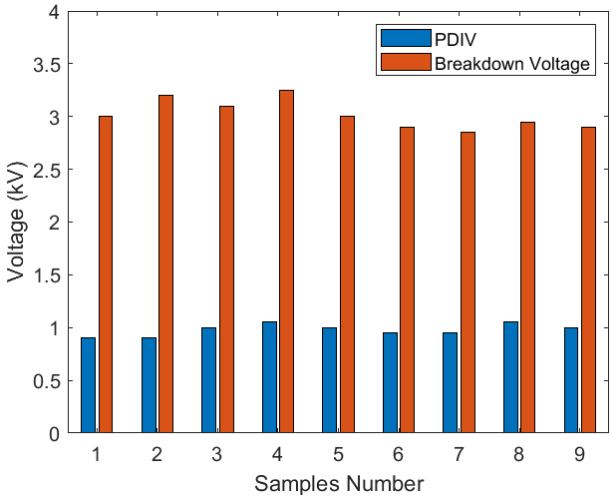

Figure 38. PDIV and breakdown voltage of Nomex film obtained from 9 samples [Paper VIII].

PDIV and breakdown voltage are measured on nine different samples under identical conditions, and the average PDIV was found to be 0.95 kV, which validates the U_i^{th}. Figure 38 shows the PDIV and breakdown voltage (V_b) of nine specimens of Nomex films found during PD measurement. The average breakdown voltage is found to be 3 kV.

5 Lifetime Study of Nomex Insulation and Stages of Aging Under the Influence of Partial Discharges

Surface discharges pose a significant threat to insulation in high-voltage transformers and aircraft equipment. Nomex film with a thickness of 0.13 mm is extensively utilized in both dry and oil-immersed transformers as interlayer insulation, offering an optimal balance of mechanical strength and electrical performance. In electrical machines, it is utilized as slot liners and phase insulation inter-turn insulation due to its lightweight and thermal endurance properties [74]. Surface erosion-based accelerated aging framework replicates the deterioration effects of partial discharges in the field operating conditions. It allows researchers and asset managers to assess the aging behavior of insulation under various operating conditions. It plays a vital role in the selection of materials, design of insulation systems, and preparation of preventive maintenance strategies [61], [72]. Several research articles are available in the literature that focus on the lifetime and condition assessment of Nomex insulation. Table VI briefly describes the related work strengths and limitations.

Table VI. Review of research related to aging and lifetime study of Nomex film.

Ref.	Strengths	Limitations
[77]	Comparison of the PDIV of Nomex and cellulose paper	No analysis of aging or long-term erosion
[78]	The reduced lifespan of Nomex is linked to PWM voltages and thermal stress	Short-term endurance tests
[79]	The behavior of PRPD patterns and PD characteristics at increasing voltage	The study was performed on a modeled cavity within Nomex insulation
[80]	Lifetime study of Nomex and monitoring of maximum charge and number of pulses during lifetime under AC and superposed inter-harmonics	The electrode configuration is not designed for surface discharges
[81]	Comparison of polyimide, polyester, and Nomex under medium frequency square voltage	Based on PDIV and endurance capability. No lifetime study is performed

None of the above studies proposed a continuous surface-erosion-based aging framework that integrates PD measurements and microscope-based analysis from the PD inception until the breakdown. The proposed study bridges that gap by mapping the aging of Nomex film using a four-stage degradation concept under AC voltages. It also sets diagnostic markers that connect Nomex insulation behavior under the influence of surface discharges, offering a useful framework for researchers and insulation designers.

For this, comprehensive PD measurements were performed during the lifetime of Nomex insulations at twice the inception voltage. The purpose of applying 2×PDIV voltage is to conduct accelerated aging and to speed up the degradation process caused by the PD activity. This allows researchers to observe insulation aging and failure mechanisms within a shorter time. By applying a voltage higher than the normal operating level (often a suitable multiple of PD inception voltage, PDIV, and well below its breakdown voltage), PD occurs more frequently and with higher energy, which accelerates chemical and physical degradation (such as erosion, treeing, or pitting) in the insulation material in a short time. This helps estimate insulation lifespan, understand failure modes, and compare the durability of varied materials or designs.

5.1 Measurement Methodology

Figure 30 (a, b) shows the laboratory-based experiment setup designed for the lifetime study of Nomex film. After finding PDIV, the voltage is raised to 2×PDIV, and lifetime PD data are recorded using PRPD patterns and PD features at 15-minute intervals during aging until breakdown. During each measurement, the PRPD pattern, Q_a, and n were recorded within an acquisition time of 1 minute, with a pulse dead time at 20 µs. Microscopic examinations are conducted at each phase of deterioration. Continuous surface erosion is conducted for 480 minutes. Trending attributes of PRPD patterns, PD characteristics, and microscopic images are examined at various stages of the lifetime.

5.2 Four-Stage Aging of Nomex Insulation

Temmen analyzed how an increase in surface conductivity, roughness, and crystal development changes PRPD patterns resulting from partial discharge activity in flat cavities. It provides a theoretical insight into how these surface alterations influence the phase-angle histograms. Figure 39 illustrates Temmen's four-stage degradation concept that correlates the evolution of PRPD patterns with increasing aging. However, Temmen's study is limited to artificial cavities modelled at the insulation surface. It does not consider the lifetime of insulation from PD inception to breakdown [70]. On the contrary, the proposed framework maps the lifetime of Nomex insulation with a stage aging concept through PRPD patterns, PD characteristics, and microscopic analysis. The images are taken from an optical microscope at 40 × magnification.

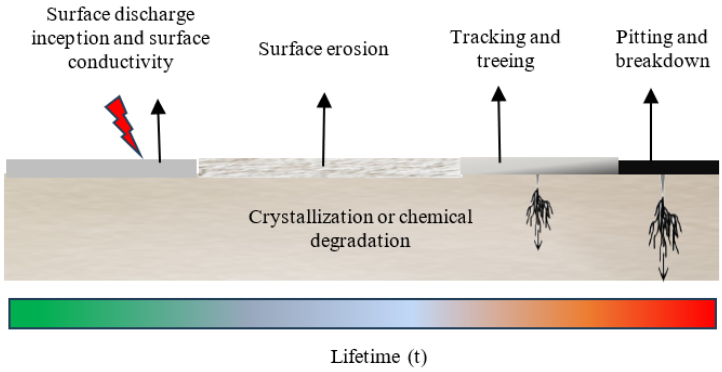

Figure 39. Four-stage degradation of solid insulation based on surface erosion accelerated aging method [Paper VIII].

5.2.1 Inception of Surface Discharges and Increase of Surface Conductivity

Surface discharge inception refers to the moment when electrical discharges initiate along the surface of an insulating material, triggered by an applied voltage. The analysis of the PRPD pattern indicates high PD activity at PDIV, as illustrated in Figure 40 (a). After one hour, the PD activity is drastically reduced, as fewer discharges of magnitude 40...79 pC were observed in the PRPD pattern, as shown in Figure 40 (b). This can be due to an increase in surface conductivity. Air and dissociation products interact with the dielectric surface, collectively enhancing surface conductivity. During PD activity, oxygen is produced that increases conductivity [4], [27], [28]. Considering PRPD patterns, asymmetric patterns were observed at this stage, characterized by increased PD activity

during the positive half-cycle relative to the negative half-cycle of the applied voltage. Considering the phase span, discharges are observed between 50°...70° during the positive half cycle and 200°...250° during the negative half cycle of the applied voltage. This activity lasted for two hours, as illustrated in Figure 40 (b, c). Figure 41 (a, b) shows a physical sample and a microscopic image of Nomex film, with a little black dot highlighting the initiation of discharge.

5.2.2 Occurrence of Surface Erosion on the Surface

During the second stage, the PD activity spread on the insulation surface. The oxidation process results in chemical deterioration and the development of a crystalline structure, making the surface rough. With increasing aging, several byproducts of oxygen, namely CO_2 and CO, are produced, leading to cross-linking, chain scission, and electrical and thermal degradation of insulation. This process changes the chemical structure of the insulation and causes surface erosion [3], [29–31]. Three significant changes were observed in the PRPD pattern. Asymmetrical partial discharge activity is observed with very high PD activity during the positive half-cycle of the applied voltage, shown by orange and yellow colours in the PRPD patterns in Figure 40 (d, e). An increase in PD magnitude is found with discharges ranging from 78...167 pC. The phase span of PD activity is increased with an increasing number of discharges recorded between 0°...60° during the positive half-cycle of the applied voltage and 180°...270° during the negative half-cycle of the applied voltage. This activity also lasted for two hours. The microscopic images show that discharges penetrate the Nomex film, showing signs of surface tracking, as illustrated in Figure 41 (c, d).

5.2.3 Tracking and Treeing

The third stage is the tracking stage; prolonged, repeating discharges result in surface tracking. Tracking under the influence of a continuous electric field forms a conductive channel within the insulation called electrical trees [27], [30]. Considering the PRPD pattern, a symmetrical pattern is observed, with significant discharges ranging from 92 to 382 pC observed at this stage. The severity of PD can be described by an increase in pulse repetition rate, as depicted by the yellow and orange colours in the PRPD patterns in Figure 40 (f, g). Repetitive PD activity is observed between 0...90° during the positive half cycle and 180°...270° during the negative half cycle of the applied voltage. At this stage, PD activity moves towards the zero crossing of the applied voltage, which indicates the tracking phenomenon. Tracking continued for two hours, as shown by PRPD patterns at stage III. The microscopic analysis shows carbonized channels within the insulation depicted in Figure 41 (e, f).

5.2.4 Occurrence of Pitting and breakdown

Continuous erosion and tracking result in pitting on the insulating surface. Pitting forms dark spots on the insulation surface as shown in Figure 41 (g). It is the final stage of degradation that leads to the breakdown [30]. The PRPD pattern shows intense PD activity with charge levels between 360 pC...1.8 nC detected between 0–90° of positive half cycle and between 180°...270° during the negative half cycle of the applied voltage, as shown in Figure 40 (h). The microscopic analysis shows deep black patches within the material's thickness, as illustrated in Figure 41 (e, f). After seven hours of aging, PD activity is intensified in both the positive and negative half-cycles of the applied voltage. After approximately 50 minutes, a breakdown occurred. Figure 40 (h) shows the PRPD pattern before the breakdown.

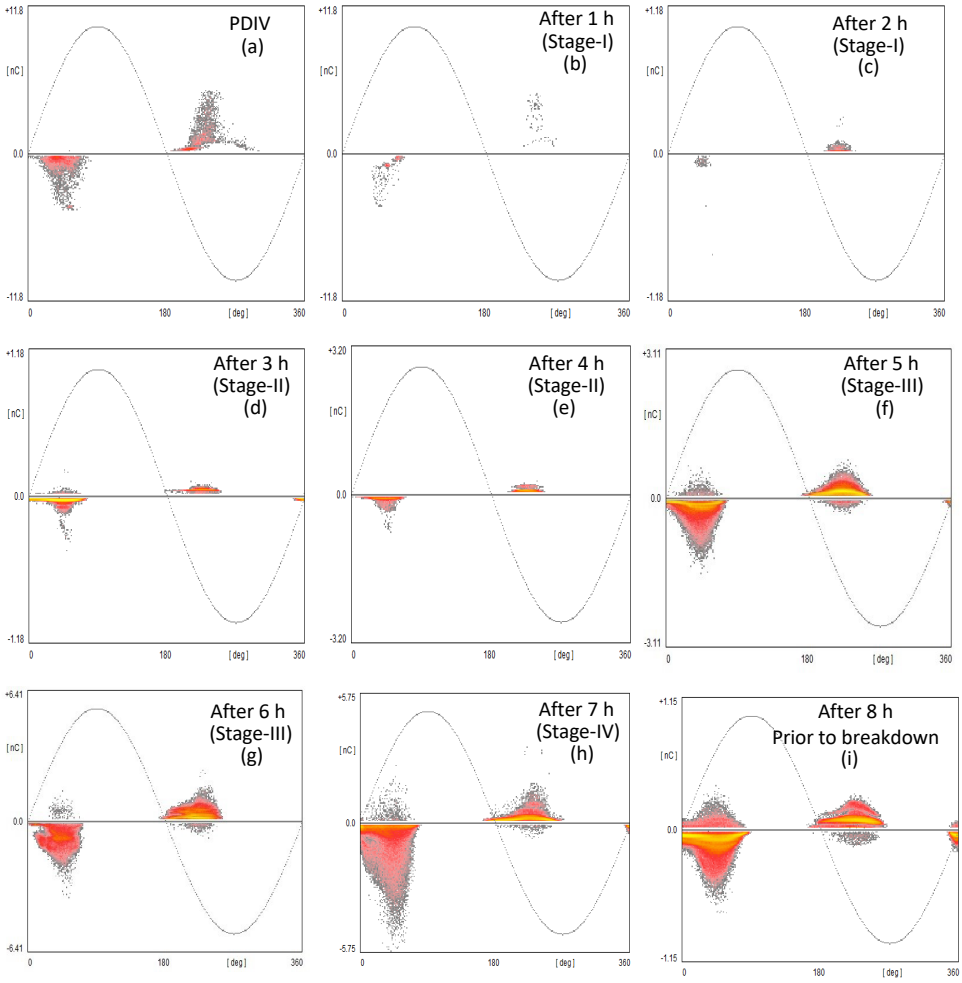

Figure 40. PRPD pattern at four stages of degradation recorded after every hour of aging from PD inception till breakdown [Paper VIII].

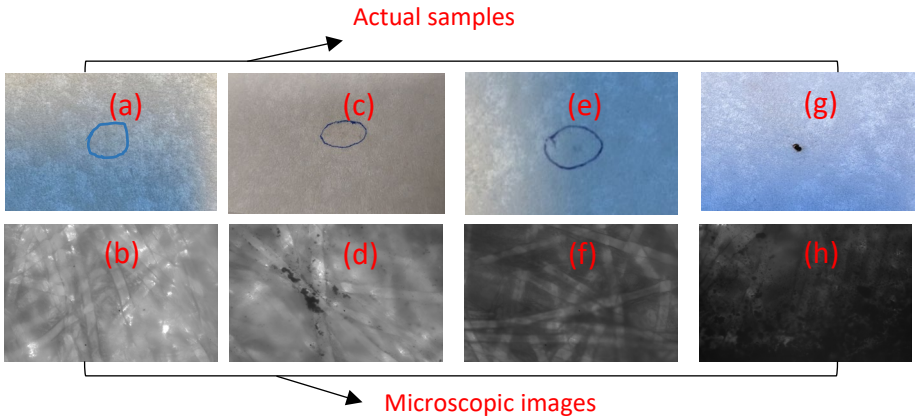

Figure 41. Nomex film specimen at different stages from partial discharge inception to breakdown: Close-up view of physical sample (top row) and microscopic view (bottom row). a and b) Surface discharge inception, c and d) Surface erosion, e and f) tracking, g and h) pitting and breakdown [Paper VIII].

5.3 Behavior of PD Characteristics, Maximum apparent charge (Q_{max}), and Number of Pulses (n_p) During the lifetime of Nomex Insulation Film

Figure 42 illustrates the behavior of Q_{max} during the lifetime of Nomex film. Moving average lines in Figure 42 and Figure 43 smooth out short fluctuations in the graph and identify the major trends the PD characteristics follow during the lifetime of Nomex film. A three-point moving average is applied to Q_{max} and n_p data.

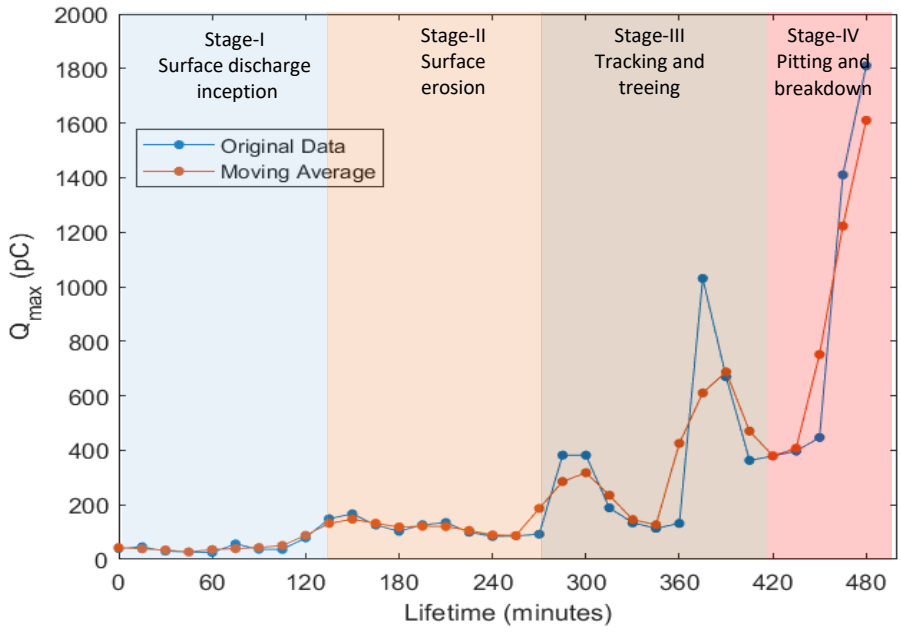

Figure 42. Behavior of Q_{max} at different stages of aging of Nomex film during the entire lifespan from PD inception until breakdown [Paper VIII].

Trendlines of Q_{max} indicate that after PDIV, when the insulating surface is subjected to a strong electric field, low-amplitude PD activity (40…125 pC) is detected. The duration of this activity was two hours. Following two hours, Q_{max} exhibits an undulating trend until seven hours, oscillating between 84 and 382 PC. After seven hours, a drastic increase in Q_{max} is observed. A few minor fluctuations are observed, particularly around 300 and 390 minutes. Tracking creates carbonized paths within the insulation, increasing the local electrical field, which may cause fluctuations in $Q_{max.}$

Figure 43 illustrates the behavior of positive and negative pulses over the lifetime of Nomex material. The trendlines for positive and negative pulses indicate that positive pulses exhibit a progressive increase over time and maintain greater stability in comparison to negative pulses. Upon considering negative pulses, initially, a minimal number of discharges was recorded for a duration of two hours. An undulating trend is observed after two hours and continues until six hours. However, a considerable increase is found in both positive and negative pulses after six hours of aging, i.e., at the third stage.

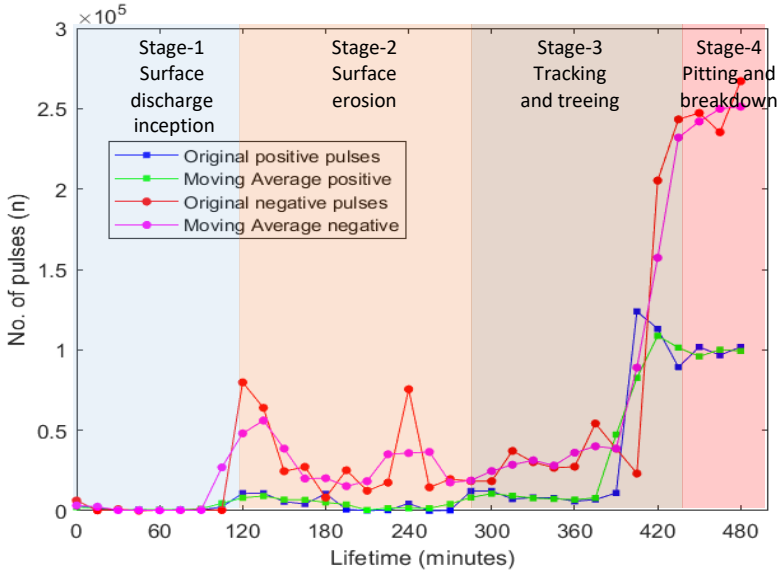

Figure 43. Behavior of the number of positive and negative pulses at different stages of aging of Nomex film during the entire lifespan from PD inception until breakdown [Paper VIII].

Initially, both negative and positive pulses exhibit a modest frequency of occurrence. During the second stage, there is a significant increase in negative pulses, while positive pulses exhibit a slow rise. In the third stage, there is a relative reduction in negative pulses compared to the preceding stage, while positive pulses increase. Before the breakdown, there is a significant increase in negative pulses. At this stage, severe black pitting is seen on the insulating surface, resulting in a breakdown after fifty minutes.

6 Conclusion and Future Work

This chapter presents conclusions drawn from this thesis and outlines potential directions for future research.

6.1 Conclusions

This thesis proposes a multi-method approach for aging and degradation studies of solid insulation, providing guidelines for researchers and asset managers to deeply understand the aging behavior of solid insulation using data-driven and FEM modeling approaches. The study begins with a thorough literature review of aging mechanisms, aging models, and the role of PD measurement in the aging and degradation study of solid insulation. This led to a foundation for a deeper understanding of aging mechanisms, major factors that contribute to aging, and the important aspects of the PD phenomenon. In addition to that, the literature review also highlighted the challenges and gaps in the aging study of solid insulation.

Phenomenological models are useful as their parameters rely on experimental data. Insulating materials can be characterized and assessed based on empirical investigations rather than physical properties. Integrated data-driven tools with signal processing and principal component analysis (PCA) based techniques can play a pivotal role in the extraction of major PD features. These features can contribute to the formulation of phenomenological models. However, the general viability of these models requires expensive experimental studies across different insulating materials and operating conditions.

This thesis proposed an efficient approach that advances the analysis of PD data. PD measurement is affected by noise, sensor oscillations, and pulse reflections, which distort original PD signals. This issue is addressed by implementing discrete DWT-based denoising and local maxima techniques. An algorithm is developed that denoises PD data and detects PD pulse peaks above a certain threshold value. The key objective is not to detect every individual peak that appears, but to detect most PD pulses that can describe the behavior of PD activity. A window method is then implemented around each peak to extract the corresponding PD pulse and relevant features for analysis of PD data.

The selection of optimum features was another major challenge, as 11 features were extracted from individual PD pulses. Principal component analysis (PCA) is an efficient dimensionality reduction technique that identifies major features that can describe PD activity. It also contributes to the classification and clustering of PD data if two or more types of PD are available in the PD dataset. For this, a machine learning based technique is implemented. It utilizes hierarchical clustering to classify different PD types. This PCA and clustering algorithm was implemented to describe the aging and degradation stages of Nomex insulation.

Experimental results on modelled cable defects illustrated that with increasing voltage, the pulse height increases to a certain level of voltage. However, as the voltage is further raised, the pulse height remains stable, while the occurrence of pulses increases near the zero crossing of the applied voltage in the PRPD pattern. The results also revealed that with increasing applied voltage, the phase span of PD activity widens, and the number of pulses also increases at a certain level of voltage.

PDIV is an important parameter used for endurance assessment and design of the insulation system in power system assets. The results showed that the three-leg approach is a validated approach for the estimation of surface PDIV in solid insulation.

It utilizes FEM modeling, a surface discharge model, and an experimental setup with a two-electrode configuration. In the first and the second leg, a FEM model is used to determine tangential field profiles across the insulation using different electrode configurations. In the second leg, field profiles are used to estimate the surface discharge inception field and inception voltage using the surface discharge model. In the third leg, the experiment setup is used to determine the PDIV of the Nomex insulation.

Lifetime assessment of Nomex insulation using surface erosion accelerated aging showed that aging on the Nomex film follows four stages of degradation, i.e., surface discharge inception, surface erosion, tracking, and finally pitting and breakdown. These four stages were validated using PRPD patterns, PD characteristics, and microscopic analysis. This study is useful, particularly for the assets that utilize Nomex insulation. Further investigations can be conducted to investigate the behavior of surface discharges under different environmental conditions, such as temperature, pressure, or other operating conditions.

In conclusion, the proposed frameworks, including data-driven tools, FEM models, and surface erosion-based lifetime studies, can advance condition monitoring and lifetime studies of solid insulation in power system assets.

6.2 Future Work

While this thesis proposed novel frameworks that can contribute to condition assessment and lifetime study of insulation used in power system assets, it also elucidates directions for future research to enhance their applicability and integration into asset management and design practices. Some of the potential areas for further research are outlined as follows:

- The implementation of ML or artificial intelligence tools to automate the optimum selection of thresholds or the detection of PD pulses in acquired PD data.
- Extensive experimental investigation on commonly used insulating materials such as XLPE, polyethylene, Nomex, and polyimide films under varying environmental conditions and defects typically encountered in field applications. The concrete PD features that describe aging can contribute to the development of phenomenological models.
- Implementation of the three-leg approach under varying environmental conditions and different insulating materials.
- Development of pattern recognition algorithms for the recognition of PRPD patterns at distinct stages of aging.

List of Figures

List of Tables

References

[1] A. Subramaniam, A. Sahoo, S. S. Manohar, S. J. Raman and S. K. Panda, "Switchgear Condition Assessment and Lifecycle Management: Standards, Failure Statistics, Condition Assessment, Partial Discharge Analysis, Maintenance Approaches, and Future Trends," *IEEE Electrical Insulation Magazine*, vol. 37, no. 3, pp. 27–41, May/June 2021, https://doi:10.1109/MEI.2021.9399911.

[2] J. He, C. Somogyi, A. Strandt and N. A. O. Demerdash, "Diagnosis of stator winding short-circuit faults in an interior permanent magnet synchronous machine," *IEEE Energy Conversion Congress and Exposition (ECCE), Pittsburgh, PA*, USA, 2014, pp. 3125–3130, https://doi:10.1109/ECCE.2014.6953825.

[3] S. H. Lee and C. K. Chang, "Separation of Transformers for Class 1E Systems in Nuclear Power Plants," *Science and Technology of Nuclear Installations*, 2017(1), 3976049. https://doi.org/10.1155/2017/3976049.

[4] W. Higinbotham, "The Premier Electrical Maintenance and Safety Event Review of Medium-Voltage Asset Failure Investigations" *The Premier Electrical Maintenance and Safety Event*, 2018.

[5] J. Densley, "Ageing mechanisms and diagnostics for power cables - an overview," in IEEE Electrical Insulation Magazine, vol. 17, no. 1, pp. 14–22, Jan.-Feb. 2001, https://doi:10.1109/57.901613.

[6] T. W. Dakin, "Electrical Insulation Deterioration Treated as a Chemical Rate Phenomenon," *Transactions of the American Institute of Electrical Engineers*, vol. 67, no. 1, pp. 113–122, Jan. 1948, doi: 10.1109/T-AIEE.1948.5059649.

[7] G. Mazzanti and G. C. Montanari, "Electrical aging and life models: the role of space charge," *IEEE Transactions on Dielectrics and Electrical Insulation*, vol. 12, no. 5, pp. 876–890, Oct. 2005, doi: 10.1109/TDEI.2005.1522183.

[8] C. Zhou, H. Yi, and X. Dong, "Review of recent research towards power cable life cycle management", *High Voltage*, 2(3), 179-187. https://doi.org/10.1049/hve.2017.0037.

[9] E. David, J., L. Parpal and J.P. Crine, "Aging of XLPE cable insulation under combined electrical and mechanical stresses," *Conference Record of the 1996 IEEE International Symposium on Electrical Insulation*, Montreal, QC, Canada, 1996, pp. 716–719 vol.2, doi: 10.1109/ELINSL.1996.549445.

[10] M. Choudhary, M. Shafiq, I. Kiitam, A. Hussain, I. Palu, and P. Taklaja, "A Review of Aging Models for Electrical Insulation in Power Cables," *Energies (Basel)*, vol. 15, no. 9, p. 3408, May 2022, doi: 10.3390/en15093408.

[11] S. Hellesø, J. T. Benjaminsen, M. Selsjord and S. Hvidsten, "Water tree initiation and growth in XLPE cables under static and dynamic mechanical stress," *2012 IEEE International Symposium on Electrical Insulation*, San Juan, PR, USA, 2012, pp. 623–627, doi: 10.1109/ELINSL.2012.6251546.

[12] J. Su, B. Du, J. Li, and Z. Li, "Electrical tree degradation in high-voltage cable insulation: Progress and challenges," *High Voltage*, 5(4), 353–364. https://doi.org/10.1049/hve.2020.0009.

[13] S. Gutierrez, I. Sancho, L. Fontan and J. D. No, "Effect of protrusions in HVDC cables," *IEEE Transactions on Dielectrics and Electrical Insulation*, vol. 19, no. 5, pp. 1774–1781, October 2012, doi: 10.1109/TDEI.2012.6311527.

[14] L. Simoni, “A General Approach to the Endurance of Electrical Insulation under Temperature and Voltage,” *IEEE Transactions on Electrical Insulation*, vol. EI-16, no. 4, pp. 277–289, Aug. 1981, doi: 10.1109/TEI.1981.298361.

[15] L. Simoni, “General Equation of the Decline in the Electric Strength for Combined Thermal and Electrical Stresses,” *IEEE Transactions on Electrical Insulation*, vol. EI-19, no. 1, pp. 45–52, Feb. 1984, doi: 10.1109/TEI.1984.298732.

[16] L. Simoni, G. Mazzanti, G. C. Montanari and L. Lefebre, “A general multi-stress life model for insulating materials with or without evidence for thresholds,” *IEEE Transactions on Electrical Insulation*, vol. 28, no. 3, pp. 349–364, June 1993, doi: 10.1109/14.236212.

[17] L. Dissado, G. Mazzanti and G. C. Montanari, “The incorporation of space charge degradation in the life model for electrical insulating materials,” *IEEE Transactions on Dielectrics and Electrical Insulation*, vol. 2, no. 6, pp. 1147–1158, Dec. 1995, doi: 10.1109/TDEI.1995.8881933.

[18] P. Cygan and J. R. Laghari, “Models for insulation aging under electrical and thermal multistress,” *IEEE Transactions on Electrical Insulation*, vol. 25, no. 5, pp. 923–934, Oct. 1990, doi: 10.1109/14.59867.

[19] E. L. Brancato, “Insulation Aging a Historical and Critical Review,” *IEEE Transactions on Electrical Insulation*, vol. EI-13, no. 4, pp. 308–317, Aug. 1978, doi: 10.1109/TEI.1978.298079.

[20] L. E. Fisher, C. D. Haries and J. M. Lehr, “Initiation and Growth of the Secondary Electron Avalanche along High-Gradient Insulators in Vacuum,” *IEEE Transactions on Dielectrics and Electrical Insulation*, vol. 28, no. 3, pp. 972–980, June 2021, doi: 10.1109/TDEI.2021.009400.

[21] “IEEE Guide for the Statistical Analysis of Electrical Insulation Voltage Endurance Data,” in *ANSI/IEEE Std 930-1987*, vol., no., pp. 1–28, 21 Aug. 1987, doi: 10.1109/IEEESTD.1987.86250.

[22] G. C. Stone and J. F. Lawless, “The Application of Weibull Statistics to Insulation Aging Tests,” *IEEE Transactions on Electrical Insulation*, vol. EI-14, no. 5, pp. 233–239, Oct. 1979, doi: 10.1109/TEI.1979.298226.

[23] G. Pattini and L. Simoni, “Discussion on modeling of voltage endurance,” *IEEE International Conference on Electrical Insulation, Boston, MA, USA, 1980*, pp. 15–15, doi: 10.1109/ICEI.1980.7470860.

[24] T. S. Ramu, “On the Estimation of Life of Power Apparatus Insulation Under Combined Electrical and Thermal Stress,” *IEEE Transactions on Electrical Insulation*, vol. EI-20, no. 1, pp. 70–78, Feb. 1985, doi: 10.1109/TEI.1985.348759.

[25] W. Nelson, “Analysis of Accelerated Life Test Data - Part I: The Arrhenius Model and Graphical Methods,” *IEEE Transactions on Electrical Insulation*, vol. EI-6, no. 4, pp. 165–181, Dec. 1971, doi: 10.1109/TEI.1971.299172.

[26] S. Sofyan, M. D. Faraby, K. Naim, A. R. Idris, S. S. Akhmad, and H. Firmansyah, “Analysis of estimated age of distribution transformer against loading at ULP Panakkukang with the Montsinger Method,” *J. Phys.: Conf. Ser.,* vol. 2596, no. 1, art. no. 012054, 2023, doi:10.1088/1742-6596/2596/1/012054.

[27] G. C. Montanari, G. Pattini and L. Simoni, “Long - Term Behavior of XLPE Insulated Cable Models,” *IEEE Transactions on Power Delivery*, vol. 2, no. 3, pp. 596–602, July 1987, doi: 10.1109/TPWRD.1987.4308151.

[28] G. Mazzanti and G. C. Montanari, “A comparison between XLPE and EPR as insulating materials for HV cables,” *IEEE Transactions on Power Delivery*, vol. 12, no. 1, pp. 15–28, Jan. 1997, doi: 10.1109/61.568220.

[29] G. C. Montanari, G. Mazzanti and L. Simoni, “Progress in electrothermal life modeling of electrical insulation during the last decades,” *IEEE Transactions on Dielectrics and Electrical Insulation*, vol. 9, no. 5, pp. 730–745, Oct. 2002, doi: 10.1109/TDEI.2002.1038660.

[30] J. P. Crine, J. L. Parpal and G. Lessard, “A model of aging of dielectric extruded cables,” *Proceedings of the 3rd International Conference on Conduction and Breakdown in Solid Dielectrics*, Trondheim, Norway, 1989, pp. 347–351, doi: 10.1109/ICSD.1989.69218.

[31] A. Cavallini, D. Fabiani and G. C. Montanari, “Power electronics and electrical insulation systems - part 2: life modeling for insulation design,” *IEEE Electrical Insulation Magazine*, vol. 26, no. 4, pp. 33–39, July-Aug. 2010, doi: 10.1109/MEI.2010.5511187.

[32] G. Mazzanti, G. C. Montanari and L. A. Dissado, “A space-charge life model for ac electrical aging of polymers,” *IEEE Transactions on Dielectrics and Electrical Insulation*, vol. 6, no. 6, pp. 864–875, Dec. 1999, doi: 10.1109/94.822029.

[33] C. L. Griffiths, J. Freestone and R. N. Hampton, “Thermoelectric aging of cable grade XLPE,” *Conference Record of the 1998 IEEE International Symposium on Electrical Insulation (Cat. No.98CH36239)*, Arlington, VA, USA, 1998, pp. 578–582, vol. 2, doi: 10.1109/ELINSL.1998.694859.

[34] G. Bahder, T. Garrity, M. Sosnowski, R. Eaton and C. Katz, “Physical Model of Electric Aging and Breakdown of Extruded Polymeric Insulated Power Cables,” *IEEE Transactions on Power Apparatus and Systems*, vol. PAS-101, no. 6, pp. 1379–1390, June 1982, doi: 10.1109/TPAS.1982.317185.

[35] G. C. Montanari, “Aging and life models for insulation systems based on PD detection,” *IEEE Transactions on Dielectrics and Electrical Insulation*, vol. 2, no. 4, pp. 667–675, Aug. 1995, doi: 10.1109/94.407031.

[36] IEC 60270: High-voltage test techniques – Partial discharge measurements, *International Electrotechnical Commission (IEC)*, Geneva, Switzerland, Standard, 3rd ed., 2000.

[37] R. Bartnikas, “Partial discharges. Their mechanism, detection and measurement,” *IEEE Transactions on Dielectrics and Electrical Insulation*, vol. 9, no. 5, pp. 763–808, Oct. 2002, doi: 10.1109/TDEI.2002.1038663.

[38] Ivar Kiitam, “Insulation durability and measurement of partial discharge,” *Tallinn University of Technology*, Tallinn, 2021.

[39] G. C. Stone, “Partial discharge diagnostics and electrical equipment insulation condition assessment,” *IEEE Transactions on Dielectrics and Electrical Insulation*, vol. 12, no. 5, pp. 891–904, Oct. 2005, doi: 10.1109/TDEI.2005.1522184.

[40] R. J. Van Brunt, “Physics and chemistry of partial discharge and corona. Recent advances and future challenges,” *IEEE Transactions on Dielectrics and Electrical Insulation*, vol. 1, no. 5, pp. 761–784, Oct. 1994, doi: 10.1109/94.326651.

[41] P. H. F. Morshuis, “Degradation of solid dielectrics due to internal partial discharge: some thoughts on progress made and where to go now,” *IEEE Transactions on Dielectrics and Electrical Insulation*, vol. 12, no. 5, pp. 905–913, Oct. 2005, doi: 10.1109/TDEI.2005.1522185.

[42] J. C. Devins, “The physics of partial discharges in solid dielectrics,” *Conference on Electrical Insulation & Dielectric Phenomena - Annual Report*, Claymont, DE, USA, 1984, pp. 15–31, doi: 10.1109/EIDP.1984.7683959.

[43] P. H. F. Morshuis, “Partial Discharge Mechanisms,” *Delft University*, Delft, Netherlands, 1993.

[44] M. Shafiq, M. Lehtonen, G. A. Hussain and L. Kütt, “Performance evaluation of PD monitoring technique integrated into medium voltage cable network for smart condition assessment,” *2014 Electric Power Quality and Supply Reliability Conference (PQ)*, Rakvere, Estonia, 2014, pp. 351–357, doi: 10.1109/PQ.2014.6866840.

[45] M. Hashmi, S. Hänninen and M. Lehtonen, “Intelligent fault diagnosis for on-line condition monitoring in smart distribution networks,” *2012 IEEE International Conference on Condition Monitoring and Diagnosis*, Bali, Indonesia, 2012, pp. 946–949, doi: 10.1109/CMD.2012.6416309.

[46] M.Muhr, T.Strehl, E.Gulski, K.Feser, E.Gockenbach, W.Hauschild, E.Lemke, “Sensors and sensing used for non-conventional PD detection”, *Proceedings 41 Cigré 2006 session international council on large electric systems*, Paris, Frace, 2006.

[47] P. L. Lewin, J. Steele-Davies, S.M. Rowland, V.Catterson, C.Johnstone, C.Walton, “The state of the art of condition monitoring: where do we go from here?”, *International Electrical Insulation Conference (INSUCON)*, Stanford, USA, 2013.

[48] R.-N. Wu and C. -K. Chang, “The Use of Partial Discharges as an Online Monitoring System for Underground Cable Joints,” *IEEE Transactions on Power Delivery*, vol. 26, no. 3, pp. 1585–1591, July 2011, doi: 10.1109/TPWRD.2011.2124474.

[49] M. M. Yaacob, M. A. Alsaedi, J. R. Rashed, A. M. Dakhil, and S. F. Atyah, “Review on partial discharge detection techniques related to high voltage power equipment using different sensors,” *Photonics Sensors*, vol. 4, no. 4, pp. 325–337, Dec. 2014, doi: 10.1007/s13320-014-0146-7.

[50] CIGRE WG D1.33 Task Force 05, “Experiences in partial discharge detection of distribution power cable systems,” *Electra*, no. 208, pp. 35–43, Jun. 2003.

[51] N. C. Sahoo, M. M. A. Salama and R. Bartnikas, “Trends in partial discharge pattern classification: a survey,” *IEEE Transactions on Dielectrics and Electrical Insulation*, vol. 12, no. 2, pp. 248–264, April 2005, doi: 10.1109/TDEI.2005.1430395.

[52] G. Stone, S. Campbell and S. Tetreault, “Inverter-Fed Drives: Which Motor Stators Are at Risk*?,” IEEE Industry Applications Magazine*, vol. 6, no. 5, pp. 17–22, Sept.-Oct. 2000, doi: 10.1109/2943.863631.

[53] G. C. Montanari, P. Seri and G. Stone, “Prospects for increasing supply voltage and design of electrical field rotating machine windings supplied from power electronics,” *IEEE Electrical Insulation Magazine*, vol. 36, no. 3, pp. 31–38, May-June 2020, doi: 10.1109/MEI.2020.9063561.

[54] G. C. Montanari, R. Hebner, P. Morshuis and P. Seri, “An Approach to Insulation Condition Monitoring and Life Assessment in Emerging Electrical Environments,” *IEEE Transactions on Power Delivery*, vol. 34, no. 4, pp. 1357–1364, Aug. 2019, doi: 10.1109/TPWRD.2019.2897905.

[55] M. Kaufhold, H. Aninger, M. Berth, J. Speck and M. Eberhardt, “Electrical stress and failure mechanism of the winding insulation in PWM-inverter-fed low-voltage induction motors,” *IEEE Transactions on Industrial Electronics*, vol. 47, no. 2, pp. 396–402, April 2000, doi: 10.1109/41.836355.

[56] G. C. Montanari, M. Shafiq, and R. Mcginnis, “Coming Challenges in Electrified Transportation and Impact on Electrical Insulation Reliability: Ships and Aircrafts,” *ATINER’s Conference Paper Proceedings Series, Athens, Greece*, 2023.

[57] H. Okubo, N. Hayakawa and A. Matsushita, “The relationship between partial discharge current pulse waveforms and physical mechanisms,” *IEEE Electrical Insulation Magazine*, vol. 18, no. 3, pp. 38–45, May-June 2002, doi: 10.1109/MEI.2002.1014966.

[58] M. Choudhary, M. Shafiq, I. Kiitam, I. Palu, and P. Taklaja, “Study on the Progression of Surface Partial Discharge in Power Cables,” *IEEE 63rd Annual International Scientific Conference on Power and Electrical Engineering of Riga Technical University* (RTUCON), 2022, doi: 10.1109/RTUCON56726.2022.9978804.

[59] T. Okamoto and H. Uehara, “Partial Discharge Current Measurements With Small Discharge Gaps Over Polyimide Film,” *IEEE Transactions on Dielectrics and Electrical Insulation*, vol. 30, no. 1, pp. 158–164, Feb. 2023, doi: 10.1109/TDEI.2022.3226133.

[60] J. P. Steiner, P. H. Reynolds and W. L. Weeks, “Estimating the location of partial discharges in cables,” *IEEE Transactions on Electrical Insulation*, vol. 27, no. 1, pp. 44–59, Feb. 1992, doi: 10.1109/14.123440.

[62] S. Sriram, S. Nitin, K. M. M. Prabhu and M. J. Bastiaans, “Signal denoising techniques for partial discharge measurements,” *IEEE Transactions on Dielectrics and Electrical Insulation*, vol. 12, no. 6, pp. 1182–1191, Dec. 2005, doi: 10.1109/TDEI.2005.1561798.

[64] A. Cavallini, M. Conti, A. Contin and G. C. Montanari, “Advanced PD inference in on-field measurements. II. Identification of defects in solid insulation systems,” in *IEEE Transactions on Dielectrics and Electrical Insulation*, vol. 10, no. 3, pp. 528–538, June 2003, doi: 10.1109/TDEI.2003.1207481.

[65] P. Seri, R. Ghosh, and G. C. Montanari, “An Unsupervised Approach to Partial Discharge Monitoring in Rotating Machines: Detection to Diagnosis with Reduced Need of Expert Support,” *IEEE Transactions on Energy Conversion*, vol. 36, no. 3, pp. 2485–2492, Sep. 2021, doi: 10.1109/TEC.2021.3050324.

[66] M. Choudhary, I. Palu, I. Kiitam, M. Shafiq, P. Taklaja, and A. Bhattarai, “Denoising and Extraction of Partial Discharge Pulse Characteristics Using Wavelet Denoising and Local Maxima Method,” *IEEE International Conference on Power and Energy (PECon),* 2024, doi: 10.1109/PECON62060.2024.10827085.

[67] X. Ma, C. Zhou and I. J. Kemp, “Automated wavelet selection and thresholding for PD detection,” in *IEEE Electrical Insulation Magazine*, vol. 18, no. 2, pp. 37–45, March-April 2002, doi: 10.1109/57.995398.

[68] F. H. Kreuger, E. Gulski and A. Krivda, “Classification of partial discharges,” *IEEE Transactions on Electrical Insulation*, vol. 28, no. 6, pp. 917–931, Dec. 1993, doi: 10.1109/14.249365.

[69] A. Contin, A. Cavallini, G. C. Montanari, G. Pasini and F. Puletti, “Digital detection and fuzzy classification of partial discharge signals,” *IEEE Transactions on Dielectrics and Electrical Insulation*, vol. 9, no. 3, pp. 335–348, June 2002, doi: 10.1109/TDEI.2002.1007695.

[70] M. Choudhary, I. Palu, I. Kiitam, M. Shafiq, and P. Taklaja, “Study of Partial Discharge Characteristics in Medium Voltage Cable Insulation with Internal Defect,” *IEEE International Conference on High Voltage Engineering and Applications (ICHVE), 2024*, doi: 10.1109/ICHVE61955.2024.10676188.

[71] M. Choudhary, M. Shafiq, A. Bhattarai, I. Kiitam, P. Taklaja, and I. Palu, “A comprehensive study of partial discharge based extrinsic aging in nomex insulation films: Modeling, simulation and measurement,” Electric Power Systems Research, vol. 245, Aug. 2025, doi: 10.1016/j.epsr.2025.111663.

[72] K. Temmen**,** “Evaluation of surface changes in flat cavities due to ageing by means of phase-angle resolved partial discharge measurement,” *Journal of Physics D: Applied Physics*, vol. 33, no. 6, pp. 603–608, Mar. 2000, doi: 10.1088/0022-3727/33/6/303.

[73] G. C. Montanari, S. Schwartz and R. Cuzner, “On the Characterization of Partial-Discharge Endurance of Dielectric Materials for Aerospace Applications,” in *IEEE Transactions on Aerospace and Electronic Systems*, vol. 59, no. 6, pp. 7590–7599, Dec. 2023, doi: 10.1109/TAES.2023.3293455.

[74] Dupont, “Nomex® Paper Protects Critical Components in Electronic Applications.” Accessed: Jun. 30, 2025. [Online]. Available: https://www.dupont.com/products/nomex-400-series.html.

[75] G. C. Montanari, M. Shafiq, S. B. Myneni, M. Lizcano, and T. S. Williams, “Electrical Characterization of Boron Nitride-Filled Insulation for Aerospace and Avionics Applications,” *Energies*, vol. 17, no. 12, Jun. 2024, doi: 10.3390/en17123016.

[76] P. Cambareri and G. Montanari, “A Surface Discharge Model for the Design of Surface Components of Insulation Systems Under AC Stress in Industrial Electronics Environments,” *IEEE Journal of Emerging and Selected Topics in Industrial Electronics*, vol. 4, no. 2, pp. 698–706, Nov. 2022, doi: 10.1109/jestie.2022.3221001.

[77] H. Moranda, H. Moscicka-Grzesiak, P. Przybylek, K. Walczak, and R. Szewczyk, “Comparative tests of partial discharges in Nomex® 910 paper and cellulose paper,” *Energies (Basel)*, vol. 13, no. 3, 2020, doi: 10.3390/en13030647.

[78] C. Zheng, Q. Wang, H. Wang, Z. Shen, F. F. Da Silva, and C. L. Bak, “Partial discharge inception and deterioration of Nomex paper under repetitive square wave voltage,” *IEEE International Conference on High Voltage Engineering and Applications* (ICHVE) 2022, doi: 10.1109/ICHVE53725.2022.9961729.

[79] S. Zhang et al., “Investigation on the partial discharge of the cavity in Nomex insulation for mining dry type transformer,” *12th International Conference on the Properties and Applications of Dielectric Materials (ICPADM)*, Xi’an, China, 2018, pp. 525–529, doi: 10.1109/ICPADM.2018.8401044.

[80] X. Li *et al.*, “Partial discharge characteristics of oil-paper insulation for on-board traction transformers under superposed inter-harmonic AC voltages,” *IEEE Transactions on Dielectrics and Electrical Insulation*, vol. 27, no. 1, pp. 240–248, Feb. 2020, doi: 10.1109/TDEI.2019.008404.

[81] C. Zheng, Q. Wang, H. Wang, Z. Shen, F. F. Da Silva, and C. L. Bak, “Comparative PDIV and endurance studies on different insulating materials used for medium frequency transformers,” in *2022 IEEE International Conference on High Voltage Engineering and Applications, ICHVE 2022*, Institute of Electrical and Electronics Engineers Inc., 2022. doi: 10.1109/ICHVE53725.2022.9961619.

Acknowledgments

This thesis is the result of the contributions of many individuals whose support, guidance, and encouragement were instrumental throughout my PhD journey.

Primarily, I would like to extend my sincere gratitude to my supervisor Prof. Ivo Palu, and co-supervisor Ivar Kiitam, for their unwavering support, constant encouragement, and invaluable guidance during my PhD journey. The quality and direction of this research have been significantly influenced by their patient mentorship, profound expertise, and insightful feedback.

I am also grateful to Muhammad Shafiq for providing me with this opportunity. His support and guidance in this endeavour are deeply appreciated. I would like to thank Abhinav Bhattarai for his support in FEM modeling and Marten Pärg for assisting with microscopic imaging of Nomex films. I would like to thank Paul Taklaja for his support in the HV Lab. I am also very thankful Electrical Power Engineering & Mechatronics Department staff for their academic support throughout the various stages of my PhD journey.

I also would like to thank the Estonian Government for investing in my future by giving financial support that facilitated the completion of my PhD journey. This research was additionally supported by the Estonian Research Council's grant PSG632 "Aging Behavior of Medium Voltage Cables under Smart Grid Operation."

Finally, I would like to extend my most profound gratitude to my family. To my parents, brothers, wife, and son. I am grateful for their unwavering love, devotion, and moral support. Special thanks to my wife Hem Lata Choudhary and son Chervic. Their confidence in me has consistently served as my greatest asset. Their patience, sacrifices, and understanding during the countless hours I gave this research have been genuinely inspiring and motivating. I dedicate this thesis to my beloved wife and my dearest son.

In the end I would like to thank all those who supported me and believed in me throughout this PhD journey. I am incredibly grateful for your participation in this endeavour.

Abstract

A Multi-Method Approach to Solid Insulation Aging Based on Partial Discharge Measurement

This thesis presents a multi-method framework for the aging and degradation behavior of solid insulation materials, focusing on Nomex and medium voltage cross-linked polyethylene (XLPE) cable insulation, utilizing efficient partial discharge (PD) data analysis, finite element method (FEM) modeling, and experimental investigation. A multifaceted approach has been adopted to examine the electrical aging process, develop data-driven tools, and validate modeling frameworks. The thesis begins with a comprehensive review of primary factors that influence the aging of insulation. Followed by an in-depth comparison of insulation aging models presented over the past three decades, highlighting their strengths and limitations and the pivotal role of PD measurement in the aging and degradation study of solid insulation. The literature thus provides a foundation for identifying existing research gaps and guiding future advancements in insulation aging and degradation studies.

An efficient data-driven toolset is designed that detects PD pulses and extracts multiple features by utilizing wavelet-based denoising and local maxima techniques. This framework is further augmented through the integration of principal component analysis (PCA) for optimum feature selection and advanced machine learning techniques such as hierarchical clustering for classification and clustering of PD data. Moreover, a fuzzy logic algorithm is employed that precisely identifies PD sources (corona, surface, internal), thereby providing a rule-based interpretation of intricate discharge patterns. The designed toolset was validated on various data sets obtained from experiments on XLPE cable insulation and Nomex film under physically modelled defects and aging scenarios.

Partial discharge inception voltage (PDIV) is a critical parameter in the assessment of insulation dielectric strength and aging behavior. It is one of the crucial markers used in insulation system design. A three-leg approach is devised that utilizes FEM based simulation and surface discharge model to estimate PDIV of Nomex film. Simulated PDIV is validated by experimental PD measurements, which confirm the model's dependability and accuracy.

The last section of the work evaluates the lifetime performance of Nomex film insulation through a surface erosion-based accelerated aging procedure. A four-stage degradation methodology is adopted to characterize the distinct stages of insulation aging from the PD inception to the breakdown. Phase resolved partial discharge (PRPD) patterns, PD characteristics, and microscopic analysis are employed to differentiate these phases. The study is useful for electrical assets utilizing Nomex insulation and where surface discharge is a major risk and causes failure of insulation. This research offers a framework for surface erosion-based accelerated aging to investigate the behavior of surface discharges under different supply and environmental conditions.

Overall, this thesis contributes to a validated framework that advances insulation diagnostics and can play a key role in condition monitoring and lifetime prediction of solid insulation systems used in electrical assets.

Lühikokkuvõte

Osalahenduste mõõtmisel põhinev mitmemeetodiline lähenemine tahke isolatsiooni vananemisele

Käesolevas väitekirjas esitatakse laiapõhjaline raamistik tahkete isoleermaterjalide vananemis- ja lagunemiskäitumise uurimiseks, keskendudes Nomex'ile ja keskpingekaablites kasutatava ristsillatud polüetüleenist (XLPE) valmistatud isolatsioonile. Uurimistöös kasutatakse osalahenduste (PD) andmeanalüüsi, lõplike elementide meetodiga (FEM) modelleerimist ning katseliselt saadud tulemusi. Rakendatud on mitmekülgset lähenemisviisi elektrilise vananemise protsessi uurimiseks, andmepõhiste vahendite väljatöötamiseks ning modelleerimisraamistike valideerimiseks. Väitekirjas antakse põhjalik ülevaade isolatsiooni vananemist mõjutavatest peamistest teguritest. Samuti teostatakse süvitsi võrdlus viimase kolmekümne aasta jooksul arendatud isolatsiooni vananemise mudelite kohta, keskendudes nende tugevustele ja piirangutele, ning käsitletakse PD mõõtmise olulist rolli tahke isolatsiooni vananemise ja lagunemise uurimisel. Kirjanduse baasil antakse ülevaade teadmuse olemasolevatest lünkadest, mille põhjal saab suunata edasist uurimistööd isolatsiooni vananemise ja lagunemise alal.

Koostatud on tõhus andmetel põhinev tarkvaravahend, mis tuvastab PD impulsse ning eraldab mitmeid tunnuseid kasutades lainikupõhist müraeemaldust ja lokaalsete maksimumide tehnikat. Seda raamistikku täiendab peakomponentide analüüs (PCA) optimaalsete tunnuste valiku jaoks ning edasijõudnud masinõppetehnikad, sh hierarhiline klasterdamine, mida kasutatakse PD andmete klassifitseerimiseks ja klasterdamiseks. Lisaks kasutatakse hägusloogika algoritmi, mis täpselt tuvastab PD allikad (koroonalahendus, pindmine ja sisemine osalahendus), pakkudes keerukate PD mustrite reeglipõhist tõlgendust. Koostatud tarkvaravahend on valideeritud erinevatel andmekogumitel, mis on saadud XLPE kaabli isolatsiooni ja Nomex'ist valmistatud kiledega teostatud katsetest füüsiliselt modelleeritud defektide ja vanandamisstsenaariumitega.

Osalahenduste alguspinget (PDIV) peetakse oluliseks parameetriks isolatsiooni dielektrilise tugevuse ja vananemiskäitumise hindamisel. See on ka üks peamisi parameetreid, mida arvestatakse isolatsioonisüsteemide projekteerimisel. Välja on töötatud kolmiklähenemisviis, mis kasutab FEM põhist modelleerimist ja pindlahenduse mudelit PDIV arvutamiseks Nomex kile puhul. Mudeldatud PDIV on valideeritud katseandmetega, mis kinnitavad mudeli tõepärasust ja täpsust.

Viimases uurimuse osas hinnatakse Nomex kilest valmistatud isolatsiooni kasutusiga kasutades pinderosioonipõhist kiirendatud vanandamise protseduuri. Rakendatakse neljast etapist koosnevat lagunemismeetodit, millega kirjeldatakse isolatsiooni vananemise erinevaid faase alates PD süttimisest kuni läbilöögini. Etappide erinevuste määramiseks kasutatakse osalahenduste faasilaotuse (PRPD) mustreid, PD tunnuseid ning mikroskoopilist analüüsi. Uuringust võib kasu olla Nomex isolatsiooniga elektriseadmete käitamisel, kus isolatsiooni rikkeid põhjustavate pindlahenduste oht on märkimisväärne. See uurimus kirjeldab raamistikku pinderosioonipõhiseks kiirendatud vanandamiseks, et uurida pindlahenduste käitumist erinevate toite- ja keskkonnatingimuste korral.

Kokkuvõttes aitab antud töö edasi arendada ja valideerida isolatsiooni diagnostikameetodeid ning panustab tahkete isolatsioonisüsteemide seisundiseiresse ning kasutusaja prognoosimisse elektrisüsteemides.

Appendix

Publication I

M. Choudhary, M. Shafiq. I. Kiitam, A. Hussain, I. Palu and P. Taklaja, “A Review of Aging Models for Electrical Insulation in Power Cables,” Energies, vol. 15, issue 9. 2022. doi: https://doi.org/10.3390/en15093408.

energies

MDPI

Review

A Review of Aging Models for Electrical Insulation in Power Cables

Maninder Choudhary [1,2,*], Muhammad Shafiq [1], Ivar Kiitam [1], Amjad Hussain [3], Ivo Palu [1] and Paul Taklaja [1]

[1] Department of Electrical Power Engineering and Mechatronics, Tallinn University of Technology, 12616 Tallinn, Estonia; muhammad.shafiq@taltech.ee (M.S.); ivar.kiitam@taltech.ee (I.K.); ivo.palu@taltech.ee (I.P.); paul.taklaja@taltech.ee (P.T.)
[2] Department of Electrical Engineering, Sir Syed University of Engineering and Technology, Karachi 75300, Pakistan
[3] Department of Electrical Engineering, American University of Kuwait, Kuwait City 15453, Kuwait; ghussain@auk.edu.kw
* Correspondence: machou@taltech.ee

Abstract: Electrical insulation is an integral part of power components. The aging of electrical insulation is an undeniable fact that limits the operational lifetime of power components. Apart from regular aging, abnormal stresses and the development of defects are real threats because of their contribution in accelerating the aging rate and thereby leading to a premature failure of the power components. Over the decades, various studies have been carried out to understand the aging behavior of electrical insulation mainly considering electrical and thermal stresses. Similarly, a number of mathematical (aging) models have been developed based on the theoretical and experimental investigations and evidences. However, a dependable formulation of the models that can provide more practical estimation of the insulation degradation profile has not been achieved yet. This paper presents a comprehensive review of the aging models considering single and multistress conditions. Further, the paper discusses possible challenges and barricades averting the conventional models to achieve a suitable accuracy. Finally, suggestions are provided that can be considered to improve the modeling approaches and their performance.

Keywords: electrical insulation; power cables; insulation degradation; aging models; partial discharge

check for updates

Citation: Choudhary, M.; Shafiq, M.; Kiitam, I.; Hussain, A.; Palu, I.; Taklaja, P. A Review of Aging Models for Electrical Insulation in Power Cables. *Energies* **2022**, *15*, 3408. https://doi.org/10.3390/en15093408

Academic Editor: Pawel Rozga

Received: 15 April 2022
Accepted: 2 May 2022
Published: 6 May 2022

Publisher's Note: MDPI stays neutral with regard to jurisdictional claims in published maps and institutional affiliations.

Copyright: © 2022 by the authors. Licensee MDPI, Basel, Switzerland. This article is an open access article distributed under the terms and conditions of the Creative Commons Attribution (CC BY) license (https://creativecommons.org/licenses/by/4.0/).

1. Introduction

While air provides the withstanding capability of 3 kV/mm between two conductors, the use of dielectric material increases this withstanding capability to the required voltage levels. In addition to increased electrical breakdown strength, the materials must be able to meet thermal and mechanical performance requirements [1]. Keeping performance in view, the reliability, cost, and environmental impacts are the major considerations during the insulation design of the components [2]. The operational lifetime of the power components depends on the reliability of the dielectrics. Insulation aging is a looming issue in all types of power components [3]. However, aging becomes more critical at medium or high-voltage operation as compared to low-voltage applications. During a survey of Stockholm, out of 1392 total failures, 263 were due to power transformers, 435 failures were caused by cables, and overhead lines were responsible for 20 failures where electrical insulation was considered as a significant cause of these failures [4]. Sudden failure of grid equipment can cause unplanned power outages, leading to huge economic and operational loss to customers and utilities. A better understanding of the aging behavior and its progression can help to foresee the incoming failures of critical network components, which in turn

reduces the associated losses and interruption of the industrial, commercial, and social processes.

Considering the nature of the mechanism, aging can be divided into intrinsic and extrinsic processes. The former is a naturally occurring process that produces gradual irreversible changes in the insulation properties. This refers to an intuitive process which leads to unusual changes in physiochemical properties of the insulating materials that may affect a major part of the insulation. The chemical kinetic process causes the breaking of the chemical bonds. These bonds are continuously broken and rearranged under the influence of the electric field that forms moieties [5,6]. The moieties increase with time and collectively bring substantial changes to the microscopic and ultimately macroscopic properties of insulation, which may lead to accelerated degradation. Intrinsic aging normally takes longer to fail and is initiated due to cavities, defects, protrusions, and voids (CDPV), which are the result of poor manufacturing, transportation, installation, or operation and contribute to intrinsic aging in the future. These defects under the influence of thermal, electrical, ambient, and mechanical (TEAM) stresses pose a significant impact on insulation aging [7].

Diagnostic tests play an eminent role in evaluating the defects' progression and impact of stresses. Research on the improvement of the proactive diagnostic capabilities has progressed well, especially considering the detection and location of insulation defects in the power components [8,9]. Similarly, prediction of lifetime has been a focus for the last 40 years [10–12]. It is well-understood that the progression of the insulation defects or insulation degradation is associated with the magnitude of stresses and condition of the insulation [13,14]. Various measurement methodologies are used to observe the insulation conditions, such as dielectric response in the time domain and frequency domain, infrared spectroscopy, degree of polymerization, moisture content, tensile strength and elongation, partial discharges (PD), and tan-delta [15]. The suitability of the adopted methodology is based on the type of equipment and the focus of diagnostics. The clarity in the interpretation of the measured quantities and their relationship with the aging mechanism or type of deterioration is vital for reliable diagnostics. Identification of the changing pattern as a reflection of progressing deterioration can provide a traceable behavior of insulation aging and prediction of its expected condition [16]. Due to stochastic characteristics of interest observed from the analyzed measurements, it is challenging to identify the degradation patterns. Therefore, reliable prediction of life expectancy of the component is a topic of increased interest for the power engineers [17].

Further in this article, Section 2 discusses aging from cause to consequence, typical cable defects, and the basic idea of the tests performed for the evaluation of insulation condition. Section 3 presents a holistic overview of various insulation aging models under thermal and electrical stress and discusses the threshold behavior of dielectric materials. Section 4 presents accelerated testing methods, limitations of available models in achieving general applicability, and prospective solutions for improved understanding of aging behavior.

2. Insulation Degradation in Solids and Aging Models

The degradation of insulation materials varies with their chemical composition, source (natural or synthetic), heat-resisting capability, and physical state, i.e., liquid, solid, and gas. Considering physical state, in liquids and gases degradation occurs due to contamination, solid impurities, and dissolved gasses. These impurities under the influence of continuous electric field lower the dielectric strength, which ultimately leads to the breakdown. In solids, electrical breakdown causes the final failure of insulation; however, electrical stress itself is not the dominant aging factor under normal operating conditions. The dominant degradation is caused by the combination of different stresses, among which thermal and mechanical stresses are more significant. Operational, physical, and environmental factors may lead to deteriorating effects and cause additional aging, such as the rise of temperature, bending or compression, contaminations or voids, moisture, etc. [18–20].

The effects mentioned above become the sources of different types of stresses that can be categorized as thermal, electrical, ambient, and mechanical stresses. Based on the magnitude of these stresses, the irreversible incipient degradation mechanisms are initiated in terms of oxidation, decomposition, electrical treeing, PDs, and space charges. As a result of these aging mechanisms, the material properties deteriorate, and dielectric strength is reduced at a localized level that is gradually extended across the insulation between conducting parts. Consequently, this leads to an electrical breakdown of the insulation, and the failure of the component occurs. An overview of the insulation degradation from initiation of aging into the possible failure is presented in Figure 1. The arrows indicate that the induced stresses are interrelated, as thermal stress is a result of mechanical stress. The bending and compression cause a temperature rise, which produces thermal stress. Cables operating in wet environments may cause corona discharges that increase electrical stress in cables. Mechanical stress relies on the operational and environmental conditions (harsh or mild). The damage to the cable sheath is due to mechanical stress, i.e., bending or compression, letting the moisture enter into the cable sheath, resulting in environment stress and vice versa. It also reduces the electrical performance of cable.

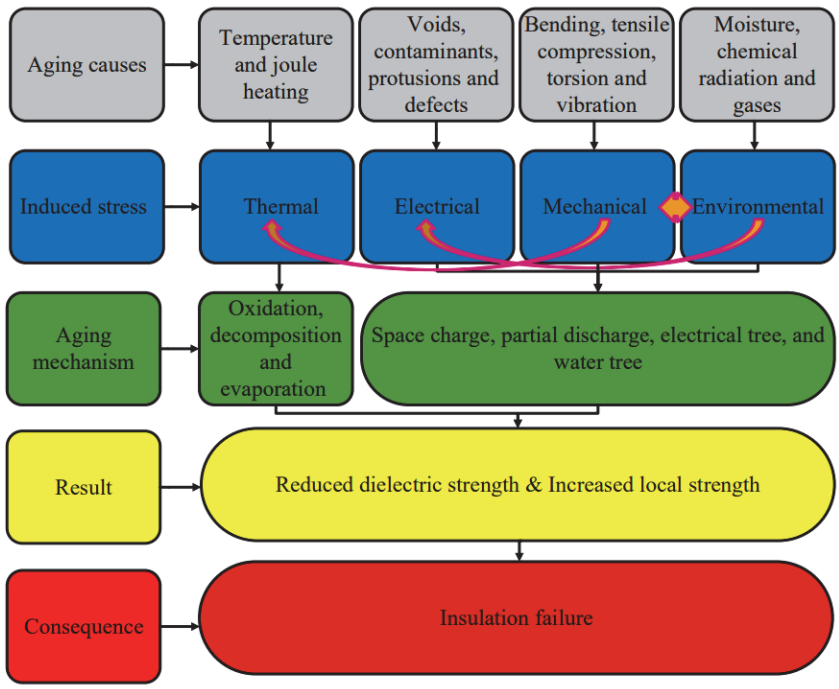

Figure 1. Aging factors, causes, mechanisms, effects, and consequences for solid insulation.

Considering underground cables as a critical component of the medium-voltage (MV) grid having dielectric a major part of its physical design, typical insulation defects are depicted in Figure 2. The most alarming defects lie within the main insulation between shielding and the conductor [21,22].

Water treeing is a serious concern in the extruded cables operating in wet environments where the potential aqueous infiltration can produce conditions that are favorable for the inception and development of water trees. These trees are effective areas inside cross-linked polyethylene (XLPE) insulation with reduced dielectric strength, and can therefore also contribute to aging, e.g., via consequent initiation of electrical treeing. Electrical trees are initiated when the insulation is subjected to high electrical stress for a sufficiently long time in the presence of (CDPVs). The electric trees are formed due to sustained PD activity,

which causes gradual local disintegration of the insulation. Both water trees and electrical trees tend to expand in the direction of the electric field they are exposed to [23,24].

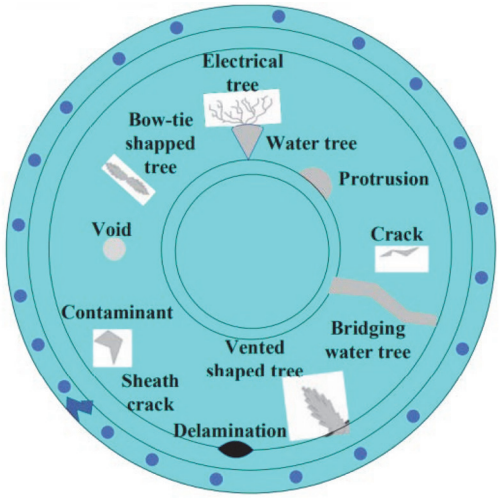

Figure 2. Typical defects in extruded power cables.

The aim of aging studies and lifetime modeling is to relate the life with the associated stresses which can be achieved by experimental studies. Considering experimentation, accelerated-aging tests can be more efficient since the routine testing methods take a longer time. Typically, underground cables are designed for a service life of 30–40 years. Accelerated aging tests can be used to estimate an asset's life in a short span with a suitable accuracy. IEEE 1407 defines well-established guidelines for accelerated tests for medium-voltage cables (5–35 kV), according to which accelerated water-treeing tests (AWTT) are performed where cables of various lengths are kept inside water-filled pipes from four months to one year. Later, the step AC breakdown voltage is applied, and insulation behavior is investigated. Another method where cables are aged in tanks instead of water pipes for a known period of time or until failure time is called the accelerated cable-life test (ACLT). In this method, the step AC voltage is applied under different temperatures and voltages. This method is very useful for the investigation of the overall aging process, i.e., from inception and growth to final failure [25]. IEEE 98 defines test procedures for thermal endurance (TE) characterization of insulating materials based on analytical methods, concluding that TE tests must be performed at three or more ranges of temperatures for a duration of more than 100 and 5000 h (about 7 months) for the shortest and longest test, respectively [26]. A shorter method for TE characterization purposed in [27] is based on the oxidation-stability measurements to estimate the activation energy (minimum energy required to initiate a chemical reaction) of degradation. Regarding measurement techniques, nondestructive tests such as insulation resistance, tan delta, and PD are comparatively popular.

IEC-60270 defines PD as an electrical discharge that partially bridges the insulation between conductors, which may or may not occur adjacent to a conductor. IEC also provides guidelines for PD measurement where the PD inception voltage (PDIV) is applied at nominal frequency i.e., 50 Hz, and PD pulses are measured at increasing voltages. These pulses can be measured by various sensors such as coupling capacitors [28]. Other devices such as high-frequency current transformer (HFCT), Rogowski coil, ultra-high-frequency (UHF) sensor, and electric-field sensors (D-dot) are also used for PD pulse measurement [14,29]. The results demonstrate the fault location, intensity, and type of PDs.

Modeling has made prominent progress from the Dakin physical model [5] to the Simoni multistress life models [30–32] and Dissado space-charge model [33]. These models predict insulation life under single or multiple stresses. The study of the insulation under multistress conditions can provide a more compressive aging response. Multiple stresses are not simply additive, but they are coactive and might have a direct or indirect impact; or the other way around, they might have sequential impact [34]. Although the accelerated-aging tests evaluate the insulation condition efficiently, the life estimation at a particular instance of service requires statistical tools and life models. Due to their significant degradation impact, thermal and electrical stress based aging models are discussed in the next section considering single-stress and multi-stress approaches, as shown in Figure 3. Multistress models are further classified into phenomenological, physical, and thermodynamic models.

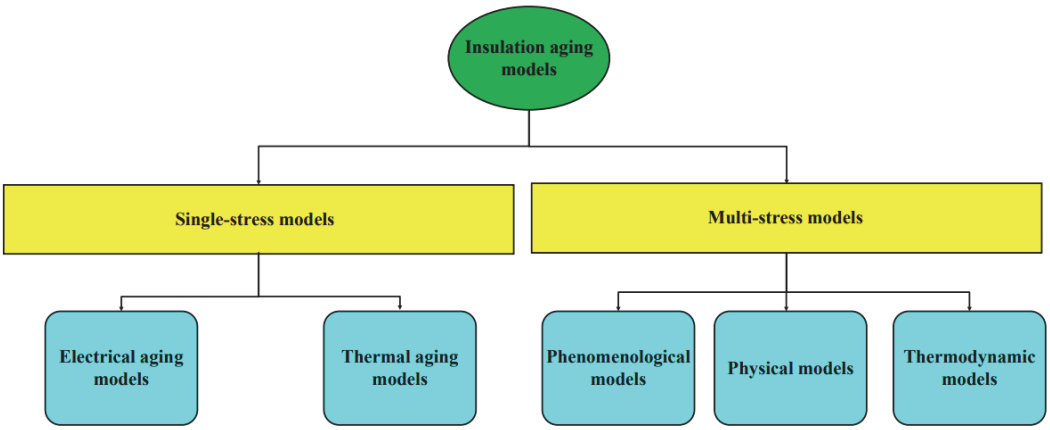

Figure 3. Classification of insulation-aging models.

3. Single-Stress Aging Models

3.1. Electrical-Aging Models

Electrical aging occurs due to the presence of free electrons and other charge carriers. The free electrons at low concentrations start colliding frequently with the lattice of dielectric materials and ionize molecules of insulating materials by transferring energy. At a high concentration, this collision liberates additional free electrons and collectively they produce an avalanche effect [35,36]. The excess of free electrons causes the current to flow within the insulation. At high stress, heating is produced due to the high current, which thermally deteriorates the material, thus contributing to aging. Introducing a relationship between electrical stress and time to breakdown, inverse power law (IPL) predicts the lifetime of the insulation as

$$t_{f\,=\,aE^{-b}} \qquad (a\ >\ 0) \tag{1}$$

where t_f is failure time, E is applied electrical stress, and a is the constant to be estimated by electrical life data. The parameter b is the voltage-endurance coefficient (VEC), which is the slope-of-life graph between applied electrical stress and life [37]. Life prediction through IPL is based on the accelerated-aging-test results, as it is the relation between electrical stress and time to failure [38]. It has been observed that electrical-endurance data or the relation between insulation life and applied stress can be best described using two-parameter Weibull distribution [39,40]. The cumulative density function for Weibull distribution is expressed as

$$f(t) = 1 - e^{-\left[\left(\frac{t}{p}\right)^q\right]},\ t \geq 0 \tag{2}$$

where f(t) is failure probability at applied stress or time, and p and q are the scale and shape parameters and are positive. The parameter p illustrates the voltage or (time) at which

f(t) becomes 63.2%, whereas q is the measure of the dispersion of data such as variance in normal distribution and t is time to failure or breakdown value of electrical stress. Figure 4a is a graphical representation of IPL that depicts an inverse relation between electrical stress and insulation life; as electrical stress increases, the insulation life decreases [38]. It is observed that at lower value of electrical stress, the insulation life graph tends towards the electrical threshold E_O This behavior is best described by the exponential model, as shown in Figure 4b. The model represents the voltage endurance of the insulation based on a threshold value that permits faster and accurate results [41], expressed as

$$t_{f = k\, e^{(-nE)}} \quad (3)$$

where k and n are the constants ought to be found by electrical-endurance experimental data [38]. Both models have wide application for electrical endurance and are extensively used to study insulation life under single and multiple stresses.

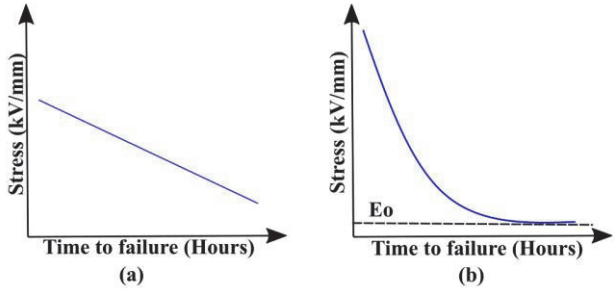

Figure 4. Relationship between applied stress and insulation life for varnished polyamide films using (**a**) inverse life graph; (**b**). exponential life graph adapted with permission from [40].

In many cases, particularly when the diagnostic tests are extended for a long time, the electrical lines show their tendency towards the electrical threshold E_O. The life graph of polyethylene terephthalate (PET) film with surface discharge shows an S-shape curve in Figure 5a. The green curve (semi-log plot) follows IPL at first and later tends towards E_O at a low value of electrical stress, showing the practical existence of the electrical threshold [42]. The same material was tested in [43] at different temperatures, as shown in Figure 5b. It was observed that the threshold value decreased with increasing temperature; however, its presence was still there even at 130 °C. The tendency of the life graph towards the electrical threshold (E_O) can be due to the extrapolation of the experimental data or due to operating conditions of the insulation.

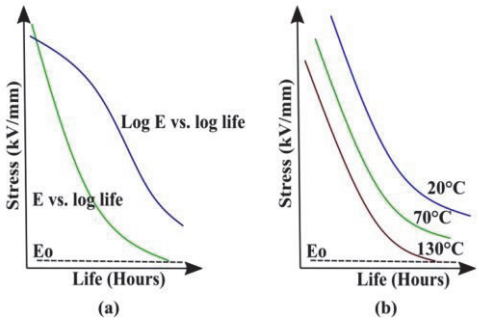

Figure 5. Electrical life curves for PET, approaching threshold E_O, (**a**) at constant temperature; (**b**) at different temperatures adapted with permission from [43].

Materials that adopt this behavior can be expressed by adding a threshold value in both inverse-power-law exponential models. Thus (1) and (3) are extended as (4) and (5). Adding a threshold value mathematically in the life equation, e.g., E_O in (5), gives precise results, since it is impractical to include stress values below the threshold.

$$t_f = t_o\left[\frac{E}{E_O}\right]^{-b} \tag{4}$$

$$t_f = t_O\left[\frac{k}{E - E_O}\right]e^{[-n\ (E-E_O)]} \tag{5}$$

where E is applied voltage, t_f is insulation remaining life, and t_O is life at stress E_O [32]. Haideo also observed threshold behavior in dielectric materials such as polyethylene and polyethylene-terephthalate. His work illustrates that the life of electrical insulation follows a Z curve called flat Z characteristics, as shown in Figure 6. Three regions of representation are provided, while region I shows linear relation between life and applied stress following IPL; it is assumed that threshold E_T appears in the third region [44].

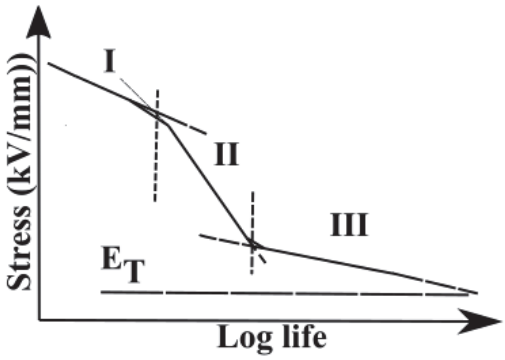

Figure 6. Representation of flat Z characteristics of insulation life in three regions adapted with permission from [44].

It can also be noticed that during region I and region III, the rate, i.e., (dv/dt_f), is lower than in region III, which implies that the degradation rate is high in the transition phase, which is region II.

3.2. Thermal-Aging Models

Thermal stress is one of the prominent causes of insulation aging, as it produces irreversible and enduring reactions that eventually affect the dielectric properties of insulation, thereby increasing the dissipation factor or conductance. Dakin et al. [27] identified three processes that lead to thermal aging of insulation, as follows:

- increase in dissipation factor and conductance due to oxidation.
- brittle hardening of the insulation due to reduction in the plasticizer effect.
- depolarization of plastic insulation at elevated temperatures.

Montsinger also described aging as a function of time and temperature. According to him, an increase in temperature (8–10 °C), reduces equipment life by half [45]. The relationship between temperature and reaction rate of a chemical reaction was first aimed at by Arrhenius in Equation (6), expressing it as the rate of a chemical reaction directly proportional to the temperature [46].

$$K = ke^{-\frac{E_a}{RT}} \tag{6}$$

where K is reaction rate, k is rate constant, T is absolute temperature, and R is general gas constant [47]. Here E_a is the activation energy that determines the rate of the chemical reaction. It is proportional to the slope of the line between the rate of reaction and the inverse of temperature. High activation energy represents slow chemical reaction. A modified form of (6) is proposed in (7), as (6) deals with the kinematics (reaction rates) only in gaseous form. [48]. However, expression (7) is able to support heterogenous reactions as well, i.e., reactions in which two or more forms of matter (liquids, gases, and solids) take part as reactants, and is presented as

$$K = \frac{K_B T}{h} e^{-\frac{\Delta H}{RT}} e^{\frac{\Delta S}{R}} \quad (7)$$

where K_B and h are the Boltzmann and Planck's constant, ΔH is activation enthalpy, ΔS is activation entropy. If life L_T is insulation life under thermal stress (assumed to be inversely proportional to the reaction rate), then (6) becomes

$$L_T = \alpha e^{\left(\frac{\beta}{T}\right)} \quad (8)$$

where $\beta = E_a/R$ is constant and function of activation energy of reaction [49]. The value of α is mainly dependent on the insulation characteristics and failure mode. The thermal graph shown in Figure 7 is obtained by extrapolation of data points and temperature indices, including temperature index TI [50,51].

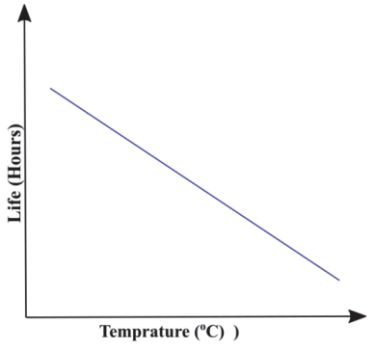

Figure 7. Thermal life graph between temperature and insulation life adapted with permission from [51].

The linearity of the thermal life graph is dependent on the constancy of rate of reaction at all ranges of temperature and on the assumption that the material only undergoes thermal stress. However, the tests performed under combined (electrical and thermal) stress showed that thermal life graph lines followed curved patterns [52,53]. Figure 8 presents the thermal lines of XLPE cable under different values of electrical stress.

It was observed that thermal lines adopt curvilinear behavior with increasing magnitude of electrical stress. The plots demonstrate that at the start, the thermal lines exhibit linear behavior, but at higher values of electrical stress, the lines tend towards thermal threshold Tt, which reflects the practical existence of the thermal threshold. Considering the threshold behavior, a modified form of (8) derived from the Eyring relationship proposed in [52] is expressed as

$$L = K_1 T^{\gamma} e^{\left(-\frac{\beta}{T}\right)} e^{\{[K_2 + K_3/T_T(S)]\}} \quad (9)$$

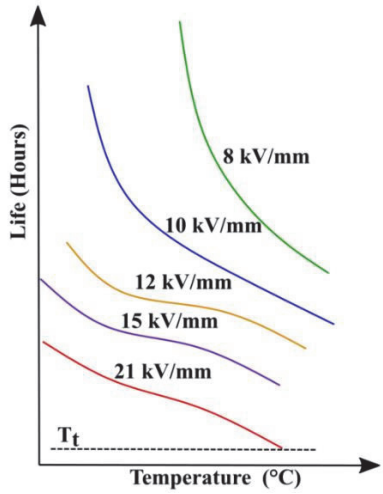

Figure 8. Thermal lifelines of XLPE cable at different values of electrical stress adapted with permission from [53].

Here, S is stress other than thermal, which can be electrical or mechanical. It can be seen from (9) that for s = $\leq$0, there will be thermal aging only. K_1, K_2, K_3, and Υ are parameters of the Eyring model, extracted by thermal-endurance data. In addition, Figure 8 shows that the insulation life reduces drastically at higher values of electrical stress even at low temperature, which indicates that electrical stress also influences thermal aging.

The models based on single (individual) stresses provide a clear understanding of the aging behavior and prediction of lifetime with good accuracy and flexibility. However, in a more practical scenario, insulating materials operate under multiple stresses, which are discussed in the next section.

4. Multistress Aging Models

During regular operation, equipment is exposed to multiple stresses simultaneously. Observing their combined impact provides a more comprehensive understanding of the aging behavior under operational conditions [46]. If any abnormality of thermal stress has primarily accelerated the aging rate due to the oxidation process in air, its interaction with electrical stress further increases the temperature and can initiate the treeing phenomenon. Conversely, the impact of electrical as the primary stress and thermal as the secondary stress substantially changes the PDIV and intensity of PD [30]. Thus, multistress models consider the synergistic effect of applied stresses that are multiplicative in nature, not additive. A generalized life model (10) for insulating materials (threshold and non-threshold) under multiple stresses, say, n, is expressed as in [49]:

$$\frac{l}{l_0} = \frac{l_1}{l_0}\frac{l_2}{l_0}\ldots\ldots\frac{l_n}{l_0}\,C(S_1S_2,\ldots\ldots S_n)\Big) \tag{10}$$

where l is life under multiple stresses. Further, $l_1, l_2 \ldots, l_n$ are individual lives for stresses S_1, $S_2 \ldots, S_n$ and l_0 is life at a certain stage called reference life. The constant C is the correction factor, which is necessary to include since at higher values of stresses, the multiplicative model yields a solid reduction in the insulation lifetime [54]. Multistress models are based on Arrhenius and Eyring's equations for thermal and mechanical endurance, inverse, and exponential models for electrical endurance. These models can be divided into three categories:

- Phenomenological Models.
- Thermodynamic Models.

- Physical Models.

4.1. Phenomenological Models

The empirical models are based on the aging phenomenon in accordance with the principal theories; however, their parameters hold no physical meaning. They are designed by analyzing the failure data of experiments or accelerated-aging-test results that cannot be found directly as material properties. Phenomenological life models are relatively successful in predicting the life of insulation at any stage. The major characteristics of these models can be stated as follows [55]:

- Depicts the relationship between stress (es) and life of the equipment based on the experimental data;
- Characterizes insulating materials based on experimental evidence rather than physical properties;
- Predicts life at any stage through extrapolation of the test data;
- Statistical and statistical or probabilistic approaches can be used to find model parameters.

Over the past three decades, a number of multistress models based on experimental results have been proposed. Among the first phenomenological multistress models, Fallou's model presented in [56] is expressed as

$$L = B_1[e^{(B_2E)}e^{\frac{C_1}{T}}\ e^{\frac{C_2E}{T}}] \tag{11}$$

where B_1, B_2, C_1, and C_2 are the electrical constants, determined by experimental results. The interesting thing about this model is that each of the three terms in (11) represents the aging process, i.e., first term—electrical aging, the second term—thermal aging, and third term—aging under combined stress (14). The model is only valid for $E > 0$; thus, it does not consider the impact of threshold value or lower value of electrical stress near to zero. The exponential term in the model holds curvilinear properties at stresses near to zero, as shown in Figure 4b. Therefore, at a lower value of applied electrical stress, the extrapolation of the data in the model does not give accurate results. The major contribution in the field of multistress aging was made by Simoni [31]. The proposed models bear high credibility as they are developed based on broad research and experimental evidence. Simoni's first multistress model is expressed as

$$L = K_n L_0 \frac{e^{(-hE-BT+bET)}}{\frac{E_G}{E_{Gto}} + \frac{\Delta T}{\Delta T_{to}} - 1} \tag{12}$$

where k_n is constant depending on insulation short-time characteristics, h and B are electrical (coefficient of inverse-power model) and thermal parameters, b is parameter for combined stress, E_G is electrical gradient, ΔT is change in temperature, and E_{Gto} and ΔT_{to} are electrical gradient and thermal threshold at room temperature, respectively. One of the major characteristics of Simoni models is the life surface, as shown in Figure 9: a three-dimensional graph that is a geometrical representation of life under combined stress. The surface intersection with axes gives electrical lifelines at constant temperature and thermal aging at constant electrical stress. Additionally, at constant life (L), the isochronal (hyperbolic) lines of thermal and electrical stress in correlation with selected life can also be acquired from the surface model.

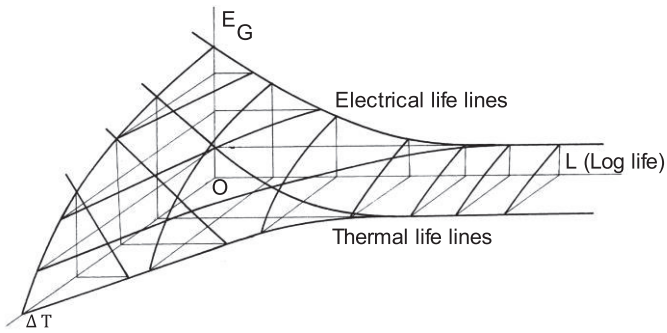

Figure 9. Life surface graph representing linear and isochronal lines adapted with permission from [31].

Simoni's observations during experiments proved to be a breakthrough in defining the threshold materials i.e., it is not material, which is threshold or non-threshold rather behaviour, depends on the value of applied stress. If at least one of the applied stresses is less than the threshold, e.g., at stress $E < E_o$ the lifelines approach thermal threshold and vice versa. Thus, the material behaves as threshold material. If all applied stresses are higher than the threshold value, the material behaves as non-threshold material [33]. This led Simoni to propose a unique model which is valid for material behavior (threshold and non-threshold) expressed as

$$L = L_0 \frac{e^{(-hE-BT+bET)}}{\left(\frac{E}{E_{to}} + \frac{T}{T_{to}} - (bTt_o\ ET)/(h\ E_{to}\ T_{to}) - 1\right)^{\beta}} \tag{13}$$

where

$$\beta = \beta_O \left[\left(\frac{E - E_{to}}{E_{to}} \right)^2 + \left(\frac{T - T_{to}}{T_{to}} \right)^2 \right] \tag{14}$$

Equation (13) has seven parameters: L_0 is life at some reference point or at room temperature, E is applied electrical stress ($E-E_{to}$), and E_{to} and T_{to} are electrical and thermal thresholds at room temperature, respectively. The value of β_O, ultimately β, defines material behavior. It can be observed that by putting $\beta = 0$ in (13) the model represents the non-threshold behavior of insulating material, which means all stresses must be greater than or equal to corresponding threshold values, i.e., $E \geq E_{to}$ and $T \geq T_{to}$. Yet if $\beta > 0$, the model represents threshold behavior, inferring that either of the applied stresses must be less than the respective threshold value, i.e., ($E < E_{Gto}$ or $T < T_{to}$). Moreover, the values of β model validity rely on the following boundary conditions:

- In absence of electrical stress in other words ($E \leq E_{Gto}$), the model must tend to the thermal model; however, at $T \leq T_{to,}$ the life function must tend to infinity.
- Likewise, in the absence of thermal stress the model must tend to the electrical model and at lower value of electrical stress ($E \leq E_{to}$), the life must follow upward curvature (tend to infinity).

In the absence of both stresses, the model must converge to the linear model. Considering the versatility of this model, it can differentiate the behavior of materials based on the values of applied stresses in contrast with the threshold. It can also predict the life or aging in multiple scenarios given that the suitable test properties and criteria for failure are used for thermal and electrical-endurance data processing. However, there are higher chances of uncertainties calculating parameters through estimating methods such as maximum likelihood, even with the high volume of experimental data [57]. The phenomenological models have the capability to be transformed into probabilistic models based on the experimental data results [38,47,58]. A probabilistic model proposed in [59]

can describe insulation aging of material subjected to thermal and electrical stress. The IPL-based model is expressed as

$$F\,(t, E; T) = 1 - e^{\left[-\frac{t}{t_s}\left(\frac{E}{E_s}\right)^{n_i}\right]^{q(E,T)}} \tag{15}$$

where $n = \frac{n_i}{\left(1-\frac{E_s-E}{E_s-E_T}\right)^{\Delta}}$. Here, n_i is the initial electrical-endurance coefficient, t is time to failure at stress E and ts is time to failure at electrical stress E_s, T represents thermal stress or temperature, and v U is shape parameter (v = v (T)). It can be observed that the value of the power term n is dependent on electrical stress E, temperature T, and v, which is different from previous models, dependent on E and T only. In addition, this model has no separate term for thermal stress like we have seen in previous models. Although it is a novel approach, implemented on XLPE-insulated cables, the general validity of the model for materials with threshold behavior still requires experimental evidence gathered on varied materials [45,46].

4.2. Physical Models

The major drawback of phenomenological models is the model validity, which solely depends on the experimental results since the parameters can only be found after the aging test. This process often takes longer and is difficult to handle a large amount of data using statistical means. On the other hand, physical models are based on the aging mechanisms, laws, and theories. These models support aging in insulation parameters of later models that have physical meaning and can be found directly from the measurement of physical quantities [55]. The physical model based on the PD phenomenon was initially proposed by Bahder et al. [60] as

$$L_E = \frac{1}{f b_1 \left[e^{b_2(E-E_{tac})} - 1\right] e^{b_3(E_b)} + b_4} \tag{16}$$

The b_1, b_2, b_3, and b_4 are constant terms and their values depend on frequency f and shape of applied stress i.e., impulse, DC, or AC. Here E_b is the voltage at which electrical breakdown occurs and E_{tac} is the threshold value of applied stress (AC). The value of E_{tac} is influenced by the shape and type of void or defect and insulation temperature. A similar model based on the tree growth and PD test is proposed in [61], expressed as

$$F(t, Q_i, E) = 1 - e^{\left[-\left(\frac{t k_5 (E-E_T)^n}{\ln\left[\left(\frac{Q_i}{k_2}\right)+1\right]^d}\right)\right]^{\beta}} \tag{17}$$

This expression describes the probability of insulation failure, where β and n are the parameters of Weibull distribution; n is also the electrical-endurance coefficient; d is tree depth and can be found from fractal characters of the tree; and k_2, k_5 are the constants, whose value relies on the material type and tree-growth phenomenon. The model is valuable in finding the residual life of the insulation at a chosen value of charge Q_i at time t.

Although the above models are based on the novel PD testing, the life estimation through this model depends on electrical tree growth. Knowing the fact that electrical treeing is one of the hazardous haps that severely affects insulation, it is therefore necessary to predict the insulation condition prior to the tree growth. In addition, this model needs sufficient PD data and processing tools for accurate estimation of the model parameters and constants.

4.3. Thermodynamic Models

Typically, thermodynamic models illustrate that the insulation degradation or aging is due to the reactions, activated by heat or temperature. These reactions form moieties that cause degradation. Both electric field and temperature are responsible for these reactions,

as temperature provides free energy to electrons to overcome the barrier, and electrical stress reduces the height of that barrier [62]. Crine et al. [63] proposed a multi-stress model based on the thermodynamic approach, expressed as

$$t_b \cong \frac{h}{K_B T} e^{\left(\frac{\Delta G - E\lambda F}{K_B T}\right)} \tag{18}$$

ΔG is Gibbs free energy, λ is scattering distance, and F is frequency. As seen from the equation as $E \rightarrow 0$, the life t_b will tend towards infinity. In this case, λ will be contingent on thermal quantities, i.e., temperature, ad must relate to physical properties (structure and size of micro voids and small cavities that grow in the material due to structural defects accelerated by electrons). The model presumes that electrons have sufficient energy to accelerate reactions that break the weakest bonds; this indicates either that there is a considerable number of defects or micro voids already present at the start of the aging process, or the presence of high-voltage stress or a simultaneous effect [63,64]. Another model proposed in [65] is based on the chemical characteristics of insulation. The breaking of chemical bonds under multiple stress(es), i.e., thermal, and electrical, form micro voids. These micro voids can defuse with each other and form cracks that contribute to deterioration that can be observed from the expression as

$$t = \int_N^{n_c} \left\{ \frac{k_B T}{h} \left[\left(e^{\left(\frac{-U_r(E)}{k_B T}\right).(N-n)} - e^{\left(\frac{-U_{b(E)}}{kT}\right).(n)} \right] \right\}^{-1} dn \tag{19}$$

Here, t is time to failure or time at which crack growth due to voids is initiated, n is number of bonds that are broken, n_c is their critical quantity, N is the quantity that can be breakable, and $U_r(E)$ and $U_b(E)$ are activation energies required for forming and breaking of bonds. Taking a similar concept Dissado described the role of space charges in insulation aging. Space charges are evolved in polymeric insulation as a result of charge injection by electrodes, where some charges may be trapped within the insulation. At high electrical stress, these trapped charges attain enough energy to break bonds thus changing chemical properties of a material at microscopic level and initialize degradation. The acceleration of degradation is a thermodynamic process [66]. This study focuses on the microscopic characteristics of insulating materials, which is different from the previous models, considering macroscopic characteristics as major cause of failure. Dissado el at. [67] proposed a model called DMM (Dissado–Mazzanti–Montanari), based on the space-charge degradation phenomenon under combined stress (thermal, and electrical) as

$$L(E,T) = \frac{h}{2K_B T} e^{\left[\frac{\frac{\Delta H}{K_B} - \frac{C' E^{2b}}{2}}{T} - \frac{\Delta S}{k}\right] \ln\left[\frac{A_e(E)}{A_e(E) - A^*}\right] \left[\text{Cosh}\left(\frac{\frac{\Delta}{k} - C' E^{2b}}{2T}\right)\right]^{-1}} \tag{20}$$

where A represents degraded moieties, A* is the critical value of A (value at which large cavities are formed, sufficient for PDs and therefore the electrical tree), Ae (E) is A when equilibrium occurs between forward and backward reactions, and Δ is the difference of free energy between reactants and products. The constant b depends on charge-trapping and insulation-degradation quantities, and constant C' depends on material properties such as element strain, permittivity, etc. Interesting results have been found with the implementation of (20) with certain assumptions. Firstly, it is assumed that the insulation holds a homogenous structure. As in the past, insulating materials were manufactured with imperfections (in small size and quantity), and thus can be considered homogeneous on macroscale level. In addition, it assumes that small voids are present during manufacturing. However, advanced manufacturing techniques produce extra clean materials, infers that there are low chances of defects at the manufacturing. On the other hand, charge carriers trapped in such materials could have a remarkable impact on aging. This concludes that there is an efficient need to investigate insulation degradation based on the space-charge-trapping mechanism in presently available materials. Secondly, the model predicts the

inception of cracks and micro voids that result in PD or breakdown later, but not the failure time or breakdown itself. This means that the model is extremely useful in cable design and manufacturing, as in-service insulation is more concerned with failure time and lifetime prediction.

5. Discussion

Improved understanding of the insulation aging and life prediction is essential for the reliable operation of power components. Development of defects as a result of manufacturing or certain stress reaching above the specified range causes initiation of the degradation mechanisms, leading to final breakdown. The complexity of the mechanisms makes it challenging to develop well-defined degradation models to predict the lifetime or failure time of the affected component with a reliable degree of accuracy.

This paper provides a comprehensive review of aging models, highlighting the competencies and barricades of the models under single and/or multiple stresses. The single-stress approach is relatively simple in terms of experimental analysis, data interpretation, and relating insulation life to the corresponding stress. However, more practically, the power components operate in multistress environments; thus, predicting lifetime under single stress can be indecisive in many cases. Multistress models offer improved estimation of insulation life, keeping in view variation of insulation characteristics. Phenomenon-based models provide good understanding of insulation-aging behavior, as model terms rely on the experimental results. Although model parameters have no physical meaning, these models can be very helpful in the comparison of different insulating materials. On the other hand, physical models consider the aging mainly caused by electrical stress. It can be noticed in (16) and (17) that the models represent electrical and fractal quantities only. Thermodynamic models—particularly the space-charge approach—bear high significance in predicting the development of defects (voids and cavities) that result from space charge, but the insulation operating in-field is much concerned about the time-to-failure approach instead.

Therefore, the available multistress models are quite useful in predicting the insulation life. However, there are certain observations that limit their general applicability:

- It has been observed that most of the models are material-oriented, as their validity is examined on certain materials. It can be seen in Table 1 that most of the models are tested on XLPE and ethylene-propylene rubber (EPR) cables. However, insulation characteristics or aging behavior varies with material type, manufacturing techniques, operating environments, and level of stress applied. The life of cables with the same insulation installed in different networks is different. This depends on the environment and operational conditions. As the operational conditions keep on changing, the degradation rate changes hence the time to failure will change. This challenges the general validity of models.
- Experimental surveys [43,68] show a wide variation in the life graphs of various insulation materials when they come under single or multiple stress. Due to randomness in experimental data points, the graph does not follow a clear pattern. Thus, it is quite unwieldy to fit data accurately in one model. Although the model in [33] is valid for threshold and non-threshold behavior of dielectric materials, the life equation relies on several parameters. Almost all models contain parameters, indicated in Table 1, that can be found by different statistical methods such as maximum likelihood, linear regression, etc. The parameter resembles variables in an equation. It is cumbersome to handle multiple variables when it comes to experimental analysis of combined thermal and electrical stress.
- Considering the operation of the new components being proliferated in the modern grid, such as power electronics converters (PEC), it is found that available models do not incorporate their effect. A model proposed in [69] considers the impact of PEC and describes overall aging or degradation rate as the sum of electrical stress (peak-

to-peak value of voltages) at nominal frequency (50 Hz) and the impulse frequency expressed as

$$L_{f_1} = \left[\left(\frac{U'_{pk}}{pk}\right)^n \left(\frac{f_1}{50}\right)\right] \quad (21)$$

where $U_{pk/pk}$ is peak-to-peak voltage, n is VEC determined from experimental results, and f_1 is the frequency at which insulation life is to be found. Unlike conventional models, it assumes no synergism between stresses, i.e., between voltage and impulse frequency. In addition to that the model does not consider the impact of thermal stress, the model terms represent the impact of electrical stress and frequency only.

Table 1. Summary of reviewed multistress aging models.

Model No.	Model Equation	Model Type and No. of Parameters	Validity Tested On	References
1.	$L = B_1\left[e^{(B_2 E)} e^{\frac{C_1}{T}} e^{\frac{C_2 E}{T}}\right]$	Phenomenological 4	Poly propylene-oil system	[56]
2.	$L = K_n L_0 \frac{e^{(-hE-BT+bET)}}{\frac{E_G}{E_{Gto}}+\frac{\Delta T}{\Delta T_{to}}-1}$	Phenomenological 6	Composite (Nomex-Mylar-Nomex), cycloaliphatic epoxy resin and polyurethane resin	[31]
3.	$L = L_0 \frac{e^{(-hE-BT+bET)}}{\left(\frac{E}{E_{to}}+\frac{T}{T_{to}}-(bT t_o\ ET)/(h\ E_{to}\ T_{to})\right)-1)^{\beta}}$	Phenomenological 7	XLPE Cables and (Composite N-M-N)	[33]
4.	$F(t,E;T) = 1 - e^{\left[-\frac{t}{t_s}\left(\frac{E}{E_s}\right)^{n}\right]^{q(E,T)}}$	Phenomenological 5	XLPE Cables	[59]
5.	$L_E = \frac{1}{fb_1\left[e^{b_2(E-E_{tac})}-1\right] e^{b_3(E_b)}+b_4}$	Physical 5	XLPE, PE (Polyethylene) and (EPR) Cables	[60]
6.	$F(t,Q_i,E) = 1 - e\left[-\left(\frac{tk_5(E-E_T)^n}{\ln[(\frac{Q_i}{k_2})+1]^{\frac{1}{d}}}\right)\right]^{\beta}$	Physical 4	XLPE Cables	[61]
7.	$t_b \cong \frac{h}{K_B T} e^{\left(\frac{\Delta G - E/F}{K_B T}\right)}$	Thermodynamic 1	Polyethene (HMW-PE), Cross linked PE, XLPE and EPR	[63]
8.	$t = \int_N^{n_c}\left\{\frac{k_B T}{h}\left[\left(e^{\left(\frac{-U_r(E)}{k_B T}\right).(N-n)} - e^{\left(\frac{-U_b(E)}{kT}\right).(n)}\right]\right\}^{-1} dn$	Thermodynamic 2	XLPE Cables	[65]
9.	$L(E,T) = \frac{h}{2K_B T} e^{\left[\frac{\frac{\Delta H}{K_B}-\frac{C' E^{2b}}{2}}{T}-\frac{\Delta S}{k}\right]\ln\left[\frac{A_e(E)}{A_e(E)-A^*}\right]\left[\mathrm{Cosh}\left(\frac{\frac{A}{K}-C' E^{2b}}{2T}\right)\right]^{-1}}$	Thermodynamic 8	PET and PP Specimen and XLPE cables	[6]
10.	$L_{f_1} = \left[\left(\frac{U'_{pk}}{pk}\right)^n \left(\frac{f_1}{50}\right)\right]$	Phenomenological 1	Enameled Wires	[69]

The operational lifetime of the equipment can be followed by the insulation's remaining life in terms of time to failure or likelihood of failure. A comprehensive aging model can be developed based on the most representative combination of both time to failure and activity to failure and considering pros and cons of reviewed aging models mentioned in Table 2. Any hard event or abnormal stress conditions can shorten life and unexpected failure may occur. To predict the breakdown moments, it should be more useful to observe the outcome of degradation instead of the mechanism of degradation. Observing the outcome of the degradation can provide a direct indication of the insulation conditions. PD measurements provide a direct illustration of the insulation conditions. Initial studies conducted by the authors demonstrate the characteristics of PD signals such as PD magnitude and pulse-repetition rate analyzed from the PDIV up to the breakdown of the insulation due to the gradual increase in electrical stress [16]. The variation in these

characteristics provides a cognizable pattern during various stages of degradation. Further characteristics of the PD signals in time and frequency domain should be investigated to understand the aging behavior in terms of insulation lifetime.

Table 2. Pros and cons of reviewed multistress aging models.

Model No.	Pros	Cons
1.	• Model parameters can be found from experimental results. • Model terms represent individual and synergetic effect of electrical and thermal stress. • Contain nominal number of parameters.	Only valid for non-threshold materials.
2.	• Valid for both threshold and non-threshold materials. • Model parameters can be found through experimental results. • The model includes term for reference life i.e., l_0.	• Increased number of parameters can increase the complexity in evaluation of the results.
3.	• The model includes additional term (β) that describe material behavior. • Valid for both threshold and non-threshold materials. • Model parameters can be found through experimental results. • The model includes term for reference life i.e., l_0.	Increased number of parameters can increase the complexity of model.
4.	• The model terms represent impact of time besides electrical and thermal stress. • Model terms only define synergetic effect of thermal and electrical stress that reduces the size of equation and parameters. • Predicts life under thermal and electrical stress.	The model doesn't represent the impact of individual stress. There is no separate term for thermal or electrical stress.
5.	• Model terms consider impact of frequency. • Nominal number of parameters. • Parameter can be found by measuring physical quantities by performing PD test.	• The model terms ´b1, b2, b3 and b4 require prior knowledge of physical properties of materials. • There is no term that directly represent thermal stress.
6.	• Model terms have physical meaning i.e., depth of electrical tree d and charge q. • Model can predict life at chosen value of charge. • Nominal number of parameters	Model parameters rely on occurrence of electrical tree. Thus, life prediction prior to tree is not possible.
7.	• Model terms includes the impact of microscopic properties of insulation, the quantity n defines number of broken bonds. • Minimum number of parameters	• Model terms rely on chemical properties of insulation. Thus, difficult to extract through convential methods. • The assumptions made about micro-voids in the model can impact the accuracy of the model.
8.	• The model is useful in analyzing insulation behavior at microscopic level as model terms also define the quantity of broken bonds i.e., n defines number of broken bonds.	• The assumptions made about the already broken bonds in the model can impact the accuracy of the model. • Increased number of parameters can increase the complexity of model.

Table 2. *Cont.*

Model No.	Pros	Cons
9.	• Well-suited for cable design and manufacturing process as model terms are extracted from microscopic properties of insulation. • Predicts time for development of micro-voids.	• The model can't predict time to breakdown or aging at macroscopic level. • Increased number of parameters can increase the complexity of model.
10.	• Consider the impact of modern grid operating conditions i.e., impulse, and high frequency switching. The parameter n can be calculated through experiments. • Minimum number of parameters.	• Model terms does not consider impact of thermal stress. • The model tested only on the enameled wires where insulation thickness is small.

The measurement methodology can play a key role in improving the accuracy of life prediction capability. Nondestructive testing is considered safe and cost-effective without causing damage to the equipment or interruption in the plant's operation. The role of accelerated aging tests is crucial in predicting insulation life in a short time span. However, the deviation of results from real operation tests or routine tests is a matter of concern, since accelerated-aging tests are performed at elevated levels of stress, which do not take into account all the dynamics associated with real operations. A term called accelerated factor A can be used to correlate accelerated-aging tests to normal routine tests [70], is expressed as

$$A = \frac{t_{normal}}{t_{accelerated}} \tag{22}$$

where the times t_{normal} and $t_{accelerated}$ are those at which the property (under test) achieves the same value after the normal and accelerated-aging test. A high value of A shows big variation in results of the normal and accelerated-aging tests.

In addition to nondestructive testing, destructive testing is needed to observe in-depth degradation behavior. Destructive testing allows for understanding the pattern of changing PD characteristics up to a certain stage of degradation. Based on the authors' own experience during recent destructive testing, the proximity of failure provides distinct behavior that must be observed.

6. Conclusions

This paper reviews various aspects of insulation aging in solids, including theoretical and experimental studies describing the aging phenomenon, aging mechanisms, useful measurement techniques, and their role in the development of efficient aging models. Major contributions in the field of insulation life modeling were made during the late 1980s and 1990s. While continuous advancements are being made on proactive diagnostic solutions, no major breakthroughs have been observed during the last two decades in developing well-defined formulation to determine the aging indices. Further, the conventional aging models discussed in this paper highlight the limitations of available models in achieving accuracy and general viability. The major limitations of the models include their viability when tested on specific materials, and also that most of the model studies do not incorporate modern grid-operating conditions. The impulsive growth in hybrid girds, DC links, impact of power electronic converters, and EV charging has raised concerns over the reliablity of insulation. As there is not enough research on insulation behavior under these conditions, future work will be oriented towards investigating all these major aspects concerning modern grid operation. The insulation samples can be tested under IEEE 1407 guidelines where samples of cable are placed in tanks for four to six months, and later, a partial-discharge test will be conducted under different scenarios. PD activity offers greater visibility and continuous tracking of the insulation-degradation process. The statistical analysis of PD data from inception to breakdown will lead to the development of the aging model. Due to the close relationship between the characteristics of the PD activity and

the mechanisms of insulation degradation, PD measurement can determine the state of the components more effectively. Low-cost nonintrusive measurement sensors such as Rogowski coils, available data-acquisition solutions, ease of installation, and simplicity of the analysis makes PD measurement an affordable methodology for aging studies. For today's developing grid, it is imperative to develop models that enable the achievement of pragmatic, well-defined, and accurate formulation for predicting the incipient faults before the equipment failure causes an unexpected outage.

Author Contributions: M.C.: literature review, conceptualization, writing—original draft, writing—review and editing, visualization; M.S.: conceptualization, writing—review and editing, supervision, resources, funding acquisition; I.K.: writing—review and editing; A.H.: writing—review and editing; P.T.: writing—review and editing; I.P.: writing—review and editing, supervision. All authors have read and agreed to the published version of the manuscript.

Funding: This work is supported by the Estonian Research Council under Grant No. PSG632 (Aging behavior of medium voltage cables under smart grid operation) and Kuwait Foundation for the Advancement of Sciences (KFAS) under Project No. PR18-18EO-01.

Institutional Review Board Statement: Not applicable.

Informed Consent Statement: Not applicable.

Conflicts of Interest: The authors declare no conflict of interest.

References

1. Saleem, M.Z.; Akbar, M. Review of the Performance of High-Voltage Composite Insulators. *Polymers* **2022**, *14*, 431. [CrossRef]
2. Campo, E.A. 4—Electrical Properties of Polymeric Materials. In *Selection of Polymeric Materials*; Plastics Design Library, Willian Andrew Inc.: Norwich, NY, USA, 2008; pp. 141–173. [CrossRef]
3. Garros, B. Ageing and reliability testing and monitoring of power cables: Diagnosis for insulation systems: The ARTEMIS program. *IEEE Electr. Insul. Mag.* **1999**, *15*, 10–12. [CrossRef]
4. Bertling, L.; Eriksson, R.; Allan, R.N.; Gustafsson, L.Å.; Åhlén, M. Survey of causes of failures based on statistics and practice for improvements of preventive maintenance plans. In Proceedings of the 14th Power Systems Computation Conference, Seville, Spain, 24–28 June 2002; pp. 1–7.
5. Dakin, T.W. Electrical Insulation Deterioration Treated as a Chemical Rate Phenomenon. *Cond. Affect. Success Main Line Electrif.* **1948**, *67*, 113–122. [CrossRef]
6. Mazzanti, G.; Montanari, G.C.; Dissado, L.A. Electrical aging and life models: The role of space charge. *IEEE Trans. Dielectr. Electr. Insul.* **2005**, *12*, 876–890. [CrossRef]
7. Densley, J. Ageing mechanisms and diagnostics for power cables—An overview. *IEEE Electr. Insul. Mag.* **2001**, *17*, 14–22. [CrossRef]
8. Van der Wielen, P.C.J.M. On-Line Detection and Location of Partial Discharges in Medium-Voltage Power Cables. Ph.D. Dissertation, Eindhoven University of Technology, Eindhoven, The Netherlands, 2005.
9. Yaacob, M.M.; Alsaedi, M.A.; Rashed, J.R.; Dakhil, A.M.; Atyah, S.F. Review on partial discharge detection techniques related to high voltage power equipment using different sensors. *Photon Sens.* **2014**, *4*, 325–337. [CrossRef]
10. Tshiloz, K.; Smith, A.C.; Mohammed, A.; Djurović, S.; Feehally, T. Real-time insulation lifetime monitoring for motor windings. In Proceedings of the 2016 XXII International Conference on Electrical Machines (ICEM), Lausanne, Switzerland, 4–7 September 2016; pp. 2335–2340. [CrossRef]
11. Zaeni, A.; Khayam, U.; Viviantoro, D. Methods for Remaining Life Prediction of Power Cable based on Partial Discharge with Regard to Loading Factor Calculation and Voltage Variation. In Proceedings of the 2019 2nd International Conference on High Voltage Engineering and Power Systems (ICHVEPS), Denpasar, Indonesia, 1–4 October 2019; pp. 180–185.
12. Srinivasan, M.; Krishnan, A. Prediction of Transformer Insulation Life with an Effect of Environmental Variables. *Int. J. Comput. Appl.* **2012**, *55*, 43–48. [CrossRef]
13. Bahadoorsingh, S.; Rowland, S. A Framework Linking Knowledge of Insulation Aging to Asset Management. *IEEE Electr. Insul. Mag.* **2008**, *24*, 38–46. [CrossRef]
14. Shafiq, M.; Kauhaniemi, K.; Robles, G.; Isa, M.; Kumpulainen, L. Online condition monitoring of MV cable feeders using Rogowski coil sensors for PD measurements. *Electr. Power Syst. Res.* **2019**, *167*, 150–162. [CrossRef]
15. Hovonen, P. Prediction of Insulation Degradation of Distribution Power Cables Based on Chemical Analysis and Electrical Measurements. Ph.D. Dissertation, Aalto University, Espoo, Finland, 2008.
16. Shafiq, M.; Kiitam, I.; Kauhaniemi, K.; Taklaja, P.; Kütt, L.; Palu, I. Performance Comparison of PD Data Acquisition Techniques for Condition Monitoring of Medium Voltage Cables. *Energies* **2020**, *13*, 4272. [CrossRef]

17. Ahmed, Z. Development of a Continuous Condition Monitoring System Based on Probabilistic Modelling of Partial Discharge Data for Polymeric Insulation Cables. Ph.D. Dissertation, Mississippi State University, Starkville, MS, USA, 2019.
18. Choudhary, M.; Suwanasri, T.; Kumpalavalee, S.; Fuangpian, P.; Suwanasri, C. Condition Assessment of Synchronous Generator Using Fuzzy Logic. *IEET Int. Electr. Eng. Trans.* **2018**, *4*, 27.
19. David, E.; Parpal, J.-L.; Crine, J.-P. Aging of XLPE cable insulation under combined electrical and mechanical stresses. In Proceedings of the 1996 IEEE International Symposium on Electrical Insulation, Montreal, QC, Canada, 16–19 June 1996. [CrossRef]
20. Zhou, C.; Yi, H.; Dong, X. Review of Recent Research Towards Power Cable Life Cycle Management. *High Volt.* **2017**, *2*, 179–187. [CrossRef]
21. Higinbotham, W. Review of Medium-Voltage Asset Failure Investigations. *Prem. Electr. Maint. Saf. Event* **2018**, *1*, 17.
22. Toshikatsu, T.; Greenwood, A. *Advanced Power Cable Technology: Present and Future*; CRC Press Inc.: Boca Raton, FL, USA, 1983; Volume 2, pp. 57–94.
23. Su, J.; Du, B.; Li, J.; Li, Z. Electrical tree degradation in high-voltage cable insulation: Progress and challenges. *High Volt.* **2020**, *5*, 353–364. [CrossRef]
24. Helleso, S.; Benjaminsen, J.T.; Selsjord, M.; Hvidsten, S. Water tree initiation and growth in XLPE cables under static and dynamic mechanical stress. In Proceedings of the 2012 IEEE International Symposium on Electrical Insulation, San Juan, PR, USA, 10–13 June 2012; pp. 623–627. [CrossRef]
25. *IEEE 1407*; IEEE Guide for Accelerated Aging Tests for Medium-Voltage (5 kV–35 kV) Extruded Electric Power Cables Using Water-Filled Tanks. IEEE: Piscataway, NJ, USA, 2017.
26. *IEEE 98*; IEEE Standard for the Preparation of Test Procedures for the Thermal Evaluation of Solid Electrical Insulating Materials. IEEE: Piscataway, NJ, USA, 2016; pp. 1–32.
27. Montanari, G.; Motori, A. Short-term thermal endurance characterization of polymeric cable insulating materials. Use of oxidative stability measurements. *IEEE Trans. Dielectr. Electr. Insul.* **1996**, *3*, 561–566. [CrossRef]
28. *IEC-60270:2000+AMD1*; High-Voltage Test Techniques-Partial Discharge Measurements. IEC: Geneva, Switzerland, 2015.
29. Hussain, G.A.; Shafiq, M.; Lehtonen, M.; Hashmi, M. Online Condition Monitoring of MV Switchgear Using D-Dot Sensor to Predict Arc-Faults. *IEEE Sens. J.* **2015**, *15*, 7262–7272. [CrossRef]
30. Simoni, L. A General Approach to the Endurance of Electrical Insulation under Temperature and Voltage. *IEEE Trans. Electr. Insul.* **1981**, *16*, 277–289. [CrossRef]
31. Simoni, L. General Equation of the Decline in the Electric Strength for Combined Thermal and Electrical Stresses. *IEEE Trans. Electr. Insul.* **1984**, *19*, 45–52. [CrossRef]
32. Simoni, L.; Mazzanti, G.; Montanari, G.; Lefebre, L. A general multi-stress life model for insulating materials with or without evidence for thresholds. *IEEE Trans. Electr. Insul.* **1993**, *28*, 349–364. [CrossRef]
33. Dissado, L.; Mazzanti, G.; Montanari, G.C. The incorporation of space charge degradation in the life model for electrical insulating materials. *IEEE Trans. Dielectr. Electr. Insul.* **1995**, *2*, 1147–1158. [CrossRef]
34. IEEE Dielectrics and Electrical Insulation Society; Multifactor Stress Committee. *IEEE Guide for Multifactor Stress Functional Testing of Electrical Insulation Systems*; IEEE: Piscataway, NJ, USA, 1991.
35. Edwards, V. *Electrons Theory*; Edtech Press: London, UK, 2018; Chapter 1; pp. 1–15.
36. Fisher, L.E.; Haries, C.D.; Lehr, J.M. Initiation and Growth of the Secondary Electron Avalanche along High-Gradient Insulators in Vacuum. *IEEE Trans. Dielectr. Electr. Insul.* **2021**, *28*, 972–980. [CrossRef]
37. *IEC 61251*; Electrical Insulating Materials and Systems-AC Voltage Endurance Evaluation. IEC: Geneva Switzerland, 2015.
38. *IEEE 930-1987*; IEEE Guide for the Statistical Analysis of Electrical Insulation Voltage Endurance Data. IEEE: Piscataway, NJ, USA, 1995.
39. Stone, G.C.; Lawless, J.F. The Application of Weibull Statistics to Insulation Aging Tests. *IEEE Trans. Electr. Insul.* **1979**, *14*, 233–239. [CrossRef]
40. Cygan, P.; Laghari, J.R. Models for insulation aging under electrical and thermal multistress. *IEEE Trans. Electr. Insul.* **1990**, *25*, 923–934. [CrossRef]
41. Pattini, G.; Simoni, L. Discussion on modeling of voltage endurance. In Proceedings of the 1980 IEEE International Conference on Electrical Insulation, Boston, MA, USA, 9–11 June 1980. [CrossRef]
42. Dakin, T.W. The Endurance of Electrical Insulation. In Proceedings of the 4th Symposium Electrical Insulation Materials, JIEE, Saclay, France, 21–23 April 1971.
43. Montanari, G.C.; Simoni, L. Aging phenomenology and modeling. *IEEE Trans. Electr. Insul.* **1993**, *28*, 755–776. [CrossRef]
44. Hirose, H. A Method to Estimate the Lifetime of Solid Electrical Insulation. *IEEE Trans. Electr. Insul.* **1987**, *22*, 745–753. [CrossRef]
45. Montsinger, V.M. Loading Transformers by Temperature. *Cond. Affect. Success Main Line Electrif.* **1930**, *49*, 776–790. [CrossRef]
46. Brancato, E. Insulation Aging a Historical and Critical Review. *IEEE Trans. Electr. Insul.* **1978**, *13*, 308–317. [CrossRef]
47. *IEEE Std 101-1987*; IEEE Guide for the Statistical Analysis of Thermal Life Test Data. IEEE: Piscataway, NJ, USA, 1988.
48. Endicott, H.S.; Hatch, B.D.; Sohmer, R.G. Application of the Eyring Model to capacitor aging data. In Proceedings of the Annual Report 1962 Conference on Electrical Insulation, Hershey, PA, USA, 15–17 October 1962; pp. 47–50.
49. Simoni, L. Application of a new geometrical approach to determination of combined stress endurance of insulating materials. *IEEE Trans. Electr. Insul.* **1988**, *23*, 489–492. [CrossRef]

50. *IEC 60216–3*; Electrical Insulating Materials—Thermal Endurance Properties—Part 3: Instructions for Calculating Thermal Endurance Characteristics. IEC: Geneva, Switzerland, 2021.
51. Nelson, W. Analysis of Accelerated Life Test Data—Part I: The Arrhenius Model and Graphical Methods. *IEEE Trans. Electr. Insul.* **1971**, *6*, 165–181. [CrossRef]
52. Mazzanti, G.; Montanari, G. A comparison between XLPE and EPR as insulating materials for HV cables. *IEEE Trans. Power Deliv.* **1997**, *12*, 15–28. [CrossRef]
53. Montanari, G.C.; Pattini, G.; Simoni, L. Long—Term Behavior of XLPE Insulated Cable Models. *IEEE Trans. Power Deliv.* **1987**, *2*, 596–602. [CrossRef]
54. Ramu, T.S. On the estimation of life of power apparatus insulation under combined electrical and thermal stress. *IEEE Trans. Electr. Insul.* **1985**, *EI-20*, 70–78. [CrossRef]
55. Montanari, G.C. Insulation Aging Models. In *Encyclopedia of Electrical and Electronics Engineering*; J. Wiley & Sons: Hoboken, NJ, USA, 1999.
56. Fallou, B.; Burguiere, C. First Approach on Multiple Stress Accelerated Life Testing of Electrical insulation. *Annu. Rep. Proc. CEIDP* **1979**, 621–628.
57. Cacciari, M.; Montanari, G. Optimum design of life tests for insulating materials, systems and components. *IEEE Trans. Electr. Insul.* **1991**, *26*, 1112–1123. [CrossRef]
58. Cacciari, M.; Montanari, G.C. Probabilistic models for life prediction of insulating materials. *J. Phys. D Appl. Phys.* **1990**, *23*, 1592–1598. [CrossRef]
59. Montanari, G.; Cacciari, M. A probabilistic life model for insulating materials showing electrical thresholds. *IEEE Trans. Electr. Insul.* **1989**, *24*, 127–134. [CrossRef]
60. Bahder, G.; Garrity, T.; Sosnowski, M.; Eaton, R.; Katz, C. Physical Model of Electric Aging and Breakdown of Extruded Pplymeric Insulated Power Cables. *IEEE Trans. Power Appar. Syst.* **1982**, *101*, 1379–1390. [CrossRef]
61. Montanari, G. Aging and life models for insulation systems based on PD detection. *IEEE Trans. Dielectr. Electr. Insul.* **1995**, *2*, 667–675. [CrossRef]
62. Zhang, Y.; Lewiner, J.; Alquie, C.; Hampton, N. Evidence of strong correlation between space-charge buildup and breakdown in cable insulation. *IEEE Trans. Dielectr. Electr. Insul.* **1996**, *3*, 778–783. [CrossRef]
63. Crine, J.-P.; Parpal, J.-L.; Lessard, G. A model of aging of dielectric extruded cables. In Proceedings of the 3rd International Conference on Conduction and Breakdown in Solid Dielectrics, Trondheim, Norway, 3–6 July 1989; pp. 347–351.
64. Sanche, L. Electronic aging and related electron interactions in thin-film dielectrics. *IEEE Trans. Electr. Insul.* **1993**, *28*, 789–819. [CrossRef]
65. Griffiths, C.; Freestone, J.; Hampton, R. Thermoelectric aging of cable grade XLPE. In Proceedings of the Conference Record of IEEE International Symposium on Electrical Insulation, Arlington, VA, USA, 7–10 June 1998; Volume 2, pp. 578–582.
66. Dissado, L.A.; Mazzanti, G.; Montanari, G.C. The role of trapped space charges in the electrical aging of insulating materials. *IEEE Trans. Dielectr. Electr. Insul.* **1997**, *4*, 496–506. [CrossRef]
67. Mazzanti, G.; Montanari, G.; Dissado, L. A space-charge life model for ac electrical aging of polymers. *IEEE Trans. Dielectr. Electr. Insul.* **1999**, *6*, 864–875. [CrossRef]
68. Gubanski, S.M. Analysis of lifetime estimation methods based on data for electro-thermally aged PET films. In Proceedings of the Conference Record of IEEE International Symposium on Electrical Insulation, Toronto, ON, Canada, 3–6 June 1990; pp. 27–30. [CrossRef]
69. Cavallini, A.; Fabiani, D.; Montanari, G.C. Power electronics and electrical insulation systems—Part 2: Life modeling for insulation design. *IEEE Electr. Insul. Mag.* **2010**, *26*, 33–39. [CrossRef]
70. Frigione, M.; Rodríguez-Prieto, A. Can Accelerated Aging Procedures Predict the Long Term Behavior of Polymers Exposed to Different Environments? *Polymers* **2021**, *13*, 2688. [CrossRef] [PubMed]

Publication II

M. Choudhary, M. Shafiq, I. Kiitam, I. Palu, and P. Taklaja, “Study on the Progression of Surface Partial Discharge in Power Cables”, IEEE 63rd Annual International Scientific Conference on Power and Electrical Engineering of Riga Technical University (RTUCON), 2022, doi: https://10.1109/RTUCON56726.2022.9978804.

2022 IEEE 63th International Scientific Conference on Power and Electrical Engineering of Riga Technical University (RTUCON)

Study on the Progression of Surface Partial Discharge in Power Cables

Maninder Choudhary
Department of Electrical Power Engineering & Mechatronics
Tallinn University of Technology
Tallinn, Estonia
machou@taltech.ee

Muhammad Shafiq
Department of Electrical Power Engineering & Mechatronics
Tallinn University of Technology
Tallinn, Estonia
muhammad.shafiq@taltech.ee

Ivar Kiitam
Department of Electrical Power Engineering & Mechatronics
Tallinn University of Technology
Tallinn, Estonia
ivar.kiitam@taltech.ee

Ivo Palu
Department of Electrical Power Engineering & Mechatronics
Tallinn University of Technology
Tallinn, Estonia
ivo.palu@taltech.ee

Paul Taklaja
Department of Electrical Power Engineering & Mechatronics
Tallinn University of Technology
Tallinn, Estonia
paul.taklaja@taltech.ee

***Abstract*—Surface discharge or surface tracking is one of the destructive types of discharge that travels along the insulation surface. In cables, surface partial discharge (SPD) can be caused due to contamination and moisture. Poor installation and maintenance are also major causes of SPD. Partial discharge (PD) measurement is an efficient technique, used for the assessment of insulation conditions in medium and high voltage assets. PD pulses contain information that describes the nature of PD and the severity of a defect in the insulation. Several characteristics such as accumulated charge, average discharging current, and discharge power are used that indirectly describe behaviour of a PD activity within the insulation. This study investigates the behaviour of quantities related to partial discharge pulse such as the number of pulses (observed during full AC cycle of the applied voltage) and pulse amplitude (peak and average) at progressive electrical stress. An algorithm has been developed that efficiently identifies the first occurring PD pulse of individual PD event, its polarity, and peak amplitude. The probabilistic analysis is also performed to investigate the behavior of pulse characteristics at progressive degradation.**

Keywords— Power cables, insulation aging, surface partial discharge, pulse analysis, electrical stress.

I. INTRODUCTION

Insulation is an essential component of power system assets including cables. The long-term and continuous partial discharge activity deteriorate insulation chemically and change the morphological properties of the insulation [1]. PD is a localized breakdown that causes degradation of insulation. Physically PD can be explained by the electron avalanche mechanism. Under high electrical or thermal stress, the free electrons in insulating materials gain sufficient kinetic energy and start colliding with other molecules of insulation or surroundings. The exponential growth of free electrons initiates an avalanche of electrons that develops fast current pulses at critical points of insulation called PD [2]-[3].

Surface partial discharge (SPD) is the most common type of discharge take place in presence of moisture, contaminants, and conducting paths which initiate from the conductor to the insulation surface. In cables, SPDs initiate due to the appearance of liquid, gas, or along the vicinity of solid dielectric surfaces in presence of both normal and tangential components of electric field strength. These discharges propagate through cracks, contaminated routes, or parts with a lack of electrical clearance. The ionization of atoms results in the development of a strong concentrated electric field on the surface and at termination, joints, and sharp edges. Poor environmental conditions like humidity, moisture, or dust accelerate the SPDs [4]. SPDs can cause electric erosion when they interact with heat and moisture and may cause erosion that changes the morphological properties of insulation [5]. The increase in the PD activity will accelerate the surface tracking and erosion phenomenon that can reduce the life of the insulation. Considering the phase-resolved partial discharge PRPD pattern of surface discharges, the occurrence of PD pulses between 0° to 90° is the result of streamer discharges present on the surface, and pulses from 180°-270° are the result of continuous discharges due to the memory effect [6] as shown in Fig. 1. The accumulated charges in the previous voltage cycle produce sustained discharges. Usually, the SPD pulses are unsymmetrical with a wide range of magnitude and have a low repetition rate.

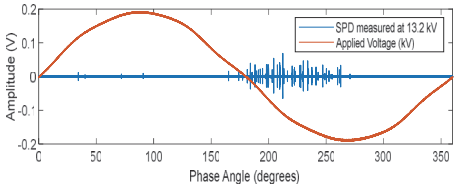

Fig. 1. PRPD pattern of SPD at 13.2 kV

PD quantification is a very useful tool for finding PD intensity, nature of the defect, and insulation degradation pattern. However, due to the random and immanent stochastic behavior of the PD phenomenon, the interpretation of PD in correlation to the aging or degradation of insulation is complex. It is important to characterize the behavior of the PD signals in relation with the degradation mechanism occurring inside the defects. During a PD event, localized breakdown causes rapid displacement of the charges that induces high frequency (HF) PD current pulses on the conductor (of the cable) and can be measured using HF sensors [7]. It is found that PD activity inside defect varies

2022 IEEE 63th International Scientific Conference on Power and Electrical Engineering of Riga Technical University (RTUCON) | 978-1-6654-6558-8/22/$31.00 ©2022 IEEE | DOI: 10.1109/RTUCON56726.2022.9978804

978-1-6654-6558-8/22/$31.00 ©2022 European Union

Authorized licensed use limited to: Tallinn University of Technology. Downloaded on October 03,2025 at 07:15:48 UTC from IEEE Xplore. Restrictions apply.

during progression. Initially the PD activity was consisted of narrow pulses of large magnitude appearing in a virgin flat cavity. Later the appearance of conductive layer at the cavity surface resulted in wider and low amplitude PD pulses [8]. Various approaches have been presented providing good understanding of quantifying the intensity of defect in power cables including accumulated charge, average charge, average discharging current, discharge power, repetition rate etc.[9]. These quantities consider all PD data including oscillations. Different dimension and noise reduction techniques were also used to reduce dimension of PD data set and to eliminate the noise [10]-[11].The probabilistic methods were also used for risk assessment and life estimation of insulation [12]. The work done in [13] studies the amplitude, number of pulses per power frequency cycle, pulse repetition rate, rise time, and pulse width to observe the traces of PD mechanism.

Valuable work has been performed over the last two decades to observe insulation degradation behavior. However, there has been lack of well formulated toolsets that can be used for simplified and efficient understanding and evaluation of the progression stages of the insulation defect. The core objective of this study is to correlate the behavior of PD pulse characteristics with progressive degradation. PD pulses, particularly the first occurring pulse in a PD event is considered as actual representation of a PD event within the insulation. The rest are the oscillations caused due to vibration and attenuation caused by sensitivity and calibration of measuring equipment. In-depth analysis of PD pulses at different degradation stages may lead to a better understanding of degradation behavior with time and increasing stress conditions. In this study, the first occurring PD pulse is extracted from a PD data without implementation of dimension reduction and noise elimination methods. The purposed algorithm detects the first occurring PD pulse at a threshold value. The comparative assessment of number of pulses and peak pulse amplitude at progressive degradation is performed which is the key finding of this study. Probabilistic analysis is also performed to estimate behavior of average and peak pulse amplitude at increasing degradation. The outcome of this study will provide a useful ground for the development of an efficient tool for the understanding aging behavior of insulation.

II. EXPERIMENTAL SETUP

The layout of an experimental setup for PD measurement in accordance with IEC 60270 is shown in Fig. 2. The setup consists of the following equipment.

A high voltage test transformer *T*, which is connected to medium voltage variable AC supply to vary the applied voltage in steps.

A coupling capacitor of range *C* of range 1 nF and 100 kV rating, connected in parallel to the test transformer and cable sample to measure the PDs.

A high-frequency current transformer (HFCT) of bandwidth 80 MHz (-3dB) and transfer ratio of 1:10 connected as a measuring sensor to a coupling capacitor for the measurement of PD pulses

A digital storage oscilloscope (DSO) of sample rate (250 MS/s) is connected to HFCT using coaxial cable.

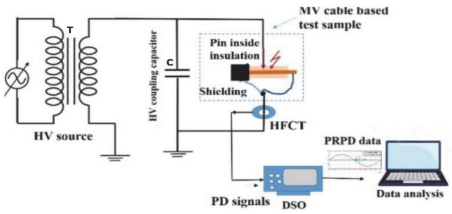

Fig. 2. Layout of PD measurement setup [14]

In this study, an MV cross-linked polyethylene XLPE cable sample of length 3 m is chosen as the test object (TO). A defect is created by damaging cable termination to produce a surface discharge as shown in Fig .3. The outer shield and jacket were removed from one end of the cable approx. 30 cm of the cable to reach the main insulation. The main conductor was grounded where HFCT was connected. The propagation of PD pulses occurs from the PD source to the ground and HFCT.

Fig. 3. Modelling of surface discharge at MV cable termination

III. PD MEASUREMENT AND EXTRACTION OF PD CHARACTERISTIC QUANTITIES

The stochastic nature of PD pulses makes it difficult to interpret the PD behavior. Each PD activity appears in the shape of a pulse in an oscilloscope or measuring equipment. These pulses may vary due to the presence of micro cavities in the neighborhood of the main cavity. This causes the random occurrence of pulses of different magnitudes. PRPD pattern during an ac cycle is an effective method that provides a variation of PD pulses in one full cycle of applied voltage. Fig. 4 shows the PRPD pattern of surface discharge PDs, at different stress levels starting from 5.9 kV to 7.12 kV and 8.1 kV, and 9.1 kV). The PD pulses (U*i*) are observed in a full cycle (20 ms) which is the reference time t_{ref} of applied AC voltage. For accuracy and preciseness, 32 readings were collected on each stress level. The core objective of this study is to analyze the behavior of PD during full cycle of applied AC voltage. Thus, the scaling of the y-axis is kept in volts according to the PD. However, the applied voltage rating is in the kV. The PD activity initiated at 5.9 kV and only one pulse is observed at partial discharge inception voltage (PDIV) as shown in Fig. 4. The peak value of the pulse is observed as 0.01 mV. The measurements were taken at an increasing electrical stress level of 1 kV approximately.

Authorized licensed use limited to: Tallinn University of Technology. Downloaded on October 03,2025 at 07:15:48 UTC from IEEE Xplore. Restrictions apply.

However, PD activity was not taken beyond 13.5 kV as breakdown occurred on that level.

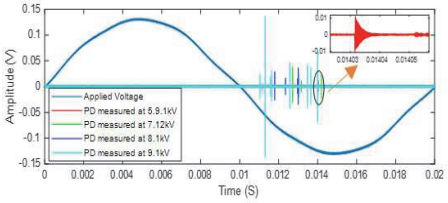

Fig. 4. PRPD Pattern at various stress levels and PD pulse at PDIV

According to IEC 60270, conventional PD measurement involves the recording of PD pulses (voltage or current) of amplitude proportional to charge results from a PD activity. Commercial diagnostic systems use PRPD patterns to represent apparent charge/pulses with respect to time or phase angle. However, for detailed analysis of PD non-conventional methods are used which involve high sensitivity and ultra-bandwidth sensors like HFCTs, due to their proven efficiency in practical implications. The PD pulse of a certain magnitude U_{PD}, measured through HFCT can be used to determine the overall charge is given by

$$q_{PD} = \frac{1}{R}\int_{t_1}^{t_2} U_{PD}(t).dt \qquad (1)$$

Where $U_{PD}(t)$ in (1) is the amplitude of sample at instant t and R is the resistance of measuring equipment. The accumulated charge q_{PD} and time t can be processed to extract different quantities like accumulated charges, average discharging current, etc., These characteristic quantities indirectly describe the actual phenomenon of a PD source. Besides the above, other characteristics of PD pulse such as the number of pulses, maximum pulse amplitude, rise time, fall time, and pulse width are also important for a deeper understanding of the PD phenomenon and location of PD. PD pulse can be represented by a double exponential function,

$$PD_{Pulse}(t) = A(e^{-a_1 t} - e^{-a_2 t}) \qquad (2)$$

Where A in (2) is the peak value of PD pulse, a_1 is the rate of rise time, a_2 rate of fall time of pulse [15]. Fig. 5 shows a typical PD pulse and the characteristics of the PD pulse. Let's say the peak value of pulse is P, then the rise time T_r is the time pulse takes to increase its magnitude from 10% to 90% of the peak value. Similarly, the fall time T_f is the time that a pulse takes to decay from 90% to 10% of its peak value. The pulse width T_w is the time interval between 50% of peak value on both sides [16].

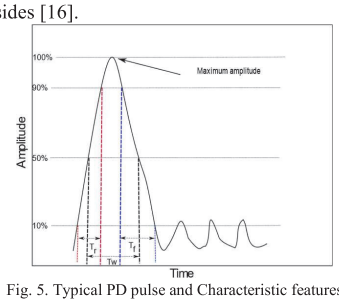

Fig. 5. Typical PD pulse and Characteristic features

An algorithm is developed that identifies and number of PD pulses their peak values (positive and negative) throughout an AC cycle of the applied voltage. Further, this algorithm also identifies the first occurring PD pulse above a threshold value Fig. 6 shows the block diagram of purposed algorithm.

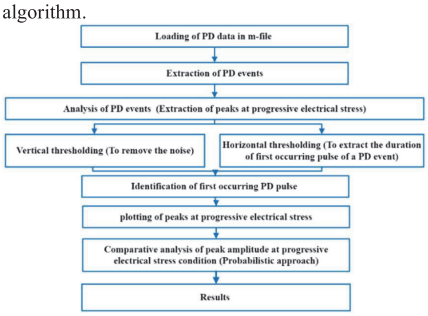

Fig. 6. Block diagram of peak detection algorithm

Fig. 7 shows the peak pulses recorded at 9.1 kV. Considering the number of pulses, 10 pulses appeared during the full ac cycle of the applied voltage.

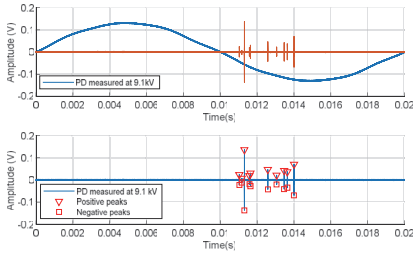

Fig. 7. PD measured at 9.1 kV and corresponding peaks (positive and negative)

The qualitative analysis of PD pulses from PDIV to breakdown follows an increasing pattern as shown in fig 7. After PDIV at 7.1 kV three pulses were observed, with a further increase, at 10.2 kV thirteen pulses were observed. Fifty-one pulses were observed near the breakdown voltage (13.2 kV). Fig. 8 shows the behavior of the number of pulses at each stress level. There is an exponential rise in the number of pulses with increasing stress during SPDs.

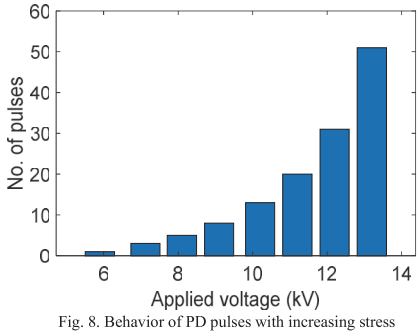

Fig. 8. Behavior of PD pulses with increasing stress

Authorized licensed use limited to: Tallinn University of Technology. Downloaded on October 03,2025 at 07:15:48 UTC from IEEE Xplore. Restrictions apply.

Considering the time-span of overall PD activity, at PDIV the PD activity appeared only at 0.014 seconds. With increasing stress levels, the activity span increased. At 7.1 kV PD activity started at 0.013 seconds and ended at 0.014 sec, and with a further increase in stress to 12.1 kV the span increased more. PD activity started at 0.010 sec and ended at 0.015 sec which indicates that as stress increases the time-span of PD activity increases. Also, as stress increases the PD activity appears in the positive half cycle of the applied voltage. Fig. 9 shows a stem plot (at different stress levels) of the first occurring PD pulses and their location during the full AC cycle. It can be seen from PDIV to 9.1 kV the PD activity appeared only in the negative half cycle of the applied voltage. However, as stress increased to 10.1 kV the PD activity appeared in both the positive and negative half cycle of the applied voltage.

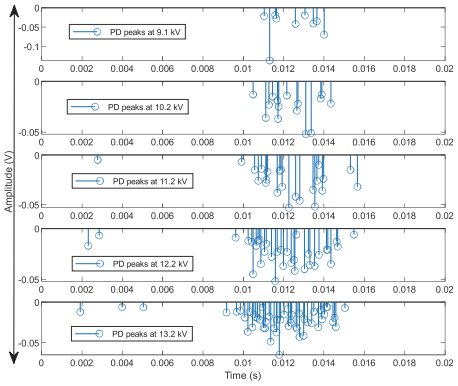

Fig. 9. First occurring peak of individual pulses at different stress levels

The statistical analysis of the number of PD pulses at different stress levels is performed. A curve fitting tool is utilized to determine the best fit distribution that efficiently characterizes the number of PD pulses observed at each stress level.

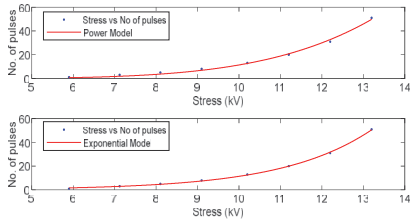

Fig. 10. Relation between stress and no. of pulses using different probabilistic models

Fig. 10 shows the behavior of number of pulses with increasing electrical stress. Two probabilistic models, exponential and power models are applied to the number of pulses data. The likelihood of any distribution model is based on the R- square values. The R-squared or coefficient of determination (COD) values for power distribution and exponential distribution was found as 0.995 and 0.999 respectively. It implies that the number of pulses (at increasing stress) during surface discharge follows an exponential distribution. Although the number of pulses is not an exact reflection of a PD activity however a trackable pattern is observed. It can be inferred that during SPD the number of pulses increases with increasing electrical stress.

The amplitude of PD pulses is a crucial parameter that describes the severity of SPD and the nature of the defect. The study of pulse amplitude and reflection is also very useful in determining the location of PD. The distribution fitting tool is utilized to determine the best-fit distribution that accurately describes the peak amplitude of PD pulses observed in the full ac cycle. Fig. 11 shows the probability density function (PDF) of various distributions (Weibull, Generalized Extreme Value distribution, and Rayleigh distribution). The skewness of 1.02 and kurtosis 4.5 represents that the data does not follow the normal distribution.

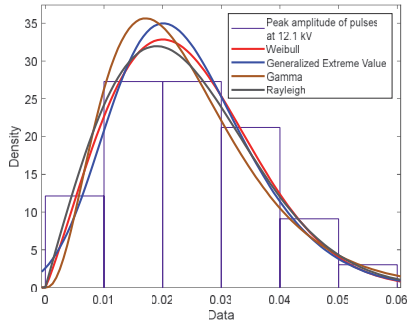

Fig. 11. Probability density function of various probability distributions applied on 13 kV peak pulse amplitude data

The goodness of fit of any probability distribution relies on the log-likelihood or COD values. Weibull distribution is an extreme value distribution that is often used to model PD data [17]. Table I shows the log-likelihood values for various distributions. The highest value of log-likelihood shows that the peak amplitude of PD pulses during the full ac cycle follows the Weibull distribution.

Table I. Log-likelihood values of various probability distributions

No.	Distribution Type	Log Likelihood
1	Gamma	100.347
2	Weibull	100.689
3	Generalized Extreme Value	99.8784
4	Rayleigh	100.607

The comparison of characteristic quantities, peak amplitude, and the average amplitude of PD pulses with increasing electrical stress is also analyzed in this study.

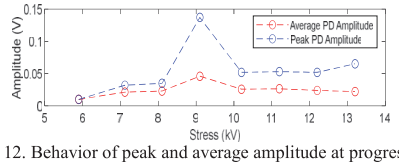

Fig. 12. Behavior of peak and average amplitude at progressive electrical stress

Authorized licensed use limited to: Tallinn University of Technology. Downloaded on October 03,2025 at 07:15:48 UTC from IEEE Xplore. Restrictions apply.

Fig. 12 shows the variation of quantitative parameters including peak PD amplitude and average PD amplitude. It can be seen that the peak amplitude of PD pulses is increasing monotonically at lower electrical stress levels i.e., from PDIV to 9.1 kV. The peak amplitude values show an extreme point at 9.1 kV where the peak value was recorded as 0.137 mV. But as electrical stress is increased beyond 9.1 kV the peak amplitude value starts decreasing. Although the number of pulses was increasing exponentially at increasing electrical stress. It can also be seen that near the breakdown voltage of 12.2 kV the peak amplitude value starts increasing. Similar pattern is observed for average values at start. However, at higher stress levels (above 10.1 kV) the average amplitude follows consistent behavior as shown in Fig. 11. It implies that the degradation rate is higher at 9.1 kV. At higher stress levels degradation follows a consistent pattern.

IV. DISCUSSION & CONCLUSION

Power cables are widely used due to their high reliability and low operational cost. The operational stresses (thermal, electrical environmental, and ambient) and growing penetration of renewables particularly the use of power electronic converters increase the degradation rate. The condition-based assessment is a key technique to prevent cables from degradation and upcoming failure.

In this paper, a PD study is carried out on a medium voltage cable sample with SPD. The key goal of this study is to relate the PD characteristic quantities with insulation aging and degradation. The progression of SPD is analyzed using PD pulse characteristics at increasing electrical stress conditions. The study is based on the PRPD pattern. Considering the number of pulses, it increases exponentially with increasing electrical stress. On the other hand, the peak amplitude of pulses at increasing electrical stress follows the Weibull distribution. The study also highlights that the insulation degradation under SPD follows a two-step behavior. From PDIV till 9.1 kV the peak and average amplitude of pulses were increasing proportionally with the number of pulses. In the second step which is above 9.1 kV the number of pulses increase but the peak values started decreasing.

The stochastic nature of PD pulses suggests that the probabilistic analysis is the best way to analyze PD data. Generally, during field measurements, the engineers are not aware of the localized stress at the defects. The PD measurement-based investigation can be useful in determining the level of stress by analyzing the variation in the PD characteristics at different stress conditions. A valid correlation between quantities and degradation can lead to the development of aging patterns that can efficiently estimate the remaining life of the insulation and avoid the sudden failure of the affect components.

ACKNOWLEDGEMENT

This work is supported by the Estonian Research Council under Grant No. PSG632.

REFERENCES

[1] R. Bartnikas, “Partial discharges their mechanism, detection and measurement,” *IEEE Transactions on Dielectrics and Electrical Insulation*, vol. 9, no. 5, pp. 763–808, Oct. 2002, doi: 10.1109/TDEI.2002.1038663.

[2] C. Laurent and G. Teyssedre, “Hot electron and partial-discharge induced ageing of polymers,” in *Nuclear Instruments and Methods in Physics Research, Section B: Beam Interactions with Materials and Atoms*, Aug. 2003, vol. 208, no. 1–4, pp. 442–447. doi: 10.1016/S0168-583X (03)00649-9.

[3] M. Hoof and R. Patsch, "A physical model, describing the nature of partial discharge pulse sequences," *Proceedings of 5th International Conference on Properties and Applications of Dielectric Materials*, 1997, pp. 283-286 vol.1, doi: 10.1109/ICPADM.1997.617583.

[4] C. Thirumurugan, G. B. Kumbhar, and R. Oruganti, “Surface Discharge Characteristics of Different Solid-Liquid Insulation Materials in Power Transformers,” *IEEE Transactions on Plasma Science*, vol. 47, no. 11, pp. 5013–5022, Nov. 2019, doi: 10.1109/TPS.2019.2943550.

[5] L. Bai *et al.*, “Influence of surface discharge on the deterioration characteristics of ethylene-propylene rubber cable insulation under alternating current high voltage,” *IET Science, Measurement and Technology*, vol. 16, no. 5, pp. 293–304, Jul. 2022, doi: 10.1049/smt2.12104.

[6] W. Deng, Z. Zheng, L. Ruan, Y. Shen, Q. Xie and H. Wang, "Power apparatus insulation diagnosis through partial discharge in a smarter grid," *2010 IEEE International Symposium on Electrical Insulation*, 2010, pp. 1-4, doi: 10.1109/ELINSL.2010.5549838.

[7] I. Kiitam, M. Shafiq, P. Taklaja, M. Parker, I. Palu and L. Kütt, "Characteristic Pulse Pattern Features of Different Types of Partial Discharge Sources in Power Cables," *2021 IEEE PES/IAS PowerAfrica*, 2021, pp. 1-5, doi: 10.1109/PowerAfrica52236.2021.9543366.

[8] P. H. F. Morshuis, "Degradation of solid dielectrics due to internal partial discharge: some thoughts on progress made and where to go now," in IEEE Transactions on Dielectrics and Electrical Insulation, vol. 12, no. 5, pp. 905-913, Oct. 2005, doi: 10.1109/TDEI.2005.1522185.

[9] I. Kiitam, M. Shafiq, P. Taklaja, M. Parker, I. Palu and L. Kütt, "Characteristic Pulse Pattern Features of Different Types of Partial Discharge Sources in Power Cables," *2021 IEEE PES/IAS PowerAfrica*, 2021, pp. 1-5, doi: 10.1109/PowerAfrica52236.2021.9543366.

[10] S. Q. Wang *et al.*, “Feature optimization selection and dimension reduction for partial discharge pattern recognition,” in *CMD 2016 - International Conference on Condition Monitoring and Diagnosis*, Nov. 2016, pp. 877–880. doi: 10.1109/CMD.2016.7757962.

[11] G. O. de Andrade, A. S. O. Avelar, and H. O. de Mota, “Comparative Analysis of Partial Discharge Denoising Techniques,” in *2021 Electrical Insulation Conference, EIC 2021*, 2021, pp. 678–681. doi: 10.1109/EIC49891.2021.9612387.

[12] W. Hassan, F. Mahmood, G. A. Hussain, and S. Amin, “Risk assessment of low voltage motors based on PD measurements and insulation diagnostics,” *Measurement (Lond)*, vol. 176, May 2021, doi: 10.1016/j.measurement.2021.109151.

[13] B. Djamal, "Pulse Sequence Analysis and Pulse Shape Analysis: Methods to Analyze Partial Discharge Processes", PhD Dissertation, University Library of Siegen, 2008.

[14] IEC-60270:2000+AMD1; High-Voltage Test Techniques-Partial Discharge Measurements. IEC: Geneva, Switzerland, 2015.

[15] M. Shafiq, I. Kiitam, K. Kauhaniemi, P. Taklaja, L. Kütt, and I. Palu, “Performance comparison of pd data acquisition techniques for condition monitoring of medium voltage cables,” *Energies (Basel)*, vol. 13, no. 6, Aug. 2020, doi: 10.3390/en13164272.

[16] M. Wu, H. Cao, J. Cao, H. L. Nguyen, J. B. Gomes, and S. P. Krishnaswamy, “An overview of state-of-the-art partial discharge analysis techniques for condition monitoring,” *IEEE Electrical Insulation Magazine*, vol. 31, no. 6, pp. 22–35, Nov. 2015, doi: 10.1109/MEI.2015.7303259.

[17] A. Contin, E. Gulski, M. Cacciari, and G. C. Montanari, “Weibull approach to the investigation of partial discharges in aged insulation systems,” in *Conference Record of IEEE International Symposium on Electrical Insulation*, 1996, vol. 1, pp. 416–419. doi: 10.1109/elinsl.1996.549369.

BIOGRAPHY

Maninder Choudhary was born in Pakistan, in 1990. He received the M.Sc. degree from TGGS, KMUTNB, Bangkok, Thailand in 2018. From 2019 to 2021 he served as Lecturer at SSUET, Pakistan. Currently, he is pursuing Ph.D. degree at Department of Electrical Power Engineering and

Authorized licensed use limited to: Tallinn University of Technology. Downloaded on October 03,2025 at 07:15:48 UTC from IEEE Xplore. Restrictions apply.

Mechatronics, Tallinn University of Technology (Taltech), Estonia. His main research interest includes partial discharge diagnostics and condition monitoring of power system assets.

Authorized licensed use limited to: Tallinn University of Technology. Downloaded on October 03,2025 at 07:15:48 UTC from IEEE Xplore. Restrictions apply.

Publication III

M. Choudhary, I. Palu, I. Kiitam, M. Shafiq, P. Taklaja and A. Bhattarai, “Denoising and Extraction of Partial Discharge Pulse Characteristics Using Wavelet Denoising and Local Maxima Method,” 2024 IEEE International Conference on Power and Energy (PECon), Kuala Lumpur, Malaysia, 2024, pp. 221–225, doi: https://doi.org/10.1109/PECon62060.2024.10827085.

Denoising and Extraction of Partial Discharge Pulse Characteristics Using Wavelet Denoising and Local Maxima Method

Maninder Choudhary
Dept. of Electrical Power Engineering & Mechatronics
Tallinn University of Technology
Tallinn, Estonia.
maninder.choudhary@taltech.ee

Ivo Palu
Dept. of Electrical Power Engineering & Mechatronics
Tallinn University of Technology
Tallinn, Estonia.
ivo.palu@taltech.ee

Ivar Kiitam
Dept. of Electrical Power Engineering & Mechatronics
Tallinn University of Technology
Tallinn, Estonia.
ivar.kiitam@taltech.ee

Muhammad Shafiq
Center for Advanced Power Systems
Florida Stage University
Florida, USA.
mshafiq@fsu.edu

Paul Taklaja
Dept. of Electrical Power Engineering & Mechatronics
Tallinn University of Technology
Tallinn, Estonia.
paul.taklaja@taltech.ee

Abhinav Bhattarai
Dept. of Electrical Power Engineering & Mechatronics
Khatmandu University
Khatmandu, Nepal.
abhbhattarai@gmail.com

2024 IEEE International Conference on Power and Energy (PECon) | 979-8-3503-6197-1/24/$31.00 ©2024 IEEE | DOI: 10.1109/PECON62060.2024.10827085

***Abstract*— Partial discharge (PD) pulse characteristics describe the nature of an insulation defect, its severity, and aging behavior of electrical insulation. However, extracting these characteristics requires sophisticated tools in order to denoise measured PD data, detect actual PD pulses, and analyze the corresponding characteristics. This paper proposes an effective tool that utilizes a simple hybrid approach based on wavelet denoising and the local maxima technique that denoises PD data acquired using a high-frequency current transducer. After denoising, it detects PD pulses from a time series dataset and identifies corresponding primary features like peak pulse amplitude and location. In addition, it can extract pulse shape (rise time, fall time and pulse width), and pulse sequence (voltage interval and time interval) features. Developed tool is computationally efficient as it precisely detects major PD events and corresponding features from a large data set while rejecting noise. Efficiency of tool is checked by implementing it on various data sets obtained from experimental investigation performed on three distinct types of defects, i.e., corona, surface, and internal discharge. Results show that this tool can be used for the identification of defect types, their progression, and aging studies to estimate the remaining lifetime based on changing PD behavior.**

Keywords—partial discharge, pulse features, electrical stress, wavelet denoising, local maxima.

I. Introduction

Electrical utilities around the world rely on the vast network of power cables to deliver power from generator to the load centres. These cables have different parts and insulation is one of the major components. The studies on power cable failure show that insulation breakdown is a primary cause of the faults in cables. These faults are the result of operating stresses and defects, occur during manufacturing and installation [1-3].

Occurrence of partial discharges is a cardinal indicator that describes the degradation and aging of electrical insulation in power system assets including cables. PD as an extrinsic aging factor impacts the dielectric properties and voltage endurance capability of insulation and can eventually cause premature failure. Therefore, it is beneficial to detect PD as early as possible to protect the cable from failure. Modern grids rely on the reliable operation of power system assets. PD measurements can provide useful information which can be helpful to identify incipient faults and develop predictive maintenance strategies, thereby improving the reliability of the overall system [4].

Three common PD types are found in cables, namely corona, surface, and internal discharge. These PD sources are found at weak points of the insulation, mainly at sharp edges or cable terminations, rough surfaces, cavities, and other defective locations. Their severity increases with time and intensity of operating stresses. Surface and internal PD are considered severe as they directly affect the insulation. Surface discharge causes surface tracking which may lead to internal PD eventually. Whereas internal PD is more severe and may lead to electrical trees with time, which is a prime cause of failure of insulation [5]. Fig.1 shows phase resolved partial discharge (PRPD) patterns obtained from PD measurement performed on three defects in the laboratory as shown in Fig.3 (a, b, c).

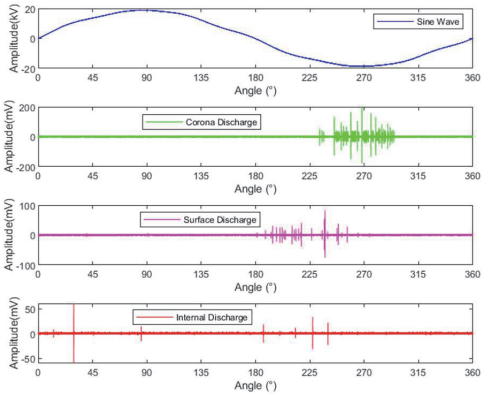

Fig.1. PRPD pattern of three types of defects, corona, surface, and internal discharge obtained through measurement on defects.

PD measurement has several advantages over other insulation diagnostic methods. Visually, a PRPD pattern can

2024 IEEE International Conference on Power and Energy (PECon) | 979-8-3503-6197-1/24/$31.00 ©2024 IEEE

Authorized licensed use limited to: Tallinn University of Technology. Downloaded on October 03,2025 at 07:16:34 UTC from IEEE Xplore. Restrictions apply.

identify the nature and severity of any defect. However, the detailed investigation about type of defect and its location or solid inferences from measurement is complex and requires field expertise. PD activity within the insulation can be described or quantified through PD features. These characterises represent actual PD activity. Several researchers have utilized various features for defect classification, pattern recognition and life assessment of insulation. In [6], IEC 60270 features including accumulated charge (Q_{acc}), average discharging current (I_{avg}), discharge power (P) and quadratic rate (D) are extracted from PD data, acquired from three defects, corona, internal and surface discharge. Behavior of these features is investigated under electrical stress. In [7], pulse shape features rise time (t_r), fall time (t_f) and pulse width (t_w) are extracted from a dataset acquired from a cable sample with a surface defect and their behavior is investigated under electrical stress. In [8], pulse features are utilized where classification of defects is performed using pulse sequential analysis and long short-term memory networks. In [9], pulse features V_m, phase of occurrence (Φ), pulse repetition rate (n) and phase span (Φ_{span}) are extracted from a cable sample with surface defects and their behavior is analysed under electrical stress. Abovementioned research studies highlight three major points.

- PD pulse features are very useful in detailed investigation of PD behavior.
- These features play a crucial role in dimensionality reduction of data which in turn decreases computational time.
- Several machine learning (ML) and artificial intelligence-based tools rely on these features.

PD measurement through HFCT requires sophisticated tools that not only denoise the incoming PD signal but also can detect PD pulses appearing in a measured time series data. Several denoising methods are available in the literature however these methods require additional ML tools for dimensionality reduction and feature extraction of PD data [10-12]. ML methods often require large amount of data and computationally intensive. This paper proposes a novel tool that uses simple hybrid approach that not only denoises PD data, but it also detects actual PD pulse and corresponding features. In this article, section II describes the methodology procedure adopted from data acquisition to feature extraction and section III shows the results obtained via developed tool.

II. STEPS FOR FEATURE EXTRACTION

Overall process from data acquisition to feature extraction is performed in four steps. Fig. 2 shows the overall procedure, which includes data acquisition, denoising, detection of actual PD pulses and extraction of characteristic features.

Fig.2. Steps for extraction of denoising and extraction of PD pulse characteristics.

A. PD Data Acquisition

PD data is acquired from a laboratory-based test setup. Fig.3 shows three types of defects. Corona defect is created by the two electrodes (pin-to-plane) configuration. PD inception was noted at 11 kV and PD measured at 11.8 kV. Surface defect was created by removing the stress cone of the cable termination. Inception of surface discharge is observed at 6.5 kV and PD measurement is conducted at 12.2 kV. The internal defect is created by introducing a cut, which protrudes into the outermost layer of the insulation. PD inception occurred at 8 kV and PD data were collected at 11.4 kV and 12.8 kV. Fig. 4 shows a schematic of the laboratory measurement setup. The experimental setup includes a high voltage variable AC source of 50 Hz frequency, coupling capacitor of 36 kV and 1 nF capacitance, high frequency current transducer (HFCT) of 1:10 transfer ratio, 11 kV XLPE cable samples with defects and digital oscilloscope set at sampling rate of 250 MS/s.

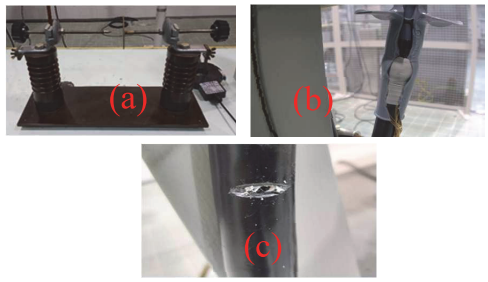

Fig.3. Three defects modelled in the laboratory a) corona discharge; b) surface discharge; c) internal discharge.

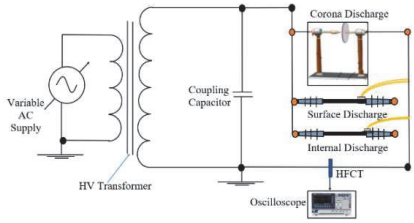

Fig.4. Schematic diagram of test setup designed for PD measurement in different types of defects.

B. Denoising of PD data

PRPD acquisition through HFCT is subject to various types of noise, including white noise, random noise, interferences due to equipment and communication systems. Removal of noise is essential to preserve original signal features for the analysis.

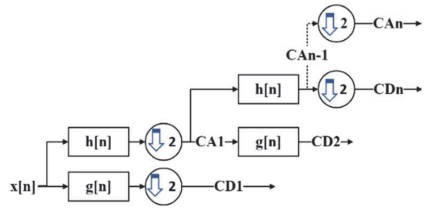

Fig. 5. Block diagram of discrete wavelet based denoising at n levels.

Several techniques including fast Fourier transform, frequency domain, and wavelet based denoising have

Authorized licensed use limited to: Tallinn University of Technology. Downloaded on October 03,2025 at 07:16:34 UTC from IEEE Xplore. Restrictions apply.

previously been used according to the literature to denoise PD data. Among all techniques, wavelet denoising is one of the more efficient techniques. Wavelets provide multiresolution analysis both in the frequency and time domain unlike Fourier transform, which only analyzes signal in the frequency domain [13].

In this study, discrete wavelet transform (DWT) is used as it is effective for signals with transient and non-stationary behavior, while also being computationally efficient. Fig. 5 shows the block diagram of DWT. It consists of three steps.

1) Decomposition: a mother wavelet is chosen along with levels and the signal is decomposed into *n* levels.
2) Thresholding: for each level, a thresholding method is chosen that performs thresholding at each level.
3) Reconstruction: finally, the reconstruction of the signal is performed based on approximation and detailed co-efficients obtained from levels 1 to *n*.

PD signals, acquired via oscilloscope are denoised using wavelet denoising technique. Initially, a mother wavelet is chosen. Choice of the mother wavelet solely depends on the shape of the PD pulse. Two Daubechies mother wavelets, db2 and db8, fulfill that criterion as their shape resembles the PD pulse. Levels define the compression and stretching of signal amplitude. Different levels are compared in this study and the maximum value of levels λ is calculated from (1), where l is the length of the signal.

$$\lambda = 2.\log(l) \tag{1}$$

In the next stage, a threshold is defined. There are several methods including soft, hard, and adaptive thresholding for denoising of PD signals. In this study, an adaptive thresholding method is used where threshold value is calculated using Stein's unbiased risk estimate (SURE) technique as it automatically calculates threshold value by observing the signal characteristics. Hard thresholding is used as it gives an improved PD signal-to-noise ratio in comparison to soft thresholding [14].

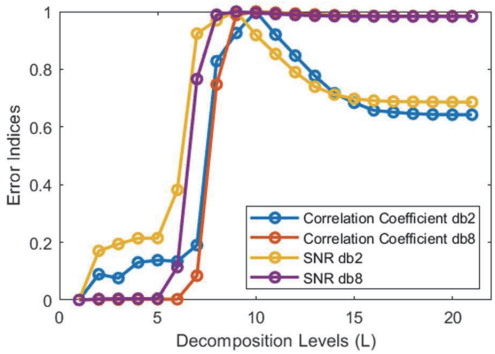

Fig. 6. Error indices for optimum level of wavelet denoising.

Different wavelet configurations based on the levels are compared and an optimum wavelet is selected based on the correlation coefficient and signal-to-noise ratio (SNR) value. Fig. 6 shows the correlation coefficient, and SNR values at different decomposition levels. Db8, level 9 shows the highest correlation with a value of 0.9954. Fig. 7 shows noisy and denoised signal obtained using DWT, db8, level 9. After denoising process (green), PD signals are more distinguished as spurious noise is removed, showing clear representation of PD events across phase angle.

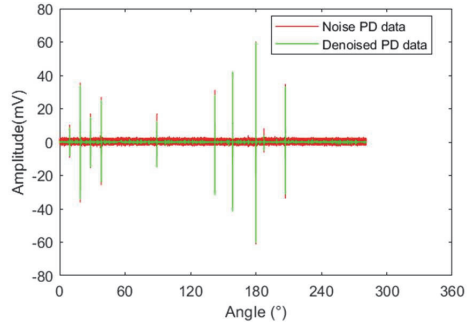

Fig. 7. Noisy signal acquired from internal defect at 12.8 kV (red) and corresponding denoised using DWT (green).

C. Detection of PD Pulse and Location

Acquisition through HFCT has the number of pulses in a PRPD pattern as shown in Fig. 7. Thus, it is cumbersome to detect individual pulses and its location from a PRPD pattern. Extraction of pulse features solely relies on the peak value of a PD pulse, its polarity, and location. For this, local maxima-based algorithm is developed. Fig. 8 shows the flowchart of the developed algorithm.

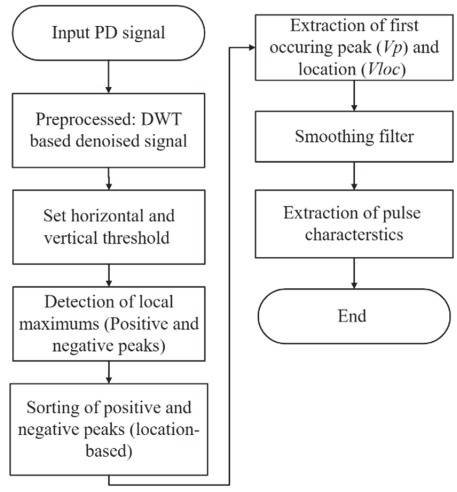

Fig. 8. Flowchart of DWT and local maxima-based algorithm.

It takes denoised signal as an input and operates based on two thresholds, i.e., horizontal, and vertical. Choice of the optimum threshold values is crucial for accurate detection of pulses and corresponding characteristics. Vertical threshold is set to detect pulses above a certain threshold value. Threshold value varies with the input signal. In this study, the maximum value obtained out of the first 2000 samples are set as vertical threshold. Whereas horizontal threshold 12.8 µs or 2000 samples is set as the deadtime of individual PD pulses in a measured PD signal. The MATLAB peak detection function is used to detect pulses in the measured signal. Although the

Authorized licensed use limited to: Tallinn University of Technology. Downloaded on October 03,2025 at 07:16:34 UTC from IEEE Xplore. Restrictions apply.

developed tool can detect actual PD pulses in a time series data or in a PRPD pattern. However, detectability is solely relied on choice of threshold values. Incorrect values may lead to inaccurate detection of PD pulses.

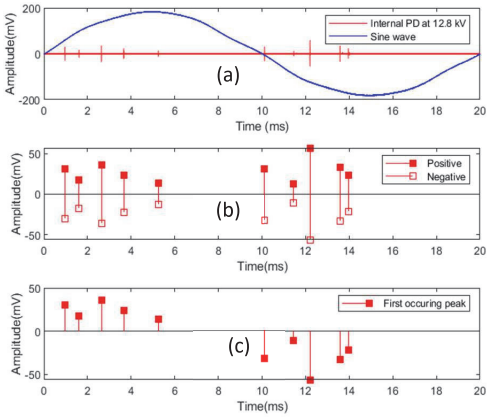

Fig. 9. PRPD pattern of Internal PD b) Corresponding negative and positive peaks of PD pulses c) First occurring PD pulses

Initially, it detects the positive and negative peaks of individual pulses. In the next stage, it sorts the positive and negative peaks based on their location. After sorting it verifies if positive peaks equal negative peaks. If this condition is met, it sets first peak of first pulse as reference and considers every third peak as peak of the following PD pulse. Fig. 9 (a) shows a measured signal of internal PD, (b) steam plot showing corresponding positive and negative peaks and (c) showing first occurring peak of individual PD pulses respectively.

D. Extraction of Pulse Charaterstics

PD charaterstics play a crucial role in investiation of PD behavior, in particular defect classfication and lifetime studies. Following are the basic charaterstics that the developed tool can detect.

a) Peak Amplitude of PD Pulse (V_m)

Maximum value attained by a PD pulse. In PD measurement first occuring pulse is an actual PD pulse, the rest is reflection or oscillation of PD signal. Its value is extracted using developed tool. It can extract the instantanous value of the applied AC voltage (V_{app}).

b) Peak Location (V_{loc})

Sample location of V_m of individual pulse (peak) in a PRPD pattern or in a AC cycle of the applied voltage.

c) Time of Occurrence (t_{loc})

Time at which PD pulse occurred in an AC cycle. It is calculated by (2)

$$t_{loc} = T_{interval} * V_{loc} \tag{2}$$

d) Phase of Occurrence (Φ_{loc})

It is defined as the angle at which PD pulse occurs in an AC cycle of the applied voltage. It is calculated by (3).

$$\Phi_{loc} = \left(\frac{t_{loc}*360}{0.02\ sec}\right) \tag{3}$$

e) Number of Pulses or Pulse Repetition Rate (n)

Number of pulses occurred in ac cycle of the applied voltage. It is calculated by (4).

$$n = \left(\frac{no.of\ pulses}{one\ cylce}\right) \tag{4}$$

f) Phase Span (Φ_{span})

Overall Span of the PD activity in positive and negative half cycle. It can be calculated as (5)

$$\Phi_{span} = \Phi_f - \Phi_i \tag{5}$$

Where Φ_i and Φ_f represent phase of occurrence of initial and final PD pulse in an AC half-cylce.

g) Pulse Sequential Charateristics

Pulse sequence analysis is one of the efficient methods widely used for the classification of defects in power cables [6]. The developed tool can extract the voltage interval (ΔU) and time interval (Δt) between sequence of pulses.

h) Pulse Shape Characteristics:

Pulse shape characteristics, particularly pulse width (t_w) that describe discharge type whether its steamer or Townsend. The pulses with small width represent streamer type breakdown and with large width are result of Townsend breakdown [15]. The developed tool can extract pulse shape characteristics including rise time (t_r), fall time (t_f), and pulse width (t_w) [7]. For this MATLAB pulse shape functions are used to extract shape characteristics.

III. RESULT

Fig.10 shows a polar plot highlighting the peak amplitude of individual pulses, phase of occurrence, phase span of PD activity. Pulses of three data sets acquired from each defect are incorporated in the polar plot.

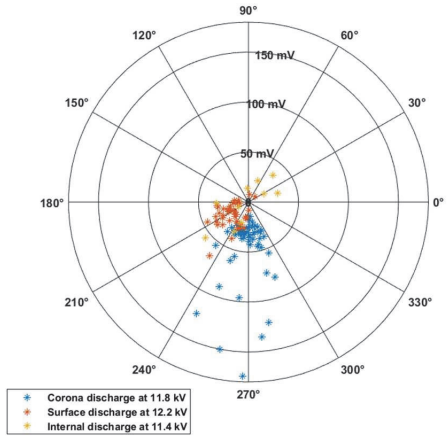

Fig. 10. Polar plot highlighting peak pulse amplitude and phase location of PD pulses acquired during full ac cycle.

Authorized licensed use limited to: Tallinn University of Technology. Downloaded on October 03,2025 at 07:16:34 UTC from IEEE Xplore. Restrictions apply.

Corona activity is observed only in the negative half cycle of the applied voltage between 230°–300°, whereas surface discharge activity is asymmetrical as few pulses are observed in positive half cycle but most of the PD activity is observed in the negative half cycle between 181°–270°. Internal discharge is symmetrical to both axis as PD activity is observed between 0°–90° in positive half cycle and 180°–270° in negative half cycle of the applied voltage. Considering the amplitude, the corona discharge pulses have higher amplitude, as some of the pulses are observed above 60 mV whereas during surface and internal activity the pulse amplitude is below 50 mV. Table I show various PD characteristics extracted from a PRPD pattern of internal discharge at 12.8 kV.

IV. CONCLUSION

This article proposes a novel tool that utilizes a simple hybrid approach consisting of wavelet denoising and local maxima techniques, which denoises PD data, detect actual PD pulse and extracts major pulse features from a PRPD pattern. Various features are extracted using developed tool. In addition to the above characteristics, statistical parameters including mean, variance skewness, and kurtosis values can be extracted using Matlab functions. Future works include PCA based investigation so that features with a higher degree of variation can be used for classification of defects, aging studies, condition monitoring and fault prediction in insulation of power cables.

TABLE I. PARTIAL DISCHARGE PULSE CHARACTERISTICS EXTRACTED FROM THE PRPD PATTERN ACQUIRED VIA CABLE SAMPLE WITH INTERNAL DEFECT AT 11.4 KV.

No.	V_m (mV)	V_{mabs} (mV)	V_{app} (kV)	V_{loc} (sample)	t_{loc} (ms)	Φ_{loc} (°)	t_r (ns)	t_f (ns)	t_w (ns)	ΔU (kV)	Δt (ms)	Φ_{span} (°)	n
1	30.7	30.7	3.9	150030	1	17.3	69.8	30.3	64.5				
2	17.7	17.7	8.4	251904	1.6	29	43.8	32.4	71.8	4.5	0.6		
3	35.9	35.9	11.8	412052	2.6	47.5	48	37.2	73.5	3.4	1	77.1	
4	23.5	23.5	14.1	571402	3.7	65.8	49.1	32.5	72.2	2.3	1.1		
5	13.6	13.6	16.5	819738	5.2	94.4	61.6	28.9	74	2.4	1.5		
6	-32.3	32.3	-0.7	1580931	10.1	182.1	46.6	31.6	61.8				10
7	-11.1	11.1	-7.9	1790254	11.5	206.2	63.8	34.3	73.9	7.2	1.4		
8	-56.2	56.2	-14.3	1906374	12.2	219.6	52.5	32.8	70	6.4	0.7	69.2	
9	-32.9	32.9	-15.7	2121417	13.6	244.4	13.1	15.1	28.8	1.4	1.4		
10	-21.7	21.7	-18.1	2181060	14	251.3	45.9	37.2	71.7	2.4	0.4		

REFERENCES

[1] M. Choudhary, M. Shafiq, I. Kiitam, A. Hussain, I. Palu, and P. Taklaja, "A Review of Aging Models for Electrical Insulation in Power Cables," Energies, vol. 15, no. 9. MDPI, May 01, 2022. doi: 10.3390/en15093408.

[2] E. M. Shaalan, S. A. Ward and A. Youssef, "Analysis of a Practical Study for Under-Ground Cable Faults Causes," 2021 22nd International Middle East Power Systems Conference (MEPCON), Assiut, Egypt, 2021, pp. 208-215, doi: 10.1109/MEPCON50283.2021.9686288.

[3] E. Maggioli, H. Leite and C. Morais, "A survey of the Portuguese MV underground cable failure," 2016 13th International Conference on the European Energy Market (EEM), Porto, Portugal, 2016, pp. 1-5, doi: 10.1109/EEM.2016.7521217.

[4] R. Bartnikas, "Partial discharges. Their mechanism, detection and measurement," in IEEE Transactions on Dielectrics and Electrical Insulation, vol. 9, no. 5, pp. 763-808, Oct. 2002, doi: 10.1109/TDEI.2002.1038663.

[5] Hartlein, N. Hampton, J.C. Hern and J. Perkel, "Overview of cable system diagnostic technologies and application", Cable Diagnostic Focus Initiative Project (CDFI), pp. 04-211, 2006.

[6] W. Hassan, M. Shafiq, G. A. Hussain, M. Choudhary and I. Palu, "Investigating the progression of insulation degradation in power cable based on partial discharge measurements", Electric Power Systems Research, vol. 221, 2023.

[7] M. Choudhary, M. Shafiq, I. Kiitam, I. Palu and W. Hassan, "Partial Discharge Pulse Shape Analysis for Progression of Insulation Degradation in Medium Voltage Cable," 2023 International Electrical Engineering Congress (iEECON), Krabi, Thailand, 2023, pp. 332-336, doi: 10.1109/iEECON56657.2023.10126589.

[8] R. Das et al., "Mathematical Morphology-Aided Bidirectional Long Short-Term Memory Network-Based Partial Discharge Pulse Sequence Classification," in IEEE Transactions on Plasma Science, vol. 51, no. 12, pp. 3454-3461, Dec. 2023, doi: 10.1109/TPS.2023.3330891.

[9] M. Choudhary, M.Shafiq, I.Kiitam, I.Palu, I.; W.Hassan, P.P.Singh, "Investigation of partial discharge characteristics in XLPE cable insulation under increasing electrical stress". Eng. Fail. Anal. 2024, 158, 108006.

[10] L. Lu, K. Zhou, G. Zhu, B. Chen and X. Yana, "Partial Discharge Signal Denoising with Recursive Continuous S-Shaped Algorithm in Cables," in *IEEE Transactions on Dielectrics and Electrical Insulation*, vol. 28, no. 5, pp. 1802-1809, October 2021, doi: 10.1109/TDEI.2021.009662.

[11] R. Hussein, K. B. Shaban and A. H. El-Hag, "Wavelet Transform With Histogram-Based Threshold Estimation for Online Partial Discharge Signal Denoising," in *IEEE Transactions on Instrumentation and Measurement*, vol. 64, no. 12, pp. 3601-3614, Dec. 2015, doi: 10.1109/TIM.2015.2454651.

[12] S. Lu, H. Chai, A. Sahoo and B. T. Phung, "Condition Monitoring Based on Partial Discharge Diagnostics Using Machine Learning Methods: A Comprehensive State-of-the-Art Review," in *IEEE Transactions on Dielectrics and Electrical Insulation*, vol. 27, no. 6, pp. 1861-1888, December 2020, doi: 10.1109/TDEI.2020.009070

[13] S. Sriram, S. Nitin, K. M. M. Prabhu, and M. J. Bastiaans, "Signal denoising techniques for partial discharge measurements," IEEE Transactions on Dielectrics and Electrical Insulation, vol. 12, no. 6, pp. 1182–1191, Dec. 2005, doi: 10.1109/TDEI.2005.1561798.

[14] X. Ma, C. Zhou and I. J. Kemp, "Automated wavelet selection and thresholding for PD detection," in IEEE Electrical Insulation Magazine, vol. 18, no. 2, pp. 37-45, March-April 2002, doi: 10.1109/57.995398.

[15] P. H. F. Morshuis, "Partial discharge mechanisms: Mechanisms leading to breakdown, analyzed by fast electrical and optical measurements ", doctoral thesis, TU Delft, 1993.

Authorized licensed use limited to: Tallinn University of Technology. Downloaded on October 03,2025 at 07:16:34 UTC from IEEE Xplore. Restrictions apply.

Publication IV

M. Choudhary, I. Palu, I. Kiitam, M. Shafiq and P. Taklaja, “Study of Partial Discharge Characteristics in Medium Voltage Cable Insulation with Internal Defect,” 2024 IEEE International Conference on High Voltage Engineering and Applications (ICHVE), Berlin, Germany, 2024, pp. 1–4, doi: https://doi.org/10.1109/ICHVE61955.2024.10676188.

Study of Partial Discharge Characteristics in Medium Voltage Cable Insulation with Internal Defect

2024 IEEE International Conference on High Voltage Engineering and Applications (ICHVE) | 979-8-3503-7498-8/24/$31.00 ©2024 IEEE | DOI: 10.1109/ICHVE61955.2024.10676188

Maninder Choudhary
Dept. of Electrical Power Engineering & Mechatronics
Tallinn University of Technology
Tallinn, Estonia.
maninder.choudhary@taltech.ee

Ivo Palu
Dept. of Electrical Power Engineering & Mechatronics
Tallinn University of Technology
Tallinn, Estonia.
ivo.palu@taltech.ee

Ivar Kiitam
Dept. of Electrical Power Engineering & Mechatronics
Tallinn University of Technology
Tallinn, Estonia.
ivar.kiitam@taltech.ee

Muhammad Shafiq
Center for Advanced Power Systems
Florida State University
Tallahassee, Florida, USA.
mshafiq@fsu.edu

Paul Taklaja
Dept. of Electrical Power Engineering & Mechatronics
Tallinn University of Technology
Tallinn, Estonia.
paul.taklaja@taltech.ee

***Abstract*— Inception of partial discharge (PD) is an important indicator of insulation degradation in power system assets, including cables. The characteristics of PD activity measured during ongoing degradation process provide information regarding the nature and severity of insulation defects. This study investigates the behavior of PD in a medium voltage (MV) cable sample with an artificial defect developed by making a cut on the outer jacket towards the shielding that extends into the main insulation. The PD activity is measured using a high frequency current transformer. A number of PD characteristics: peak pulse height, phase of occurrence, and pulse repetition rate are extracted from the PD measurements using a local maxima-based algorithm. The behavior of the PD activity based on these characteristics is analyzed under increasing electrical stress. This study can be useful in analyzing the aging and degradation behavior of solid insulating materials.**

Keywords—Power cable, partial discharge, condition monitoring, electrical stress.

I. Introduction

European electricity distribution grids are connected to almost 260 million customers. These customers heavily rely on a vast network of medium and low-voltage cables. Reliability of large networks is indeed a significant challenge for utilities and asset managers. According to a survey of cable failures conducted in Portugal, it was found that 68 percent of faults in cables occur due to different component failure. Out of these, 84% of faults occur due to insulation degradation and 14% due to intrinsic aging [1]. Thus, insulation degradation is one of the prominent causes of failure in cables. Operating stresses i.e., thermal, electrical, ambient, and mechanical (TEAM), and manufacturing defects are two main causes that contribute to degradation and extrinsic aging [2]. These stresses may initiate partial discharges (PD) at the weakest points of insulation, mainly at cable terminations, rough surfaces, voids, cavities, and other defective regions. These discharges increase with time and level of stress depending on the type of defect and eventually cause premature failure of the insulation.

PD measurement is efficient diagnostic techniques used for the condition monitoring of power system components [3]. According to IEC 60270, PD is a localized breakdown that partially bridges the insulation [4]. In cables, this localized breakdown occurs as one of three different types, i.e., corona, surface, and internal discharge. Corona discharge occurs at sharp edges, near the conductor. High electrical field strength ionizes the air surrounding the conductor and causes corona. Cables operating at medium or high voltages may create favorable conditions for surface corona at the conductor surface or braid layer in rubber-insulated cables. Surface discharges occur at exposed surfaces such as cable terminations and along the creepage discharge or surface of insulating material. These discharges are the result of poor installation, moisture, and contamination and in long run track across the insulation surface and may eventually cause internal PD. Internal PD occurs due to voids and cavities caused due to poor manufacturing and installation. These cavities, under the impact of TEAM stresses, may result in electrical trees and water trees in the presence of moisture which are considered as major causes of insulation failure [5-6]. Thus, it is customary to detect the type and severity of defects so that utility can take preventive measures to enhance the reliablity of the overall system. PD measurement is a very useful technique as it can be used to identify the nature and severity of a defect.

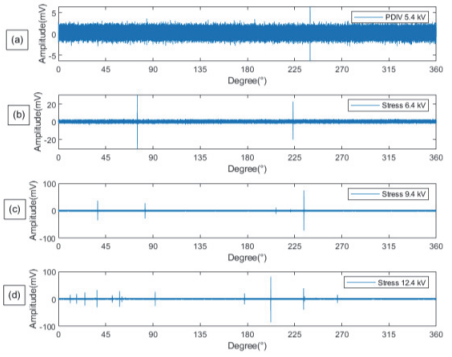

Fig. 1. PD data obtained from an internal defect modelled in MV cable insulation at different electrical stress levels a) PDIV (5.4 kV) (b) 6.4 kV c) 9.4 kV d) 12.4 kV.

Fig. 1 (a-d) presents phase-resolved partial discharge (PRPD) patterns of internal defect at different stress levels. Internal PD

979-8-3503-7498-8/24/$31.00 ©2024 IEEE

Authorized licensed use limited to: Tallinn University of Technology. Downloaded on October 03,2025 at 07:17:05 UTC from IEEE Xplore. Restrictions apply.

is mostly symmetrical regarding both positive and negative cycles of the applied ac voltage. The symmetrical pulses mainly occur between 0-90° of the positive half cycle and 180°-270° of the negative half cycle of the applied voltage. PRPD pattern due to the internal cavity follows a wave-like shape in both ac cycles. Intensity of discharges or pulses at the leading edge of PRPD pattern describes the physical geometry of the cavity within the insulation [7]. The following discharges or pulses are the by-product of discharges occurring within the cavity. Several research studies have been conducted to observe insulation degradation behavior under various scenarios i.e., nature of defects, type of stress, and supply conditions. This research shows that each insulation defect follows a distinct trend reflected by PD characteristics [8]. In [9], a surface discharge defect is created at one end of cable termination and PD data is collected via a high-frequency current transformer (HFCT) sensor. The behavior of pulse shape characteristics i.e., peak pulse height (V_m), rise time (t_r), fall time (t_f), and pulse width (t_w) is analysed under progressive electrical stress. The results show that pulse characteristics show an upward trending pattern with applied electrical stress. The statistical analysis shows that pulse shape characteristics follow a gaussian distribution with increasing electrical stress. In [10], three defects (internal, surface, and corona) are created in a cable sample, and the behavior of four characteristics including apparent charge (Q), average discharging current (I_{avg}), discharge power (P_D), and quadratic rate (D) is observed under electrical stress. A tobit regression model is implemented to model trending behavior of PD characteristics with applied stress. In [11], an internal void is created in a high temperature superconducting DC cable, and pulse sequence analysis is performed. The results show that although the charge magnitude and pulse repetition rate vary with the void size and applied voltage, the patterns, or trending attributes that different voids create are consistent. The studies highlight two major points, i.e., PD measurement is a key technique that can indicate the nature and severity of a defect and secondly, each defect follows a unique pattern or trend which is shown by PD characteristics.

This article investigates the behavior of PD characteristics obtained from a comprehensive data set. PD measurements were performed on an internal PD defect modelled in the MV cable sample. Electrical stress is applied from PDIV up to higher stress levels using the step stress accelerating testing method.

II. Experiment Setup and PD Measurement

Fig. 2 (a) shows the schematics of the experimental setup used for PD measurement. Major equipment includes a high voltage test transformer connected to a 230 V regulated AC supply for stepping up the voltage, a coupling capacitor of rating 1 nF, and 36 kV for PD measurement. A HFCT sensor with a 1:10 transfer ratio and 500 kHz – 80 MHz (–3 dB) bandwidth for measuring PD pulses, a 4-channel oscilloscope, with a bandwidth of 300 MHz-1 GHz. The PD was recorded at a sampling rate of 250 MS/s. A cable sample with a cavity created by cutting the outer layer and creating a superficial groove in the insulation of the cable was used as shown in Fig. 2(b). Measurements are collected at different stress levels after PDIV using step stress test method. Initially, a voltage of up to 13 kV is applied for a few minutes without the test object to check if the setup is PD free. During the test, the voltage is raised with step size of 0.25 kV until PDIV is obtained. The measurements are recorded at a sampling rate of 250 MS/s and considering the stochasticity of pulses, 10 cycles are recorded at each stress level from PDIV to 12.4 kV.

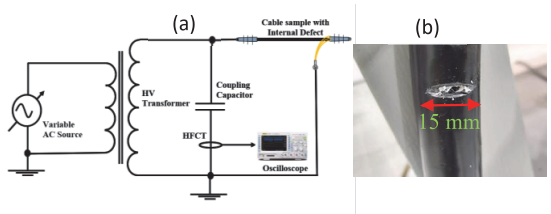

Fig. 2. Schematic diagram of PD experiment and measurement setup: a) schematic, b) cable sample with internal defect.

III. Results

A. Analyis of PRPD pattern via polar plot

Fig. 3 (a, b) shows PRPD via polar plots at various stress levels. A polar plot shows three major characteristics which include PD pulse height (V) phase of occurrence (ϕ) and number of pulses (n_p) in an ac cycle. ASTM D1868–13 defines PDIV as voltage after which continuous PD pulses above a stated magnitude (based on the background noise) occur. In this experimental investigation, PDIV is found as 5.4 kV where PD pulse of magnitude 4.9 mV is observed at 242.5° as shown in Fig. 1(a).

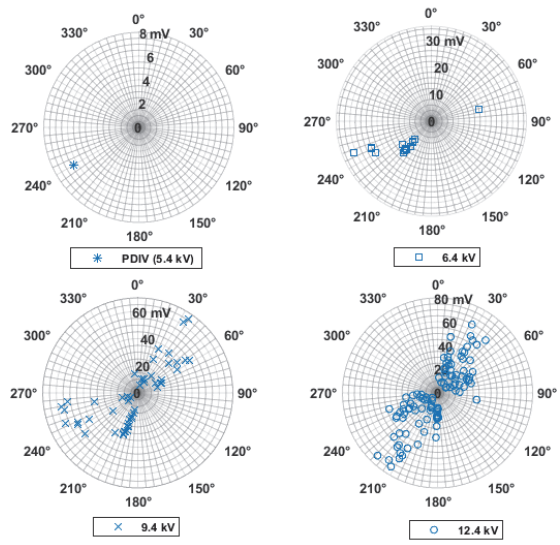

Fig. 3. Polar plots representing the behavior of pulse height, phase of occurrence, and number of pulses at PDIV (5.4 kV) 6.4 kV, 9.4 kV, and 12.4 kV.

PD characteristics show obvious variation at different stress levels as shown in Fig. 3 (a, b). Considering the pulse amplitude and number of pulses, both of these characteristics show an upward trend at increasing electrical stress. At 6.4 kV 15 pulses, at 9.4 kV 49 pulses and at 12.4 kV, 109 pulses were observed during ten cycles of the applied voltage. A similar trend is observed in the phase span of PD activity. At 6.4 kV, PD pulses are observed between 30°-60° during positive and 210-250° during the negative half cycle of the

Authorized licensed use limited to: Tallinn University of Technology. Downloaded on October 03,2025 at 07:17:05 UTC from IEEE Xplore. Restrictions apply.

applied voltage. Whereas at 12.4 kV, the PD activity phase span is increased, as pulses are observed between 0-30° and 180-270°.

B. PD Characteristics

PD characteristics are very useful for obtaining a deeper understanding of PD behavior. In this study, the behavior of three characteristics including pulse height, phase of occurrence, and pulse repetition rate is analyzed in correlation to progressive electrical stress. These characteristics are defined as follows.

a) PD pulse height (V_m)

PD pulse is a direct reflection of PD activity within the insulation. Pulse features are very helpful in locating and determining the severity of PD within the insulation [6]. In this study, peak amplitudes of individual pulses are extracted using the local maxima tool, and behavior of pulse height is analyzed. Pulses above a certain threshold value are considered in this study.

b) Phase of occurrence (φ)

It is defined as the angle at which PD pulses occur in individual AC cycles. The phase angles of PD pulses are calculated by (1), where t is the time of occurrence of a PD pulse in an AC cycle.

$$\varphi = t * 360/0.02 \tag{1}$$

c) Pulse repetition rate (n)

Pulse repetition rate *(n)* is defined as the number of PD pulses *(n_p)* in a specified time (T_r) period. Mathematically it is defined as (2)

$$n = n_p/T_r \tag{2}$$

IV. Local Maxima-based Peak Detection Tool

Fig. 1 shows PRPD patterns of various types of defects. These patterns contain noise and PD events, occurring in one AC cycle. For effective analysis PD it is customary to denoise the data and extract denoised PD signals. A local maxima-based algorithm is developed that extracts individual PD pulses with their corresponding locations. It efficiently extracts the pulses and their features without using advanced denoising methods, as the experiments were performed under low-noise laboratory conditions without excessive levels of background noise interference. [12]. The operating principle of the algorithm is demonstrated as Algorithm A using pseudocode given in Table I.

TABLE-I. Algorithm A pseudocode used for Extraction of PD pulse using local maxima method.

```
Input: PD data = N1
Sampling Frequency = Fs
Set β1
Set β2
[Pp, lp] = find peaks(x_data,'MinPeakHeight', β1,'MinPeakDistance', β2);
[Pn, ln] = find peaks(x_data,'MinPeakHeight', β1,'MinPeakDistance', β2);
Sorting: [peak_locations, sort_idx] = sort([lp', ln'])
Output: first occurring PD pulse = m
```

Initially, PD data (N_1) and sampling frequency (F_s) are given as input. Subsequently, two thresholds (β_1) as horizontal threshold and (β_2) as vertical thresholds are set that denoise and detect individual PD events in a recorded PD detector output time series [8]. Based on the threshold values, it detects positive peaks (P_p), negative peaks (P_n), and their corresponding locations as l_p and negative peaks l_p. These values are sorted and stored sequentially based on their location in a PRPD pattern. Afterward, the first occurring peak (m) of an induvial pulse is extracted. Fig. 4 (a) shows a measurement at 11.4 kV, which is given as input to the algorithm. Fig. 4(b) shows extracted P_n, P_p pulses and their location in the time domain. Whereas Fig. 4(c) shows the first occurring pulse which is an actual PD pulse representing a PD event. After detecting the pulses, it extracts the PD characteristics. Table II shows four major characteristics including peak pulse height (V_m), peak pulse height magnitude (V_{mabs}), pulse location (P_{loc}), time of occurrence (P_t), and phase of occurrence (P_φ), extracted using the developed algorithm. Various features can be utilized to analyze behavior of PD sources [13].

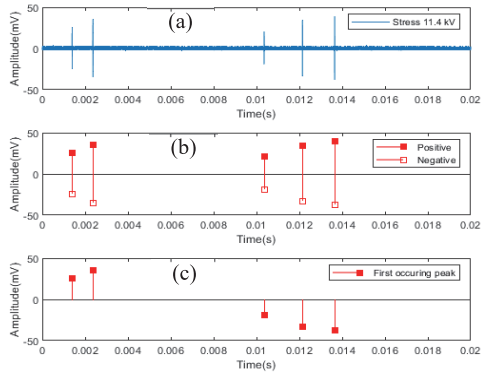

Fig. 4. PD events or pulses extracted using local maxima-based algorithm a) Measured PD data at 11.4 kV b) Detected positive and negative pulses c) first occurring PD pulses.

TABLE II. PD characteristic features extracted using local maxima-based algorithm.

Quantity	1	2	3	4	5
V_m (mV)	25.31	35.28	-19.15	-33.43	-38.03
V_{mabs} (mV)	25.31	35.28	19.15	33.43	38.03
P_{loc} (sample)	217610	369749	1618059	1897639	2132519
P_t (s)	0.0014	0.0024	0.0104	0.0121	0.0136
P_φ (°)	25.1	42.6	186.4	218.6	245.7

V. Behavior of Pulse Characteristics

A. Behavior of pulse height (V_m) and phase of occurrence (φ)

Pulse amplitude and phase of occurrence are presented on the scatter plot shown in Fig. 5. The plot represents the relation between φ and V_m. It is observed that at a lower stress level (6.4 kV), the majority of pulses occur during the negative half of the applied voltage and their occurrence is found between 219° to 249°. Considering the phase of

Authorized licensed use limited to: Tallinn University of Technology. Downloaded on October 03,2025 at 07:17:05 UTC from IEEE Xplore. Restrictions apply.

occurrence, pulses of magnitude 13-15 mV repeatedly occurring between 219°-223°. There is only a single pulse found during the positive half cycle at 75.6°. At medium stress (9.4 kV), the PD activity is observed in both positive and negative half cycles of the AC voltage. During the positive half cycle, pulses of magnitude 5-70 mV are observed between 15°-75°. A scattered PD activity is observed during the positive half cycle. During the negative half cycle, pulses of 5-57 mV are observed between 19°-350°. However, the majority of occurrences are found between 190°-192°. At high stress level (12.4 kV), the activity is symmetric during both positive and negative half cycles of applied AC voltage. PD pulses of 8-64 mV are observed between 0°-90°. During negative half cycle, pulses of 10-75 mV are observed, and their occurrence is found between 180-270°.

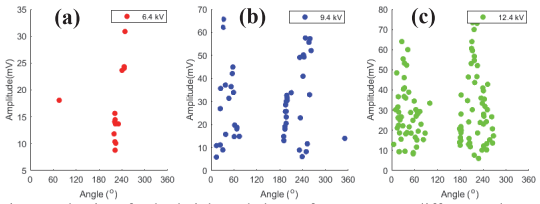

Fig. 5. Behavior of pulse height and phase of occurrence at different voltages a) 6.4 kV b) 9.4 kV c) 12.4 kV.

B. Pulse repetition rate (n)

Fig. 6 shows the behavior of positive, negative, and total pulses/PD events that occurred in T_r. In this study, T_r= 200 ms i.e., ten full ac cycles are considered. Fig. 6 shows a bar chart of the number of pulses. It is observed that there was only a single positive pulse at 6.4 kV, which is increased to 15 at 9.4 kV and 53 pulses at 12.4 kV. A similar trend is observed with negative pulses. Considering the overall behavior of pulses at increasing electrical stress, an uptrend is observed.

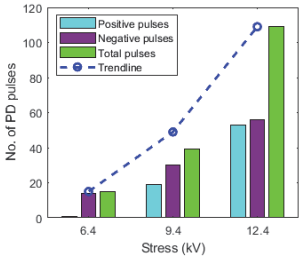

Fig. 6. Behavior of positive, negative, and total PD pulses at increasing electrical stress.

CONCLUSION

This study is based on an experimental investigation performed on an 11 kV XLPE with an internal defect/cavity at its outer layer. PD data was collected at different levels of voltage, i.e., from PDIV at 6.4 kV to 12.4 kV with a step size of 3 kV. A local maxima-based algorithm is designed that detects actual PD events, corresponding pulses, and major pulse characteristics including peak pulse height, phase of occurrence, and pulse repetition rate obtained from PD data. Considering the behavior of pulse magnitude, it is observed that despite electrical stress increasing, the magnitude of most of the pulses is 10-40 mV. Only a few pulses of magnitude over 50 mV are observed, which shows that the severity of PD is not only described by pulse amplitude but also by number and density of pulses. Similar behavior is observed with phase as most of the pulses are observed between 0°-60° and 180°-240° of the applied AC voltage. However, it can be seen that with increasing electrical stress, the phase span of PD activity increases. An uptrend is observed between electrical stress and pulse repetition rate.

REFERENCES

[1] E. Maggioli, H. Leite and C. Morais, "A survey of the Portuguese MV underground cable failure," 2016 13th International Conference on the European Energy Market (EEM), Porto, Portugal, 2016, pp. 1-5, doi: https://10.1109/EEM.2016.7521217 .

[2] M. Choudhary, M. Shafiq, I. Kiitam, A. Hussain, I. Palu, and P. Taklaja, "A Review of Aging Models for Electrical Insulation in Power Cables," Energies, vol. 15, no. 9, 2022, doi: https://10.3390/en15093408 .

[3] IEC, Evaluation and qualification of electrical insulation systems; IEC 60505. "International Electrotechnical Commission: Geneva, Switzerland", 2017.

[4] IEC, High-voltage test techniques: partial discharge measurements; IEC 60270. International Electrotechnical Commission: Geneva, Switzerland, 2015.

[5] P. Hyvönen, "Prediction of Insulation Degradation of Distribution Power Cables Based On Chemical Analysis and Electrical Measurements" Aalto University, 2008.

[6] P.H. Morshuis, "Degradation of solid dielectrics due to internal partial discharge: some thoughts on progress made and where to go now", IEEE Trans. Dielectr. Electric. Insulation 12 (5) (2005) 905–913.

[7] H. Illias, Teo Soon Yuan, A. H. A. Bakar, H. Mokhlis, G. Chen and P. L. Lewin, "Partial discharge patterns in high voltage insulation," 2012 IEEE International Conference on Power and Energy (PECon), Kota Kinabalu, Malaysia, 2012, pp. 750-755, doi: https://10.1109/PECon.2012.6450316 .

[8] Maninder Choudhary, Muhammad Shafiq, Ivar Kiitam, Ivo Palu, Waqar Hassan, Praveen Prakash Singh, "Investigation of partial discharge characteristics in XLPE cable insulation under increasing electrical stress", Engineering Failure Analysis, Volume 158, 2024, https://doi.org/10.1016/j.engfailanal.2024.108006.

[9] M. Choudhary, M. Shafiq, I. Kiitam, I. Palu and W. Hassan, "Partial Discharge Pulse Shape Analysis for Progression of Insulation Degradation in Medium Voltage Cable," 2023 International Electrical Engineering Congress (iEECON), Krabi, Thailand, 2023, pp. 332-336, doi: https://10.1109/iEECON56657.2023.10126589 .

[10] Waqar Hassan, Muhammad Shafiq, Ghulam Amjad Hussain, Maninder Choudhary, Ivo Palu, "Investigating the progression of insulation degradation in power cable based on partial discharge measurements", Electric Power Systems Research, Volume 221,2023, 109452,ISSN 0378-7796, https://doi.org/10.1016/j.epsr.2023.109452.

[11] D. -H. Oh, H. -S. Kim and B. -W. Lee, "Novel Diagnostic Method of DC Void Discharge in High-Temperature Superconducting Cable Based on Pulse Sequence Analysis," in IEEE Transactions on Applied Superconductivity, vol. 30, no. 4, pp. 1-5, June 2020, Art no. 9000905, doi: https://10.1109/TASC.2020.2974437 .

[12] S. Sriram, S. Nitin, K. M. M. Prabhu, and M. J. Bastiaans, "Signal denoising techniques for partial discharge measurements," in IEEE Transactions on Dielectrics and Electrical Insulation, vol. 12, no. 6, pp. 1182-1191, Dec. 2005, doi: 10.1109/TDEI.2005.1561798.

[13] I. Kiitam, M. Shafiq, P. Taklaja, M. Parker, I. Palu and L. Kütt, "Characteristic Pulse Pattern Features of Different Types of Partial Discharge Sources in Power Cables," 2021, IEEE PES/IAS PowerAfrica, Nairobi, Kenya, 2021, pp. 1-5, doi: https://10.1109/PowerAfrica52236.2021.9543366 .

Authorized licensed use limited to: Tallinn University of Technology. Downloaded on October 03,2025 at 07:17:05 UTC from IEEE Xplore. Restrictions apply.

Publication V

M. Choudhary, M. Shafiq. I. Kiitam, I. Palu, W. Hassan, P. Singh, “Investigation of Partial Discharge Characteristics in XLPE Cable Insulation Under Increasing Electrical Stress,” Engineering Failure Analysis, Elsevier, 2024. doi: https://doi.org/10.1016/j.engfailanal.2024.108006.

Engineering Failure Analysis 158 (2024) 108006

Contents lists available at ScienceDirect

Engineering Failure Analysis

journal homepage: www.elsevier.com/locate/engfailanal

Investigation of partial discharge characteristics in XLPE cable insulation under increasing electrical stress

Maninder Choudhary [a,*], Muhammad Shafiq [b], Ivar Kiitam [a], Ivo Palu [a], Waqar Hassan [c], Praveen Prakash Singh [a]

[a] Department of Electrical Power Engineering and Mechatronics, Tallinn University of Technology, Tallinn, Estonia
[b] Florida State University, USA
[c] Institute of Power Engineering (IPE), Universiti Tenaga Nasional (UNITEN), Malaysia

ARTICLE INFO

Keywords:
XLPE cable
Partial discharge measurement
PD characteristics
Regression analysis

ABSTRACT

Insulation degradation in power components is a looming issue that can have a significant impact on the reliability of power system if not attended timely. Partial discharge (PD) diagnostics is a key technique used for the condition monitoring and health assessment of insulation. Inception of PD is a primary indicator which shows degradation and decreased local dielectric strength of the insulation. PD magnitude can increase with time and level of stress, which may result in failure of insulation. This article investigates the behavior of PD characteristics in a medium voltage (MV) cross-linked polyethylene (XLPE) cable sample, containing a defect at the cable termination, under elevated electrical stresses. PD behavior is studied by investigating the key PD characteristics, such as partial discharge inception voltage *(PDIV)*, phase of occurrence *(ϕ)*, mean amplitude *(V_{mean})*, pulse repetition rate *(PRR)*, and phase span (ϕ_{span}). These quantities are extracted from a phase-resolved partial discharge (PRPD) pattern using a pulse detection algorithm. Later, these characteristics are analyzed in correlation with the electrical stress. Various regression models are implemented and compared to find the best fit model that represents trending attributes of major PD characteristics. The presented study can be used as an effective process to analyze the measured PD data for evaluation of the insulation condition in the power components.

1. Introduction

European distribution grids are connected to almost 260 million customers that rely on a vast network of medium and low-voltage overhead lines and cables. Due to the increased security of supply and comparatively decreasing cost of underground cables, there is a gradual shift from overhead lines to underground cables [1]. With the growing number of cable networks, failure rates are also increasing as a result of imperfections during manufacturing, poor workmanship, and aging at normal or abnormal operating stresses i.e., thermal, electrical, mechanical, and ambient (TEAM) [2]. A survey was conducted in Portugal about medium voltage cable failures in substation network. The study reveals that approximately 80 % of the faults in the cables occur due to electrical insulation [3].

The occurrence of PD is a primary indicator that can describe the cause of insulation failure and its aging behavior [4]. IEC 60270 describes PD as a localized breakdown confined in a local region of insulation where the electric field strength exceeds the local

* Corresponding author.
E-mail addresses: maninder.choudhary@taltech.ee (M. Choudhary), waqar.hassan@uniten.edu.my (W. Hassan).

https://doi.org/10.1016/j.engfailanal.2024.108006
Received 8 October 2023; Received in revised form 7 January 2024; Accepted 21 January 2024
Available online 23 January 2024
1350-6307/© 2024 Elsevier Ltd. All rights reserved.

Nomenclature

MV	Medium voltage
PD	Partial discharge
PDIV	Partial discharge inception voltage
HFCT	High frequency current transformer
XLPE	Cross-linked polyethylene
PRPD	Phase resolved partial discharge
PRR	Pulse repetition rate
DSO	Digital storage oscilloscope
Q_{avg}	Accumulated average charge
Q_{acc}	Accumulated apparent charge
E_c	Cumulative energy function
P_d	Discharge power
I_d	Average discharging current
PSA	Pulse sequence analysis
ΔU	Change of voltage
ΔT	Change of time
t_r	Reference time
V_{mean}	Mean pulse height
φ_{span}	Phase span
SVM	Support vector machine
GPR	Gaussian process regression

dielectric strength [5]. Surface discharge and internal PD are two critical PDs, that occur in cables. Surface discharge occurs where there is an interface between solid and gas or liquid and gas. It propagates across the surface of the insulation, where the electric field is strong enough. The discharge activity is intensified in the presence of dust, contaminants, and moisture. Over time, surface discharge may cause internal PDs and electrical trees which may lead to failure of insulation. Internal PD normally occurs in the voids and gas filled cavities. Internal PDs particulary in large cavities contain more discharges of smaller magnitude due to increase in overall surface area. However, they have a more severe impact compared to surface discharges [6,7].

PD measurements are playing a vital role in the condition monitoring of power system assets including cables, by facilitating a reliable asset operation while also saving on maintenance costs [8]. Thus, it is crucial to track the PD behavior to predict upcoming failures which in turn provides an opportunity to plan maintenance activities accordingly to avoid sudden failures and unplanned disruptions and outages [9,10].

Experimental research is most efficient method to investigate PD behavior. Several state-of-the-art research studies have been conducted based on the PD measurements in different power system assets [11–16]. In [11] a lab based experimental investigation is performed on ethylene propylene rubber (EPR and XLPE cable) under AC and DC supply by creating artificial defects. The study found that DC voltages reduce the cable size without affecting the service life. In [12] a cavity is created under low temperature. It is found that like internal PDs in gas filled cavities surface discharge can also occur at low temperature. In [13] three types of defects (internal, surface and corona) are created and investigated under increasing electrical stress. The result found that PD characteristics including Q_{acc}, I_{avg}, P_D and quadratic rate shows an increasing trend. A tobit regression model is developed to correlate PD characteristics and electrical stress. In [14] two step regression model is developed for multi-source identification of PD. In [15], PD behavior is analyzed in relation to the cavity size. Two PD parameters, Q_{acc} and partial discharge inception voltage (PDIV) were analyzed in relation to defect size and shape. It is observed that PDIV and magnitude both vary with the variation in the shape of the defect. In [16], pulse sequence analysis (PSA) was performed where behavior of consecutive pulses was analyzed to elucidate the physics behind the PD mechanism. It is found that characteristics pertaining to consecutive pules, i.e., change of voltage (ΔU) and change of time (ΔT) follow a well-defined pattern under increasing stress conditions.

The above-described studies highlighted two major points. Firstly, the insulation degradation caused by any type of defect or stress follows a distinct trend or pattern which can be analyzed by utilizing PD characteristics. Secondly, from the literature review, it is found that an ample amount of work has been done to investigate PD characteristics under various scenarios such as various defects (types and size), multi-stress conditions, and modern grid operating conditions (impact of power electronic converters) for lifetime estimation. Their main focus is to analyze the impact of defects or grid operating conditions on the insulation rather understanding the degradation behavior.

This article aims at investigating the PD behavior using PD characteristics extracted from comprehensive data sets, obtained through PD measurement from PD inception to increasing voltage levels. Furthermore, the trending behavior of major characteristics is analyzed using various regression models including linear regression, support vector machine *(SVM)* and gaussian process regression *(GPR)*.

Three major points describe the novelty of this work which includes comprehensive experimental investigation performed at each stress level, development of an effective algorithm for detection of PD pulses from PRPD pattern and extraction of PD characteristics

from a PRPD pattern without using denoising or signal processing techniques. Third is analysis of trending attributes of PD characteristics and regression analysis to map those attributes.

Further on in this paper, Section 2 describes the overall process or methodology of study including XLPE cable sample preparation, experimental setup, equipment, and measurement parameters chosen for this study. Section 3 elaborates PRPD patterns and behavior of PD characteristics considered in this study. Section 4 explains various aspects of the developed peak detection algorithm. Section 5 presents the results obtained from the experimental investigation and PD data analysis. Section 6 describes the regression analysis performed to demonstrate the correlation between the PD characteristics and progressive electrical stress and Section 7 is based on the comprehensive discussion and conclusion of this study.

2. Experimental study of on the XLPE cable

Fig. 1 depicts schematic of overall process from sample preparation to regression analysis.

The first task was the preparation of a suitable sample for PD measurement. As XLPE has a vast application in the MV power system network, an XLPE cable section of three meters is used in this study. A defect was created by removing the stress cone at one end of the cable sample for the production PDs. A measurement setup was established in a low-noise laboratory environment. PD data are visualized and stored in the form of PRPD patterns in a digital storage oscilloscope (DSO) at a sampling rate of 156 mega samples per second (MS/s). In the next stage the PRPD patterns are analyzed at various stages of insulation degradation, and major PD characteristics were extracted to investigate PD behavior at increasing degradation. A PD pulse detection algorithm is developed for extraction of PD characteristics from a PRPD pattern. Later the behavior of PD characteristics is investigated under elevated electrical stress. Finally, a regression analysis is performed to investigate the trending behavior of PD characteristics. Nine regression models from three regression families including linear, SVM and GPR are trained to find the best-fit line representing the relationship between two major PD characteristics and progressive electrical stress. Several measurements were taken into account to find the best-fit model that develops a strong correlation between stress and PD characteristics. Further, the validation of each model is evaluated using performance indices i.e., R-squared, root mean square error *(RMSE)* and mean absolute error *(MAE)*. Based on the results, a comprehensive discussion is made considering the behavior of PD characteristics in correlation to increasing electrical stress and regression analysis.

2.1. Cable sample preparation

An XLPE cable of medium voltage rating i.e., 11 kV with copper conductor area of 50 mm^2, Semi-conducting layer thickness of 1.2 mm, XLPE insulation thickness of 5.5 mm, Cross tape screen thickness of 0.9 mm, minimum bending radius of 416 mm, aluminum tape screen thickness of 1.6 mm and outer sheath thickness of 0.9 mm is considered for this study. An artificial defect is created by dismantling the stress cone of the cable terminal and removing the top layer outer sheath, an aluminum-copper layer, bedding, and copper tape layer by dismantling the cable terminal as shown in Fig. 2.

2.2. Experimental setup

Fig. 3 shows the schematic diagram of the experimental setup developed for PD measurement in the laboratory. Equipment details are given as follows:

(1) A 220 V AC source connected to a step-up test transformer of MV rating via a voltage regulator for variation of voltage in steps.
(2) A coupling capacitor (CC) of voltage rating 16 kV and capacitance of 1 nF is connected in parallel to supply for measurement of PDs emitted by the PD source.
(3) A high-frequency current transformer (HFCT) of bandwidth 500 kHz–80 MHz (-3 dB) and 1:10 transfer ratio is connected in series to cable sample shielding for the measurement of high-frequency PD pulses.
(4) A digital storage oscilloscope (DSO), connected to the HFCT via a 50 Ω coaxial cable is used for data acquisition, i.e., to visualize and record PD pulses

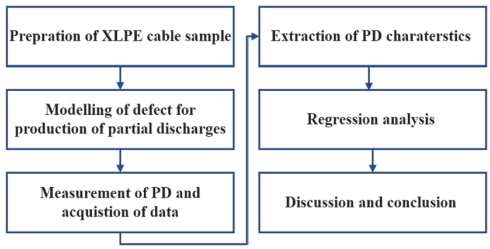

Fig. 1. Process for the investigation of PD behavior at progressive electrical stress.

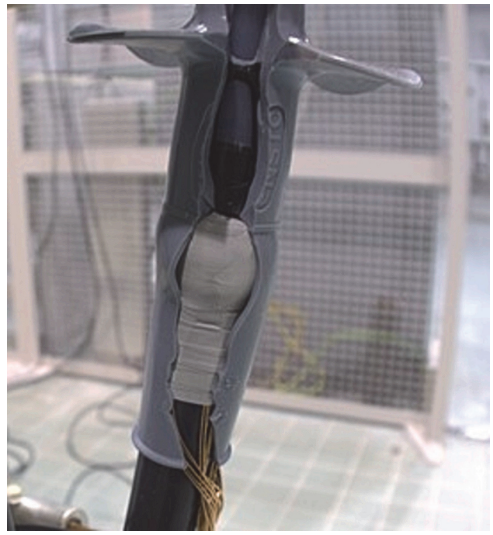

Fig. 2. Modeling of the defect at one end of XLPE cable to produce PD.

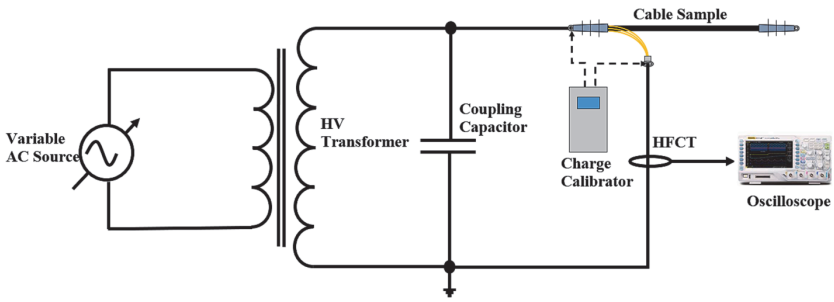

Fig. 3. Schematic of laboratory experimental setup for PD measurement.

2.3. Measurement procedure

In this investigation, the step stress test method is implemented to observe PD activity at various stress levels. Prior PD testing at voltages up to 12 kV was applied, to ensure that the setup is PD free. With the cable sample, 3 kV was initially applied and later it was increased with a step size of 0.2 kV until PDIV. In IEC 60270, the PDIV is defined as the applied voltage at which repetitive partial discharges are first observed in the test object, when the voltage applied across the test object is gradually increased from a lower value at which no partial discharges are observed. Afterwards, the voltage was increased to higher levels and PD behavior was observed at voltage intervals of 1 kV up to 13.3 kV.

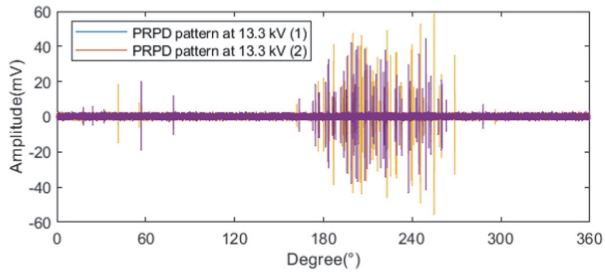

Fig. 4. PRPD pattern contains two measurements at 13.3 kV with changes in pulse amplitude, location, and number of pulses.

Due to the stochastic nature of PD, the pulses appearing during any AC cycle are different in magnitude and phase location to the pulses observed at the next cycle. There is always a variation in the presentation of the PD activity, which is also reflected in the PD characteristics, i.e., pulse location, pulse height, and the number of pulses. Fig. 4 presents PD data captured over two AC cycles at an applied voltage of 13.3 kV. There were 49 pulses, observed during the first measurement and 42 pulses of different magnitudes at different phase locations, observed during the second measurement. A single measurement or PD data over one AC cycle may not provide an adequate representation of the ongoing PD activity. For a comprehensive analysis multiple measurements are required. Thus, the oscilloscope was configured to record the PD data over ten consecutive cycles at each voltage level.

3. Investigation of PRPD pattern and selection of PD characteristics

3.1. Investigation of PRPD pattern

PRPD pattern is direct reflection of a PD activity and plays key role in the investigation of the PD mechanism. Commercial PD measurement systems use PRPD patterns to identify the type of defect and its intensity. It represents the PD activity with respect to the phase of the applied voltage. In general form, the PRPD pattern is based on three major parameters: phase angle ϕ, charge magnitude q, and the number of discharges n, also called the ϕ-n-q pattern. In HFCT-based measurement, a PRPD pattern is represented as ϕ-V-n, where n represents the number of pulses, V represents pulse peak voltage and ϕ represents its phase of occurrence. In this study, in-depth analysis of the PRPD pattern is performed. Initially, the PRPD pattern is analyzed at various stages of degradation, i.e., from PDIV to 13.3 kV.

Fig. 5 (a and b) shows PRPD patterns at various electric stress levels. It can be observed that the degradation occurs in two stages. At the early stage of degradation from PDIV to 9.1 kV as shown in Fig. 5(a), the PD activity is concentrated at the negative half cycle as most of the pulses are observed during the negative half cycle of the applied AC voltage. At a later stage as shown in Fig. 5(b), when electrical stress is increased above 9.1 kV, the PD activity starts appearing at the rising edge of the positive half cycle of the AC cycle. The appearance of pulses in the positive half cycle of the applied voltage may be the result of surface tracking. Under increasing stress for longer durations, surface discharges start to track by forming irreversible conducting or carbonized paths across the insulation surface. In wet and contaminated environments this tracking may cause leakage current or simplify the occurrence of flashover that damages insulating materials and degrades the dielectric properties of insulation. Long-term tracking generates electric trees or internal PDs, which are a major cause of failure of insulation [21,22]. Thus, these pulses can be an indication of the initiation of internal PDs. The pulses in the positive half-cycle can also be a byproduct of charge deposition onto the surface of the insulation as a result of discharges which have occurred during the previous negative half-cycle.

3.2. Selection of PD characteristics

It is important to observe the PD characteristics for in-depth understanding of the degradation behavior in insulation systems. This investigation is based on captured PRPD patterns. Ref-s [17,18] provide a comprehensive guide for feature extraction and classification methods for PD analysis. Considering the PRPD pattern in Fig. 6, the four characteristics i.e., phase of occurrence of PD, pulse height of an individual PD event, number of pulses across full AC cycle or pulse repetition rate, and phase span of overall PD activity show considerable pattern variations at each cycle and at increasing electrical stress. Therefore, the above mentioned four characteristics are

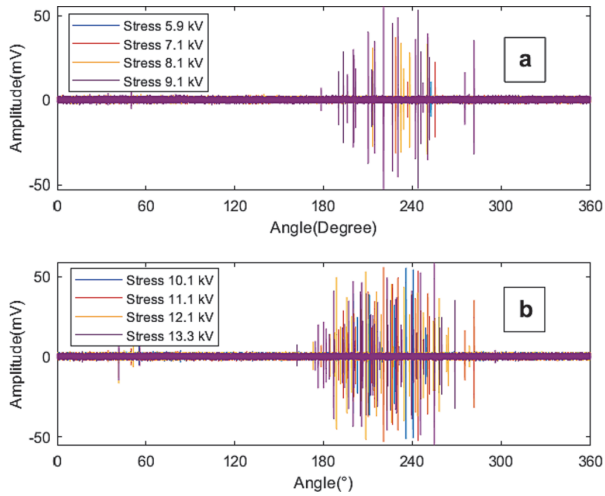

Fig. 5. PRPD pattern and phase span of PD activity at two stages of degradation (a) initial level of degradation (b) higher level of degradation.

considered in this study. These characteristics are illustrated in Fig. 6 and can be defined as follows.

(1) Phase of occurrence (ϕ)

It is defined as the phase angle at which the PD pulse occurs in a full AC cycle, excluding the oscillations of the signal illustrated in Fig. 6, where the PD pulse occurred at an angle of 226.55°.

(2) Mean pulse height (V_{mean})

Pulse height is defined as peak value *Vp* of a PD pulse representing a PD event as shown in Fig. 6. The mean pulse height (V_{mean}) can be found by adding the V_p of individual PD pulses in an AC signal and dividing it by the number of pulses *n* presented as

$$V_{mean} = \frac{\sum_{i=1}^{n} V_{p(i)}}{n} \tag{1}$$

(3) Pulse repetition rate (PRR)

Pulse repetition rate is defined as the total number of pulses *n* observed over a reference time interval T_r Pulses above a certain threshold are considered for the analysis as shown in Fig. 6. Mathematically, it is represented as [5].

$$PRR = \frac{n}{T_r} \tag{2}$$

(4) Phase span (φ_{span})

Phase span describes the overall span of PD activity over an AC cycle or half-cycle. It is the difference in ϕ of the last PD pulse ϕ_{end} and the first PD pulse ϕ_{start} as shown in Fig. 6. Mathematically, phase span is represented by

$$\varphi_{span} = \varphi_{end} - \varphi_{start} \tag{3}$$

4. Implementation of the PD pulse detection algorithm for PD analysis

Commercial systems use the PRPD pattern as a graphical tool that represents the nature and properties of the defect. Amplitude of the individual PD pulse reflects the extent of the ongoing aging of insulation, however, PRPD pattern provides the amplitude of the overall PD activity. Therefore, an algorithm is developed that detects individual PD pulse. After detecting the pulse, it extracts the peak amplitude based on the first rising peak from the PD signal, representing a single PD event. Due to the low level of background noise, it was not necessary to implement advanced denoising techniques, although several are available. Previous researchers have used wavelet-based denoising methods and advanced filters before extraction of characteristics to denoise the PD signal and detect actual PD signal [19,20].

The developed tool is effective in detecting PD pulses, their location, ϕ, and the applied voltage at which the pulses occur. Fig. 7 (a) shows the flowchart of the developed algorithm. It efficiently detects individual PD events from a PRPD pattern. Initially, two thresholds are needed, i.e., horizontal, and vertical thresholds as shown in Fig. 7(b). Their value is defined based on the variation of data throughout the measurements. For this study, a range of 5–8 mV was chosen for the vertical threshold and 19.2 μs was chosen for the horizontal threshold. The performance of the algorithm heavily relies on the choice of threshold values. In case of deviation from optimal values, the algorithm will detect pulses which are oscillations or reflections of individual PD pulses as shown in Fig. 7. Both thresholds function simultaneously to remove noise, oscillations, and attenuation of PD signals without using advanced denoising techniques [19,20].

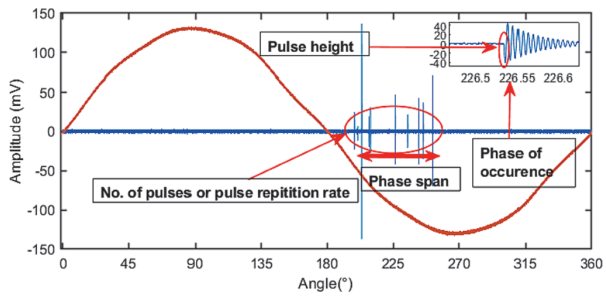

Fig. 6. PD characteristics considered for ageing study.

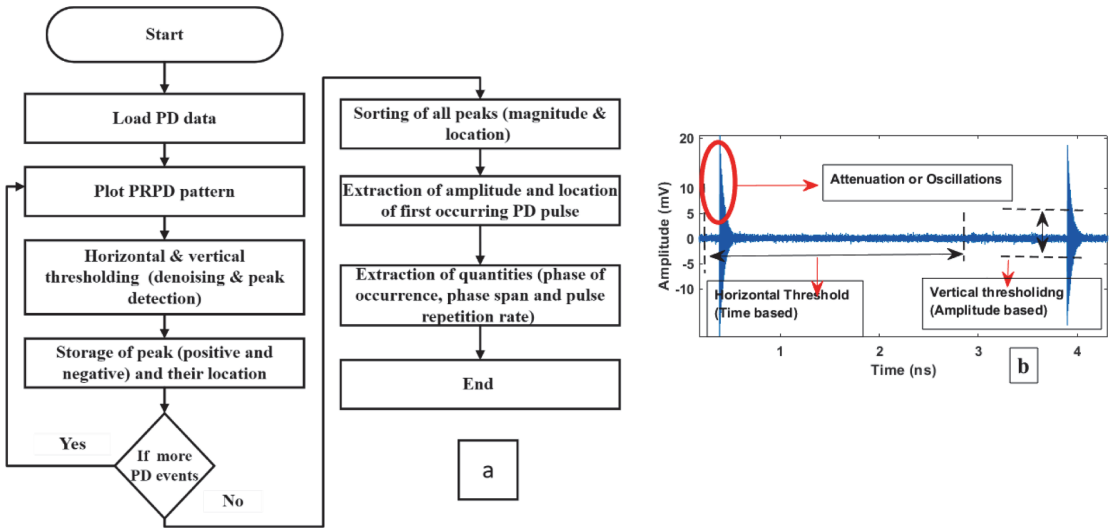

Fig. 7. (a) Flowchart of the algorithm developed for the extraction of PD characteristics (b) Horizontal and vertical threshold defined for the algorithm.

The key purpose here is to detect the actual PD pulses, and their positive and negative peaks and store them sequentially. Besides the detection of PD pulses, it also extracts the characteristics such as the peak values of the individual pulse, pulse polarity, time of occurrence, phase angle of occurrence, instantaneous test voltage, number of pulses, or pulse repetition rate. In addition to that, the algorithm can also extract characteristics for pulse sequence analysis (PSA) such as ΔU and ΔT and characteristics for pulse shape analysis, e.g., rise time, fall time, and pulse width of individual PD pulses from a PRPD pattern. Thus, it can analyze PD data using different approaches, i.e., based on shape and pulse sequence characteristics.

5. Analysis of PD characteristics

In this section, PD characteristics are analyzed in correlation to electrical stress and prospective trends are visualized using polar and line plots. As mentioned above, four characteristics including ϕ, V_{mean}, PRR, and φ_{span} of PD activity in PRPD pattern are investigated.

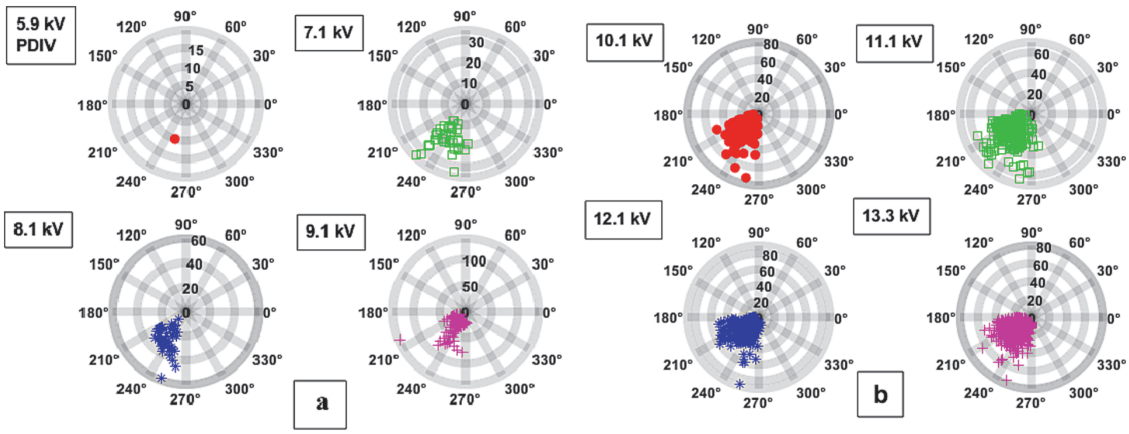

Fig. 8. (a) Polar plots representing amplitudes (mV) and phase angles of individual PD pulses at following stress levels: 5.9 kV (PDIV), 7.1 kV, 8.1 kV, 9.1 kV (b) Polar plots representing amplitudes and phase angles of individual PD pulses at following stress levels: 10.1 kV, 11.1 kV, 12.1 and 13.1 kV.

5.1. Behavior of phase of occurrence (ϕ)

Similar to a PRPD pattern, a polar plot can also represent PD behavior, i.e., pulse height, angle of occurrence and number of pulses occurring during a full AC cycle. Fig. 8 a and b show polar plots representing individual PD pulse heights and locations over a 360° full AC cycle. As displayed previously in Fig. 5, the ϕ was showing an obvious variation in the PRPD pattern at different measurements and at increasing electrical stress. Ten measurements at different electrical stress levels above PDIV are incorporated in the respective polar plots.

At PDIV, a single pulse of magnitude 10 mV was observed at 252.5° as shown in Fig. 8(a) (PDIV). The PD progression of the PD activity occurs in two stages. Initially, from 7.1 to 9.1 kV, the PD activity is concentrated at the first half of the negative half cycle of the applied voltage, between 210°–270°. Scattered PD activity at an amplitude range between 10 and 40 mV was observed at 7.1 kV and 8.1 kV, as shown in Fig. 8(a). At 9.1 kV, the PD activity shows a similar trend, although the amplitude of pulses has increased to a range of 10–100 mV.

At later stages of degradation, the PD activity started increasing with a larger density of pulses near the zero crossing of the applied voltage (transitioning from positive to negative), i.e., from 180°–270°, and also few pulses were observed during the positive half cycle of the applied voltage as shown in Fig. 5(b). This behavior resembles the surface PD activity observed in prior research [23]. At 12.1 kV and 13.3 kV stress levels, the phase span of PD activity decreased by a few degrees. Also, it is evident from the polar plots that at higher electrical stresses (10.1–13.3 kV), there is no significant rise in height of pulses, but there is an increase in the number of PD pulses at increasing stress, which is reflected by the denser scattering on the polar plots i.e., from 10.1 kV to 13.3 kV as shown in Fig. 8(b).

5.2. Behavior of mean pulse height

Pulse height is the second important characteristic of the PRPD pattern. Fig. 9 shows the behavior of V_{mean} at various stress levels i.e., from 7.1 kV to 13.3 kV. The figure includes 10 measurements taken at each stress level. The developed algorithm extracts the mean peak value of all PD pulses in an AC signal and plots these against electrical stress. For voltages exceeding 9.1 kV, despite a rise in electrical stress, V_{mean} demonstrates a decreasing pattern. This can be caused by inception of PD at other locations in the test object, which creates more PD pulses, with a lower peak value. In the initial stages of degradation, specifically from PDIV to 9.1 kV, the V_{mean} increases proportionally with the applied stress. However, at 9.1 kV, there is a distinct peak in the V_{mean}, as illustrated in Fig. 9. A similar trend is observed with the maximum and minimum values of pulse height concerning electrical stress, as documented in reference [24]. There is a minor increase in V_{mean} at 11.1 kV. This spontaneous change in V_{mean} at 9.1 kV and 11.1 kV may show high charge movement at intermediate voltage levels after PDIV and at higher stress levels prior to breakdown, i.e., at 9.1 kV and 11.1 kV. The mean values in Fig. 9 and demonstrate that at 12.1 kV and 13.3 kV, there is a decrease in V_{mean} which shows that at higher stress level pulse heights, on average, decrease.

5.3. Behavior of pulse repititon rate

Pulse repetition rate is the third most important characteristic. As depicted in Fig. 8a and b, there is a significant increase in the number of pulses in correlation to the electrical stress. At 7.1 kV, 36 pulses occurred over ten AC cycles (T_r = 200 ms), while at a medium stress level (9.1 kV), 78 pulses were observed, at highest level i.e., at 13.3 kV, 491 pulses were recorded. As the PRR is directly proportional to the number of pulses, this similar trend was consistently observed throughout all ten measurements, Fig. 10 shows minimum average and maximum value of PRR at stress level. It can be seen that PRR varying in three stages i.e., near PDIV, intermediate stage and higher stage. Initially from 7.1 to 8.1 kV PRR found between 150 and 250 s^{-1} i.e., there is monotonic increase in pulse repetition rate. At intermediate stage (9.1–10.1 kV) PRR observed between 350 and 950 s^{-1}. At higher levels (10.1–13.3 kV) the PPR rise significantly ranges between 1000 and 2500 s^{-1}.

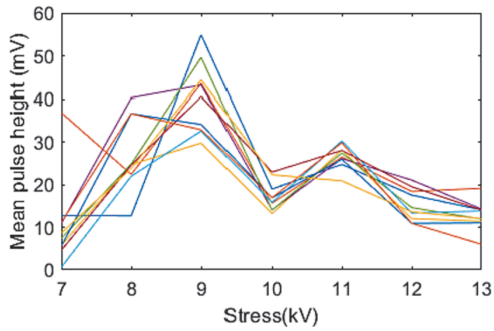

Fig. 9. Behavior of mean pulse height (10 cycles) in correlation to progressive electrical stress.

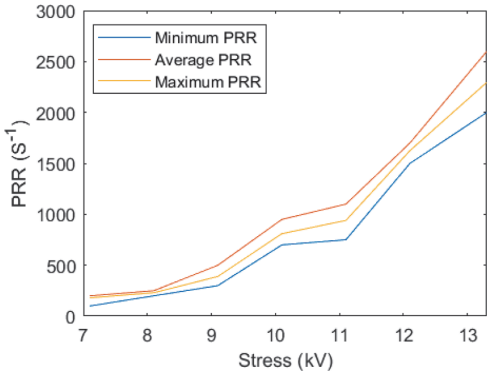

Fig. 10. Relationship between pulse repetition rate and increasing electrical stress.

5.4. Behavior of phase span

Phase span is a significant characteristic that describes the duration or span of a PD activity. In this study activity span of only negative half-cycle is considered. The selection is made based on the occurrence of PD pulses at all stress levels. Fig. 11 show trendlines of phase span data containing minimum, average, and maximum value at each stress level. Ten measurements into account. Similar to PRR φ_{span} trendline varies in three stages.

Immediately after PDIV the φ_{span} of PD activity observed between 26° and 46° which increased further at intermediate level (9.1–10 kV) and found between 49° and 79°. At higher level this range significantly increased the phase 80°–101°. It is also observed that high stress level above 12.1 kV the span of PD activity decreased as depicted in the graph. Thus, it can be said that at high level of degradation the φ_{span} of actvity does not vary much it decreases or stay consistent. Considering variation of data at each stress level, the skewness value shows that the φ_{span} data is positively skewed.

6. Regression analysis

Regression analysis is one the methods used to find the correlation between variables or quantities. Regression techniques are widely used in forecasting, prediction, and analysis of time series data. Previous researches have used state-of-the-art methods such as decision functions, distance, and likelihood functions, artificial neural networks, and trainable classifiers described in [17]. These methods are useful for the classification of PRPD patterns and defects. However, initially, the degradation trend must be investigated, which is very useful for ageing studies and condition monitoring of cables. Thus, regression analysis is performed. The regression analysis consists of the following stages, from data collection to training and evaluation of regression models.

6.1. Data collection and selection of characteristics for regression analysis

PD data are collected through experimental and measurement setup in the first stage. Considering the nature of the data, two characteristics, PRR and φ_{span}, are chosen as the dependent variable and electrical stress is chosen as the independent variable.

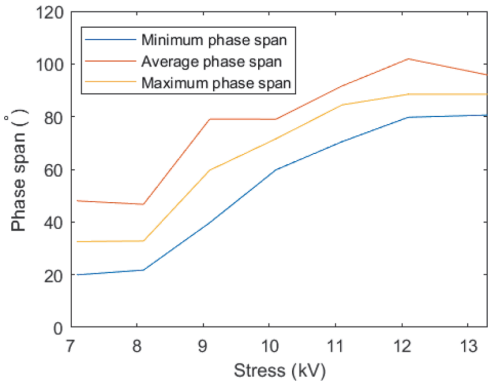

Fig. 11. Behavior of PD activity negative polarity phase span values in correlation to progressive electrical stress.

6.2. Selection and training of regression models

In this study, nine models from three families including linear, SVM and GPR families are chosen to find best correlation between phase span and PRR data with applied electrical stress. The models are defined as follows.

(1) Linear regression models

Linear models are one of the simplest regression models used to correlate two or more than two variables, also called the response and predictor variables. Mathematically, the linear regression models are expressed as [25]

$$f(x) = a_o + a_1x_1 + a_2x_2 + e \tag{4}$$

where a_o is the y-intercept, a_1 and a_2 are co-efficients of regression, x_1 and x_2 are response variables and e represent the error. In this study, three linear models are selected including simple linear, linear interaction and linear robust. The linear interaction model includes an interaction term in addition to the constant and linear terms as shown in (5) [26]. The interaction term x_1x_2 represents interaction between two response variables. The linear model with robust function reduces the sensitivity of the model to outliers by assigning lower weights to the points which are expected to be outliers.

$$f(x) = a_o + a_1x_1 + a_2x_2 + a_3x_1x_2 + e \tag{5}$$

(2) Support vector Machine (SVM) regression models

SVM models are extensively used in classification. SVM regression models use the hyperplane (boundaries which predict the output) to fit the data. In addition to that these use different kernel functions, which transform input data into a suitable format. In this study, three kernel functions are used: linear, quadratic, and fine gaussian [27].

(3) Gaussian process regression (GPR) models

GPR is a non-parametric and probabilistic regression, which is based on kernel functions. It calculates the probability distribution over all allowable functions, which best fit the data, calculating it from parameters of any function. However, firstly it requires prior distribution and based on that, it predicts a posterior distribution on points of interest. GPR models are widely used in the field of machine learning for classification and regression.

There are two major advantages of GPR. Firstly, it performs well on small data sets and secondly, it provides uncertainty values on its own estimation. Let us consider a data set $\{(x_i, y_i);\ i = 1, 2, 3, \cdots..n\}$ where $x_i \in \mathbb{R}^d$ is the predictor variable with dimension d and $y_i \in \mathbb{R}$ is the response variable. We can assert that for any input vector $x = [x_1, x_3, \cdots, x_n]^T$ the vector of outputs $y = [y_1, y_3, \cdots, y_n]^t$ is normally distributed. The gaussian process is defined by mean $m(x)$ and covariance or kernel function $K(x, x')$ as [28]

$$f(x)\ GP\,[m(x),\ K(x, x')\,] \tag{6}$$

The choice of kernel function is important for obtaining the best fit model. It is essential that the kernel function must be symmetrical, i.e., $K(x_i\,,\,x_j) = K(x_j\,,\,x_i)$ and have a positive value for any set of inputs. Three types of kernels are used in this study: rational quadratic, squared exponential, and Matérn kernels.

6.3. Response plots and error indices

Comparison of models is an important aspect in evaluating the best model representing correlation between quantities. In this study, the comparison is made based on graphical and error indices. All models are trained with the respective data sets where cross-validation is kept at 5 folds for all models.

Response plot is a graph between predicted response versus the actual response. If the regression line of the model and actual data lies on identical lines, it means the model best fits actual data. Performance indices are statistical quantities which are useful in evaluating the fit of any regression model. In this study, four error indices including R-squared, RMSE, MAE and training time are used to evaluate and compare the performance of the trained regression models.

(1) R-squared error

This is a statistical error index, describing the effectiveness of fitting any regression line. Its value ranges between 0 and 1. A higher R-squared value shows better fitting of regression model [29].

(2) Root means square error (RMSE)

This represents the deviation of residuals (shows how far the actual data is from predicted response). Essentially, it defines the

distance of residuals from original data points. Mathematically it is defined as [29]

$$RMSE = \sqrt{\frac{\sum_{i=1}^{m}(x_i - x'_i)^2}{m}} \tag{7}$$

where $\acute{x}_i$ represents predicted values, $x_{(i)}$ represents actual values and m represents number of data points.

(3) Mean absolute error (MAE)

MAE is used to evaluate the performance of regression models. It is the difference of the average of actual and estimated data points. Mathematically, it is represented as [29]

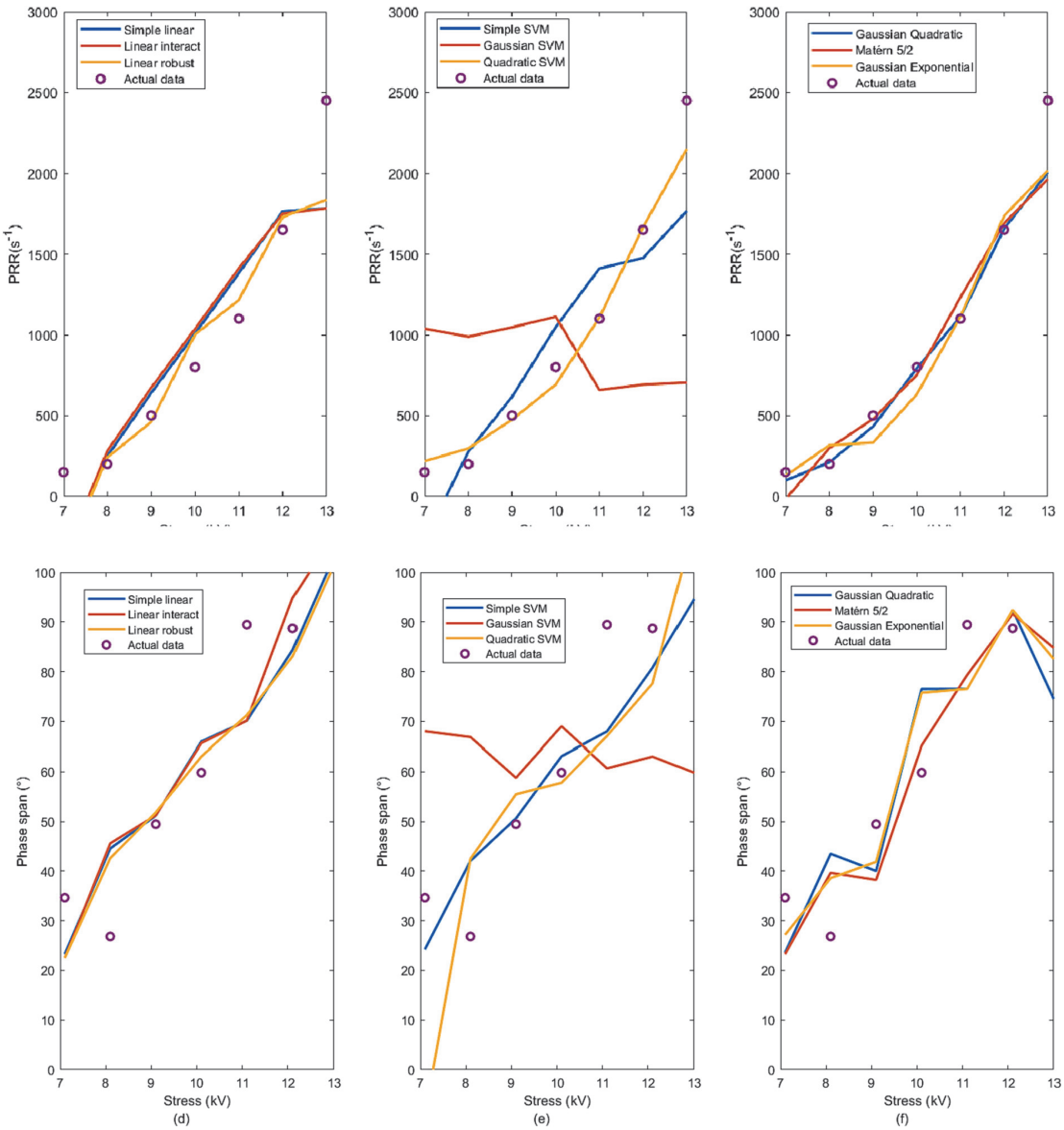

Fig. 12. Regression lines of three families of regression models (a) Linear models for PRR data, (b) SVM models for PRR data (c) GPR models for PRR data (d) Linear models for phase span data, (e) SVM models for phase span data (f) GPR models for phase span data.

$$MAE = \frac{\sum_{i=1}^{m} |x_i - x_i'|}{m} \tag{8}$$

where $\acute{x}_i$ represents predicted values, x_i represents actual values and m represents number of data points.

6.4. Performance comparison of regression model

Fig. 12(a–c) includes plots containing actual PRR data at increasing electrical stress and response plots of trained linear, SVM and GPR family models respectively. The regression lines along with performance indices show that linear SVM, SVM with quadratic kernel and models of gaussian process regression (quadratic, squared exponential and Matérn) best fit the PRR data at increasing electrical stress. Performance indices presented in Table 1 indicate that SVM quadratic and all models of the GPR family, i.e., quadratic, squared exponential and Matérn best fit the PRR data as R-squared values range between 0.95 and 0.98. RMSE and MAE values show that the GPR model with quadratic kernel has the lowest RMSE values of 160.67 s^{-1} and 118.29 s^{-1}. This shows that GPR regression model with quadratic kernel best fits the PRR data at increasing electrical stress. Fig. 12 (d–f) shows response plots of linear, SVM and GPR families respectively. The regression lines along with performance indices show all GPR models, i.e., quadratic, squared exponential, and Matérn, best fit the phase span data at increasing electrical stress.

7. Discussion

Medium voltage cables are integral part of the power system network. These cables composed of two major parts i.e., conductor and insulation. During operation cables undergo various types of stresses. Various tests are conducted for quality assurance and condition monitoring of cables. In [30] different testing methods are implemented to determine the quality of a conductor in optical ground wire (OGW). These tests include stress strain, tensile strength, creep test which are used to test the mechanical properties of insulation, thermal endurance test which is used to find the thermal capability of material to sustain certain temperature levels during operation, vibration test, galloping test to evaluate the fatigue performance and lighting test to see the behavior of cables during lighting strike. Insulation is second most important components of the cable. Thus, it is crucial to investigate the behavior of insulation under TEAM. Different testing methods including insulation resistance and tan delta used to determine insulation condition. Partial discharge measurement is latest technique used to assess insulation. Inception of PD indicates that cable undergoing degradation. This article investigates the PD progression behavior in XLPE insulation. An experimental investigation was performed where PD tests were conducted on a medium voltage cable sample containing an artificial defect. PD data were stored in the form of PRPD patterns. An algorithm is developed that extracts major PD characteristics from a PRPD pattern. Later, the behavior of those characteristics was analyzed at increasing electrical stress. The following conclusions can be made based on this investigation.

Four PD characteristics phase of occurrence, mean pulse height, pulse repetition rate and phase span were analyzed under elevated electrical stress. Analysis of φ shows that at lower stress levels, PD pulses were recorded between 210° to 270°. However, at higher stress levels the pulses are more concentrated towards the zero crossing of negative half cycle of the applied voltage as the majority of pulses were recorded between 180°-240°. The denser PD activity near the zero crossing can be the result of surface tracking.

Analysis of V_{mean} indicates that at lower stress levels V_{mean} of PD events varies proportionally to the applied electrical stress. However, at higher stress levels the strength of PD activity i.e., occurrence of pulses increases rather than pulse height which shows that pulse height doesn't indicate the severity of PD, but rather the density or number of pulses near zero crossing. It is also notable that the mean amplitude of PD pulses is high at intermediate voltage levels after PDIV, i.e., at 9.1 and 11.1 kV, rather than at higher stress levels, which also shows that severity is not proportional to pulse height. Also, it is noticed that the pulses with maximum amplitude do not occur near the peak of the applied voltage, but rather during the first half of the negative cycle of the applied voltage, i.e., between 190°-250°.

Analysis of PRR shows that at increasing electrical stress there is rise in number of pulses. At low stress levels pulses increases linearly with applied electrical stress, however at higher levels there is a significant rise in pulses which makes PRR an important indicator that represents severity of PD activity.

Analysis of φ_{span} indicates that at lower stress levels, the span of PD activity was increasing proportionally to electrical stress. However, at higher stress levels, there is consistency in φ_{span} values which implies that at higher stress levels there is not much variation in φ_{span} of PD activity. Regression analysis of φ_{span} and PRR data in correlation to elevated stress shows that GPR models best represent trending attributes of both PD characteristics.

8. Conclusion

This study uses a simple approach to investigate degradation behavior of insulation under light of PD characteristics. For this an experimental investigation is performed. PD data is collected by creating an artificial defect on cable surface in form of a PRPD pattern. A tool is developed that extract major PD characteristics. A correlation between PD characteristics and various levels of electrical stress is shown using graphical representation. The results shows that there an increase in PD activity at middle voltage levels i.e., 9 10 and 11 kV compared to high voltage levels, reflected by the behavior of PRR and mean pulse height. The trending attributes of major characteristics are mapped using regression analysis which shows that the PRR and phase span data follows GPR. The core objective of this study is to determine how partial discharge characteristics vary with increasing degradation or aging. The outcomes of this investigation can contribute to lifetime assessment, failure prediction and condition monitoring of power cables. Similar

Table 1
Performance indices of regression models trained for PRR and for $_{span}$ data under increasing electrical stress.

Regression Models	R-Squared		RMSE		MAE	
	PRR (s^{-1})	Phase span (°)	PRR (s^{-1})	Phase span (°)	PRR (s^{-1})	Phase span (°)
Linear	0.84	0.80	326.29	15.75	316.49	13.05
Linear interact	0.84	0.80	438.27	15.79	316.49	13.02
Linear robust	0.82	0.80	389.31	15.71	323.74	12.93
SVM	0.85	0.81	346.14	15.42	308.06	12.73
SVM quadratic	0.98	0.59	785.98	22.37	85.54	16.85
SVM gaussian	0.01	−0.03	147.94	35.61	809.43	33.05
GPR quadratic	0.98	0.92	160.67	10.18	118.29	6.55
GPR Squared exponential	0.95	0.92	204.21	10.18	152.36	6.55
GPR Matérn	0.96	0.92	487.81	9.97	156.23	7.35

methodologies can be implemented to investigate insulation degradation behavior in other power system assets.

CRediT authorship contribution statement

Maninder Choudhary: . **Muhammad Shafiq:** Methodology, Project administration, Supervision, Writing – review & editing. **Ivar Kiitam:** . **Ivo Palu:** . **Waqar Hassan:** Methodology, Writing – review & editing. **Parveen Prakash Singh:** .

Declaration of competing interest

The authors declare that they have no known competing financial interests or personal relationships that could have appeared to influence the work reported in this paper.

Data availability

The authors do not have permission to share data.

Acknowledgement

This work is supported by the Estonian Research Council under Grant No. PSG632.

References

[1] Europacable, An Introduction to Medium and Low Voltage Cables in Distribution Networks as support of Smart Grids, 2014.
[2] M. Choudhary, M. Shafiq, I. Kiitam, A. Hussain, I. Palu, and P. Taklaja, A review of aging models for electrical insulation in power cables, Energies 15(9), MDPI, May 01, 2022.
[3] E. Maggioli, H. Leite, and C. Morais, A survey of the Portuguese MV underground cable failure, International Conference on the European Energy Market, (EEM), Porto, Portugal, 2016.
[4] G.C. Montanari, A. Cavallini, Partial discharge diagnostics: from apparatus monitoring to smart grid assessment, IEEE Electr. Insul. Mag. 29 (3) (2013) 8–17.
[5] IEC-60270:2000+AMD1; High-Voltage Test Techniques-Partial Discharge Measurements, International Electrotechnical Commission, 2015.
[6] R. Bartnikas, Partial discharges their mechanism, detection and measurement, IEEE Trans. Dielectr. Electr. Insul. 9 (5) (2002) 763–808.
[7] H.V.P. Nguyen, B.T. Phung, Void discharge behaviours as a function of cavity size and voltage waveform under very low-frequency excitation, High Voltage, IET, 2018.
[8] K. Temmen, Evaluation of surface changes in flat cavities due to ageing by means of phase-angle resolved partial discharge measurement, J. Phys. d: Appl. Phys. 33 (2000) 603.
[9] S. Boggs, J. Densley, Fundamentals of partial discharge in the context of field cable testing, IEEE Electr. Insul. Mag. 16 (5) (2000) 13–18.
[10] P.H.F. Morshuis, Degradation of solid dielectrics due to internal partial discharge: some thoughts on progress made and where to go now, IEEE Trans. Dielectr. Electr. Insul. 12 (5) (2005) 905–913.
[11] X. Feng, Q. Xiong, A.L. Gattozzi, R.E. Hebner, Partial discharge experimental study for medium voltage DC cables, IEEE Trans. Power Deliv. 36 (2) (2021) 1128–1136.
[12] L. Zhou, L. Bai, J. Zhang, W. Cao, E. Xiang, Measurement and diagnosis of PD characteristics of industrial cable terminations in extreme cold environment, IEEE Trans. Instrum. Meas. 70 (2020) 1–11.
[13] W. Hassan, M. Shafiq, G.A. Hussain, M. Choudhary, I. Palu, Investigating the progression of insulation degradation in power cable based on partial discharge measurements, Electr. Pow. Syst. Res. 221 (2023).
[14] H. Janani, B. Kordi, M.J. J.ozani, Classification of simultaneous multiple partial discharge sources based on probabilistic interpretation using a two-step logistic regression algorithm, IEEE Trans. Dielectr. Electric. Insulation 24 (1) (2017) 54–65.
[15] O.E. Gouda, A.A. El Farskoury, A.R. Elsinnary, A.A. Farag, Investigating the effect of cavity size within medium-voltage power cable on partial discharge behaviour, IET Gener. Transm. Distrib. 12 (5) (2018) 1190–1197.
[16] R. Patsch, F. Berton, Pulse Sequence Analysis-a diagnostic tool based on the physics behind partial discharges, J. Phys. d: Appl. Phys. 35 (2002) 25.
[17] N.C. Sahoo, M.M.A. Salama, R. Bartnikas, Trends in partial discharge pattern classification: a survey, IEEE Trans. Dielectr. Electr. Insul. 12 (2) (2005) 248–264.
[18] S.-H. Park, H.-E. Jung, J.-H. Yun, B.-C. Kim, S.-H. Kang, K.-J. Lim, Classification of defects and evaluation of electrical tree degradation in cable insulation using pattern recognition method and weibull process of partial discharge. International Conference on Condition Monitoring and Diagnosis, Beijing, China, 2008.
[19] J. Tang, S. Zhou, C. Pan, A Denoising algorithm for partial discharge measurement based on the combination of wavelet threshold and total variation theory, IEEE Trans. Instrum. Meas. 69 (6) (2020) 3428–3441.
[20] X. Ma, C. Zhou, I.J. Kemp, Interpretation of wavelet analysis and its application in partial discharge detection, IEEE Trans. Dielectr. Electr. Insul. 9 (3) (2002) 446–457.

[21] S. Chandrasekar, et al., Investigations on leakage current and phase angle characteristics of porcelain and polymeric insulator under contaminated conditions, IEEE Trans. Dielectr. Electr. Insul. (2009).
[22] F. Sk Wong, W. Rowe, Detection of corona and dry-band arc discharges on nano-composite epoxy insulators using RF sensing, Prog. Electromagn. Res. 2012 (125) (2012) 237–254.
[23] I. Kiitam, M. Shafiq, P. Taklaja, M. Parker, I. Palu, L. Kütt, Characteristic pulse pattern features of different types of partial discharge sources in power cables, IEEE PES/IAS Power Africa, Nairobi, Kenya 2021 (2021) 1–5.
[24] M. Choudhary, M. Shafiq, I. Kiitam, I. Palu, P. Taklaja, Study on the progression of surface partial discharge in power cables, in: IEEE 63rd International Scientific Conference on Power and Electrical Engineering of Riga Technical University (RTUCON), 2022.
[25] J. Neter, M.H. Kutner, C.J. Nachtsheim, W. Wasserman, Applied Linear Statistical Models, The McGraw-Hill Companies Inc, IRWIN, 1996.
[26] G.A.F. Seber, L.R. Analysis, Wiley Series in Probability and Mathematical Statistics, John Wiley and Sons Inc, 1977.
[27] A.J. Smola, B.J.S. Scholkopf¨, Computing. In: A tutorial on support vector regression. 14, 2004, p. 199–222.
[28] E. Schulz, M. Speekenbrink, A.J.Jo.M.P. Krause, A Tutorial on Gaussian Process Regression: Modelling, Exploring, and Exploiting Functions 85 (2018) 1–16.
[29] D. Chicco, M.J. Warrens, G. Jurman, The coefficient of determination R-squared is more informative than SMAPE, MAE, MAPE, MSE and RMSE in Regression Analysis Evaluation, 2021.
[30] Karabay, Sedat, E.A. Güven, A.T. Ertürk, Performance testing of an optical ground wire composite, Mater. Technol. 47 (2013) 1.

Publication VI

M. Choudhary, M. Shafiq, I. Kiitam, I. Palu and W. Hassan, “Partial Discharge Pulse Shape Analysis for Progression of Insulation Degradation in Medium Voltage Cable,” 2023 International Electrical Engineering Congress (iEECON), Krabi, Thailand, 2023, pp. 332–336, doi: https://doi.org/10.1109/iEECON56657.2023.10126589.

Partial Discharge Pulse Shape Analysis for Progression of Insulation Degradation in Medium Voltage Cable

Maninder Choudhary
Department of Electrical Power Engineering & Mechatronics
Tallinn University of Technology
Tallinn, Estonia
maninder.choudhary@taltech.ee

Muhammad Shafiq
Department of Electrical Power Engineering & Mechatronics
Tallinn University of Technology
Tallinn, Estonia
muhammad.shafiq@taltech.ee

Ivar Kiitam
Department of Electrical Power Engineering & Mechatronics
Tallinn University of Technology
Tallinn, Estonia
ivar.kiitam@taltech.ee

Ivo Palu
Department of Electrical Power Engineering & Mechatronics
Tallinn University of Technology
Tallinn, Estonia
ivo.palu@taltech.ee

Waqar Hassan
University of Engineering & Technology,
Lahore, Pakistan
2017phdelect10@uet.edu.pk

023 International Electrical Engineering Congress (iEECON) | 979-8-3503-3236-0/23/$31.00 ©2023 IEEE | DOI: 10.1109/IEECON56657.2023.10126589

***Abstract*—Measurement of partial discharge (PD) pulses is a method used in quantifying PD activity within defective insulation. PD pulses propagate away from the defect along the cable and can be measured by sensors such as high frequency current transformers (HFCT). These PD pulses contain information that describes the behavior of PD activity in the degrading insulation. Pulse shape analysis (PSA) is an efficient method to analyze the degradation behavior of insulation. In this study, the PSA is performed on a medium voltage cable sample with surface discharges emerging from a damaged cable termination. PSA is performed based on rise time, fall time, and pulse width of individual PD pulses that are extracted from the PD data measured in the form of phase resolved PD pattern under increasing electrical stress conditions. The Gaussian model is implemented to find best-fit lines which describe the correlation of PSA quantities and electrical stress. The presented study results can be useful in improving the diagnostics of aging power cables.**

Keywords— Power cables, insulation aging, surface partial discharge, pulse analysis, electrical stress.

I. INTRODUCTION

The use of power cables is gradually increasing to improve the reliability of power networks [1]. The increasing use of polymeric-insulated cables is due to their improved electrical behavior (low discharging current and dielectric loss), low transmission loss, reduction in faults, protection against abrasion, tear, ozone, and improved chemical and morphological properties. Insulation aging is a general phenomenon that reduces the lifetime of the cable. Aside from normal aging, defects emerge during operation due to associated operating stresses (thermal, electrical, mechanical, and ambient), overvoltages, and transients and surges due to the operation of power electronics converters accelerate the aging and cause premature failure [2], [3].

Therefore, it is crucial to protect the insulation prior to failure. Partial discharge (PD) measurement is a well-known testing method utilized for the assessment and prediction of insulation condition [4]. PDs are confined discharges that degrade the insulation locally at the defect site and with increasing stress or time this activity spread across the surrounding insulation between the conductor and shielding and finally causes breakdown [5]. PD activity can be best explained by the avalanche theory. The electric field is amplified at the defect site compared to normal electric field stress in the surrounding insulation. Due to the high electric field strength, free electrons are accelerated and obtain sufficient kinetic energy to ionize other gas molecules upon colliding with them. This generates an avalanche of electrons [6]. This avalanche creates a multiplicative effect with increasing stress and time which ultimately cause degradation and ultimately causes breakdown. This avalanche produces high-frequency pulses from the defect site termed PD [7]. The emerging PD pulses travel in both directions toward the ends of the cable and can be sensed by the high-frequency current transformer (HFCT) sensor.

Mainly three types of discharges occur in the power cables that include surface discharge, internal discharge, and corona discharge. Surface discharges occur at interfaces where there is the interaction of gaseous and solid dielectrics under the presence of an electrical field, commonly found on insulation surfaces and at critical points such as cable terminations, joints, and sharp edges [8]. These discharges are the result of contamination, dust, cracks, and sharp edges (termination) in the cable insulation. Lack of electrical clearance and poor environmental conditions promote surface discharges. Their interaction with moisture and heat results in erosion which in turn affects the chemical structure of the insulation [9]. Surface partial discharges can cause tracking on the surface of the insulation and initiate electrical trees which can cause the breakdown of the insulation.

Different methods are used to investigate insulation degradation behavior. PRPD pattern analysis is the most common method. PRPD pattern represents three basic quantities including charge magnitude q, number of discharges n and phase of occurrence Φ. Several derived quantities, accumulated charge Q_{acc}, average discharging current I_{avg}, discharge power P_d, and pulse repetition rate PRR can be extracted from basic quantities for a deeper understanding of PD behavior. In [10] Q_{acc}, P_d, $I_{avg,}$ and PRR are analyzed in correlation to the increased lifetime of MV cables.

979-8-3503-3236-0/23/$31.00 ©2023 IEEE

Restrictions apply.

Pulse sequence analysis is the second important method where, peak height of pulses V_P, corresponding instantaneous applied voltage U_{ins}, and time of occurrence t are first stored sequentially (in full ac cycle), and later frequency distribution of quantities and their sequential behavior is analyzed. In [11] pulse sequence analysis is performed *where* V_P, U_{ins}, t and derived quantities ΔU_{ins} and Δt are analyzed to understand the physics of PD mechanism. In addition, pulse pattern features can be used to differentiate between different types of cable defects, which present a variable risk of failure [12]. Although the above methods are very useful in determining the degradation behavior of insulation.

PD pulse shape itself contains useful information which can help to understand degradation behavior in cables. Insulation degradation from initiation to breakdown occurs in two steps. Initially, short, and narrow pulses of small pulse width occur however the frequency of occurrence happens after several ten nanoseconds. These pulses are due to streamer-like discharges that initiate at the start of a PD activity. Later with increasing degradation wider pulses occur (pulse width proportional to the defect size). These pulses are due to Townsend-like discharges [11]. Therefore, it is crucial to investigate the behavior of pulse shape characteristics. Pulse shape analysis (PSA) is a comparatively simple and efficient method. Fig. 1 shows a PD pulse with its shape characteristics.[13]. Pulse shape characteristics vary with type of defect and type of insulation. These characteristics can be utilized to track the degradation trend of insulation[14]. There are three major characteristics of a PD pulse.

Rise time (t_r) is the time it takes for the PD pulse to reach from 10% to 90% of the peak value.

Fall time (t_f) is the time it takes for the PD pulse to decrease from 90% to 10% of the peak value.

Pulse width (t_w) is the time interval between 50% peak values at both the rising and falling edges.

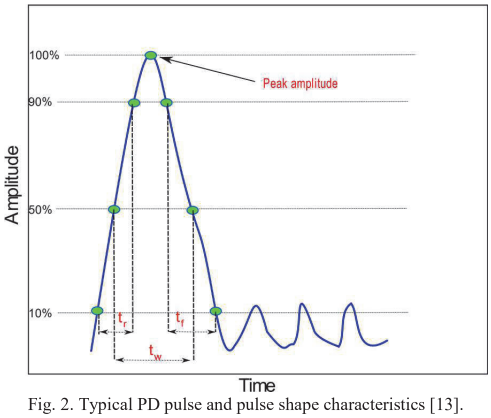

Fig. 2. Typical PD pulse and pulse shape characteristics [13].

In this study pulse shape characteristics (t_r, t_f, t_w) are analyzed with increasing electrical stress. In the end, statistical analysis is performed to find the best fit line that defines PSA quantities. The core objective of this study is to correlate PSA quantities with progressive electrical stress or increasing degradation.

II. Experimental Setup and PD Measurements

For data collection, a PD measurement experiment setup was established in the laboratory. Fig. 2 shows the schematic of the measurement setup. The setup includes the following major components required for the PD measurement.

PD setup includes a high voltage AC source and a voltage regulator for variation of voltage in steps. A coupling capacitor (CC) of rating 100 kV and 1 nF charge storing capacity for storing the charges emitted by the defect site. A

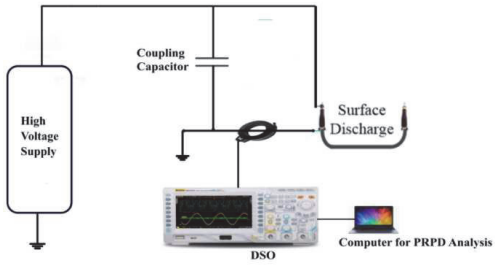

Fig. 1. Schematic of PD experiment and measurement setup

high-frequency current transformer (HFCT) with a bandwidth of 500 kHz to 80 MHz (-3dB) and a 1:10 transfer ratio connected with CC to measure PD pulses. A digital oscilloscope for visualization and storage of PD data and a computer for analysis of PRPD pattern. A small piece of 11 kV XLPE cable main insulation thickness 1.2 mm with conductor area of 50 mm^2 , continuous current capacity of 230 A and length 3 m is considered for the experimental study. A defect is made by removing the stress cone at one terminal of MV cable sample that produces surface discharges as shown in Fig. 3. The shield at other end of the cable is connected to the ground while an HFCT sensor is installed around the grounded wire for measurement of PD pulses.

Fig. 3. 11 kV XLPE cable with defect by removing stress cone at the terminal for surface discharge.

The measurements were taken at rising voltages. Initially, the voltage increased up to 3 kV where no activity observed. Later the voltage is increased by a step of approximately 0.3 kV until partial discharge inception voltage (PDIV). ASTM D1868-13 defines PDIV as the voltage at which a single pulse stays for a minute. In this measurement, PDIV was observed at 5.9 kV. After PDIV the voltages are raised at a step of 1

Authorized licensed use limited to: Tallinn University of Technology. Downloaded on October 03,2025 at 07:18:09 UTC from IEEE Xplore. Restrictions apply.

kV and data is stored until near the breakdown voltage (13.3 kV).

Stochasticity is a major concern during PD measurement. As PD activity in an insulation exhibit random pulses (PD pulses in PRPD pattern appear and flee in a fraction of milliseconds). Thus, the measurement at one instant varies at another instant. The variation mainly occurs in the phase of occurrence, pulse amplitude, and the number of pulses. To cope with this stochastic behavior ten measurements are captured at each stress level (7.1-13.3 kV).

III. Characteristics of Surface Discharge and Extraction of PSA quantities

Surface discharge phenomenon can be explained by a PRPD pattern. Fig.4. shows the PRPD patterns obtained from a surface discharge defect at increasing electrical stress. Considering phase span, surface discharge pulses occur between 0°-90° in the positive half cycle and between 180°-270° in the negative half cycle of the applied voltage. Four measurements at different stress levels are shown in Fig.4 (a) 10.1 kV, (b) 11.1 kV (c) 12.1 kV (d) 13.3 kV. There are two main features of surface discharge in a PRPD pattern. First, the PD pulses are asymmetrical in both positive and negative cycles and most of the pulses occur in the negative half cycle of the applied voltage. Secondly, the amplitude of pulses due to surface discharge is comparatively high compared to internal PDs and there is a wide range of pulses that occur in a full cycle.

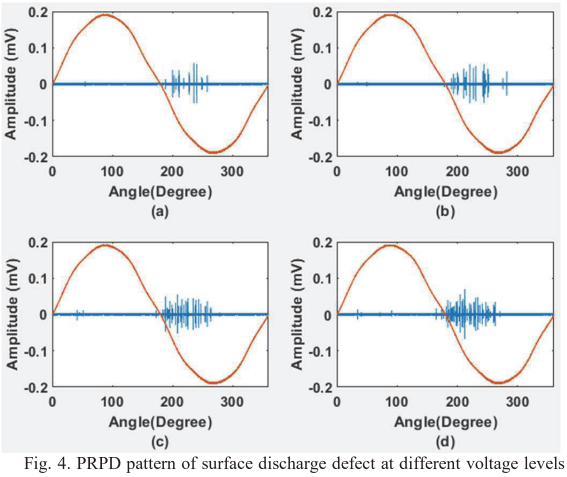

Fig. 4. PRPD pattern of surface discharge defect at different voltage levels a) 10.1 kV b)11.1 kV c) 12.1 kV d)13.3 kV.

In this study, a MATLAB based tool is developed which extracts the rise time (t_r), fall time (t_f), and pulse width (t_w) of the individual pulse from a PRPD pattern and stores it in the corresponding variable. Fig. 5 shows the flow chart of the developed tool. First of all, it detects the first occurring peak of an individual PD event then an iteration is run that moves 25 sample locations back and 25 sample locations forward to and form a PD pulse. After forming the pulse, a pulse smoothing filter is utilized that soothes the PD pulse and finally t_r, $_f$, and t_w are extracted.

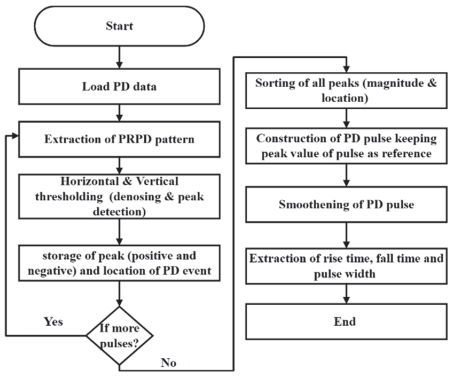

Fig. 5. Flow chart of an algorithm for extraction of pulse shape analysis characteristic quantities.

IV. Results & Discussion

In this section, the behavior of the above-extracted pulse characteristics is investigated at increasing electrical stress. The key goal is to correlate the changes that appeared in the values of these characteristics/quantities with increasing degradation or increasing electrical stress.

A. Behavior of rise time

Fig. 6 shows the box and whisker plot describe the variation of rise time values of PD pulses at different stress levels. It can be seen that at lower-stress levels (7-9 kV) the rise time values were found in the range of 63-73 ns. At high-stress levels (10 kV-13.3 kV) 25% of rise time values exceed 75 ns. The interquartile range (IQR) or width of the box which is the difference between upper and lower quartile ranges (Q3-Q1). It represents middle 50% of values of a data set i.e., from 25th to 75th percentile. IQR shows that 50 % of the values still reside in the range of 65 to 75 ns. Considering median value, it varies in three stages. At lower stress (7-10 kV) it stays consistent at 68 ns at high electrical stress (11-12.2 kV) it is increased to 70 ns and nearest the breakdown (13.3 kV) it is 72 ns. It means that with increasing stress, the median value follows a trending pattern. Whiskers at different stress levels which represent the remaining 50% of data show that at lower stress levels there is a small variation in rise time values but at increasing stress this variation increases. There are more outliers near to breakdown (13.3 kV) than at lower stress levels.

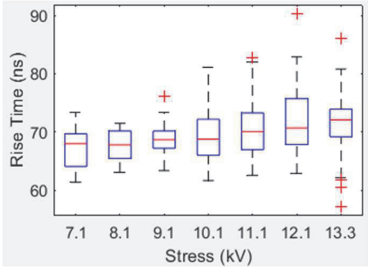

Fig. 6. Box and whisker plot showing the variation of rise time data at different stress levels.

Authorized licensed use limited to: Tallinn University of Technology. Downloaded on October 03,2025 at 07:18:09 UTC from IEEE Xplore. Restrictions apply.

B. Behavior of fall time

Fig. 7 shows the box and whisker plot of fall time at different electrical stress levels. IQR at each stress level shows that 50% of fall time values reside between 47 to 52 ns. It can be seen that that at 7.1, 9.1, 11.1, and 13.3 kV the overall fall time values are concentrated, however at 8.1, 10.1, and 12.1 Kv there seems a slight increase in IQR as shown by width of box. There is random variation in the IQR at increasing stress. The whiskers which represent the remaining 50% fall time values of a data set show that at increasing stress there is a big variation in the fall time data since whiskers spread out from both sides. The median values follow a similar pattern to rise time. From 7.1 kV to 10.1 kV the median value observed as 50.9 ns, which is slightly increased to 51.2 ns at middle stress levels (10.1 to 11.1 kV), and further increased to 52 ns near to breakdown. The number of outliers values are high at higher stress levels particularly at 11.1 kV and near breakdown (13.3 kV).

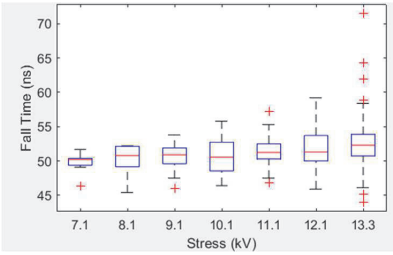

Fig. 7. Box and whisker plot showing the variation of fall time data at different stress levels.

C. Behavior of pulse width

Fig. 8 shows the box-and-whisker plot of pulse widths at progressive electrical stress. It can be observed that pulse width values follow an upward trend. Initially, pulses of small duration below 100 ns were observed at (7.1-8. kV). With increasing stress, the width of pulses increased, and near-to-breakdown (12.1 kV) pulses of width 110 ns were observed. According to breakdown theory, there are two mechanisms, steamer and Townsend breakdown which are responsible for the breakdown of gases. The streamer breakdown is characterized by pulses of small pulse width and the Townsend phenomenon is characterized by wider pulse widths. The median value varies in three stages. From 7.1 to 8.1 kV, it is 102 ns, from 9.1 kV to 11.1 kV it slightly increases to 103 ns, and at 13.3 kV it is considerably increased to 106 ns. The whiskers at higher stress levels (10.1-13-3 kV) which represent the remaining 50% of data show that there is a large variation of pulse width values at high voltage levels.

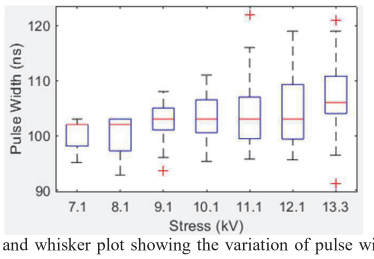

Fig. 8. Box and whisker plot showing the variation of pulse width data at different stress levels.

To understand the degradation behavior based on PSA it is necessary to observe the variation of t_r, t_f, and t_w at increasing electrical stress. Fig. 8 shows the behavior of these three parameters based on the mean value. It can be seen that all three quantities are increasing with the increasing electrical stress. Although Pulse width shows a random behavior after PDIV i.e., at 7.1 kV and 8.1 kV. However, at higher stress levels the pulse width varies proportionally with applied electrical stress.

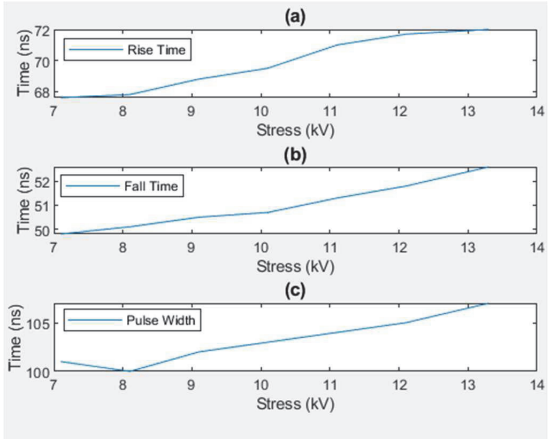

Fig. 9. Behavior of (a)rise time, b) fall time c) pulse width in correlation to electrical stress.

Statistical analysis is performed to find the best fit lines that represent the trend of three quantities. Table I shows skewness S_k and kurtosis k_u values of t_r, t_f, and t_w at increasing stress. The results show that data is slightly skewed to Gaussian distribution.

TABLE I. SKEWNESS AND KURTOSIS OF PSA QUANTITIES AT PROGRESSIVE ELECTRICAL STRESS

Parameter	Rise Time	Fall Time	Pulse Width
Skewness	0.016	0.59	0.24
Kurtosis	-2.0	-0.5	-0.78

Keeping in view S_k and k_u Gaussian model is implemented using MATLAB curve fitting tool to find the best fit line that represents the relation between applied electrical stress and PSA quantities. Fig. 10 shows the curve fitting lines (a) of t_r, (b) t_f, and (c) t_w with 95%f prediction bounds. All the quantities show an upward trend with progressive electrical stress. Prediction lines show that the gaussian model best describes the relationship between PSA quantities and electrical stress. However, the validity of any model relies on the coefficient of determination (COD) or R-Square and RMSE values. Table II shows COD and RMSE values for each best fit line representing t_r, t_f, and t_w respectively.

TABLE II. R-SQUARE AND RMSE VALUES OF GAUSSIAN MODEL

Quantity	R Square	RMSE
Rise time	0.96	0.41
Fall time	0.97	0.19
Pulse width	0.93	0.76

Authorized licensed use limited to: Tallinn University of Technology. Downloaded on October 03,2025 at 07:18:09 UTC from IEEE Xplore. Restrictions apply.

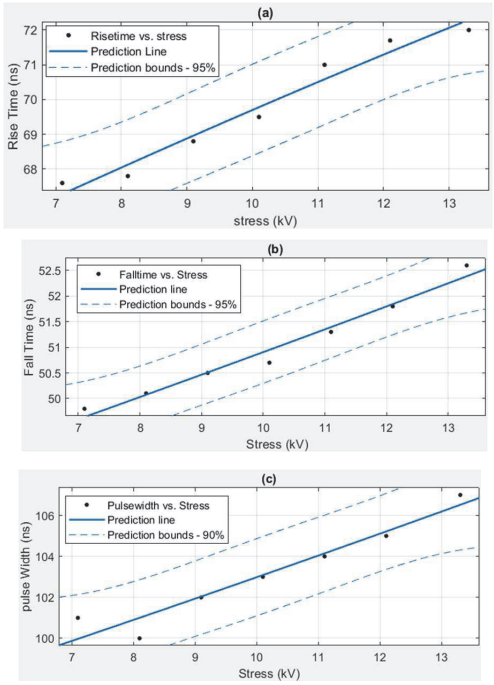

Fig. 10. Gaussian models prediction lines and 95% confidence bounds describe the relation between a) Rise time b) fall time c) pulse width and progressive electrical stress.

V. CONCLUSION

In this study, PD pulse shape characteristics (rise time, fall time, and pulse width) are investigated in correlation to increasing electrical stress. To achieve this, PD tests were conducted on medium voltage cable samples with surface discharge defects. A tool is developed that extracts PSA quantities. The results show that all three quantities follow a trending pattern with increasing electrical stress that is their value is proportional to the level of applied electrical stress. R square values, obtained from best-fit lines of t_r, t_f, and t_w show that the PSA quantities follow gaussian distribution at increasing electrical stress. These results might be useful for developing a diagnostics algorithm, which can help utilities monitor the insulation condition of the critical network asset without having specific expertise in the area of PD.

VI. REFERENCES

[1] Europacable, "An Introduction to Medium and Low Voltage Cables in Distribution Networks as support of Smart Grids," 2014. [Online]. Available: www.europacable.com

[2] M. Choudhary, M. Shafiq, I. Kiitam, A. Hussain, I. Palu, and P. Taklaja, "A Review of Aging Models for Electrical Insulation in Power Cables," *Energies*, vol. 15, no. 9. MDPI, May 01, 2022. doi: 10.3390/en15093408.

[3] A. Cavallini, D. Fabiani and G. C. Montanari, "Power electronics and electrical insulation systems - part 2: life modeling for insulation design," in *IEEE Electrical Insulation Magazine*, vol. 26, no. 4, pp. 33-39, July-Aug. 2010, doi: 10.1109/MEI.2010.5511187.

[4] "IEEE Guide for Partial Discharge Testing of Shielded Power Cable Systems in a Field Environment," in *IEEE Std 400.3-2006*, vol., no., pp.1-44, 5 Feb. 2007, doi: 10.1109/IEEESTD.2007.305045.

[5] *IEC-60270:2000+AMD1; High-Voltage Test Techniques-Partial Discharge Measurements*. 2015.

[6] L. Testa, S. Serra, and G. C. Montanari, "Advanced modeling of electron avalanche process in polymeric dielectric voids: Simulations and experimental validation," *J Appl Phys*, vol. 108, no. 3, Aug. 2010, doi: 10.1063/1.3359713.

[7] R. Bartnikas, "Partial discharges their mechanism, detection and measurement," *IEEE Transactions on Dielectrics and Electrical Insulation*, vol. 9, no. 5, pp. 763–808, Oct. 2002, doi: 10.1109/TDEI.2002.1038663.

[8] L. Bai *et al.*, "Influence of surface discharge on the deterioration characteristics of ethylene-propylene rubber cable insulation under alternating current high voltage," *IET Science, Measurement and Technology*, vol. 16, no. 5, pp. 293–304, Jul. 2022, doi: 10.1049/smt2.12104.

[9] J. Densley, "Ageing mechanisms and diagnostics for power cables - an overview," *IEEE Electrical Insulation Magazine*, vol. 17, no. 1, pp. 14–22, Jan. 2001, doi: 10.1109/57.901613.

[10] Zeeshan Ahmed, "Development of a continuous condition monitoring system based on probabilistic modelling of partial discharge data for polymeric insulation cables," *Mississippi State University*, 2019.

[11] D. Benzerouk, "Pulse Sequence Analysis and Pulse Shape Analysis: Methods to Analyze Partial Discharge Processes," 2008.

[12] I. Kiitam, M. Shafiq, P. Taklaja, M. Parker, I. Palu and L. Kütt, "Characteristic Pulse Pattern Features of Different Types of Partial Discharge Sources in Power Cables," 2021 IEEE PES/IAS PowerAfrica, 2021, pp. 1-5, doi: 10.1109/PowerAfrica52236.2021.9543366.

[13] P. H. F. Morshuis, "Partial discharge mechanisms: Mechanisms leading to breakdown, analyzed by fast electrical and optical measurements," *Delft University of Technology (TU Delft)*, 1993.

[14] M. Wu, H. Cao, J. Cao, H. L. Nguyen, J. B. Gomes, and S. P. Krishnaswamy, "An overview of state-of-the-art partial discharge analysis techniques for condition monitoring," *IEEE Electrical Insulation Magazine*, vol. 31, no. 6, pp. 22–35, Nov. 2015, doi: 10.1109/MEI.2015.7303259.

Maninder Choudhary was born in Pakistan, in 1990. He received the M.Sc. degree in Energy and Power Engineering from TGGS, KMUTNB, Bangkok, Thailand in 2018. He is student member of IEEE Estonia. Currently, he is pursuing Ph.D. degree at Department of Electrical Power Engineering and Mechatronics, Tallinn University of Technology (Taltech), Estonia. From 2019 to 2021 he served as Lecturer at SSUET, Pakistan. His main research interest includes partial discharge diagnostics and condition monitoring of power system assets. Maninder honors and award Global UGRAD & Exchange Scholarship by Department of State USA during his undergraduate studies.

Authorized licensed use limited to: Tallinn University of Technology. Downloaded on October 03,2025 at 07:18:09 UTC from IEEE Xplore. Restrictions apply.

Publication VII

M. Choudhary, M. Shafiq, A. Bhattarai, I. Kiitam, I. Palu, P. Taklaja, “A Comprehensive Study of Partial Discharge based Extrinsic Aging in Nomex Insulation Films: Modeling, Simulation and Measurement”, Electric Power Systems Research, Elsevier, 2025, doi: https://doi.org/10.1016/j.epsr.2025.111663.

Electric Power Systems Research 245 (2025) 111663

Contents lists available at ScienceDirect

Electric Power Systems Research

journal homepage: www.elsevier.com/locate/epsr

A comprehensive study of partial discharge based extrinsic aging in nomex insulation films: Modeling, simulation and measurement

Maninder Choudhary [a,*], Muhammad Shafiq [b], Abhinav Bhattarai [c], Ivar Kiitam [a], Paul Taklaja [a], Ivo Palu [a]

[a] Department of Electrical Power Engineering & Mechatronics, Tallinn University of Technology, Tallinn, Estonia
[b] Center for Advanced Power Systems, Florida State University, FL, USA
[c] Department of Electrical and Electronics Engineering, Department of Electrical and Electronic Engineering, Kathmandu University, Dhulikhel, Nepal

ARTICLE INFO

Keywords:
Surface discharge
Electrical field
Partial discharge
Insulation aging
Nomex film
FEM model

ABSTRACT

Electrical insulation plays a critical role in ensuring reliability and performance of electrical assets. However, operational stresses can degrade insulation over time, highlighting the need to understand insulation degradation behavior for development of reliable electrical systems. Nomex 410 insulation, known for its durability and thermal stability, is extensively used in electrical assets and aerospace systems. This work presents aging study of Nomex from perspective of insulation reliability assessments. It is based on a so-called three-leg approach that can be used as a valuable tool to conduct a surface partial discharge (PD) based aging study of insulating materials. This approach is used in this paper for estimation of surface partial discharge inception voltage (PDIV) of Nomex films of selected thickness. Additionally, accelerated aging tests are performed at elevated voltages (multiples of PDIV). These voltages caused accelerated surface aging, leading to gradual degradation of starting from the surface, extending towards the bulk of the material, posing more serious threat to the insulation condition. PD activity is measured in the form of phase-resolved PD (PRPD) patterns. PD characteristics and trending attributes extracted from PRPD patterns, apparent charge (Q_a), and number of pulses (n) are analyzed. Results provide insights into PD behaviour during electrical aging of Nomex. The presented methodology can be implemented to conduct reliability assessments and lifetime studies of other insulating materials.

1. Introduction

Nomex is a widely used electrical insulation material in AC and DC electrical machines, transformers, large generators, and chokes due to its excellent dielectric properties, and low dissipation factor at higher temperature and frequency ranges [1–4]. It is also used in cryogenic applications due to its moisture resistance and high mechanical strength [5].

Insulation aging is a complex process that results in the reduction of insulation service life. Insulation system in electrical assets is subjected to various types of stresses during operation, which include thermal, electrical, ambient, and mechanical (TEAM) stresses [6]. Modern operational conditions pose an additional stress, particularly due to increased voltage levels, high power density, and higher harmonic frequencies, which contribute to electrical and thermal stress. Therefore, the resiliency of the insulation system is becoming challenging from a design and operation perspective [7,8]. PD is one of the most deleterious processes affecting insulation as it accelerates intrinsic and extrinsic aging of the insulation material. PD diagnostics are performed for condition monitoring, aging, and lifetime studies and to observe the ongoing degree of deterioration within the insulation system of electrical assets [9,10].

While condition monitoring and study of aging mechanisms in insulation materials has long been of interest to researchers, there remains a critical need to understand further aging and degradation, particularly considering the progression of partial discharge activity which is not only a key indicator of insulation deterioration but also a contributor of extrinsic aging. Considering PD activity, each PD event results in a high frequency current pulse (based on the charge released during a discharge process) and a number of current pulses emerge during PD activity. The key PD quantities such as the amplitude of each PD (current pulse) and the number of pulses per second (pulse repetition rate) emerged depend on the various factor, such as type, size, and location of insulation defect, and environmental and electrical stress conditions. Therefore, in addition to the PRPD patterns, apparent charge

* Corresponding author.
E-mail address: maninder.choudhary@taltech.ee (M. Choudhary).

https://doi.org/10.1016/j.epsr.2025.111663
Received 12 November 2024; Received in revised form 10 March 2025; Accepted 27 March 2025
Available online 1 April 2025
0378-7796/© 2025 Elsevier B.V. All rights are reserved, including those for text and data mining, AI training, and similar technologies.

Nomenclature

PD	Partial discharge
PDIV	Partial discharge inception voltage
n	Number of pulses
FEM	Finite element method
E_s	Surface discharge inception field
$PDIV_{th}$	Theoretical *PDIV*
E_i	Internal discharge inception field
E_{pmax}	Maximum tangential field
k_s	Scaling factor
V_s	Applied voltage
HFCT	High frequency current transformer
CC	Coupling capacitor
Q_a	Apparent charge
n	number of pulses

(Q_a) and number of pulses (n) are the major PD characteristics to study the aging and lifetime studies of an insulation [11,12].

Nomex films are widely preferred as electrical insulation due to their exceptional thermal stability, mechanical strength, and dielectric properties. Nomex paper claims to offer an increased endurance to electrical and environmental stresses [13] making them ideal for use in transformers, motors, generators, cables, and aerospace applications. Literature shows that the research on electrical aging of Nomex paper induced by PD is scarce. Some available articles focus on investigation of aging behavior under thermal stress or Nomex immersed in liquid nitrogen and under boiling conditions [14–16]. These researchers utilized frequency domain spectroscopy, measurement of degree of polymerization and dissipation factor measurement as testing methods. A detailed aging study is performed in [17] that uses dielectric spectroscopy. While surface discharges can be considered as a major cause of insulation degradation, *PDIV* of surface PD is studies for Nomex considering its application for transformers [18]. A recent on Nomex paper presents the impact of PD under high-frequency stresses on oil-impregnated Nomex paper, by analyzing surface morphology, molecular bond degradation, and damage mechanisms [19].

This work focuses on PD behavior at *PDIV* in terms of surface discharge initiated at the surface of the film and gradual transition of PD activity from surface discharge based on three leg approach [8]. During the aging caused by surface discharge, the PD activity starts to transform into internal discharge that is more harmful to an insulation, leading to a possible breakdown. Three-leg approach is an effective way for characterizing insulation behavior, designing, lifetime estimation of insulation system [8,10,20]. The first two legs consist of FEM-based simulation and modeling used for the estimation of theoretical PD inception voltage ($PDIV_{th}$) through field profiles and parameters acquired from simulation and surface discharge model. Considering third leg, the $PDIV_{th}$ is validated with *PDIV* measured experimentally.

The electrodes' profile used in this study is custom designed in such a way that surface discharge is initiated at a voltage that is lower than that of internal discharge, allowing the insulation to age under surface discharge activity. The electrode configuration is simulated in COMSOL environment. Electrical field profiles are calculated through a simulation model. Later these profile and surface discharge model is used to calculate $PDIV_{th}$ of Nomex films. The surface PD based aging/erosion was carried out at higher voltage for accelerated aging of Nomex films at three voltage levels, i.e., above inception voltage level i.e., 2PDIV, 2.5PDIV, and 2.7PDIV. The highest applied voltage level is kept below the flashover/breakdown voltage level which was found as 3 kV during breakdown test under designed electrode configuration. By analyzing the onset and progression of PD, this research aims to reveal how these discharges contribute to the degradation of insulation materials over time.

Considering the organization of this paper, Section 1 presents the first leg, which describes behavior of normal and tangential electric fields at triple point. It also describes model geometry, boundary conditions, implementation of optimized meshing, and simulation model. Section 2 presents second leg where surface discharge models and tangential field profiles are used to estimate surface discharge inception field (E_s) and theoretical $PDIV_{th}$. Section 3 presents third leg describing experimental analysis that validates three-leg approach thereby validating $PDIV_{th}$ with measured *PDIV*. It also describes measurement methodology adopted for surface erosion based experimental investigation. Methodology includes data acquisition in form of PRPD pattern and PD characteristics. Section V presents results obtained from the experimental investigation. In this section behavior of PRPD patterns Apparent charge (Q_a) and number of pulses (n) are analyzed at elevated voltages. Section 4 presents Discussion and Section 5 presents conclusion.

2. COMSOL based simulation model – 1st leg

Electrode design plays a key role in surface erosion based accelerated aging tests. Fig. 1 shows electrode configuration used in this study where the Nomex film is positioned between electrodes.

A 2D axisymmetric simulation model is developed that demonstrates the spatial arrangement of electrical field profiles on solid insulation. Electrical field profiles computed using the electrostatics (es) module in the AC/DC branch. Fig. 2 depicts the methodology utilized to compute electrical field profiles. The study consists of five stages.

2.1. Geometry

Fig. 3 shows geometrical model of electrode configuration used in this study, which consists of two electrodes, a cylindrical high voltage electrode and a circular/disk type ground electrode. High voltage electrode has a diameter of 6 mm and a corner contour of 1 mm, while the ground electrode has a diameter of 51.5 mm.

Nomex specimen of square shape (5 × 5) cm with a thickness of 0.13 mm is positioned between two electrodes such that the surface of the electrodes is in good contact with it (without a substantial airgap). A 2D axisymmetric model offers an alternative way to simplify 3D model into a 2D geometric representation. There are three main advantages of utilizing this modelling approach:

- It provides advantage of enhanced computational efficiency compared to 3D models.

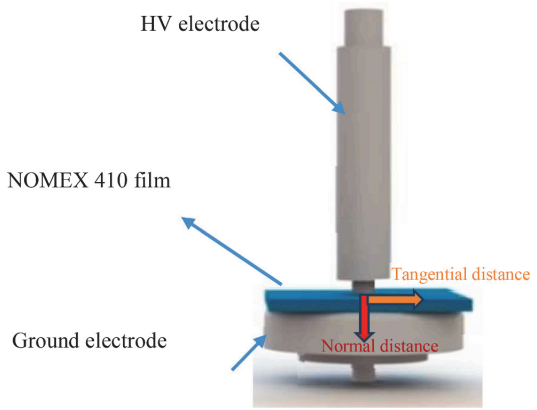

Fig. 1. Two-electrode configuration with Nomex film insulation.

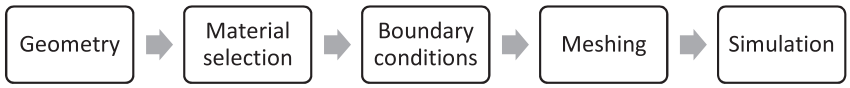

Fig. 2. Methodology adopted for FEM-based study.

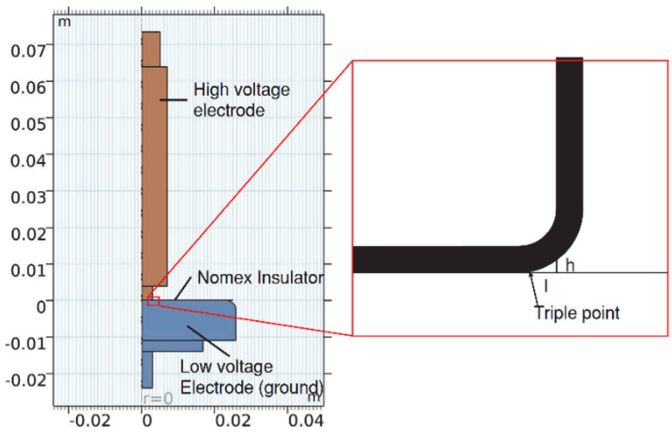

Fig. 3. Geometrical model designed for calculation of normal and tangential electric field profiles on Nomex film.

- It helps in determining behavior of electrical field at contour closely as shown in Fig. 3.
- It facilitates the implementation of boundary conditions and accelerates the process of creating meshes.

2.2. Material selection

Nomex has a vast application in electrical equipment due to its high dielectric strength, exceptional mechanical toughness, and excellent thermal stability. Nomex 410 film 0.13 mm thickness bear AC dielectric strength of 28 kV/mm and full wave impulse strength 55 kV/mm, is used in this study. Further information regarding material is given in [21].

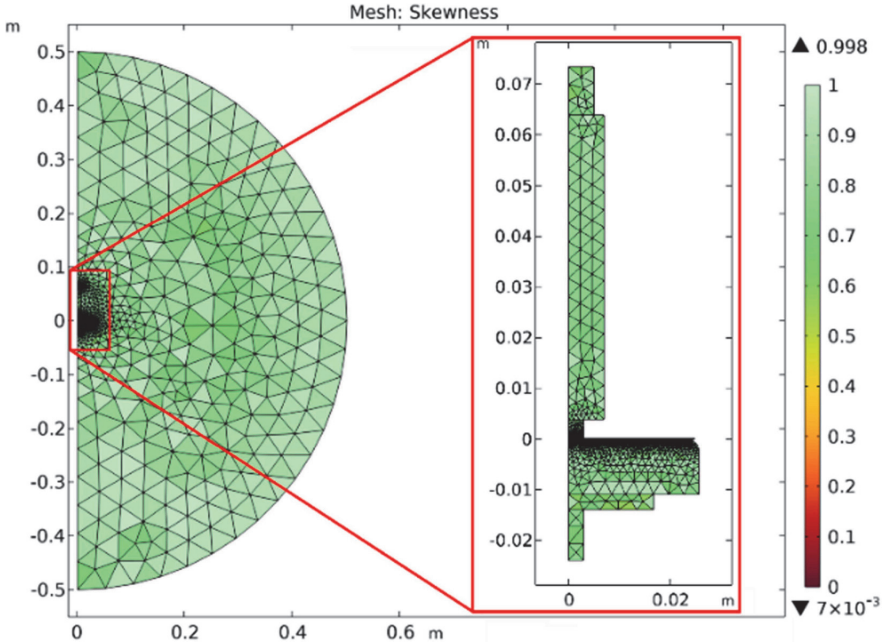

Fig. 4. Dirichlet boundary conditions and meshing implemented for calculation of normal and tangential electric field profiles at triple point.

2.3. Boundary condition

Boundary conditions are set to observe behavior of electric field at desired locations and scenarios. Dirichlet boundary conditions are implemented in this study as they have wide application in mechanics, heat transfer, fluid dynamics, and electrostatics. They offer two major advantages. Firstly, input parameters or boundary conditions are constant throughout the solution. In this study, the potentials on the high voltage and ground electrodes are kept constant throughout the solution.

Secondly, these are very useful in mapping experimental investigation to FEM solution since they can be controlled initially. Therefore, solution can be obtained under various scenarios. In this study, behavior of tangential and normal fields is observed under various voltage levels between *PDIV* to 3PDIV, i.e., from *PDIV* to breakdown voltage (found during breakdown test under designed electrode configuration).

2.4. Meshing

Mesh size and quality are two major characteristics of FEM based study. Fig. 4 shows meshing performed in COMSOL environment. Entire geometry has been meshed using triangular mesh components as they bear effective surface approximation and adequately describe complex shapes. Electrodes and air surrounding these are meshed with a predefined, coarser mesh as it utilizes less computational time. The specimen is set with maximum mesh element size limit of 9.74 μm and a minimum size limit of 0.195 μm. Mesh size is set such that it can adequately cover the triple point and contour. Model has 179,806 degrees of freedom for resolution. This choice was made considering the balance between computational efficiency and precision of solution.

2.5. Simulation study

Simulation study describes behavior of required parameters under set boundary conditions by solving partial differential equations. In this study, electric field strength and potential calculations were performed at different AC voltage levels between 1 and 3 kV. Fig. 5 shows FEM based 2D simulation model of electrodes (including the contour profile of HV electrode) and illustrates the distribution electrical field (scaled with respect to maximum value) at 3 kV throughout the geometry. Two distinct electric fields were observed based on simulated electrode geometry as shown in Fig. 5. Firstly, along the horizontal direction, called tangential electric field on the surface of the specimen (along *l*) as shown by red arrow and field distribution shown by red/orange color and second in vertical direction along (*h*) called normal field distribution shown by yellow color in Fig. 5. Space between electrode contour at the corner and insulation surface creates an air cavity. Based on its phenomenological and physical characteristics it is considered as gas or internal discharge [20,22]. Figs. 6 and 7 show tangential and normal field profiles at different voltage levels along *l* and along *h* respectively. Three points were concluded from these profiles.

- Tangential field is increasing exponentially from zero to maximum near the triple point whereas the normal field is maximum at triple point. An exponential decrease in both fields is observed as the distance from the triple point is increased along *l and h*. Whereas the normal field is maximum at the triple point at point O. Both fields decrease exponentially as the distance from the triple point increases as shown in Figs. 6 and 7.
- It is important to note both tangential and normal fields reduce to significantly smaller values (which can be considered as zero) after a certain distance. A constant reduction is observed. Tangential field reduces to approximately zero after ≈ 0.75 mm and the normal field reaches to zero after ≈ 0.22 mm. A constant reduction is observed.
- Although the magnitude of the normal field is larger than the tangential field but the as the surface *PDIV* is lower than that of the internal *PDIV*, therefore the degradation of specimen will be caused by the surface PD (derived from the tangential field), leading to the surface erosion of the specimen. Tangential field induces extrinsic aging processes and hot spots, leading to localized breakdown due to thermal instability. These factors can further accelerate aging and as progressive dielectric material degradation continues to occur, this finally leads to premature breakdown. This degradation is primarily driven by high-energy electron bombardment from PD pulses—microscale discharges that occur on the insulation surface [7].

3. Estimation of partial discharge inception voltage (PDIV) – 2nd leg

Partial discharge inception voltage is an important parameter that describes the level of degradation and behavior of PD activity in insulation. According to IEC 60270:2000, *PDIV* is lowest voltage at which

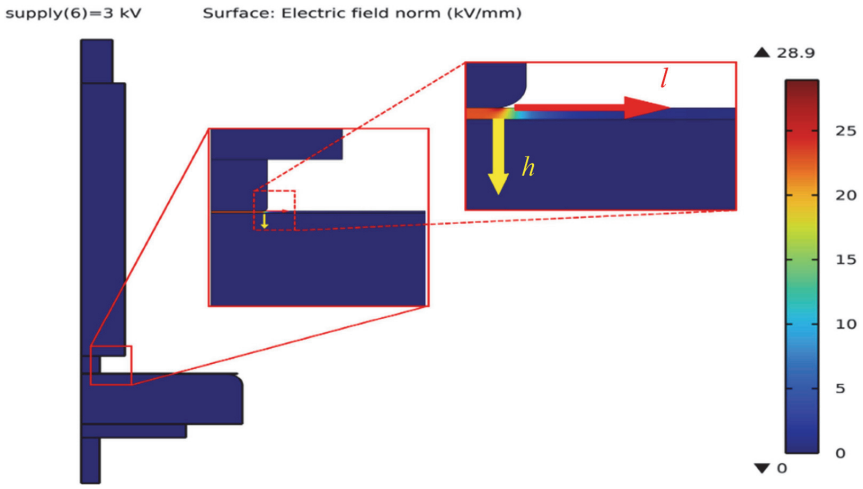

Fig. 5. FEM based 2D simulation model with red area showing distribution of tangential electric field along *l* and yellow area showing distribution of normal electric field along *h*.

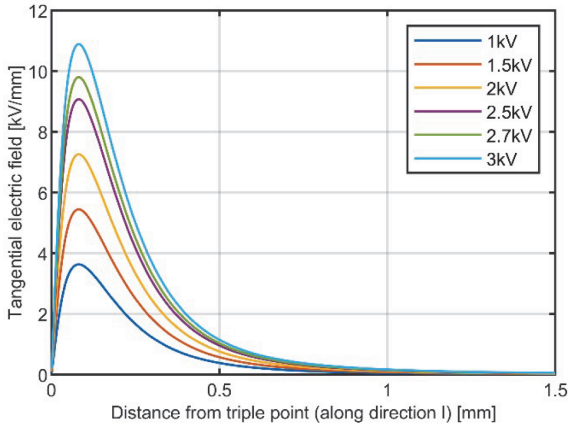

Fig. 6. Tangential field profiles at different voltage levels along l obtained from simulated model.

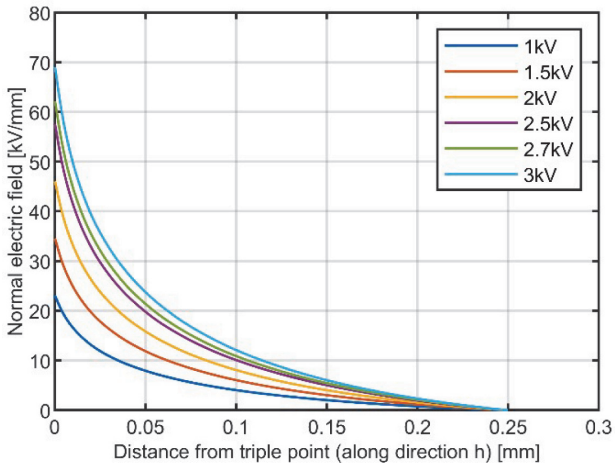

Fig. 7. Normal field profiles at different voltage levels along h obtained from simulated model.

repetitive partial discharges are first detected. *PDIV* is caused due to inception electric field (E_s). In [22] E_s is described using (1) called surface discharge model. It is modified form of the Niemeyer equation [23], which describes PD inception field surface discharge. While gas discharge (E_i) i.e., internal discharges in an air-filled cavity can be determined from the expression modified as (3). $PDIV_{th}$ is calculated using (4).

$$E_s = 8p\left[1+\frac{4.3}{\sqrt{pk_s l}}\right] \tag{1}$$

$$k_s \sim \left[\frac{l_2(0.95E_{max})^{+} - l_1(0.95E_{max})^{-}}{l}\right] \tag{2}$$

$$E_g = 25.2p\left[1+\frac{8.6}{\sqrt{ph}}\right] \tag{3}$$

$$\frac{V_S}{E_{Ps}} = \frac{PDIV_{th}}{E_{sinc}} \tag{4}$$

Where p is air pressure its value is 101.325 kPa, E_{max} is the maximum/peak value of tangential electric field calculated from field gradient profile of electric field, which is found as 3.6 kV/mm, l_1 and l_2 are the points where the tangential field attains a value of $0.95E_{max}$ obtained from a tangential field profile as shown in Fig. 8.

The rationale behind this assumption ($E = 0.95$ Emax) lies in the fact that, if a PD event occurs, it will most likely happen in the region close to the maximum field. Therefore, a rectangle is drawn at 0.95 E_{max} on tangential field profile. Intersecting points are considered for calculation for scaling factor (k_s) [22], l is the creepage distance or tangential distance from the triple point along the surface of the specimen, h is the height of the cavity for internal discharge in terms of normal distance from the triple point. k_s is the field-dependent factor calculated from the tangential field profile.

Normal field is not discussed here further since tangential field is responsible for the surface discharge, E_s is calculated using (1). Table 1 shows values of parameters. By matching this simulated tangential electric field profile with surface PD-inception field calculated from PD-inception model (1) is E_s is found as 3.3 kV/mm and estimated $PDIV_{th}$ is 0.96 kV.

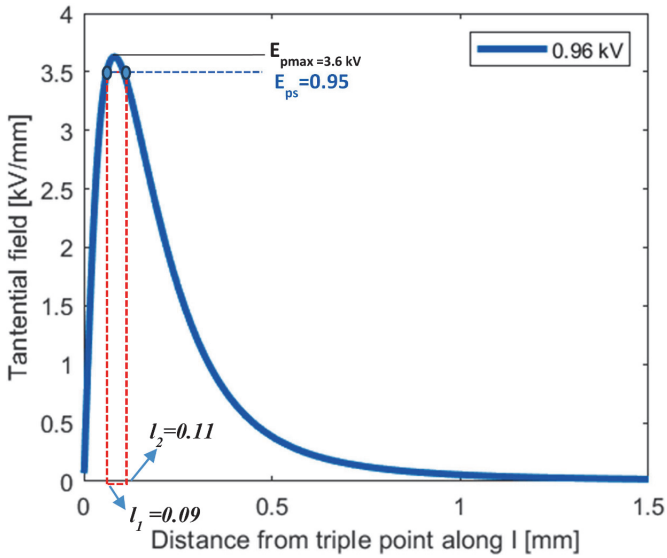

Fig. 8. Tangential field profile at 0.96 kV and points l_1 and l_2 are the distances when Ep= 0.95Emax corresponding field marked by blue circles [20].

Table 1
Parameter values for estimation of inception field E_s and theoretical $PDIV_{th}$.

Parameter	Value
V_s	1 kV
E_{ps}	3.3 kV/mm
K_s	0.0004
l	50 mm

4. Experimental setup and measurment methodolgy- 3rd leg

Validation of the simulation model is necessary for completion this three-leg approach. In this study $PDIV_{th}$ is validated through measured *PDIV*. For this experimental setup is designed in the laboratory. Fig. 9(a) shows schematic diagram and Fig. 9(b) shows two-electrode configuration with triple point. Following are the major components.

- A voltage regulator that controls AC voltage is attached to a test transformer with a 150 kV rating.
- A two-electrode arrangement in which the ground electrode is composed of aluminum and the high voltage electrode is made of copper. charge calibrator for commercial PD measuring system calibration.
- A 1 nF capacitance capacitor with a 36 kV voltage rating used as a PD sensor to measure discharges. It has two electrode configurations, and a supply linked in parallel.
- An HFCT sensor with a transfer ratio of 1:10 linked to CC via a ground wire. The sampling rate is 1 GS/s.
- A digital oscilloscope for recording PD pulses, which emerge in durations of 20 ms or one AC cycle.
- Quadrupoles and a commercial PD measurement equipment for recording PD traits and PRPD patterns.

Measuremnt methodology includes data acquisition, recording of PRPD patterns, extraction of PD characters. Initially, calibration is performed to calibrate the conventional PD measurement system using a PD calibrator. In order to ensure that the experimental setup is PD free, the voltage was applied to the PD test setup without the insulation test specimen up to 5 kV, and no PD activity was observed.

In the next stage, Nomex film was placed in between electrodes. Voltage increased from zero in steps of 0.1 kV, until PD activity was initiated. Repeated measurements were performed on nine samples due to stochastic nature of PD. Average *PDIV* found as 1 kV. which matches the $PDIV_{th}$ estimated in the second legs. Considering the PRPD shown in

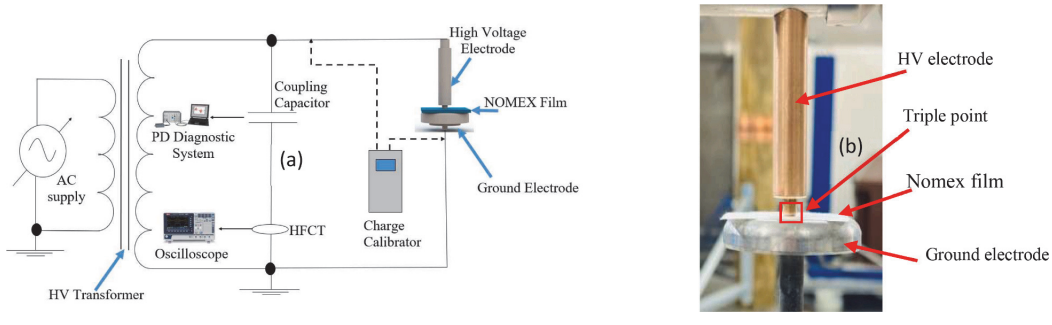

Fig. 9. Experimental setup a) Schematic layout of laboratory-based experiment setup b) Two-electrode.

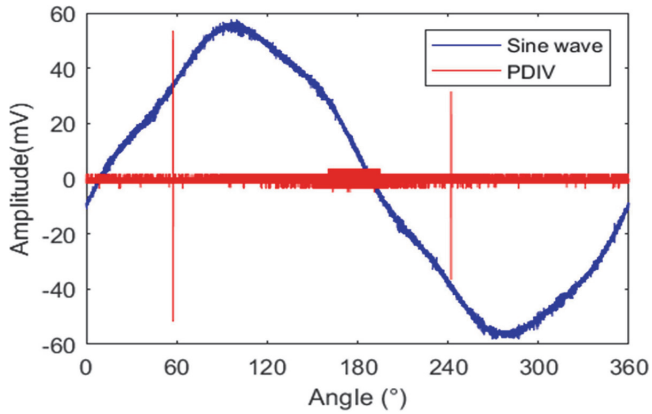

Fig. 10. Measured PD signal at partial discharge inception voltage (*PDIV*) using HFCT.

Fig. 10, it can be seen that captured PD activity presents surface discharges, which further validates the type of PD activity provided by the first leg using simulation study.

After finding *PDIV* additional measurements are conducted to observe PD behavior at elevating voltages. Usually aging under PD activity can be a time-consuming process, accelerated aging, can provide an estimate of the aging behavior of the specimens, which is obtained by applying multiples of *PDIV* as:

- 2PDIV ≈ 2 kV
- 2.5PDIV≈ 2.5 kV
- 2.7PDIV ≈ 2.7 kV

Each test was performed on a new (unaged) specimen under a constant voltage level for 3 h (180 min). PD data in terms of PRPD were acquired using a conventional PD measurement system and oscilloscope.

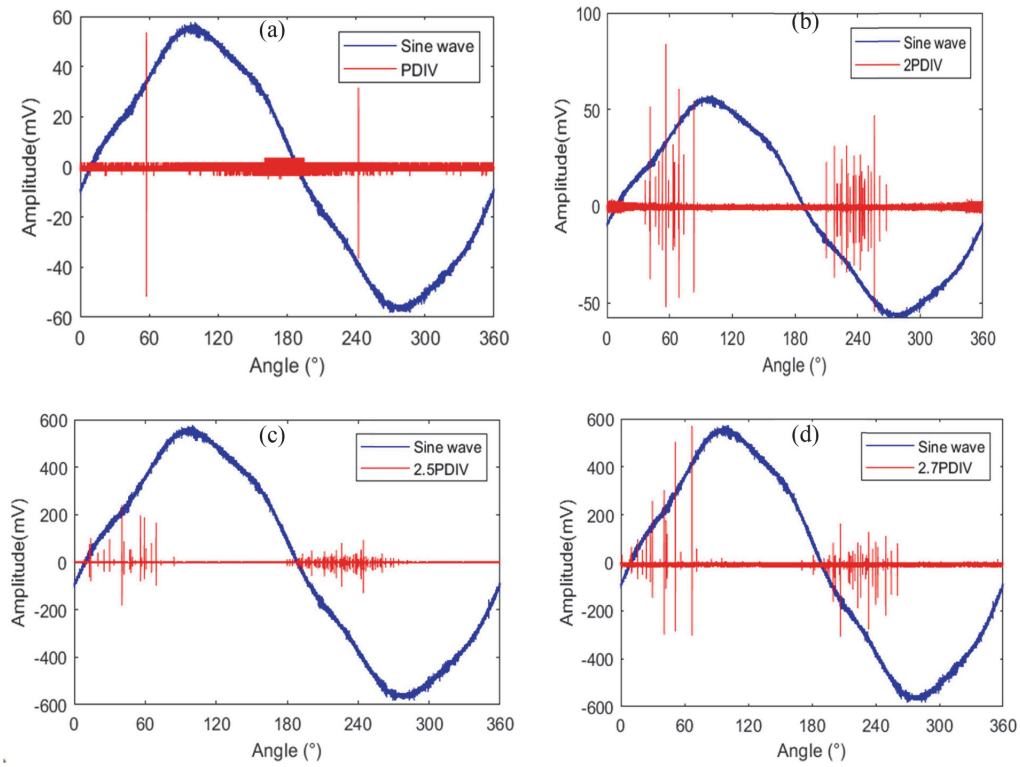

Fig. 11. PRPD patterns at different voltage levels obtained after aging of 180 min (a) *PDIV*, (b) 2PDIV, (c) 2.5 PDIV, (d) 2.7 PDIV.

5. Results

5.1. Analysis of PRPD pattern

While it is known that surface discharge activity tends to remain within 0–90°, during the experimental study it is observed that PD activity is dominantly surface when it tends to be away from 0°, or in other words, more concentrated towards 90°. However, as the PD activity starts to spread between 0–90°, it is more likely the combination of internal and surface discharge activity [24]. A detailed investigation is performed in [25,26], where automated software separates, identifies and detects the type of PD using the PD current pulse. Automated tools show two types of discharges, surface and internal were found for a given electrode configuration.

- There is a proportional increase of pulse amplitude with applied electrical stress. At *PDIV*, the maximum pulse amplitude is 50 mV, at 2PDIV it is 83 mV, at 2PDIV it is 241 mV and at 2.7PDIV it is found as 600 mV.
- At increasing electrical stress, the phase span of PD activity increases. This increase in activity span is observed in both the negative and positive half-cycles of the applied voltage.
- Considering the behavior of the number of pulses, there is a proportional increase in the number of pulses with applied electrical stress. However, the number of pulses decreased at 2.7PDIV which is near breakdown voltage as shown in Fig. 11(d). this reduction in pulses can be due to increased conductivity caused by surface tracking.
- Considering pulse amplitude, pulses in the negative half-cycle have a lower peak value than the positive half-cycle of the applied voltage in all stress levels, which shows an unsymmetric pattern likely a surface discharge activity on insulation.

Fig. 12 shows polar plot illustrating the behavior of PD pulse amplitude and corresponding phase of occurrence. These peaks are extracted using novel peak detection algorithm [27]. Approximately 800 pulses were considered in this investigation. Considering peak amplitude of pulses at different voltage levels. It can be seen in Fig. 12 amplitude of pulses increases with the increasing in voltage. Initially at 2 PDIV pulse amplitude range was under 300 mV which is increased to 400 mV on 2.5 PDIV and 600 mV on 2.7 PDIV. Considering number of pulses, the polar plot Fig. 12 the number of pulses increased with applied voltage from PDIV to 2.5 PDIV. However, a reduction of positive and negative pulses observed at 2.7 PDIV. Various studies [7,28,29] have reported different observations. It can be speculated that as the insulation ages under PD activity, localized dielectric degradation leads to erosion and the formation of carbonized conductive paths, which reduce the PD pulse repetition rate at 2.7 PDIV.

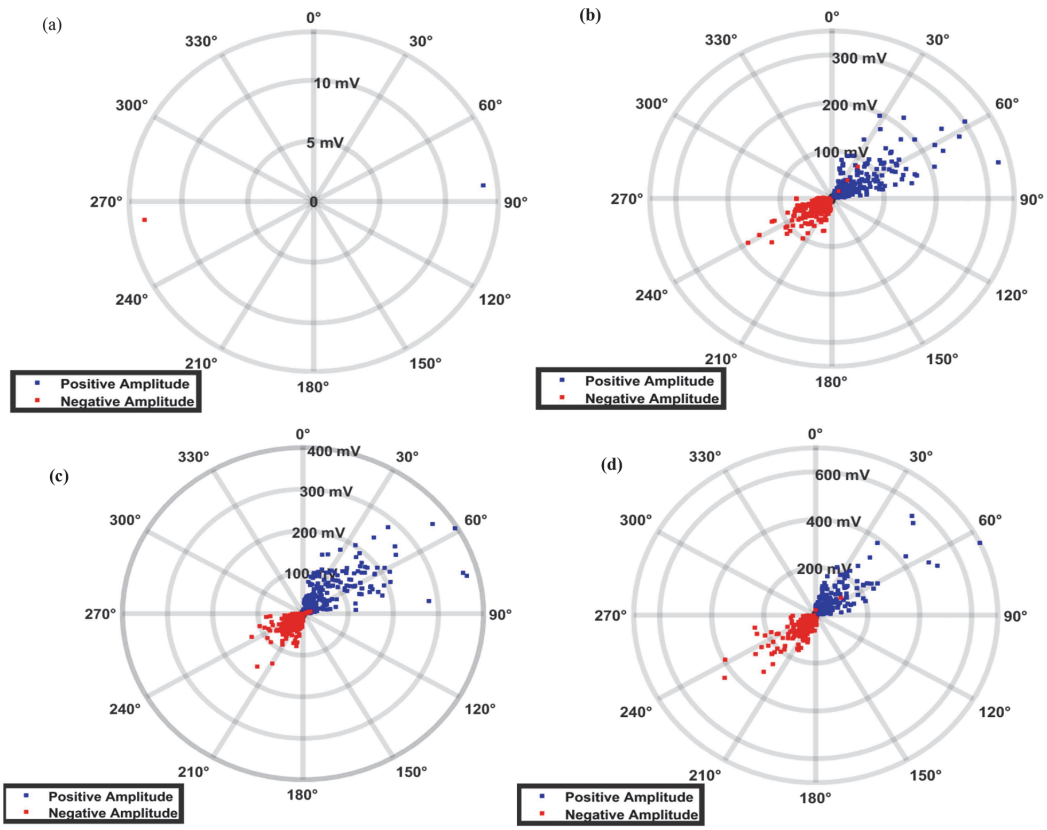

Fig. 12. Polar plots illustrating the behavior of peak pulse amplitude and phase of occurrence at different voltage levels after aging of 180 min (a) PDIV, (b) 2PDIV, (c) 2.5 PDIV, (d) 2.7 PDIV.

5.2. Behavior of accumulated apparent charge (Q_a) and number of pulses (n)

Accumulated apparent charge (Q_a) and number of pulses (n) or pulse repetition rate are two major characteristics that effectively describe behavior of PDs within insulation [11,12]. IEC 60,270 describes Q_a as the amount of charge if injected into test circuit which gives the same magnitude as PD current pulse. In this study it is measured in an acquisition time of 60 s at each voltage level. At *PDIV*. Q_a is found between range of 0.9–1 nC during three measurements. Fig. 13(a) shows Q_a follows upward trend at elevated voltages. Fig. 13 (b and c) shows behavior of positive and negative pulses respectively. Considering number of pulses *PDIV* until 2.5PDIV, an upward trend is observed as the number of pulses are increasing during both the negative and positive half cycles of the applied voltage as shown in Fig. 13(b and c). However, near breakdown voltage i.e., at 2.7PDIV, the number of pulses start decreasing which is also visible in Fig. 11(d). This shows that number of pulses or pulse repetition rate decreases near breakdown voltage. Based on the experimental investigation, it is observed that immediately after increasing the applied voltage, PD activity increases, either in terms of PD amplitude, PD repetition rate, or both, depending on the type of PD defect, i.e., surface PD, internal PD, or a combination of both. Regarding the behavior of PD activity after a certain period of aging, various studies [28,29] have reported different observations. In some cases, PD amplitude increases with aging, while in others decreases, as observed in [28]. Also, it varies at different aging stages (initial, middle, or final), often accompanied by a decrease in the PD repetition rate [28]. Most studies, including the present work, indicate a general trend where PD pulse repetition rate decreases. As also mentioned in [29], this may be attributed to changes in surface and bulk conductivity. It can be speculated that as the insulation ages under PD activity, localized dielectric degradation leads to erosion and the formation of carbonized conductive paths, which reduce the PD pulse repetition rate.

6. Discussion

This article is based on a three-leg approach implemented on flat film type specimens, Nomex 410 films of thickness 0.13 mm. Two-electrode configuration is used where Nomex films are sandwiched between electrodes. In the first leg, FEM model is developed. An electrostatic solver was implemented to investigate the behavior of normal and tangential fields at different voltage levels and along the distances away from the triple point. Study shows that there are two discharges that mainly occur under designed electrode configuration. Surface discharge due to tangential component of electric field and internal discharge due to normal field component. Virgin specimen used in this study means a health insulation under electrical stress. In a healthy insulation system, the surface discharge inception voltage is typically lower than the internal discharge inception voltage. This is because surface discharge requires a lower electric field to initiate PD because the breakdown strength of air is much lower than that of solid insulation. Therefore, in this study the electrode configuration is developed such that surface discharge occurs at a voltage lower than internal discharges. Therefore, the degradation specimen will be caused by the surface PD (derived from the tangential field), leading to the surface erosion of the specimen. In the second leg $PDIV_{th}$ is estimated using a surface discharge model and tangential field profile obtained via FEM simulation. $PDIV_{th}$ is validated with measured *PDIV* using the experimental study which is called the third leg.

Analysis of PRPD shows as the voltage level increases PD activity is more visible near zero crossing of the applied voltage. The same trend is observed with the increase in aging time. This is an increase in phase span PD activity is also observed with increasing voltage level. Analysis of apparent accumulated charge (Q_a) shows an increasing trend with applied stress; however, both number of pulses (n) including positive and negative pulses decrease near the breakdown voltage at 2.7PDIV. It can be speculated that as the insulation ages under PD activity, localized dielectric degradation leads to erosion and the formation of carbonized conductive paths, which reduce the PD pulse repetition rate at 2.7 PDIV.

7. Conclusions

This article demonstrates how three leg approach can be affectively implemented by simulating electrical field profiles and estimating inception fields that cause inception of PD on insulation surface. This approach is useful particularly for electrical assets where surface discharge is a major risk for its insulation system and affects reliability of the asset. First and second leg can be utilized for estimation of inception fields and *PDIV* of various insulating materials. These parameters are very crucial for material characterization and PD free design of insulation systems. The variation of apparent charge and pulse count with applied voltage indicates that, at elevated voltages, the charge amplitude exhibits an upward trend. However, under surface discharge conditions on Nomex paper, the PD pulse repetition rate decreases before breakdown. This study provides valuable insights into the trending attributes of PD characteristics over time, aiding in the assessment of aging and lifetime degradation.

The three-leg approach provides a predictive tool set for estimating partial discharge (PD) inception without extensive experimental studies, making insulation design more efficient and cost-effective. By considering key parameters such as thickness, relative permittivity, and electrode-insulation geometry, it enables systematic optimization. It also highlights the influence of electrode type on PD behavior, aiding in refining electrode-insulation interface design to minimize field intensification.

Considering application of three-leg approach in a wide variety of applications, while the three-leg approach provides valuable insights into the study of surface and internal PD for the design of solid

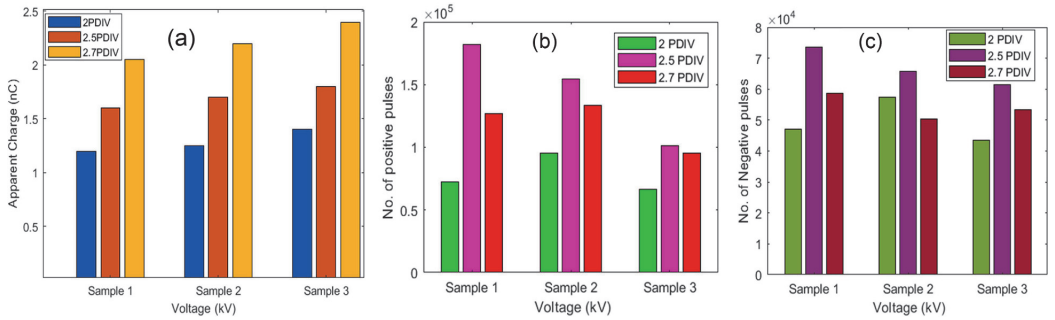

Fig. 13. Behavior of PD characteristics a) Accumulated apparent charge b) Positive pulses c) Negative pulses.

insulation, particularly in the form of films and flat surfaces, its application to liquid and gaseous insulation needs to be investigated. Although atmospheric pressure has been considered in the three-leg approach, inception of PD also depends on the environmental conditions such as humidity and temperature. The possible impact of these factors on the estimation of PDIV using three leg approach needs to be investigated.

CRediT authorship contribution statement

Maninder Choudhary: Writing – review & editing, Writing – original draft, Resources, Methodology, Investigation, Formal analysis, Data curation, Conceptualization. **Muhammad Shafiq:** Writing – review & editing, Supervision, Conceptualization. **Abhinav Bhattarai:** Writing – review & editing, Methodology, Formal analysis. **Ivar Kiitam:** Writing – review & editing, Supervision, Conceptualization. **Paul Taklaja:** Writing – review & editing. **Ivo Palu:** Writing – review & editing, Supervision, Resources, Funding acquisition, Conceptualization.

Declaration of competing interest

The authors declare that they have no known competing financial interests or personal relationships that could have appeared to influence the work reported in this paper.

Data availability

Data will be made available on request.

References

[1] B. Daguse, H. Gressinger, T. Lebey, R. Acheen, S. Ayat, Comparison between modelling and measurements of PDIV on electrical machines for aeronautics, in: ICD 2022 - IEEE 2022 4th International Conference on Dielectrics, Proceedings, IEEE Inc., 2022, pp. 230–233, https://doi.org/10.1109/ICD53806.2022.9863481.

[2] M. Wen, J. Song, Y. Song, Y. Liu, C. Li, P. Wang, Reliability assessment of insulation system for dry type transformers, in: IEEE Transactions on Dielectrics and Electrical Insulation, 20, 2013, pp. 1998–2008, https://doi.org/10.1109/TDEI.2013.6678847. December.

[3] H. Suzuki, T. Takahashi, T. Okamoto, S. Akita, Y. Ozawa, Electrical insulation characteristics of cold dielectric high temperature superconducting cable, IEEE Transact. Dielectr. Electr. Insulat. 9 (6) (2002) 952–957, https://doi.org/10.1109/TDEI.2002.1115489. December.

[4] S. Zhang, et al., Investigation on the partial discharge of the cavity in Nomex insulation for mining dry type transformer, in: 2018 12th International Conference on the Properties and Applications of Dielectric Materials (ICPADM), Xi'an, China, 2018, pp. 525–529, https://doi.org/10.1109/ICPADM.2018.8401044.

[5] M. Yazdani-Asrami, A. Sadeghi, S. Seyyedbarzegar, W. Song, Role of insulation materials and cryogenic coolants on fault performance of MW-scale fault-tolerant current-limiting superconducting transformers, IEEE Transact. Appl. Superconduct. 33 (1) (2023) 5500215, https://doi.org/10.1109/TASC.2022.3217967.

[6] M. Choudhary, M. Shafiq, I. Kiitam, A. Hussain, I. Palu, P. Taklaja, A review of aging models for electrical insulation in power cables, Energ. (Basel) 15 (9) (2022) 3408, https://doi.org/10.3390/en15093408.

[7] G.C. Montanari, M. Shafiq, M.S.B. Myneni, M. Lizcano, T.S. Williams, Electrical characterization of boron nitride-filled insulation for aerospace and avionics applications, Energies 17 (2024) 3016.

[8] G.C. Montanari, M. Shafiq, R. Mcginnis, Coming challenges in electrified transportation and impact on electrical insulation reliability: ships and aircrafts, in: 10th Annual International Conference on Technology & Engineering as part of the Annual Academic Meetings of the Sciences Division and the Engineering Division of ATINER Program, 2023.

[9] A. Cavallini, D. Fabiani, G.C. Montanari, Power electronics and electrical insulation systems - part 2: life modeling for insulation design, IEEE Electr. Insulat. Magaz. 26 (4) (2010) 33–39, https://doi.org/10.1109/MEI.2010.5511187.

[10] D. Nath, Q. Yang, G.C. Montanari, W. Yin, K. Younsi, Modelling and characterization of surface discharges in insulating material for spacer: electrode shape, discharge mode and revision of the creepage concept, Mater. (Basel) 9 (2022) 989.

[11] E. Kantar, K.K. Eie-Klusmeier, T.A. Ve, M.-H. Ese and S. Hvidsten, "Electrical aging of fluoropolymer cable insulation materials induced by partial discharge," in IEEE Transact. Dielectr. Electr. Insulat., 10.1109/TDEI.2024.3402663.

[12] W. Hassan, M. Shafiq, G.A. Hussain, M. Choudhary, I. Palu, Investigating the progression of insulation degradation in power cable based on partial discharge measurements, Electr. Power Syst. Res. 221 (2023).

[13] Nomex® Paper Protects Critical Components in Electronic Applications, Dupont. https://www.dupont.co.uk/electrical-insulation/electronics.html.

[14] S. Mishra, A. Baral, D. Mishra, S. Chakravorti, A novel method to predict severity of thermal aging and degree of polymerization for reliable diagnosis of dry-type insulation, IEEE Transact. Dielectr. Electr. Insulat. 29 (2) (2022) 631–640, https://doi.org/10.1109/TDEI.2022.3157922.

[15] R. Liao, C. Guo, K. Wang, L. Yang, S. Grzybowski, H. Sun, Investigation on thermal aging characteristics of vegetable oil-paper insulation with flowing dry air, IEEE Transact. Dielectr. Electr. Insulat. 20 (5) (2013) 1649–1658, https://doi.org/10.1109/TDEI.2013.6633695.

[16] Z. Jin, A. Lapthorn, M. Staines, The dielectric strength of nomex 410 paper in liquid nitrogen under boiling situations, IEEE Transact. Appl. Superconduct. 27 (7) (2017) 5500710, https://doi.org/10.1109/TASC.2017.2732282.

[17] S. Maity, et al., Sensing the aging state of nomex-based nanocomposite insulation by dielectric spectroscopy, IEEE Sens. J. 24 (22) (2024) 37586–37594, https://doi.org/10.1109/JSEN.2024.3472281.

[18] Hubert Moranda, et al., Comparative tests of partial discharges in Nomex® 910 paper and cellulose paper, Energies 13 (3) (2020) 647.

[19] X. Li, et al., Surface degradation of oil-immersed nomex paper caused by partial discharge of high-frequency voltage, J. Electron. Mater. 52 (2) (2023) 1094–1103.

[20] G.C. Montanari, S. Schwartz, R. Cuzner, On the characterization of partial-discharge endurance of dielectric materials for aerospace applications, IEEE Trans. Aerosp. Electron. Syst. 59 (6) (2023) 7590–7599.

[21] Dupont, "Nomex 410 Technical Data Sheet" [Online].Available: https://www.dupont.com.

[22] P. Cambarieri, G. C.Montanari, Derivation of a surface discharge model for the design of the surface components of insulation systems used in industrial electronics environments, IEEE J. Emerg. Sel. Top. Ind. Electron. 4 (2) (2023) 698–706.

[23] L. Niemeyer, A generalized approach to partial discharge modeling, IEEE Trans. Dielectr. Elect. Insul. 2 (4) (1995) 510–528.

[24] H. Illias, T.S. Yuan, A.H.A. Bakar, H. Mokhlis, G. Chen, P.L. Lewin, Partial discharge patterns in high voltage insulation, in: 2012 IEEE International Conference on Power and Energy (PECon), Kota Kinabalu, Malaysia, 2012, pp. 750–755, https://doi.org/10.1109/PECon.2012.6450316.

[25] P. Seri, R. Ghosh, G.C. Montanari, An unsupervised approach to partial discharge monitoring in rotating machines: detection to diagnosis with reduced need of expert support, IEEE Transact. Energy Convers. 36 (3) (2021) 2485–2492, https://doi.org/10.1109/TEC.2021.3050324.

[26] G.C. Montanari, M. Shafiq, S.B. Myneni, Insulation defect modelling and partial discharge typology identification: a robust and automatic approach, Appl. Sci. 14 (15) (2024) 6715, https://doi.org/10.3390/app14156715.

[27] M. Choudhary, I. Palu, I. Kiitam, M. Shafiq, P. Taklaja, A. Bhattarai, Denoising and extraction of partial discharge pulse characteristics using wavelet denoising and local maxima method, in: 2024 IEEE International Conference on Power and Energy (PECon), Kuala Lumpur, Malaysia, 2024, pp. 221–225, https://doi.org/10.1109/PECon62060.2024.10827085.

[28] M. Niasar, N. Taylor, P. Janus, X. Wang, H. Edin, R. Kiiza, Partial discharges in a cavity embedded in oil-impregnated paper: effect of electrical and thermal aging, IEEE Trans. Dielectr. Electr. Insul. 22 (2) (2015) 1071–1079.

[29] H.V.P. Nguyen, B.T. Phung, T. Blackburn, Effects of aging on partial discharge patterns in voids under very low frequency excitation, in: In 2016 IEEE International Conference on Dielectrics (ICD), July 1, 2016, pp. 524–527.

Publication VIII

M. Choudhary, I. Kiitam, I. Palu, “Electrical Aging and Lifetime Study of Nomex Insulation Influenced by Partial Discharges”, Electric Power Systems Research, Volume 249, 2025, doi: https://doi.org/10.1016/j.epsr.2025.112000.

Electric Power Systems Research 249 (2025) 112000

Contents lists available at ScienceDirect

Electric Power Systems Research

journal homepage: www.elsevier.com/locate/epsr

Electrical aging and lifetime study of nomex insulation influenced by partial discharges

Maninder Choudhary *, Ivar Kiitam, Ivo Palu

Department of Electrical Power Engineering & Mechatronics, Tallinn University of Technology, Tallinn, Estonia

ARTICLE INFO

Keywords:
Surface erosion
Partial discharges
Nomex insulation
Lifetime
PRPD pattern
PD characteristics
Microscope analysis

ABSTRACT

Surface erosion-based accelerated aging testing has emerged as an efficient alternative to traditional accelerated life testing methods, as it requires significantly short time for insulation assessment throughout its lifetime i.e., from partial discharge (PD) inception to breakdown. It is an efficient method for evaluating assets where surface discharge critically impacts the reliability and cause insulation failure particularly in cryogenic applications. PD is a key factor in insulation degradation and its inception marks the onset of extrinsic aging. This study presents a comprehensive investigation carried out on 0.13 mm thick nomex insulation film which is widely used in transformer layered insulation and electrical machine insulation. Surface erosion based accelerated aging tests were conducted on square shape nomex specimen by applying twice of partial discharge inception voltage (PDIV) from PD inception until breakdown. Comprehensive PD measurements were taken at an interval of 15 min. Phase resolved partial discharge (PRPD) patterns, apparent charge (Q_a), number of pulses (n) were recorded via an IEC 60270 complaint PD measurement system. The aging process is categorized into four distinct stages, identified through PRPD patterns, PD characteristics and microscopic observations. Results demonstrate correlation between PRPD patterns, microscope observation, and the progression of Q_{max} and n over the lifetime. The proposed methodology offers a practical and efficient approach for lifetime estimation of solid insulating materials in electrical assets.

1. Introduction

Solid insulation is an integral part of power system assets including transformers, wind turbines, cables, generators, and electric vehicles. Modern materials, including nomex offer suitable dielectric properties under high frequencies and temperatures and have vast application in cryogenic environments [1,2].

Aging is an inevitable factor that causes life reduction and affects the reliability of assets. Aging mechanism in polymers under electrical stress entails physical and chemical mechanisms activated by high intensity discharges, which cause erosion on the material surface. Prolonged erosion generates micro voids or conducting paths within the material matrix which results in reduction in the dielectric strength of material and eventually leads to premature failure of insulation [3,4]. Thus, the durability of insulating materials under impact of partial discharges (PD) is a significant challenge for insulation system designers and asset operators [5,6]. Surface discharges are major concern for insulation in high-voltage transformers, and aerospace appliances. Nomex film of 0.13 mm thickness is widely used in transformers, both dry and oil-immersed as interlayer insulation as it provides a balance between mechanical strength and electrical performance. In electrical machines, it is used as slot liners, phase insulation interturn insulation due to lightweight and thermal endurance capability [7]. Surface erosion based accelerated ageing lifetime tests mimic the degradation effects of partial discharges in the real world, allowing for quicker and more precise lifetime evaluations. To ensure reliability in critical electrical assets, these tests are useful for selection, design and development of preventive maintenance strategies [8].

Several researches related to aging and lifetime study of nomex insulation are available in the literature. These researches are broadly fragmented. In [9] nomex and cellulose paper are compared in terms of partial discharge inception voltage (PDIV). It was found that nomex paper withstands higher PDIV than cellulose. However, the work does not consider the impact of long-term erosion or degradation stages. In [10] PDIV is observed at rising temperatures and under repetitive square shape pulse voltages. It was found that with increasing temperature PDIV and lifetime of nomex paper decreases. Also, it was found that high frequency pulse width modulation (PWM) voltages cause fast decay of nomex insulation under the influence of PD. However, this study is

* Corresponding author.
E-mail address: maninder.choudhary@taltech.ee (M. Choudhary).

https://doi.org/10.1016/j.epsr.2025.112000
Received 28 April 2025; Received in revised form 16 June 2025; Accepted 3 July 2025
Available online 11 July 2025
0378-7796/© 2025 Elsevier B.V. All rights are reserved, including those for text and data mining, AI training, and similar technologies.

Nomenclature

PD	Partial discharge
PDIV	Partial discharge inception voltage
Q_a	Apparent charge
n	Number of pulses
CC	Coupling capacitor
HV	High voltage
Q_{max}	Maximum apparent charge
PWM	Pulse width modulation
FTIR	Fourier transform infrared spectroscopy
SEM	Scanning electron microscopy
XRD	X-ray diffraction
EDS	Energy dispersive spectrometry

limited to the impact of thermal stress and square shape voltage on PDIV under short-term endurance tests. In [11] PD behavior is investigated in a cavity modelled in nomex insulation used in mining dry-type transformer; the results show behavior of PRPD patterns and PD characteristics at different voltage levels. Key findings show that with increasing voltage, the phase distribution widens, and the pulse amplitude and, number of pulses are increased. In [12] PD based lifetime study of nomex film (oil-paper insulation) is performed under needle to plane electrode configuration. Results show that PDIV and breakdown voltage of nomex paper decreases under superposed Inter-harmonic AC voltage in comparison to pure AC voltage. Also, it is observed that maximum charge (Q_{max}), discharge current and discharge power have consistent behavior till 115 min of aging of nomex film and, after that a sharp rise is observed. Considering the number of pulses (n), it is observed that n rises initially but after 90 minutes itstarts decreasing. In [13] polyimide films, polyester films and nomex films are compared in terms of PDIV and endurance capabilities during lifetime. The results show that polyimide and polyester bear better PD resisting capability than nomex paper under medium frequency square voltage. In [14] reliability assessment of nomex paper is performed by extracting quality parameters from three different tests including degree of polymerization, partial discharge measurement. The results show that quality parameters can be used for condition monitoring of insulation in dry type transformer. In [15] PD surface degradation of oil immersed nomex film is analyzed under high frequencies. It utilizes different techniques including PD measurement, fourier transform infrared spectroscopy (FTIR), scanning electron microscopy (SEM), X-ray diffraction (XRD), and energy dispersive spectrometry (EDS). The result shows that high frequency voltage causes more degradation of nomex film than AC voltage. In [16] surface discharge characteristics of nomex and Cellulose board are investigated under different voltage levels using PRPD patterns and PD characteristics. In addition to above researches, different testing methods are used to investigation of aging behavior under thermal stress, including nomex immersed in liquid nitrogen and under boiling conditions [16–19]. These researchers utilized frequency domain spectroscopy, measurement of degree of polymerization and dissipation factor measurement as testing methods. A detailed aging study is performed in [20] that uses dielectric spectroscopy.

Consequently, none of the above provides a continuous surface-erosion-based ageing map that couples PRPD evolution, quantitative PD measurements and microscopic evidence from inception to breakdown. Mapping the aging of nomex film with four-stage degradation concept under 2 x PDIV AC voltage, the present work closes that gap and generates diagnostic markers linking nomex insulation behavior under the impact of surface discharges, so providing a practical framework for insulation designers and asset managers.

Electrode configuration plays a key role in production of surface erosion [21,22]. Although the research in [12] provides a comprehensives study of behavior of PD under pure AC and under superposed inter-harmonic AC voltage during lifetime of nomex insulation. However, the study utilized needle to plane configuration. Under this configuration three types of discharges can be incepted: Corona discharge, frequently produced as a result of the extremely uneven electric field close to the needle tip characterised by a strong localised discharge with high electric stress caused by the gas surrounding the needle tip becoming ionised. Secondary Surface discharge occurs at the tip of the needle positioned on insulation surface. Under some circumstances, the localised electric field may result in surface discharges by causing charge movement along the insulation surface. Internal discharge near the triple point, the place near triple point may act an air cavity therefore internal PD may induce. In proposed research electrode configuration is designed in such a way that it only produces surface discharges on insulation surface. Fig. 1(b) shows two electrode configuration used in this study. Based on the physical geometry of electrodes two types of discharges can be incepted, surface discharge under the plane surface of HV electrode and internal discharge near the contours as it creates an air cavity near triple point. However, since surface PDIV is lower than the internal PDIV, only surface erosion occurs on insulation surface thereby producing surface discharges, which will further lead to surface tracking, treeing and finally breakdown [8,21,22]. Studies showed that PRPD patterns and PD characteristics played a cardinal role in lifetime study of XLPE (Cross-linked Polyethylene) and fluoropolymer cable insulations [23–25]. Using a similar approach this article focuses on aging/lifetime study of nomex 410 paper film under impact of AC voltage.

A comprehensive investigation is carried out in this article. The PD measurement test setup is designed in the laboratory, where a two-electrode configuration (high voltage and ground electrode) is used. square shape nomex films of 0.13 mm thickness and an area of 25cm^2 are sandwiched between electrodes, thereby creating a triple point. Initially, pre-tests were conducted to observe the PDIV and breakdown voltage of nomex specimens. Later, accelerated electrical stress twice the inception voltage is applied. The choice of 2 × PDIV is made to is to carry out accelerated aging to speed up the degradation process caused by the PD activity, allowing researchers to observe insulation aging and failure mechanisms within a shorter time. By applying a voltage higher than the normal operating level (often a suitable multiple of PD inception voltage, PDIV and well below its breakdown voltage), PD occurs more frequently and with higher energy, which accelerates chemical and physical degradation (such as erosion, treeing, or pitting) in the insulation material in short time. This helps estimate insulation lifespan, understand failure modes, and compare the durability of different materials or designs. Continuous surface erosion is performed for 480 min until it breaks down. PRPD patterns, apparent charge (Q_a) and number of pulses (n) were recorded via a commercial PD measurement system. A four-stage degradation is observed from inception to breakdown, which is recorded through PD measurement and microscopic analysis. Trending attributes of PRPD patterns, PD characteristics and microscopic investigations are analyzed at different stages of lifetime. Considering the novelty of proposed work, the following are the major points.

- **Comprehensive lifetime assessment of nomex film under the impact of PD:** In contrast to previous works that mainly concentrate on PDIV behavior or lifetime studies under high frequency, inter-harmonics, this study offers a full-cycle degradation analysis of 0.13 mm nomex film, from partial discharge inception to electrical breakdown under AC voltage. Real-time measurements show the gradual progression of partial discharge (PD) activity, starting as purely surface discharges, then transitioning into a mix of surface and internal discharges, and finally evolving into entirely internal PD in the final stages before breakdown. This provides valuable insight into the complete aging process of insulation.
- **Surface Erosion based accelerated aging:** This innovative approach to surface erosion-based accelerated lifetime testing was

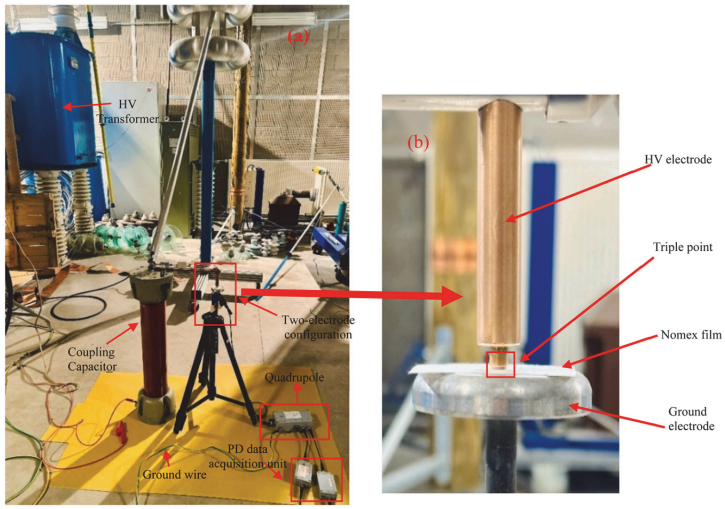

Fig. 1. (a) Laboratory based experimental setup and (b) Electrode configuration used for the surface erosion of nomex film [19].

used to target environments where surface discharges predominate, especially in compact insulation systems and aerospace applications.

- **Four stage aging characterization via PRPD patterns and microscopic investigation:** Using correlated PRPD patterns, PD characteristics (Q_m, n), and surface morphology, the ageing process is separated into distinct stages. This is a novel framework that has not been documented before.
- **Design of Electrode configuration for production of surface erosion:** In contrast to conventional needle-plane configurations that produce a variety of discharge types, the experimental setup employs a specially created flat electrode geometry intended to produce surface discharges [8–22]. This creates a realistic electrode configuration for surface discharge dominance.
- **Framework for aging and lifetime studies of solid insulating materials:** By facilitating consistent data collection across ageing stages, the suggested methodology establishes the groundwork for future integration of AI models for real-time insulation health prediction for various solid insulating materials.

2. Experimental setup and measurement methodology

2.1. Experiment setup

Fig. 1(a) depicts a laboratory-based experiment setup, and Fig. 1(b) shows two-electrode configuration. Details of major components are mentioned as follows:

- A Test transformer of 150 kV rating is connected to a voltage regulator.
- A two-electrode configuration where high voltage (HV) electrode is made of brass while the ground electrode is made of aluminum. Upper electrode as HV electrode has a flat surface and diameter of 6 mm with a contour (radius of curvature) of 0.25 mm at the corners. Ground electrode has a flat surface and diameter of 51.5 mm.
- A Charge calibrator for calibration of commercial PD measurement system.
- A Capacitor of capacitance 1 nF and 36 kV voltage rating connected in series with PD sensor for measurement of discharges and in parallel with the two-electrode configuration and high voltage AC supply as shown in Fig. 1(a).
- A Commercial PD measurement system and quadrupole for capturing PRPD patterns and PD characteristics as shown in Fig. 1(a).

2.2. Measurement methodology

Prior to lifetime PD measurements, pre-tests were performed on different specimens. Partial discharge inception voltage (PDIV) and breakdown voltage are measured, since the aging behaviour of insulating materials relies on the PDIV and breakdown voltage. PDIV is defined as the minimum voltage at which PD activity is initiated, and breakdown voltage is the voltage at which insulation fails [25]. To ensure a free PD setup, a test voltage of 5 kV is applied without test specimen and no PD activity was found. In the next stage voltage is increased in steps with a step size of 0.1 kV, until consistent PD signals are observed in the commercial PD system and the oscilloscope. PDIV of nine identical specimens was measured under the same test conditions and electrode setup. The mean PDIV was then calculated (as 0.9 kV) and validated using the three-leg approach [22], where FEM based model and surface discharge model are used to estimate PDIV.

After determining PDIV, the applied voltage is increased to 2 × PDIV, and lifetime PD data are recorded via PRPD patterns and PD characteristics at every fifteen minutes of aging until breakdown. At each measurement, PRPD pattern, Q_a and n were recorded over an acquisition time of 60 s and the pulse dead time set as 20 μs. Subsequently microscopic investigations are performed at each stage of degradation.

3. Results

3.1. Pre-test results

Fig. 2 shows pre-tests result of 9 specimens. Mean PDIV is found to be 0.9 kV and mean breakdown voltage is observed as 3.1 kV. After obtaining PDIV a continuous electrical stress of 2 × PDIV is applied for lifetime studies.

3.2. Four stage aging of nomex film under partial discharges

Aging of nomex insulation film is divided into four stages as initiation of surface conductivity or inception of PD, localized surface erosion, surface tracking and material pitting and finally breakdown. The concept of four stages of aging is readapted from [4]. Fig. 3 shows

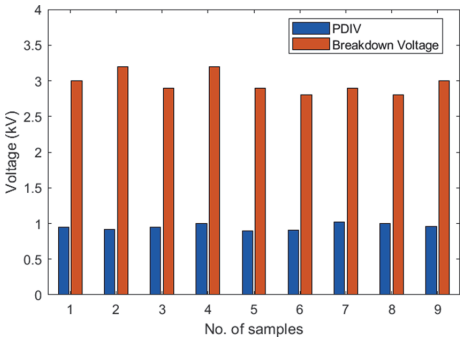

Fig. 2. PDIV and breakdown voltage of nine specimens.

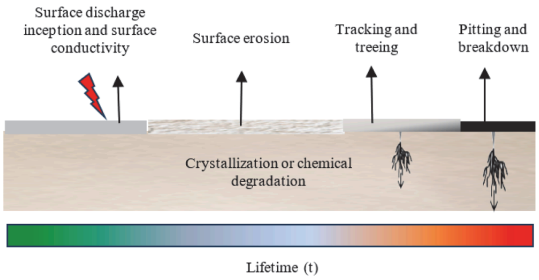

Fig. 3. Four stages of degradation of nomex film adapted from [4].

various stages of degradation aging induced by PD. Both the fundamental elements and the distinctive contributions of our study are revealed by a thorough comparison with Temmen's work.

Temmen examined how increases in surface conductivity, roughness, and crystal growth drive progressive changes in the phase-angle resolved PD patterns caused by PD activity in flat cavities, which mimic delamination-induced defects. However, it was mainly limited to artificial cavity structures and did not incorporate the lifetime of insulation from inception to breakdown, even though it offered significant theoretical insights into how these surface changes modulate the phase-angle histograms. This study, on the other hand, directly connects the evolution of PRPD patterns to specific ageing stages and lifetime to breakdown by applying similar phase-resolved PD measurement principles to a real-world insulation material, nomex 0.13 mm films under continuous AC voltage stress. Furthermore, by combining direct microscopic confirmation of material degradation with quantitative lifetime data (apparent charge and pulse counts), this work goes beyond indirect surface change inference. Our study provides a more comprehensive picture of asset reliability in actual high-voltage applications by bridging the gap between basic surface degradation behaviour and its direct impact on insulation lifetime.

3.2.1. *Surface discharge inception and surface conductivity*

Surface discharge inception is the point at which electrical discharges start occurring along the surface of an insulating material when the applied voltage exceeds a critical level. Analysis of PRPD patterns in Fig. 4. PRPD patterns and (Q_a and n) values collected from three specimens. PRPD patterns exhibits consistent patterns across all samples. The general pattern in the four ageing stages was strong, despite minor fluctuations in charge magnitude brought on by inherent variations in sample surfaces. Initially, an intense PD activity is observed at PDIV as shown in Fig 4(a).

However, after one hour PD activity has decreased significantly as the apparent charge reduced from nC to pC, which can be the result of an increase in surface conductivity. Air and dissociation products interact with the dielectric surface and together they increase surface conductivity. As PD activity continues, oxygen is regenerated faster than it is consumed sustaining high conductivity [4,26,27]. Asymmetric PRPD patterns were observed at this stage, with Q_a values between 30 pC and 40 pC observed. Considering phase span PD activity is mainly observed between 50°−70° in the positive half cycle and 200°−230° in the negative half cycle of the applied voltage. This activity lasted for two hours after PD inception as shown in Fig. 4(b, c). Fig. 5 (a, b) shows physical sample and microscopic view of nomex film with small black dots indicating discharge inception.

3.2.2. *Surface erosion*

In the second stage, the PD activity propagated along the insulation surface. Increased oxidation process leads to chemical degradation and formation of a crystal structure which makes the surface rough. As aging increases several byproducts of oxygen i.e., CO_2 and CO are formed which results in cross-linking, chain scission and electrical and thermal degradation of insulation thereby altering the chemical structure of insulation and producing surface erosion [3,28]. Considering PRPD patterns, three major changes are observed. A symmetrical PD activity is observed with intense activity observed in the positive half cycle of the applied voltage, depicted by orange and yellow color. An increase in PD magnitude as discharges in the range 78–167 pC is observed. Also, the phase span of PD activity slightly increased with an increasing number of discharges observed between 20°−60° in the positive half cycle of applied voltage and 190°−270° in the negative half cycle of applied voltage. This activity also lasted for two hours as shown in Fig. 4 (d, e). From microscopic investigation it is found that the discharges occur slightly within the material indicating traces of surface tracking as shown in Fig. 5(c, d).

3.2.3. *Tracking and treeing*

The Third stage is tracking stage, long run repetitive discharges cause surface tracking and carbonized paths within the insulation. Continuous field enhancement at surface particularly crystal locations results in initiation of tree growth [26,29]. Considering PRPD patterns, a symmetrical pattern like internal PD is observed with severe discharges of magnitude 92–382 pC are observed at this stage. PD severity is increased as pulse repetition rate is increased illustrated by yellow and orange colors in PRPD patterns. Considering phase span, repetitive PD activity is observed between 0–90° in positive half cycle and 180°−270° in the negative half cycle of the applied voltage. At this stage PD activity is more tend towards the zero crossing of the applied voltage. This can be an indication of surface tracking. Tracking lasted for two hours illustrated by PRPD patterns in Fig. 4(f, g) and microscopic investigation which shows carbonized channels within the insulation films, as shown in Fig. 5 (e, f).

3.2.4. *Pitting & breakdown*

Continuous erosion and discharges form pitting on the insulation surface which is visible in the form of dark spots on insulation surface as shown in Fig. 5(g). Continual growth in trees and pitting ultimately causes breakdown of insulation [29]. Considering the PRPD patterns, an intense PD activity with charges ranging from 360 pC to1.8 nC were observed between 0–90° in the positive half cycle of the applied voltage and 180°−270° in the negative half cycle of the applied voltage as shown in Fig. 4 (g, h). Microscopic investigation found dark spots within the thickness of material as shown in Fig. 5(h). After seven hours of aging PD activity became more intense in both positive and negative half cycles of the applied voltage. At this stage dark pitting is observed on the insulation surface as shown in Fig. 5(g). After approximately 50 min of pitting breakdown occurred. Fig. 4(i) shows PRPD pattern prior to breakdown.

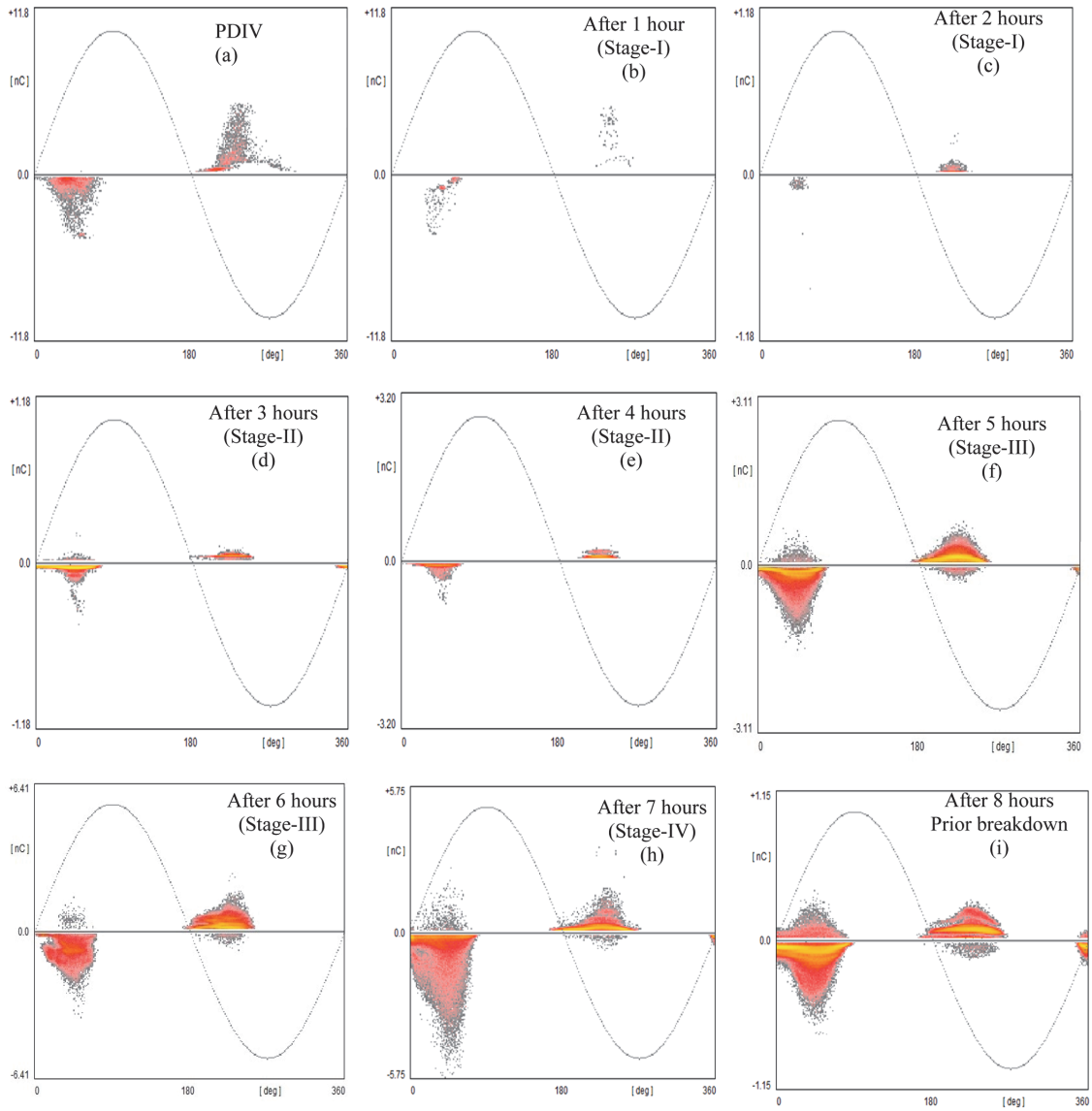

Fig. 4. PRPD patterns illustrating four stages of aging a) Inception b) Surface erosion c) tracking and treeing d) pitting and breakdown.

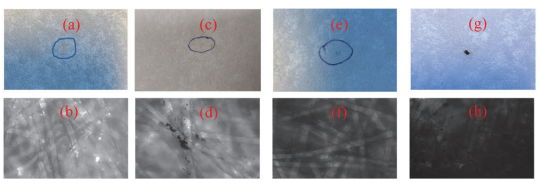

Fig. 5. Nomex film specimen at different stages from partial discharge inception to breakdown: Close-up view of physical sample (top row) and microscopic view (bottom row). a and b) Surface discharge inception, c and d) Surface erosion, e and f) tracking and treeing, g and h) Pitting and breakdown.

3.3. Behavior of apparent charge (Q_m) and number of pulses (n) during lifetime of nomex insulation film

Apparent charge and number of pulses are two major characteristics that define severity of PD activity within the insulation. According to IEC 60,270 apparent charge is defined as the charge of pulse if injected at terminals of test object gives same reading at measuring equipment [25]. Q_a is collected after every fifteen minutes of aging till breakdown from 3 samples. Fig. 6 shows behavior of maximum apparent charge (Q_{max}) obtained via lifetime testing on three samples.

The trendline of Q_{max} shows that after PDIV initially, when the insulation surface exposed to high electric field, PD activity low amplitude (40–125 pC) is observed. This activity lasted for two hours. After two hours Q_{max} followed an undulating trend until seven hours,

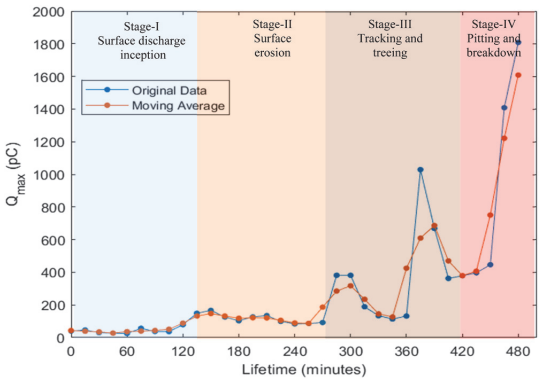

Fig. 6. Behavior of apparent charge at different stages and lifetime of nomex insulation film.

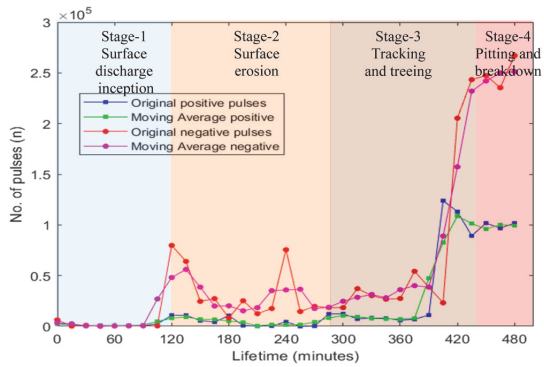

Fig. 7. Behavior of number of pulses (positive and negative) at different stages and lifetime of nomex insulation film.

fluctuating between 84–382 pC. However, after seven hours an intense PD activity of Q_{max} 1.8 nC is observed. There were a few charge spikes at 300 min and 390 min. The tracking causes discharges of high amplitude since carbonized channels are formed creating localized breakdown paths [3].

Fig. 7 shows the behavior of positive and negative pulses during the lifetime of nomex film. Trendlines of positive and negative pulses show that the positive pulses have a gradual increase over lifetime and are relatively stable compared to negative pulses. Considering negative pulses initially, very low number of discharges was observed for 2 h. After two hours an undulating trend is observed till 6 h. However, there is a significant increase is observed in both positive and negative pulses after 6 h of aging at third stage.

Initially, both negative and positive pulses have a low occurrence. At the second stage, there is notable growth in negative pulses and a gradual increase in positive pulses. At the third stage, initially there is a relative decrease in negative pulses compared to the previous stage. However, there is an increase in positive pulses. Prior breakdown there is a high rise in negative pulses. At this stage, dark black pitting is observed on insulation surface that caused breakdown after fifty minutes.

4. Conclusion

This article is based on the lifetime study of nomex film. A prolonged surface erosion accelerated aging test is performed on nomex film. PD data were recorded during the lifetime of nomex film i.e., from PD inception to breakdown. Considering the physics of degradation, a four-stage degradation is observed which is recorded in the form of PRPD patterns, PD characteristics (apparent charge and number of pulses) and microscope-based investigation. The behavior of PRPD patterns shows that initially, an asymmetrical PD activity is observed. After three hours at second stage, PD activity gets more symmetrical as PRPD patterns similar to internal PD are observed. After 5h at third stage PD activity start moving towards zero crossing of the applied voltage, thereby tracking into the insulation. After seven hours at the fourth stage PD activity became more severe as high-density discharges were observed in both negative and positive half cycle of the applied voltage. This four-stage degradation of PRPD patterns is validated through microscope-based investigation from discharge inception till pitting. Behavior of PD characteristics show taht shows that initially a minor surface discharge activity is observed reflected by stable behavior of Q_{max} *and n* showing minor chemical changes and erosion on material surface. At mid-life region PD activity shows an undulating trend as Q_{max} oscillates between 80–380pC. PD activity surges at stage IV as Q_{max} increased to 1.8 nC. A similar pattern is observed in *n,* low at stage I, an undulating increase in mid-life region and sharp rise of pulses at stage IV. This framework can be useful for real-time condition monitoring of insulation system particularly for assets where surface discharge is major risk. PRPD patterns and the evolution of Q_a and *n.* can be used as prognostic indicators for insulation health in real-world applications, such as online PD monitoring (e.g., through machine learning or data-driven models).

CRediT authorship contribution statement

Maninder Choudhary: Writing – review & editing, Writing – original draft, Visualization, Resources, Methodology, Investigation, Formal analysis, Data curation. **Ivar Kiitam:** Writing – review & editing, Supervision, Resources, Conceptualization. **Ivo Palu:** Writing – review & editing, Supervision, Resources, Funding acquisition.

Declaration of competing interest

There are no conflicts of interest.

Data availability

Data will be made available on request.

References

[1] Z. Wang, F.F. da Silva, H. Sørensen, Q. Wang, C.L. Bak, The interactions analysis for high frequency transformers insulation under multi-stress of high voltage, high frequency, and high temperature, in: 2023 IEEE 2nd International Power Electronics and Application Symposium (PEAS), Guangzhou, China, 2023, pp. 734–738, https://doi.org/10.1109/PEAS58692.2023.10395853.

[2] B. Dagusé, H. Gressinger, T. Lebey, R. Acheen, S. Ayat, Comparison between modelling and measurements of PDIV on electrical machines for aeronautics, in: 2022 IEEE 4th International Conference on Dielectrics (ICD), Palermo, Italy, 2022, pp. 230–233, https://doi.org/10.1109/ICD53806.2022.9863481.

[3] L.A. Dissado, J.C. Fothergill, Electrical degradation and breakdown in polymers, IET (1992).

[4] K. Temmen, Evaluation of surface changes in flat cavities due to ageing by means of phase-angle resolved partial discharge measurement, J. Phys. D Appl. Phys. 33 (6) (Mar. 2000) 603–608, https://doi.org/10.1088/0022-3727/33/6/303 [Online]. Available.

[5] M. Lizcano, T.S. Williams, E.S.E. Shin, D. Santiago, and B. Nguyen, "Aerospace environmental challenges for electrical insulation and recent developments for electrified aircraft," Nov. 01, 2022, *MDPI*. doi: 10.3390/ma15228121.

[6] T. Lebey, A. Rumi, A. Cavallini, Challenges for electrical insulation systems in high voltage aviation applications, IEEE Electr. Insul. Mag 38 (6) (2022) 5–11, https://doi.org/10.1109/MEI.2022.9916178. November/December.

[7] Nomex® 400 series features proven performer—Nomex® 410", [Online]. Available: https://www.dupont.com/products/nomex-400-series.html.

[8] G.C. Montanari, D. Nath, P. Cambareri, A new approach to the design of surface subsystems of polymeric insulators for HV and MV apparatus under AC voltage, High Volt 8 (2023) 651–658.

[9] H. Moranda, H. Moscicka-Grzesiak, P. Przybylek, K. Walczak, R. Szewczyk, Comparative tests of partial discharges in Nomex® 910 paper and cellulose paper, Energies 13 (2020) 647, https://doi.org/10.3390/en13030647.
[10] C. Zheng, Q. Wang, H. Wang, Z. Shen, F.F. Da Silva, C.L. Bak, Partial discharge inception and deterioration of Nomex paper under repetitive square wave voltage, in: 2022 IEEE International Conference on High Voltage Engineering and Applications (ICHVE), Chongqing, China, 2022, pp. 1–4, https://doi.org/10.1109/ICHVE53725.2022.9961729.
[11] S. Zhang, et al., Investigation on the partial discharge of the cavity in Nomex insulation for mining dry type transformer, in: 2018 12th International Conference on the Properties and Applications of Dielectric Materials (ICPADM), Xi'an, China, 2018, pp. 525–529, https://doi.org/10.1109/ICPADM.2018.8401044.
[12] X. Li, et al., Partial discharge characteristics of oil-paper insulation for on-board traction transformers under superposed inter-harmonic AC voltages, IEEE Trans. Electr. Insul. 27 (1) (2020) 240–248, https://doi.org/10.1109/TDEI.2019.008404. Feb.
[13] C. Zheng, Q. Wang, H. Wang, Z. Shen, F.F. Da Silva, C.L. Bak, Comparative PDIV and endurance studies on different insulating materials used for medium frequency transformers, in: 2022 IEEE International Conference on High Voltage Engineering and Applications (ICHVE), Chongqing, China, 2022, pp. 1–4, https://doi.org/10.1109/ICHVE53725.2022.9961619.
[14] M. Wen, J. Song, Y. Song, Y. Liu, C. Li, P. Wang, Reliability assessment of insulation system for dry type transformers, IEEE Trans. Electr. Insul. 20 (6) (2013) 1998–2008, https://doi.org/10.1109/TDEI.2013.6678847. December.
[15] X. Li, W. Zhang, H. Wang, X. Ma, H. Zhang, K. Li, T. Qin, K. Liu, Y. Yang, G. Wu, Surface degradation of oil-immersed Nomex paper caused by partial discharge of high-frequency voltage, in: Journal of Electronic Materials, vol.52, Springer, 2023, https://doi.org/10.1007/s11664-022-10044-8 pages 1094-1103.
[16] C. Thirumurugan, G.B. Kumbhar, R. Oruganti, Surface discharge characteristics of different solid–Liquid insulation materials in power transformers, IEEE Trans. Plasma Sci. 47 (11) (Nov. 2019) 5013–5022, https://doi.org/10.1109/TPS.2019.2943550.
[17] S. Mishra, A. Baral, D. Mishra, S. Chakravorti, A novel method to predict severity of thermal aging and degree of polymerization for reliable diagnosis of dry-type insulation, IEEE Trans. Electr. Insul. 29 (2) (April 2022) 631–640, https://doi.org/10.1109/TDEI.2022.3157922.
[18] R. Liao, C. Guo, K. Wang, L. Yang, S. Grzybowski, H. Sun, Investigation on thermal aging characteristics of vegetable oil-paper insulation with flowing dry air, IEEE Trans. Electr. Insul. 20 (5) (Oct. 2013) 1649–1658, https://doi.org/10.1109/TDEI.2013.6633695.
[19] Z. Jin, A. Lapthorn, M. Staines, The dielectric strength of Nomex 410 paper in liquid nitrogen under boiling situations, IEEE Trans. Appl. Supercond. 27 (7) (Oct. 2017) 1–10, https://doi.org/10.1109/TASC.2017.2732282. Art no. 5500710.
[20] S. Maity, et al., Sensing the aging State of nomex-based nanocomposite insulation by dielectric spectroscopy, IEEE Sens. J. 24 (22) (2024) 37586–37594, https://doi.org/10.1109/JSEN.2024.3472281, 15 Nov.15.
[21] G.C. Montanari, S. Schwartz, R. Cuzner, On the characterization of partial-discharge endurance of dielectric materials for aerospace applications, IEEE Trans. Aerosp. Electron. Syst. 59 (6) (2023) 7590–7599, https://doi.org/10.1109/TAES.2023.3293455. Dec.
[22] M. Choudhary, M. Shafiq, A. Bhattarai, I. Kiitam, I.Palu P.Taklaja, A comprehensive study of partial discharge based extrinsic aging in nomex insulation films: modeling, simulation and measurement, Electr. Power Syst. Res. 245 (2025) 111663.
[23] C. Hudon, R. Bartnikas, M. Wertheimer, Surface conductivity of epoxy specimens subjected to partial discharges, IEEE Int. Symp. Electr. Insul. (1990) 153–155. JuniSSN: 1089-084X.
[24] E. Kantar, K.K. Eie-Klusmeier, T.A. Ve, M.-H. Ese and S. Hvidsten, "Electrical aging of fluoropolymer cable insulation materials induced by partial discharge," in IEEE Trans. Electr. Insul., doi: 10.1109/TDEI.2024.3402663.
[25] IEC, IEC 60270: high-voltage test techniques – Partial discharge measurements, Int. Electrotech. Comm. (2015). Geneva, Switzerland.
[26] P. Morshuis, Degradation of solid dielectrics due to internal partial discharge: some thoughts on progress made and where to go now, IEEe Trans. Dielectr. Electr. Insul. 12 (5) (Oct. 2005) 905–913.
[27] P.G. Kelleher, Thermal oxidation of thermoplastics, J. Appl. Polym. Sci. 10 (6) (Jun. 1966) 843–857, https://doi.org/10.1002/app.1966.070100602.
[28] L. Wang, A. Cavallini, G.C. Montanari, L. Testa, Evolution of PD patterns in polyethylene insulation cavities under AC voltage, IEEe Trans. Dielectr. Electr. Insul. 19 (2) (Apr. 2012) 533–542.
[29] C. Hudon, R. Bartnikas, M.R. Wertheimer, Analysis of degradation products on epoxy surfaces subjected to pulse and glow type discharges, in: Proc. Annu. Report. Conf. Electr. Insul. Dielectric Phenomena, Oct. 1991, pp. 237–243.

Curriculum Vitae

Personal data

Name:	Maninder Choudhary
Date of birth:	26. 04. 1990
Place of birth:	Umerkot, Pakistan
Citizenship:	Pakistan

Contact data

E-mail:	maninder.choudhary@taltech.ee

Education

2021–2025	Tallinn University of Technology, PhD
2016–2018	The Sirindhorn International Thai German Graduate School of Engineering (TGGS), KMUTNB, MSC
2009–2013	Mehran University of Engineering & Technology, B.Eng
2010–2012	Government Qazi Sultan Higher Secondary School

Language competence

English	Fluent
Estonian	Basic
Urdu	Native
German	Basic
Thai	Basic
Sindhi	Fluent

Professional employment

2021–2025	Tallinn University of Technology, Early-Stage Researcher
2019–2021	Sir Syed University of Engineering & Technology, Lecturer
2014–2016	Bahria University (Karachi, Campus), Lab Engineer

Elulookirjeldus

Isikuandmed

Nimi:	Maninder Choudhary
Sünniaeg:	26. 04. 1990
Sünnikoht:	Umerkot, Pakistan
Kodakondsus:	Pakistani

Kontaktandmed

E-post:	maninder.choudhary@taltech.ee

Hariduskäik

2021–2025	Tallinna Tehnikaülikool, PhD
2016–2018	The Sirindhorn International Thai German Graduate School of Engineering (TGGS), KMUTNB, MSC
2009–2013	Mehran University of Engineering & Technology, BSC
2010–2012	Government Qazi Sultan Higher Secondary School

Keelteoskus

Inglise keel	kõrgtase
Eesti keel	algtase
Urdu keel	emakeel
Saksa keel	algtase
Tai keel	algtase
Sindhi keel	kõrgtase

Teenistuskäik

2021–2025	Tallinna Tehnikaülikool, doktorant-nooremteadur
2019-2021	Sir Syed University of Engineering & Technology, lektor
2014–2016	Bahria University (Karachi, Campus), laboriinsener

ISSN 2585-6901 (PDF)
ISBN 978-9916-80-410-0 (PDF)